



| | | | |
|---|---|---|-----------------|
| Report Title: Analysis and Modelling of induced pore pressures due to pile driving. | Date: June 25, 2012 | | |
| | Number of pages (including appendices): 172 | | |
| | Masteroppgave | X | Prosjektoppgave |
| Name: Fahmid Al Mahid. | | | |
| Professors in charge/Supervisor: Lars Olav Grande (NTNU). | | | |
| Other external professional /Supervisor: Tefera Tewodros Haile (NPRA). | | | |

Abstract:

This Master's Thesis discusses about the development of pore water pressures in the surrounding soil during pile driving. Several studies have already been done on this ground. These papers and books have been used to establish the background. The thesis can be divided into three parts. The first part describes the extensive literature survey of piling activities, effects on soil properties as well the mechanism of the pore pressure development especially for clay.

In the second part, the pore pressure measurements during driving from the Øvre Sund bridge project, Drammen, Norway has been analyzed and compare with the theory. It has been observed that pore water pressure increases when piles are driven and this increase is higher if the driven pile is closer to the piezometer station. The pore pressure development has also described with the theory of expanding cavity.

The last part focuses on Numerical analysis to model the excess pore pressure development during piling activity using PLAXIS and the effect on the stability of the slope. LE method using GeoSuite-Stability, SLIDE have been used to study the effect of piling on the stability.

Key words:

- | |
|-------------------------------|
| 1. Excess pore pressure. |
| 2. Pile driving. |
| 3. Cavity expansion. |
| 4. Pore pressure dissipation. |

(Signature)

MASTER DEGREE THESIS

Spring 2012

for

Student: Fahmid Al Mahid

Analysis and Modelling of induced pore pressures due to pile driving.

BACKGROUND

Pile installation in soft clay may temporarily reduce the stability of nearby buildings or slopes. The remoulding of soil during pile driving may decrease the strength of sensitive clay sufficiently to cause bearing capacity failure or slope instability. Dissipation of the excess pore pressures generated during pile driving may allow pore pressure to rise in the vicinity of slope, thus leading to failure of slope, even where the soil has not been remoulded.

The Øvre Sund Bridge project in Drammen, eastern Norway, is the recently completed bridge construction across Drammen River which was officially open to public on the 10th of September 2011. The bridge connects the Grønland part with the Hamborgstrøm part of the city. The bridge is 148 m long, 23,1 m wide and has 5 spans of 25,8 m and 32 m long. The soil conditions on both sides of the river and in the river bed are relatively similar. The soil condition is composed of three layers. Relatively thin layer of silty sand soil is overlying relatively thick layer of soft clay. The thick soft clay is overlying dense moraine. A total of 191 concrete piles on the Grønland side, 32 steel pipe piles in the river and 100 concrete piles on the Hamborgstrøm side were installed. In order to control the stability problem during construction different measures were taken. Follow up of the development of excess pore pressure during piling activity was one of the measures taken. A total of 8 piezometers in the Grønland side of the river, 6 piezometers in the river and 8 piezometers on the Hamborgstrøm side of the river were installed.

TASK DESCRIPTION

The intension of this study is to analyse the measured excess pore pressure data and model the excess pore pressure development during piling activity using PLAXIS. The candidate is also expected to study the effect of piling on the stability of the slope by FE method using PLAXIS and LE method using GeoSuite – Stability and SLIDE. The Grønland side of the river will be the main focus of the study.

The task of the thesis includes but is not limited to the following:

1. Extensive literature survey.
The focus is to explain the mechanism how the development of pore pressure affects the strength of the surrounding soil.
2. Analysis of data.
The focus is to explain the effect of pile driving by comparing the magnitude of the subsequent mass displacement, thickness of the soft clay layer and the measured pore pressure.
3. Numerical simulation.
The focus is to model the excess pore pressure development during piling activity using PLAXIS and the effect on the stability of the slope. LE method using GeoSuite – Stability, SLIDE will also be used to study the stability.

Professor in charge: Lars Grande, NTNU

Other supervisors: Tewodros Tefera, NPRA

Department of Civil an Transport Engineering, NTNU

Trondheim, June 21, 2012.



Professor in charge (sign)

Supervisor NPRA(sign)

Acknowledgement

This master's thesis has been carried out at the Geotechnical Division, Department of Civil and Transport Engineering, Norwegian University of Science and Technology, NTNU under the supervision of Professor Lars Olav Grande (NTNU), Dr. Tewodros Tefera and Grete Tevdt (NPRA). I would like to express my deepest gratitude to my supervisors. I am very grateful for their valuable comments, guidance and encouragement throughout the work.

I would like to give special thanks to Professor Arnfinn Emdal and Professor Thomas Benz for their continuous support.

I also like to express my gratitude to the Norwegian Public Roads Administration, NPRA for arranging the excursion to Oslo and Drammen to get a clear overview of piling activities and pore pressure measurement.

I am also grateful to the Norwegian Public Roads Administration, NPRA for giving the opportunity to work with them and to provide the necessary materials of Øvre Sund Bridge project.

List of Symbols

Roman Letters

| | |
|-------------------|---|
| a | -Attraction |
| a_u | - Cavity radius |
| a_0 | - Initial radius of cavity |
| c | - Cohesion |
| c' | - Effective Cohesion |
| c_v | - Coefficient of consolidation |
| d | - Pile diameter |
| e | - Void ratio |
| e_{cs} | -Value of e at unit p' on the critical state line in $e - \ln p'$ space |
| E | - Young's modulus. |
| F'_c and F'_q | - Cylindrical cavity expansion factors |
| G | - Shear modulus |
| H | -Drainage distance |
| I_r | - Rigidity Index |
| L | - Pile length |
| L_1 | - Depth of penetration |
| M_{nc} | - Oedometer modulus in the normally consolidated range |
| M_{oc} | - Oedometer modulus in the overconsolidated range |
| M | - Slope of the critical state line in the $p' - q$ plane |
| p | -Initial internal pressure |
| p | -Total mean stress |
| p' | - Effective mean stress |
| p' | - Initial consolidation pressure |
| p_0 | -Initial total mean stress |
| P'_c | -Initial mean preconsolidation stress. |
| P'_0 | - Mean effective normal stress at the state of in-situ |
| P'_f | - Mean effective normal stress at the state of failure |
| p_u | - Ultimate pressure for the expansion of cylindrical cavity |
| q | - Deviatoric stress |

Analysis and Modelling of induced pore pressures due to pile driving.

| | |
|--------------------|--|
| q_u | - Ultimate deviatoric stress |
| q_p | - The deviator stress at the elastic-plastic boundary |
| r | - Distance to the center of cavity |
| r_o | - Radius of pile |
| R | - Isotropic overconsolidation ratio |
| R | - Initial radial distance |
| R_o | - Outer pile radius |
| R_i | - Initial pile radius |
| R_u | - Cavity radius |
| R_p | - Radius of plastic zone |
| s | - Radial distance from the pile |
| s_u | - Undrained shear strength |
| s_t | - Sensitivity |
| t_p | - Primary consolidation time |
| T | - Dimensionless time factor |
| u | - Hydrostatic pore pressure |
| u_o | - Hydrostatic pore pressure. |
| u_d | - Displacement |
| u_m | - Measured pore pressure |
| u_w | - Pore water pressure |
| Δu | - Excess pore water pressure |
| Δu_m | - Maximum excess pore pressure |
| Δu_a | - Excess pore pressure from the change in total ambient pressure |
| Δu_s | - Shaft pore pressure |
| Δu_T | - Tip pore pressure |
| Δu_{oct} | - Excess pore pressure resulting from changes in octahedral normal stress. |
| Δu_{shear} | - Excess pore pressure resulting from changes in octahedral shear stress. |
| v | - The radial displacement of a soil particle. |
| k_o | - Coefficient of earth pressure at rest |
| w | - Water content |
| z | - Depth from the water table at which u is calculated. |

Greek Letters

| | |
|----------------------|---|
| α and β | - Henkel's pore pressure parameter |
| λ | - Slope of the virgin consolidation line in $e - \ln p'$ space. |
| ν | - Specific volume |
| ν | - Poisson's ratio. |
| ν' | - Effective poisson's ratio |
| κ | - Mean slope of the expansion and recompression line in $e - \ln p'$ space. |
| τ | - Shear strength |
| $\Delta\tau_0$ | - Octahedral stress change |
| σ | - Total stress |
| σ_0 | - initial internal pressure |
| $\Delta\sigma_0$ | - Mean normal stress change |
| σ' | - Effective stress |
| σ'_c | - preconsolidation stress |
| σ_n | - Total normal pressure |
| σ'_n | - Effective normal stress |
| σ'_p | - Preconsolidation pressure |
| σ_r | - Radial normal stress |
| σ_{rr} | - The total radial stress |
| σ'_{rr} | - The effective radial stress |
| σ_θ | - Circumferential normal stress |
| σ_{h0} | -Total horizontal stress |
| σ_{vo} | - Total overburden pressure |
| σ'_{vo} | - Effective overburden pressure |
| φ | - Friction angle |
| φ' | - Effective friction angle |
| γ | - Unit weight |
| γ_w | - Unit weight of water |
| Λ | - Plastic volumetric strain ratio |

Contents

| | |
|---|------------|
| Acknowledgement ----- | v |
| List of Symbols ----- | vii |
| List of Figures ----- | xv |
| List of Tables ----- | xix |
| Introduction ----- | 1 |
| Background ----- | 1 |
| Scope of the study ----- | 1 |
| Methodology ----- | 1 |
| Structure of the report ----- | 2 |
| Chapter I ----- | 3 |
| Pile foundation ----- | 3 |
| 1.1 Classification of pile ----- | 3 |
| 1.2 Pile driving method ----- | 5 |
| 1.2.1 Hammer driving----- | 6 |
| 1.2.1.1 Drop hammer----- | 6 |
| 1.2.1.2 Diesel hammers----- | 6 |
| 1.3 Problems in pile driving ----- | 7 |
| 1.3.1 Design and manufacture----- | 7 |
| 1.3.2 Installation----- | 7 |
| 1.3.3 Control of final set----- | 8 |
| 1.3.4 Noise from piling operation----- | 8 |
| 1.3.5 Ground vibration----- | 8 |
| Chapter II ----- | 9 |
| Effects of pile driving in clays ----- | 9 |
| 2.1 Pore pressure during driving ----- | 9 |
| 2.2 Displacement caused by pile driving ----- | 11 |
| 2.2.1 Vertical movement of soil----- | 12 |
| 2.2.2 Horizontal soil movement----- | 16 |
| 2.2.3 Pile heave----- | 17 |
| 2.3 Influence of pile driving on soil properties ----- | 19 |
| 2.3.1 Water content----- | 19 |
| 2.3.2 Consistency limit----- | 20 |
| 2.3.3 Shear strength----- | 20 |
| 2.3.3.1 Investigation----- | 22 |
| 2.3.3.2 The mechanism of shear strength reduction----- | 24 |
| Chapter III ----- | 27 |

Analysis and Modelling of induced pore pressures due to pile driving.

| | |
|---|-----------|
| Excess pore pressure generation due to pile driving ----- | 27 |
| 3.1 Pile driving induced pore pressure ----- | 28 |
| 3.1.1 Lo and Stermac (1965) approach ----- | 29 |
| 3.1.1.1 Modification of the approach by Lo and Stermac Approach ----- | 30 |
| 3.2 Variation of pore pressure generation at pile tip and pile shaft ----- | 32 |
| 3.3 Pore pressure variation during driving through different soil layers ----- | 35 |
| 3.4 Excess pore pressure dissipation ----- | 38 |
| 3.5 Techniques to reduce pore pressure during pile driving ----- | 38 |
| Chapter IV ----- | 39 |
| Theory of Cavity Expansion ----- | 39 |
| 4.1 Expansion of cavity with perfectly plastic soil model ----- | 40 |
| 4.1.1 Ultimate pressure, pu ----- | 41 |
| 4.1.2 Excess pore pressure ----- | 42 |
| 4.2 Expansion of cavity by Modified cam clay model ----- | 44 |
| 4.2.1 Modified cam clay parameter ----- | 45 |
| 4.2.2 Cavity expansion solution ----- | 46 |
| 4.2.2.1 Basic assumption and definition ----- | 46 |
| 4.2.2.2 Elastic analysis ----- | 47 |
| 4.2.2.3 Plastic analysis ----- | 48 |
| 4.2.2.4 An approximate closed form solution ----- | 49 |
| 4.2.3 Factors affecting cavity pressure and excess pore pressure ----- | 49 |
| 4.3 Cavity expansion in pile driving ----- | 54 |
| 4.3.1 Total stress analysis with perfectly plastic soil model ----- | 54 |
| 4.3.2 Effective stress analysis with critical state soil model ----- | 56 |
| Chapter V ----- | 59 |
| Soil condition and Geotechnical report ----- | 59 |
| 5.1 Project description ----- | 59 |
| 5.2 Soil condition ----- | 60 |
| 5.3 Available test data ----- | 60 |
| 5.3.1 Total sounding ----- | 61 |
| 5.3.2 Index test ----- | 62 |
| 5.3.3 Cone penetration test ----- | 63 |
| 5.3.4 Triaxial test ----- | 64 |
| 5.3.5 Oedometer test ----- | 67 |
| Preconsolidation stress ----- | 67 |
| Coefficient of consolidation, cv ----- | 68 |
| Modulus, M ----- | 68 |
| 5.3.6 Undrained Shear Strength of clay layer ----- | 69 |
| Chapter VI ----- | 71 |
| Analysis of Pore pressure measurement of Øvre sund Project ----- | 71 |

Analysis and Modelling of induced pore pressures due to pile driving.

| | | |
|---------------------------|---|------------|
| 6.1 | Pore pressure measurements by Piezometers | 71 |
| 6.2 | Piling activities in the project | 73 |
| 6.3 | Measures taken to control pore pressure development | 74 |
| 6.4 | Other factors that increase pore pressure | 76 |
| 6.5 | Analysis of data | 77 |
| 6.5.1 | Pore pressure situation before driving | 77 |
| 6.5.2 | Overview of Pore pressure increase | 78 |
| 6.5.3 | River water fluctuation | 81 |
| 6.5.4 | Excess pore pressure with distance from driven pile | 82 |
| 6.5.5 | Excess pore pressure with soil type | 86 |
| 6.5.6 | Induced pore pressure variation with the depth of clay layer | 87 |
| 6.5.7 | Pore pressure variation during driving through different soil layer | 88 |
| 6.5.8 | Driving pore pressure at øvre sund by Lo and Stermac approach | 89 |
| 6.5.9 | Pore pressure as a function of overburden pressure | 90 |
| 6.6 | Analysis of øvre sund data with cavity expansion theory | 91 |
| 6.6.1 | Perfectly plastic soil model | 91 |
| 6.6.1.1 | Radial cavity pressure | 92 |
| 6.6.1.2 | Radius of the plastic zone | 93 |
| 6.6.1.3 | Excess pore pressure within the plastic zone | 94 |
| 6.6.1.4 | Excess pore pressure within the elastic zone | 95 |
| 6.6.1.5 | Excess pore pressure at cavity wall | 96 |
| 6.6.1.6 | Comparison of measured and calculated value by cavity expansion | 97 |
| 6.6.2 | Modified Cam clay model | 97 |
| 6.6.2.1 | Radial cavity pressure | 97 |
| 6.6.2.2 | Radius of the plastic zone | 98 |
| 6.6.2.3 | Excess pore pressure distribution in the plastic zone | 101 |
| 6.6.2.4 | Excess pore pressure at cavity wall | 103 |
| 6.7 | Pore pressure dissipation | 103 |
| 6.7.1 | Calculation of primary consolidation time | 106 |
| Chapter VII | | 109 |
| Numerical analysis | | 109 |
| 7.1 | Stability analysis by SLIDE | 109 |
| 7.1.1 | Geometry and input parameter | 110 |
| 7.1.2 | The stability of the slope before pile driving | 111 |
| 7.1.3 | The stability considering the piling activity | 113 |
| 7.2 | PLAXIS | 114 |
| 7.2.1 | Geometry and material properties | 114 |
| 7.2.2 | Mesh generation | 115 |
| 7.2.3 | Stability of the slope without pile | 116 |
| 7.2.3.1 | Effects of river water | 118 |
| 7.2.4 | Effects of piling | 119 |
| 7.2.4.1 | Volumetric expansion | 119 |
| 7.2.4.2 | Prescribed displacement | 124 |
| 7.2.5 | Limitations | 126 |

Analysis and Modelling of induced pore pressures due to pile driving.

| | | |
|---|------------------------------|------------|
| 7.3 | GeoSuite-stability | 126 |
| 7.3.1 | Analysis without pile effect | 127 |
| 7.3.2 | Considering pile effect | 129 |
| Conclusion and Recommendations | | 131 |
| References | | 133 |
| Appendix | | 137 |
| Appendix-A: Data from Øvre sund Project | | 137 |
| Appendix-B: Analysis of piezometric data from Øvre sund Project | | 149 |

List of Figures

Figure 1. 1 a) Concrete pile connecting detail. b) Squared pre-cast concert pile. (36) -----4
Figure 1. 2 Protecting timber piles from decay. a) By pre-cast concrete upper section above water level. b) By extending pile cap below water level. (36) -----4
Figure 1. 3 a) End bearing piles (b) Friction or cohesion pile. (36)-----5
Figure 1. 4 Pile driving rig (3) -----6
Figure 1. 5 Damage to head of precast concrete pile. (15) -----7
Figure 1. 6 Schematic of squeezing –out or consolidation of clay (15)-----8

Figure 2. 1 Dimensionless distribution of excess pore pressures in a slope with pile group placed in the middle of the slope and varied pile group with. (12) 10
Figure 2. 2 Safety factor verses excess pore pressure for variation in the pile group position in the slope for relative pile group width, ($B/bH=0.25$). (12) 11
Figure 2. 3 Safety factor verses excess pore pressure for varying relative width of the pile group. (12)..... 11
Figure 2. 4 Surface heave due to pile driving (after Hagerty and Peck, 1971) (16)..... 12
Figure 2. 5 Movements of nearby buildings caused by pile-driving operations (after D’Appolonia and Lambe, 1971). (24)..... 13
Figure 2. 6 Relation between heave of ground surface and distance from group of piles. (4) 14
Figure 2. 7 Normalized ground heave profile (data from sharp, 1982) (16)..... 15
Figure 2. 8 Comparison of measured and theoretical radial soil displacements (Randolph, Carter and Wroth, 1979) (16)..... 16
Figure 2. 9 Balance of forces along driven piles (Hagerty and Peck, 1971). (24) 17
Figure 2. 10 Photogrammetric measurements of horizontal pile movements due to pile driving in successive zone. (4)..... 18
Figure 2. 11 Computed movements of adjacent pile due to installation of end-bearing pile. (23)..... 19
Figure 2. 12 Variation in water content (14)..... 20
Figure 2. 13 Mohr circle and failure envelope. (36)..... 21
Figure 2. 14 Shear strength measured by Swedish cone, in-situ vane shear strength and cone penetrometer resistance. (4) 22
Figure 2. 15 Variation of the normalized in-situ vane strength with the radial distance immediately after driving. (26)..... 24
Figure 2.16 Mohr circle during pile driving (2) 25

Figure 3. 1 Pore pressures in an equipotential line (1) 27
Figure 3. 2 Summary of measured pore pressures (after Poulos and Davis 1979) (24)..... 28
Figure 3. 3 Variation of $\Delta u/p'$ in function of the consolidation pressure in CIU tests on Saint-Alban clay. (26) 30
Figure 3. 4 Comparison of the pore pressure measured on the pile shaft and calculated from the original and modified Lo and Stermac (1965) solution. (26)..... 31
Figure 3. 5 Details of typical instrumented pile in Saint-Alban test site. (26)..... 32
Figure 3. 6 Pore pressures measured on the pile shaft during the driving of test pile 6 in Saint-Alban test site. (26)..... 33
Figure 3. 7 Variation of the normalized Pore pressures with the radial distance from the pile surface at Saint-Alban test site. (26) 34
Figure 3. 8 Pore water pressures during driving in soft clay (first driving phase) near piezometer P1 (11) .. 36
Figure 3. 9 Pore water pressures during driving in soft clay (first driving phase) near piezometer P3. (11) .. 36

Analysis and Modelling of induced pore pressures due to pile driving.

| | |
|--|----|
| Figure 3. 10 Pore water pressures during driving in soft clay (second driving phase) near piezometer P1. (11) | 37 |
| Figure 3. 11 Pore water pressures during driving in soft clay (second driving phase) near piezometer P3. (11) | 37 |
| Figure 4. 1 Expansion of a cylindrical cavity. (38) | 40 |
| Figure 4. 2 Cylindrical cavity expansion factor | 42 |
| Figure 4. 3 Modified Cam clay parameter. (7) | 46 |
| Figure 4. 4 Expansion of a cylindrical cavity. (8) | 47 |
| Figure 4. 5 Variation of normalized cavity pressure with cavity radius during the expansion of a spherical cavity. (8) | 50 |
| Figure 4. 6 Variation of normalized cavity pressure with cavity radius during the expansion of a cylindrical cavity. (8) | 51 |
| Figure 4. 7 Variation of normalized excess pore pressure at the cavity wall and normalized cavity pressure with cavity radius during the expansion of a spherical cavity.(8) | 52 |
| Figure 4. 8 Variation of normalized excess pore pressure at the cavity wall and normalized cavity pressure with cavity radius during the expansion of a cylindrical cavity.(8) | 52 |
| Figure 4. 9 Stress distribution around a (a) Spherical Cavity (b) cylindrical Cavity at the ultimate state. (8) | 53 |
| Figure 4. 10 Variation of elastic-plastic boundary with isotropic overconsolidation ratio.(8) | 54 |
| Figure 4. 11 Prediction of pile shaft normal stresses for normally consolidated Huntspill clays (Data from Coop and Wroth,1989). (35) | 55 |
| Figure 4. 12 Prediction of pile shaft normal stresses for heavily overconsolidated Madingley clays (Data from Coop and Wroth,1989). (35) | 56 |
| Figure 4. 13 Variation of excess pore pressure at cavity wall with overconsolidation ratio. (35) | 57 |
| Figure 5. 1 View of øvre sund bridge project, Drammen | 59 |
| Figure 5. 2 Boring Plan | 61 |
| Figure 5. 3 Total sounding result in Borehole 14. | 62 |
| Figure 5. 4 Index test at borehole 12. | 63 |
| Figure 5. 5 CPTU result at borehole 13. | 64 |
| Figure 5. 6 Triaxial test result in a $12 \sigma_d$ vs σ_3' diagram. | 65 |
| Figure 5. 7 q vs p' diagram for triaxial test at borehole 12. | 66 |
| Figure 5. 8 q vs p' diagram for triaxial test borehole 19. | 66 |
| Figure 5. 9 Oedometer test results at borehole 12 | 67 |
| Figure 5. 10 Undrained shear strength for clay layers. | 69 |
| Figure 6. 1 Piezometer location at Grønland part. (30) | 71 |
| Figure 6. 2 Piezometer location at station P4. (Photo : Tefera T.) | 72 |
| Figure 6. 3 Piling in progress at Grønland side. (Photo : Tefera T.) | 73 |
| Figure 6. 4 The four vertical drains installed on the outside wall of the open ended steel pipe piles in axis 5 in the river. (30) | 74 |
| Figure 6. 5 The soft clay material (clay sausage) drilled/sucked out of the hole before driving the concrete pile. (30) | 75 |
| Figure 6. 6 Schedule of piling work at the axis of G6. (31) | 76 |
| Figure 6. 7 Comparisons of hydrostatic pore pressure and piezometric pore pressure before pile driving at P4 station. | 78 |
| Figure 6. 8 Comparison of hydrostatic pore pressure and piezometric pore pressure before pile driving | 79 |
| Figure 6. 9 Excess pore pressure at P4 (-9.9m) with time | 80 |

Analysis and Modelling of induced pore pressures due to pile driving.

| | |
|---|-----|
| Figure 6. 10 Piezometer level in meter during piling. | 80 |
| Figure 6. 11 Pore pressure response at different piezometer after driving half of G194..... | 81 |
| Figure 6. 12 River water fluctuation during driving. | 82 |
| Figure 6. 13 Pore pressure response with distance..... | 83 |
| Figure 6. 14 Normalized pore pressure with distance-pile diameter ratio at P3. (-10)..... | 84 |
| Figure 6. 15 Excess pore pressure response at all piezometers for driving of different pile..... | 85 |
| Figure 6. 16 Induced pore pressure variation with distance..... | 85 |
| Figure 6. 17 Pore pressure responses from the clay layer | 86 |
| Figure 6. 18 Pore pressure response from the sand layer | 87 |
| Figure 6. 19 Induced pore pressure variation with clay layer depth. | 88 |
| Figure 6. 20 Induced pore pressure variation with clay layer depth. | 89 |
| Figure 6. 21 Comparison of measured and calculated pore pressure at piezometer location P2 in Øvre sund project, Drammen. | 90 |
| Figure 6. 22 Comparison of measured pore pressure at piezometer location P3 with the effective and total overburden pressure in Øvre sund project, Drammen..... | 91 |
| Figure 6. 23 Radial pressure to expand the cavity with depth. | 92 |
| Figure 6. 24 Radius of plastic zone with undrained shear strength..... | 94 |
| Figure 6. 25 Comparison of the development of pore pressure in the plastic and elastic zone by cavity expansion and øvre sund. | 97 |
| Figure 6. 26 Excess pore pressure at plastic zone by MCC at different depth..... | 102 |
| Figure 6. 27 comparison of excess pore pressure at plastic zone by MCC and perfectly plastic model..... | 102 |
| Figure 6. 28 Excess pore pressure dissipation with time after driving at P3 (-14)..... | 104 |
| Figure 6. 29 Excess pore pressure dissipation with time after driving at P3 (-10)..... | 105 |
| Figure 6. 30 Excess pore pressure dissipation with time after driving at P1 (-7)..... | 105 |
| Figure 6. 31 Excess pore pressure dissipation with time after driving at P4 (-9.9)..... | 106 |
| | |
| Figure 7. 1 Profile section for numerical analysis..... | 109 |
| Figure 7. 2 Section of Soil profile used in Slide..... | 110 |
| Figure 7. 3 Effective stress analysis considering river water. | 111 |
| Figure 7. 4 Undrained total stress analysis considering river water. | 112 |
| Figure 7. 5 Effective stress analysis without considering river water..... | 112 |
| Figure 7. 6 Undrained total stress analysis without considering river water..... | 113 |
| Figure 7. 7 Effective stress analysis considering the pile effect. | 114 |
| Figure 7. 8 Working mesh with 454 elements..... | 116 |
| Figure 7. 9 Failure surface for effective stress parameter..... | 117 |
| Figure 7. 10 Failure surface for total stress parameter..... | 117 |
| Figure 7. 11 FOS for effective stress parameter. | 117 |
| Figure 7. 12 FOS for total stress parameter..... | 118 |
| Figure 7. 13 Reduced stability of slope without river water | 118 |
| Figure 7. 14 Effects of river water on failure surface. | 119 |
| Figure 7. 15 Soil movement due to pile driving. (32) | 120 |
| Figure 7. 16 short time stability of the slope including pile effect. | 121 |
| Figure 7. 17 Horizontal displacement by volume expansion..... | 122 |
| Figure 7. 18 Total displacement by volume expansion..... | 122 |
| Figure 7. 19 Excess pore pressure developed due to pile effect | 122 |
| Figure 7. 20 Excess pore pressure generation in clay layer..... | 122 |
| Figure 7. 21 excess pore pressure with distance from plaxis analysis | 123 |
| Figure 7. 22 Total and effective verticle stress with horizontal displacement. | 123 |
| Figure 7. 23 failure surface with sand layer cohesion=5. | 123 |

Analysis and Modelling of induced pore pressures due to pile driving.

| | |
|---|------------|
| <i>Figure 7. 24 Prescribed displacement.....</i> | <i>124</i> |
| <i>Figure 7. 25 Failure surface with prescribed displacement</i> | <i>125</i> |
| <i>Figure 7. 26 Excess pore pressure with prescribed displacement.....</i> | <i>125</i> |
| <i>Figure 7. 27 Excess pore pressure generation in clay layer with prescribed displacement.....</i> | <i>125</i> |
| <i>Figure 7. 28 Stability of slope using effective stress parameter before piling starts without considering river water.....</i> | <i>127</i> |
| <i>Figure 7. 29 Stability of slope using effective stress parameter before piling starts considering river water.</i> | <i>128</i> |
| <i>Figure 7. 30 Stability of slope using total stress parameter before piling starts without considering river water</i> | <i>128</i> |
| <i>Figure 7. 31 Stability of slope using total stress parameter before piling starts considering river water.....</i> | <i>129</i> |
| <i>Figure 7. 32 Stability of slope considering pile effect</i> | <i>130</i> |

List of Tables

| | |
|--|-----|
| <i>Table 3. 1 Induced pore pressure expressed in function of σ_{vo}', σ_{vo}, σ_p'. (26)</i> | 34 |
| <i>Table 5. 1 The oedometer modulus M.</i> | 69 |
| <i>Table 5. 2 Summerized results of clay layer at øvre sund project, Drammen.</i> | 70 |
| <i>Table 6. 1 Locations of piezometer (30)</i> | 72 |
| <i>Table 6. 2 Pore pressure generation in plastic zone by cavity expansion theory.</i> | 95 |
| <i>Table 6. 3 Pore pressure generation in the elastic zone by cavity expansion theory.</i> | 96 |
| <i>Table 6. 4 Radial cavity pressure with MCC model for different depth.</i> | 98 |
| <i>Table 6. 5 Different parameters to calculate size of the plastic zone.</i> | 100 |
| <i>Table 6. 6 Size of the plastic zone with depth.</i> | 100 |
| <i>Table 6. 7 Ultimate deviatoric stress with depth.</i> | 101 |
| <i>Table 6. 8 Excess pore pressure at cavity wall at different depth wih MCC model.</i> | 103 |
| <i>Table 7. 1 Input parameters of soil.</i> | 111 |
| <i>Table 7. 2 Input parameters of soil in Plaxis.</i> | 115 |
| <i>Table 7. 3 General informations of mesh generation</i> | 116 |
| <i>Table 7. 4 Effective stress parameter.</i> | 130 |

Introduction

Background

Development of pore water pressure during piling activities is a fact that must be taken into consideration during construction. Indeed, when piles are driven, pore water pressure increase in the surrounding soil and so the strength of the soil reduces. This can lead to slope instability or bearing capacity failure. Excess pore water pressure dissipates with time and the soil regain its strength. Dissipation of excess pore water pressure is function of time and soil type. Proportion of pore water pressure generated varies with distance to the driven pile.

Scope of the study

The scope of this study includes extensive literature survey of pile driving pore pressure, analysis and interpretation of data and numerical modelling of excess pore pressure development and the effect on stability. The available data has been supplied by “Norwegian Public Roads Administration, NPRA” from a bridge project in Drammen, Norway.

Methodology

For the literature survey, it books and journals have been used from the library and internet. Then we had to use efficiently the data that the company gave us. With water level measurements from piezometers at different time, it was possible to find pore water pressure generation before and after driving. Then these measurements have been combined with time, depth and distance from piezometer to driven pile to compare the predicted and measured value. It has also been described the mechanism of pore pressure development.

Structure of the report

This report is composed of three main parts. The first part, focuses on literature survey, explains how pore pressure generate and how the development of pore pressure have influences on soil properties and soil strength, introduces cavity expansion theory to predict pore pressure development. The second part deals with analysis and interpretation of pore pressure data during driving from the Øvre Sund bridge project, Drammen.

In the last part, the excess pore pressure development and the effect on the stability of the slope is modelled by numerical analysis using PLAXIS. LE method GeoSuite – Stability and SLIDE were also used to study the effects of piling on the stability.

Chapter I

Pile foundation

When the soil close to the ground surface has not enough capacity to support a structure, deep foundations are essential which transfer the loads to a deeper firm strata. For this purpose, piling may be the most common and useful method.

Pile foundation is appropriate for the following condition:

- When the soil below the ground surface is very weak to support the load from the structure.
- To reduce differential settlement.
- For structure that are subjected to horizontal loads.
- To avoid erosion or scour from underneath a shallow foundation.
- Suitable for offshore structures.

1.1 Classification of pile

Piles may be classified under five different categories: (3)

- Material types.
- Method of Load transfer.
- Method of Construction.
- Type of use.
- Amount of ground disturbance.

The materials used for piles are generally steel, concrete and timber. Steels are used for piling in the form of thick pipes or rolled steel H-sections. These steel piles may be open or closed at the end. Cement concrete and reinforcement are used as the material of concrete piles. Concrete piles can be precast or cast-in-situ. Precast piles may be square, circular, triangular or octagonal in shape and they are produced in short length and can easily be connected to get the required length.

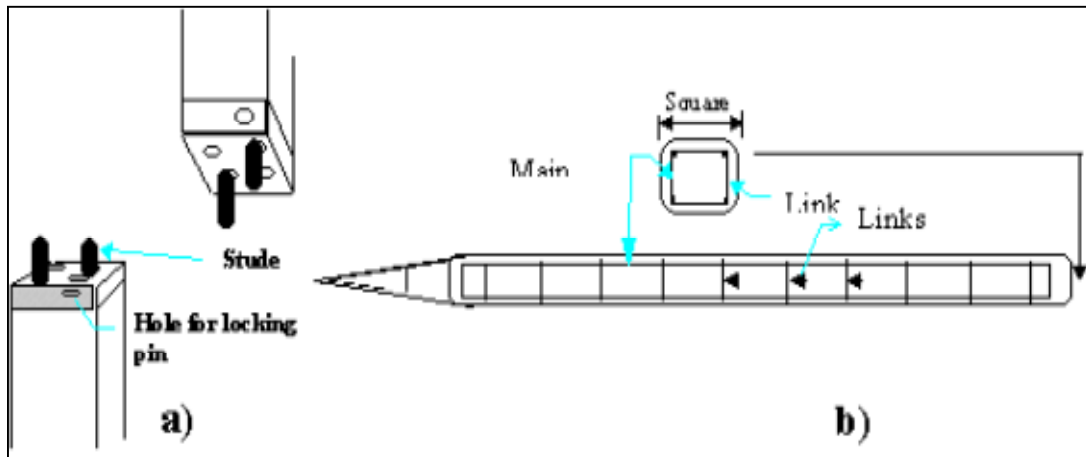


Figure 1. 1 a) Concrete pile connecting detail. b) Squared pre-cast concert pile. (36)

Timbers are also used as pile material in limited cases. Timber can be used suitably for long cohesion piling. A composite pile is made by combination of different materials. In some cases, concrete piles are driven above the ground water level while timber is used below the ground water level to protect the timber from insect attack and decay.

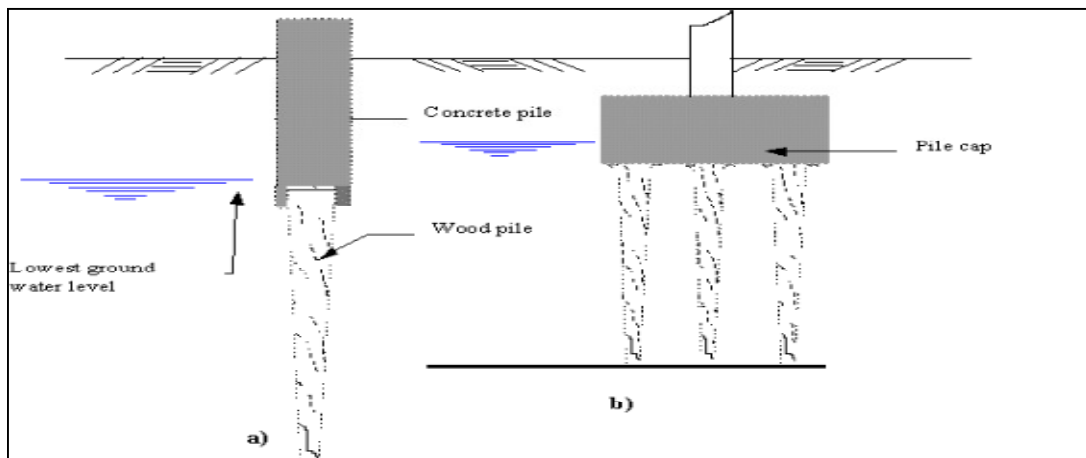


Figure 1. 2 Protecting timber piles from decay. a) By pre-cast concrete upper section above water level. b) By extending pile cap below water level. (36)

According to the method of load transfer, piles are classified as end bearing and friction piles. End bearing piles are those that transfer the loads through bottom tips. When the loads are carried by friction on the sides of the piles, it is termed as friction pile. While combinations of both methods occur, the loads are carried by tip and friction.

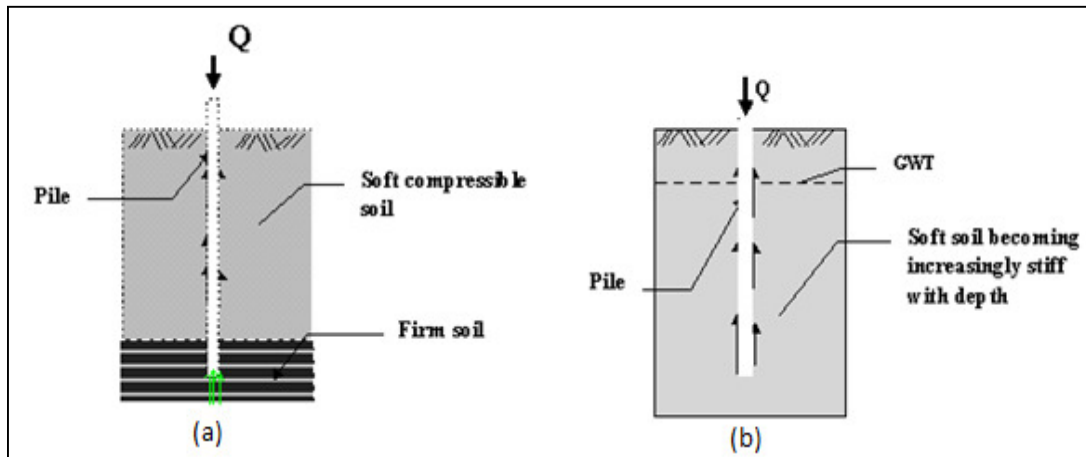


Figure 1.3 a) End bearing piles (b) Friction or cohesion pile. (36)

The classification of pile is based on method of installation also. Piles can be driven by applying blows of a heavy hammer or can be installed by making hole and then filling them with concrete which can be termed as driven piles and bored piles respectively.

Depending upon their use pile is classified as load bearing piles, compaction piles, and tension piles. Load bearing piles are transferring the loads to suitable strata by end bearing, by friction or by both. Compaction piles are driven to increase the soil condition. The piles those resist uplift and overturning forces are known as tension piles.

Displacement piles and non-displacement piles are the two types based on ground disturbance. Displacement piles cause the soil to be displaced radially as well as vertically while the pile shaft is driven or jacked into the ground.

1.2 Pile driving method

Piles can be either driven or bored depending on various parameters. Pile driving methods fall into the following categories. (3)

- Hammer driving.
- Vibratory pile driver.
- Jetting technique.
- Partial auguring method.

Analysis and Modelling of induced pore pressures due to pile driving.

A short description of Hammer driving method is described below.

1.2.1 Hammer driving

The hammers used for pile driving are following types:

1.2.1.1 Drop hammer

This is the traditional method of pile driving. Due to slow rate of hammer blows, it is rarely used these days. Fig 1.4 shows, pile driving rig. A drop hammer generally weights from 0.5 to 2 times the pile weight, allowed to drop from 0.2 to 2 m height under gravity.

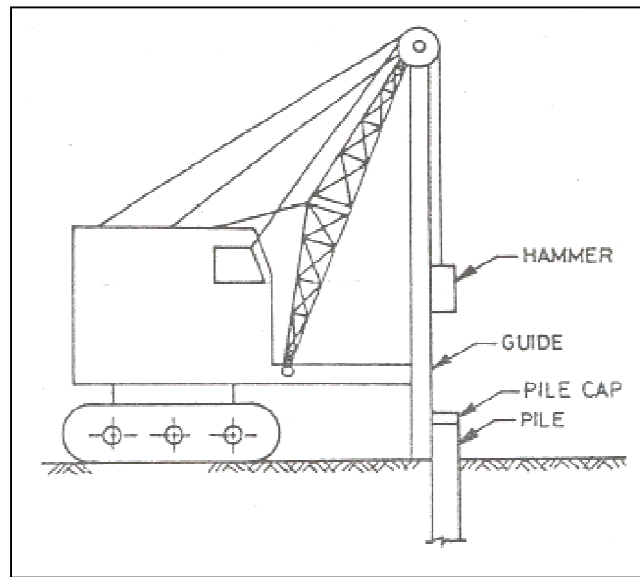


Figure 1. 4 Pile driving rig (3)

1.2.1.2 Diesel hammers

Fuel injection system is used in case of diesel hammer. It also consists of a ram and anvil block at the lower end. Fuel is injected near the anvil, hammer drops and ignition takes place by compressing the air fuel mixture. The pressure developed pushes the pile downward and raises the ram. The process is then repeats.

1.3 Problems in pile driving

Pile driving or pile boring techniques meet different types of problems as installation methods are different. Each system has particular advantages and disadvantages. Problems in manufacture and installation, movement of ground, noise and ground vibration are the major problems caused by driving. (15)

1.3.1 Design and manufacture

Shrinkage cracks in concrete piles form due to lack of adequate curing. The piles should be acceptable if the cracks are not too wide. The acceptable limit of transverse hair crack is 0.15 to 0.3mm in width.

In case of steel H-piles, it may be fitted shoe or rock point for heavy driving while as for hexagonal piles care must be given for welding. Bulking is another problem for steel piles.

1.3.2 Installation

The most common type of problem during installation of concrete pile is distortion of the head of the pile. Choice of material is important in this case. Steel piles are suitable for heavy driving and driving through strata containing rock and boulder as they rarely break. For a closely spaced group flexible piles, alignment is an important factor of consideration.



*Figure 1. 5 Damage to head of precast concrete pile.
(15)*

1.3.3 Control of final set

When pile driving is performed through strata of blocky rock with the presence of clay in between the blocks, unexpected settlement may create problem (Fig 1.6). It may occur because under static loading the clay may squeeze out from between the blocks.

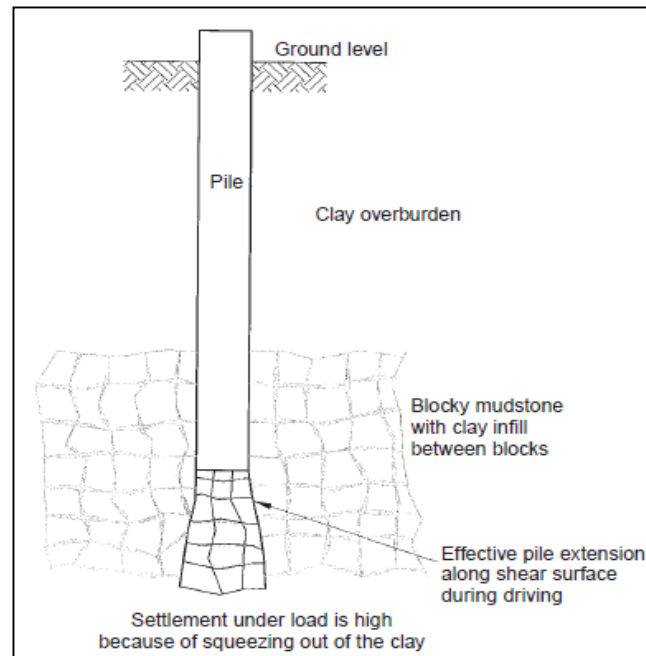


Figure 1. 6 Schematic of squeezing -out or consolidation of clay (15)

1.3.4 Noise from piling operation

Pile operation produce excessive noise from hammering, engine etc. During driving more than 85 decibel noise level is common within 10m of the piling plant (15). By improving the design of the pile rig noise can be reduced.

1.3.5 Ground vibration

Ground vibration is the other serious problem caused by pile driving. Due to vibration of ground, it may disturb adjacent structures. Vibration causes settlement in case of loose sand. This has effect within 400m from the source of vibration. (15).

Chapter II

Effects of pile driving in clays

Effects of driven piles are a major concern in Geotechnical Engineering. Pile driving has a pronounced effect on nearby soil though sands and clays behave differently. When driving is carried out through a saturated layer, a disturbed zone occurs around the pile. The soil is displaced and excess pore pressure developed which affect the strength of soil directly. In case of sensitive clay, instability of slopes may occur due to increase of pore pressure. This excess pore pressure dissipates gradually, the surrounding soil consolidates and the strength is increased which is known as the thixotropy behavior of soil.

According to De Mello (1969) the effects of pile driving in clays may be described under four major categories: (25)

- Remolding or disturbance to structure of the soil surrounding the pile.
- Alteration of the state of stress of the soil in the vicinity of the pile.
- Dissipation of excess pore pressures developed around the pile.
- Long term phenomena of strength regain in the soil.

2.1 Pore pressure during driving

Driving of high displacement piles in cohesive soil results pore pressure development around the piles. The magnitude of excess pore pressure depends on various factors such as distance from pile, soil type, diameter and length of pile, drainage facility, soil density etc. Around the piles a zone of influence developed where this pore pressure response is very high. This may reduce the undrained shear strength of clay, leads to failure of slopes and damages nearby buildings or structures. After certain time, this excess pore pressure reduced and the soil regain its strength depending on the permeability and distance from the pile. Bjerrum and Johannessen (1960) showed that, considerable excess pore pressure still remained in the clay 3 to 4 months after the driving. (13)

Analysis and Modelling of induced pore pressures due to pile driving.

According to Lo and Stermac (1965), the maximum induced pore pressure for normally and very slightly overconsolidated clays or loose silts can exceed the effective overburden pressure by up to 30%. (13)

During driving two single 12 in. precast concrete piles in sensitive clay, Fellenius and Broms (1969) measured pore pressures close to the piles that exceeded locally the total overburden pressure by 20% and dissipated within 120 days. (13)

D'Appolonia and Lambe (1971) reported small induced pore pressure 10m away from the pile. Piles were driven in a preaugered holes which reduced the pore pressure development but did not eliminate. (13)

Bozozuk et al. reported most induced pore pressure within 20 pile diameter from the pile group. Fellenius and Samson (1976) studied and reported maximum induced pore pressure around the pile exceeds 2 times the initial effective overburden and most of the pore pressure dissipates within 3 months.

Hoem (1976) studied the sensitivity of slope due to the pile driving induced pore pressure. He worked with different inclination and slope height. In figure 2.1 the relation x/bH represents the location of the pile group center, B/bH determines the ratio between pile group width and slope width. Figure 2.2 shows dramatic reduction in factor of safety when the pile group is located in the center of the slope i.e. $x/bH = 0.5$. Figure 2.3 shows the FOS with pore pressure ratio for different relative width of pile group.

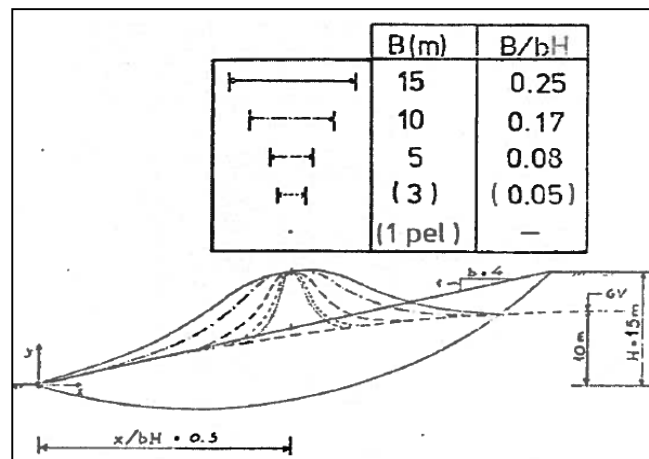


Figure 2. 1 Dimensionless distribution of excess pore pressures in a slope with pile group placed in the middle of the slope and varied pile group width. (12)

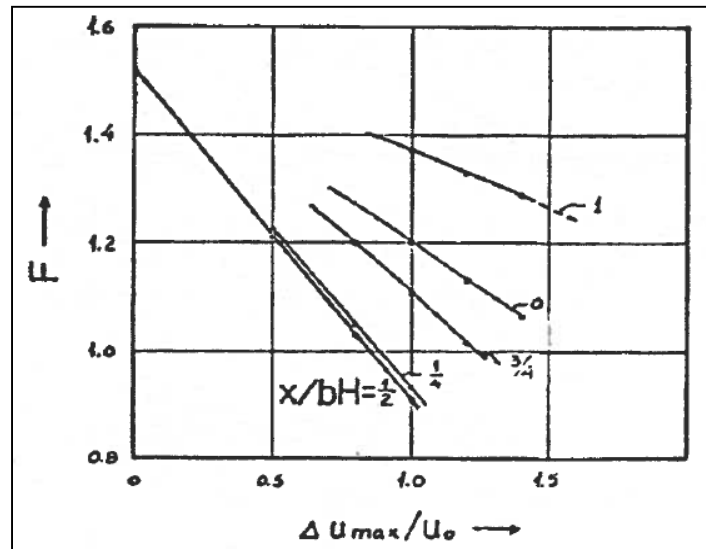


Figure 2.2 Safety factor verses excess pore pressure for variation in the pile group position in the slope for relative pile group width, ($B/bH=0.25$). (12)

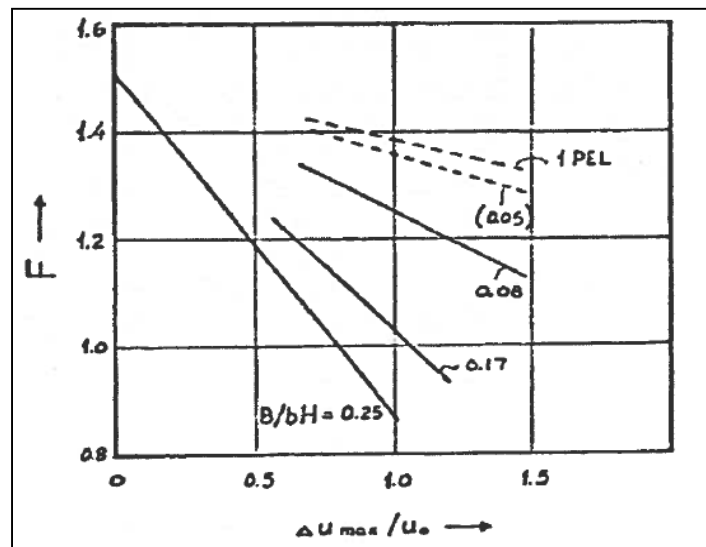


Figure 2.3 Safety factor verses excess pore pressure for varying relative width of the pile group. (12)

2.2 Displacement caused by pile driving

Whenever piles are driven, soil is displaced. This movement of soil caused by pile driving has several undesirable consequences including lift or lateral displacement of previously driven pile and significant effects on nearby structures. This effect varies greatly on how piles are transferring the loads to the soil. For end bearing piles it is

Analysis and Modelling of induced pore pressures due to pile driving.

seriously affects the load carrying capacity and should be redriven, while for frictional pile this effect is less pronounced. The soil movement effect from pile driving can be described under three ways:

2.2.1 Vertical movement of soil

Due to pile driving, some of the soil moves upward. The Vertical movement of soil during driving is termed as ground heave. The total volume of initial ground heave can be related with the total volume of driven pile. According to Adams and Hanna (1970), this ratio is 100% for steel H-piles in a firm till while it is 50% for piles in clay by Hagerty and Peck (1971). For precast concrete pile in soft, sensitive, silty clay the ratio is 30% by Orrje and Brooms (1967), 60% by Avery and Wilson (1950) and 40% by Torstensson. (25)

Hagerty and peck (1971) studied the heave caused by pile driving at 16 sites with diverse soil conditions. The average soil heave normalized by the length of the piles had determined for the 8 of the 16 sites as a function of the ratio of total volume of the inserted piles to the volume of the soil enclosed or surrounded by those piles, (Volume displacement ratio). This relationship shows in figure 2.4, the volume of soil displaced within the pile group is about one half of the total volume of pile inserted. (16)

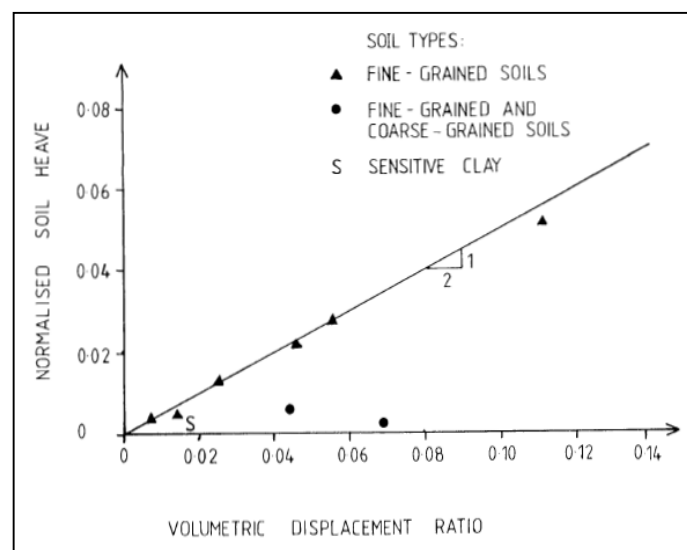


Figure 2. 4 Surface heave due to pile driving (after Hagerty and Peck, 1971) (16).

Analysis and Modelling of induced pore pressures due to pile driving.

Cooke and Price (1973) also studied the soil movement due to driving of a closed ended pile into London clay. They reported that during initial penetration up to about 12 pile radius, most of the ground heave occurs. They made a relationship between ground heave and distance from pile axis. It was reported highest displacement within 4 pile radius from the pile axis and small but measurable beyond 20 pile radius. (16)

Lambe and Horn (1965) reported the movement of an existing building due to driving of piles for the construction of a new building. It was found that, at the near corners of the existing building, a heave of about 0.3 in. occurred during driving. A net settlement of about 0.35 in. had occurred at the end of construction. (25)

D'Appolonia and Lambe (1971) reported measurements of heave during driving of concrete filled pipe piles in preaugered holes in Boston blue clay. Adjacent structures heaved from 0.01 to 0.03 ft. (3-10mm). But no damage was observed (13). Figure 2.5 shows some measurements of heave and settlement of buildings caused by pile driving by D'Appolonia and Lambe (1971). The settlement data plotted are for net settlement one to three years after the end of construction. Larger movements than those measured by Lambe and Horn (1965) were found, although the piles were again preaugered to within 20 to 30ft. of the final tip elevation. (24)

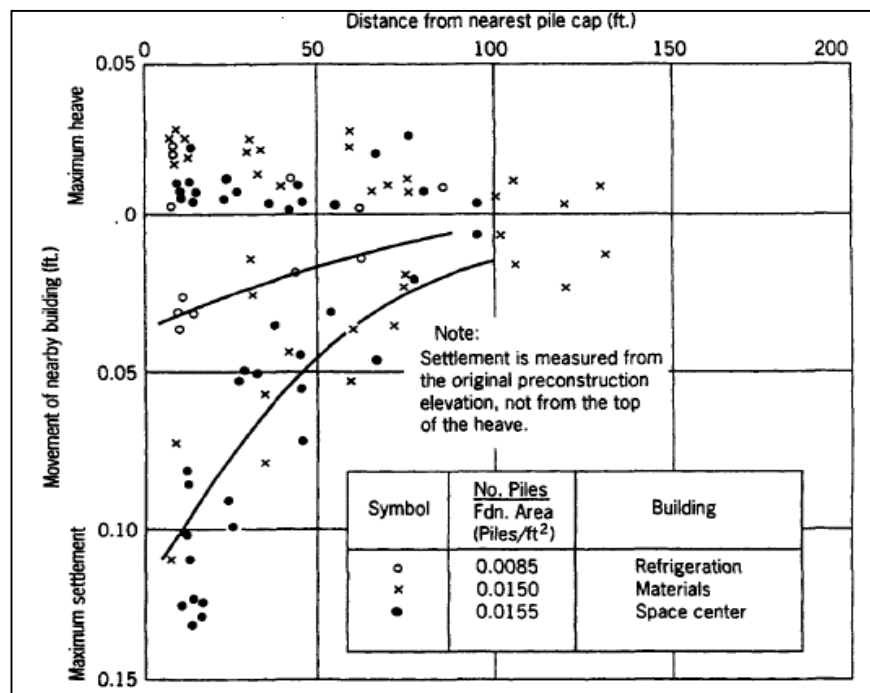


Figure 2. 5 Movements of nearby buildings caused by pile-driving operations (after D'Appolonia and Lambe, 1971). (24)

Analysis and Modelling of induced pore pressures due to pile driving.

Fellenius and Broms (1969) measured the soil heave with depth from driving two single 12 in. precast concrete piles at a spacing of 30 ft. (10m) in normally consolidated sensitive clay. They reported surface heave of 0.8 in. (20mm) close to the piles. They also showed the decreased heave with increasing depth. At a point located at 16 ft. and 36 ft. away from the two piles they reported ground heave 0.2 in. (6mm). (13)

Tortensson (1973) measured heave of 5 in. (12cm) within the pile group in a soft sensitive clay. He had also suggested that heave can be reduced by pre-boring. (13)

According to Lambe and horn (1965), soil heaved to about 0.2 ft. (60mm) during driving groups of partially preaugered and partially driven long concrete piles. The adjacent building foundation (less than 10 ft away) heaved to 0.02ft. (6mm). (13)

Bozozuk et al. (1978) reported soil heave for driving of two groups of 116 concrete piles in sensitive marine clay in Eastern Canada. They measured vertical heave of 450mm (18in.) within the pile group which decreased rapidly with distance. It was plotted the measured vertical heave at the ground surface with distance from the group of piles. The average soil heave outside the pile group to a distance of 3m was 110mm. (Fig. 2.6).

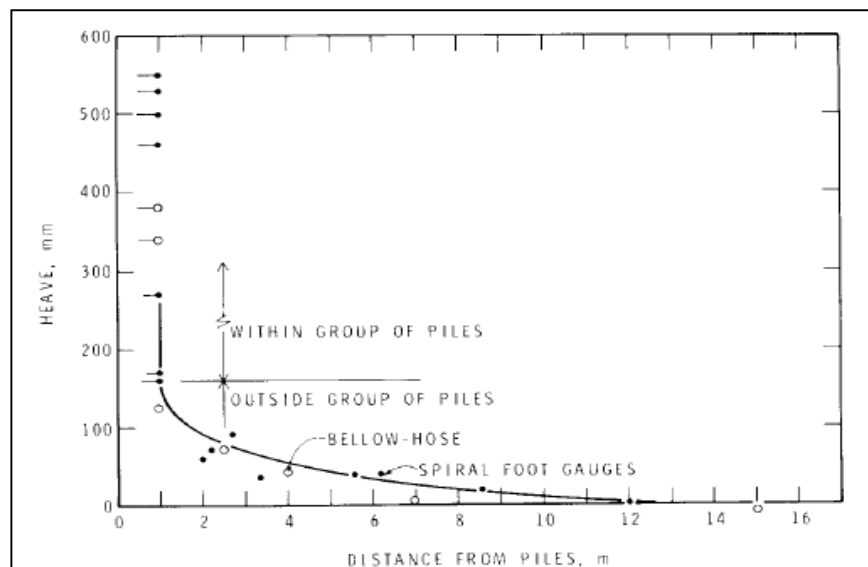


Figure 2. 6 Relation between heave of ground surface and distance from group of piles. (4)

The investigation of Fellenius and Samson (1976) was to study the disturbance caused by the driving of displacement piles. The test site was located on the Sidbec property at

Analysis and Modelling of induced pore pressures due to pile driving.

Contrecoeur, Quebec in Canada. The soil consists of sensitive marine clay. A group of thirteen precast concrete piles of diameter of 12 in. (30 cm) were driven. The ground surface heave by the pile driving was measured at three points. The heave within the pile group was 0.23 ft. (70mm) and 0.12ft. (30mm) at a distance of 8 pile diameter outside the pile group. The zone of influence around the pile group to a distance of at least 8ft. (2.5m) and probably 20 ft. (6m).

Sharp (1982) provided some ground heave measurements for open and closed end piles in stiff clay at Cowden, Hull. Their investigation agreed fairly with Cooke et al. (1979) for closed ended piles. The maximum ground heave of closed ended piles were 5-6 times that of a similar open ended piles. (16)

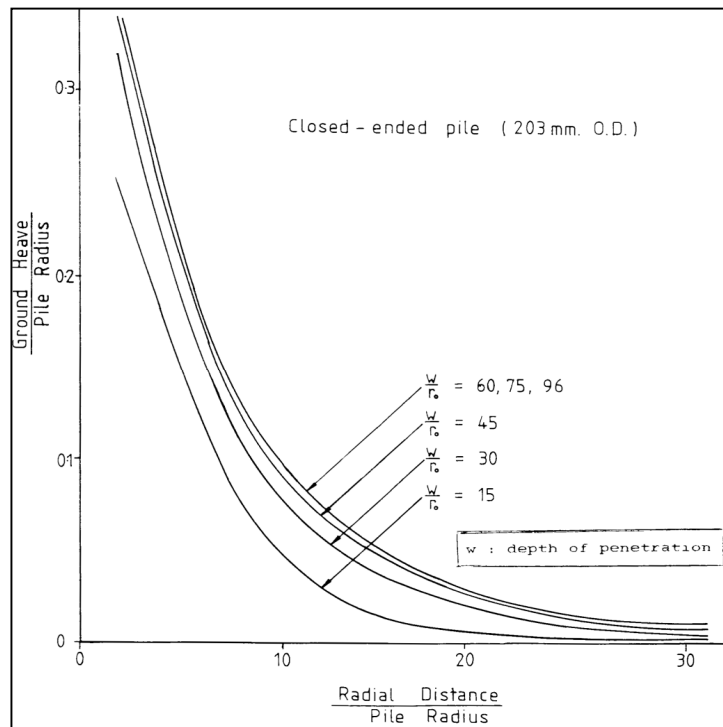


Figure 2. 7 Normalized ground heave profile (data from sharp, 1982) (16)

Figure 2.7 shows highest ground heave near the pile wall and decrease gradually with distance from the pile axis.

2.2.2 Horizontal soil movement

Lateral movement of soil and piles are also an effect of pile driving. Lateral movement of soil normally occurs at higher depth. At greater depth, the soil is displaced predominantly outwards in the radial direction. Therefore, pile driving results in movement of soil not only vertically but also laterally.

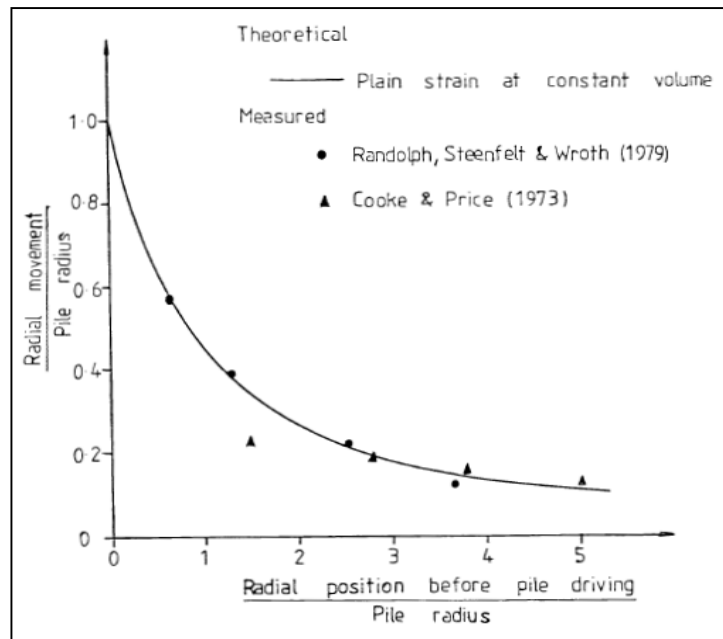


Figure 2. 8 Comparison of measured and theoretical radial soil displacements (Randolph, Carter and Wroth, 1979) (16)

Figure 2.8 shows a comparison of theoretical and measured radial movement of soil due to pile driving by Randolph, Carter and Wroth (1979). The figure combines the results from the model test of Randolph, Steenfelt and Wroth (1979) together with field measurement of Cooke and price (1973) those fit very well with the theoretical value.

The radial displacement, v of a soil particle at an initial radial distance, R away from the axis of a closed ended pile before installation,

$$\frac{v}{R_0} = \left[\left(\frac{R}{R_0} \right)^2 + 1 \right]^{1/2} - R/R_0 \quad \dots \dots \dots (2.1)$$

Where R_0 the outer pile radius. The area ratio is defined by Carter, Randolph and Wroth

(1980) as $1 - \left(\frac{R_i}{R_0}\right)^2$, where R_i is the inner pile radius. The equation is then altered for open ended piles with various area ratios as,

$$\frac{v}{R_0} = \left[\left(\frac{R}{R_0}\right)^2 + \rho \right]^{1/2} - \frac{R}{R_0} \quad \dots \dots \dots (2.2)$$

The model test piles were closed ended and therefore the theoretical curve (Fig 2.8) is plotted for $\rho = 1$.

2.2.3 Pile heave

When piles are closely spaced in a multiple pile system, piles driven earlier may rise during driving of later piles. Klohn (1961) concluded that pile heave causes a serious foundation problem for end bearing piles, redriving of all heaved piles necessary. In the case of friction pile, heave has no adverse effect on the capacity of the piles. (16)

A simple procedure to estimate pile heave was suggested by Hagerty and peck (1971). Piles driven in clay may be lifted due to relative heave of upper part while some downward adhesive forces act on lower part of the vertical pile. Assuming no soil heave below the section a-a in figure 2.9.

$$Pile\ heave = \frac{(L - d)(soil\ heave)}{L} \quad \dots \dots \dots (2.3)$$

Where d is the depth by adjusting upward and downward forces along pile Length, L .

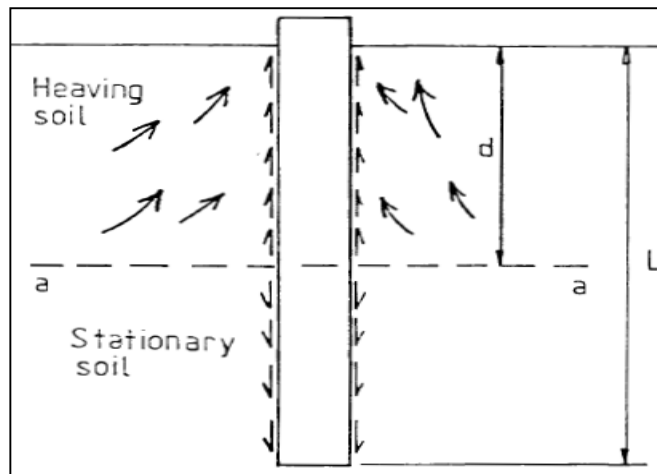


Figure 2. 9 Balance of forces along driven piles (Hagerty and Peck, 1971). (24)

Analysis and Modelling of induced pore pressures due to pile driving.

Bozozuk et al. (1978) studied the movement of piles during driving of two groups of 116 piles in sensitive marine clay in eastern Canada. Terrestrial photogrammetric technique was used to monitor the vertical and lateral movement of installed piles due to driving of additional piles in the same group. In figure 2.10 the situation has been described. The pile driving area was divided into four zones. Driving of piles in zone II, III and IV were indicated by dashed, solid and dotted line respectively. When driving in zone II, the pile no.28 which was driven earlier in zone I, moved about 175mm (7in.) Similarly when driving in zone IV, pile 66 in zone III was also moved as high as 75mm (3in.)

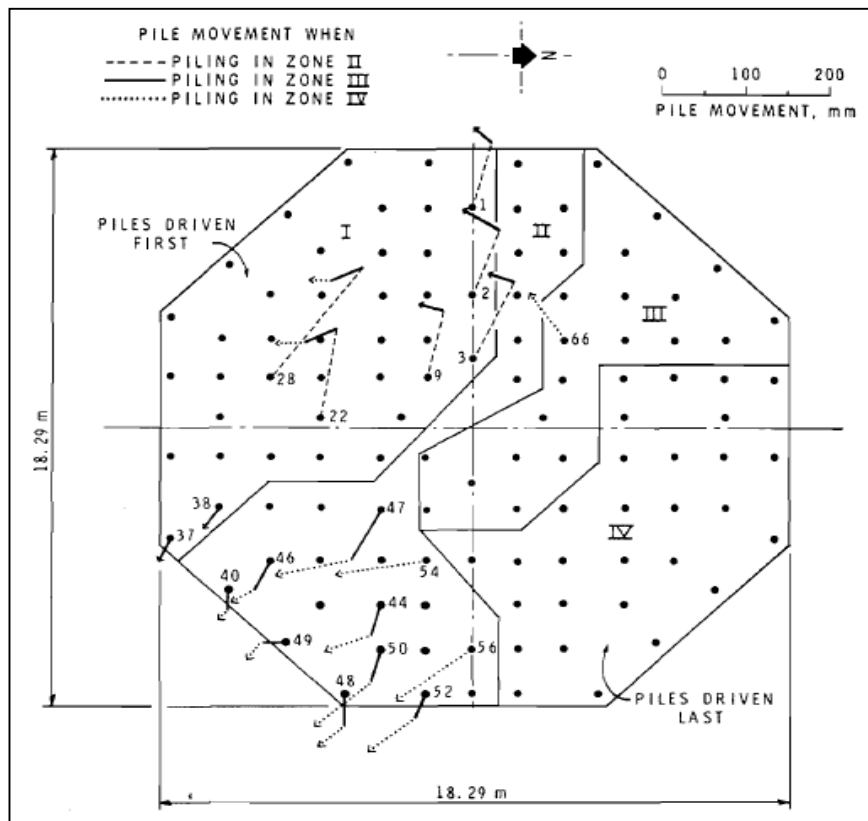


Figure 2. 10 Photogrammetric measurements of horizontal pile movements due to pile driving in successive zone. (4)

Bergdahl and Nilsson (1974) reported the movement of 4 test piles which were driven prior to the driving of large pile group. They measured the movement of previously driven test piles ranging from 0.3-1.1 ft. with an average from 0.4 ft. (11cm). (13)

Olko (1963) reported maximum pile heave of 11 in. (275mm) which was observed for steel H-piles driven into medium to stiff blue clay at 1m spacing.

Analysis and Modelling of induced pore pressures due to pile driving.

H.G Poulos (1994) plotted the movement of existing pile 1 as a function of r/d and L_1/L , where L_1/L represent different depth of penetration, for full penetration $L_1/L = 1$, d is the pile diameter of pile 2. For pile L_1/L greater than 0.5 of pile 2, pile 1 moved upward and the maximum is about 3% for $r/d = 3$ (Figure 2.11). r is the distance between piles.

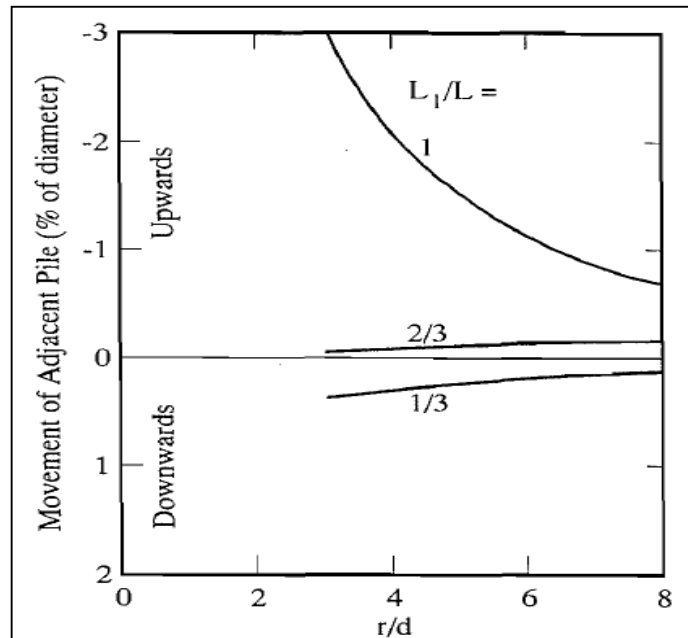


Figure 2. 11 Computed movements of adjacent pile due to installation of end-bearing pile. (23)

2.3 Influence of pile driving on soil properties

2.3.1 Water content

Water content changes in soil due to pile driving was studied by Cummings et al (1950) and Reese and Seed (1955). According to Cummings et al (1950) water content reduced after 1 month near the pile and additional reduction occurred after 11 months. Any change between the piles was not detected. (14)

Flate (1968) investigated piling effect at Nitsund Bridge project in Norway due to driving of 8 timber piles with 2 test piles I and II. The samples were taken from different depth. The figure 2.12 shows, the water content adjacent to the piles reduced

significantly, however slight increase between the piles compared to the normal range of water content.

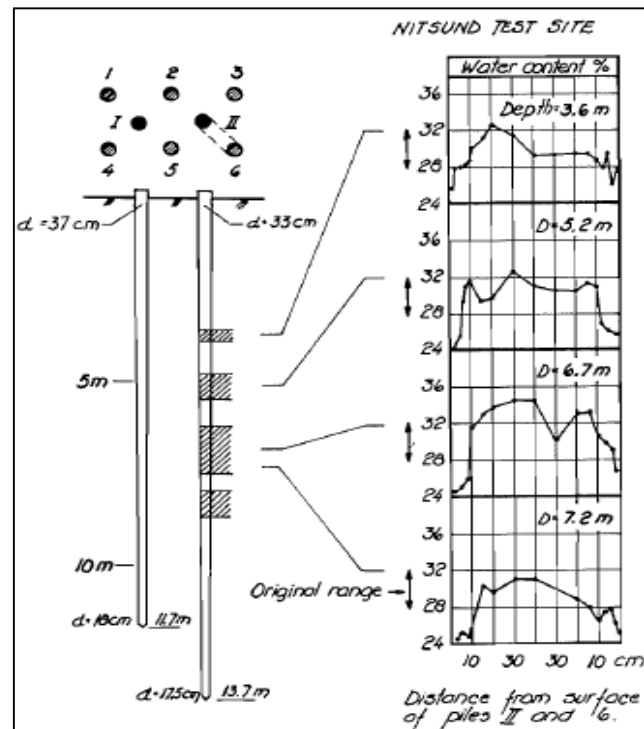


Figure 2. 12 Variation in water content (14)

2.3.2 Consistency limit

By M. Bozozuk, B. H. Fellenius and L. Samson (1978), geotechnical tests related to consistency limits have been conducted on soil samples just after pile driving and three months later in order to compare their values to the initial ones. Results showed that pile driving had no influence on water content, consistency limits and density of the soil. With the help of photographs of thin vertical section of the soils, they proved that the soil had not been subjected to physical distortion. According to them, all the soil layers were distinct and horizontal, as they were before any piles had been driven.

2.3.3 Shear strength

The shear strength of a soil is its maximum resistance to shear stresses just before the failure. Shear strength in soil depends primarily on interactions between particles. Shear failure occurs when the stresses between the particles are such that they slide or roll

past each other.

Soil derives its shear strength from two sources:

- Cohesion between particles which is a stress independent component. It means cementation when it is about sand grains and electrostatic attraction in case of clay particles.
- Frictional resistance between particles which is a stress dependent component. The internal friction angle, ϕ is the measure of the shear strength of soil due to friction.

Considering saturated soils, the relation of the initial shear strength based on effective stress,

$$\tau = c' + \sigma'_n \tan \phi' = c' + (\sigma_n - u) \tan \phi' \quad \dots \dots \dots (2.4)$$

Where,

τ is the shear strength

σ_n is the total normal stress

σ'_n is the effective normal stress

ϕ' is the effective friction angle

c' is the effective cohesion

u is the hydrostatic pore water

Pressure which is find with

$$u = z * \gamma_w$$

Where γ_w is the unit weight of water

z is the depth from the water table level to the point at which u is calculated.

This relation is valid for cohesive-frictional soils but it changes for other types of soils. Indeed, for cohesionless soils, for example sands and gravels, $c' = 0$. Therefore, $\tau = \sigma'_n * \tan \phi'$. For purely cohesive soils, for example saturated clays and silts under undrained conditions, equation 2.4 becomes $\phi' = 0$. Therefore, $\tau = S_u$.

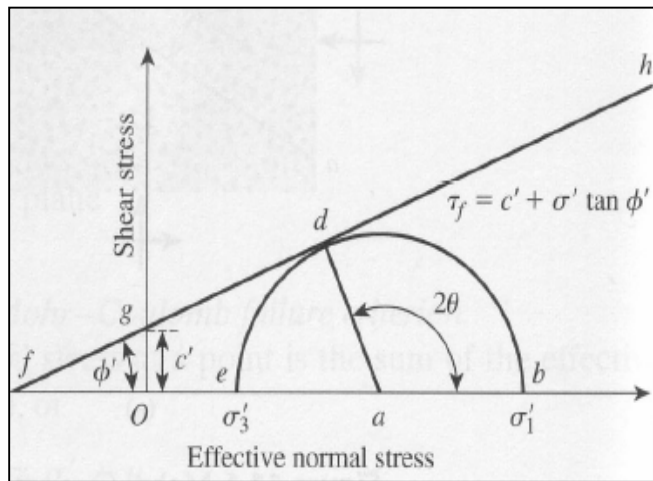


Figure 2. 13 Mohr circle and failure envelope. (36)

2.3.3.1 Investigation

The potential disturbance to the subsoil and possible danger to adjacent structure is much pronounced in sensitive marine clay. Because of these facts, concrete or other types of piles with high displacements have not been used extensively to support heavy loads. Fellenius and Samson (1976) reported that, concrete piles could be safely used (4). Their study in 1974 was limited on a group of thirteen 30 cm precast concrete piles. They extended their study together with M. Bozozuk in 1976 to two large groups of 116 piles with a pile length of 270 m (900 ft.) in a construction project in eastern Canada. Though the vertical and lateral soil movement, pore pressure changes due to driving of piles were monitored, however determination of influenced zone were the main objective of the study. It had also measured the change in shear strength to evaluate the disturbance of the sensitive marine clay. The shear strength change was measured using Swedish fall cone, in situ vane test and static cone penetrometer. The tests were performed prior to piling, immediately after and 3 month after the driving to compare the effects of driving.

Swedish fall cone shear strength:

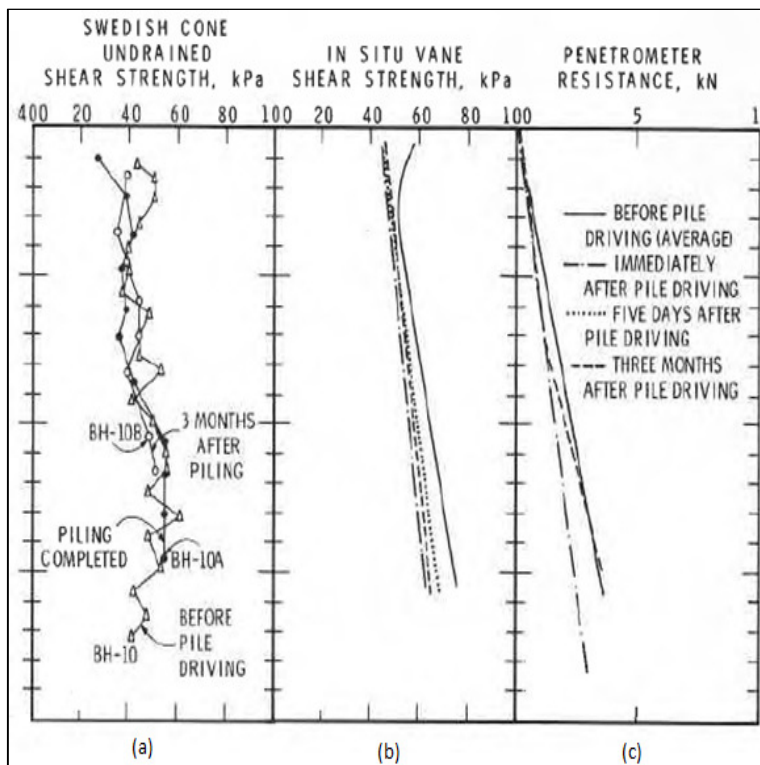


Figure 2. 14 Shear strength measured by Swedish cone, in-situ vane shear strength and cone penetrometer resistance. (4)

A small reduction of shear strength was observed in the test which was more pronounced within the upper depth up to 3m. At lower depth the reduction was not very significant. The shear strength before pile driving, immediately after driving and 3 months after driving for different borehole 2.14 (a).

In-Situ Vane Shear Strength:

Vane tests boring made immediately after pile driving highlight a diminution of in situ shear strength caused by pile driving of about 15%. (Figure 2.14 b) They noticed, with help of others tests done later, that this reduction was not recovered within the following three months.

Static Cone End Resistance:

From penetrometer soundings before piling, immediately after and three months after, they observed a decrease in cone resistance of about 30% due to pile driving. This loss was just partially regained three month after the end of pile driving. (Figure 2.14 c.)

Orrje and Broms (1967) studied the influence of pile driving on undrained shear strength. They reported shear strength reduction for closely spaced piles within a zone of 1.5 pile diameter. On the other hand, shear strength was unaffected for piles which were spaced 4 pile diameters. (13)

Shear atrength reduction in the clay by 20-30% had reported by Broms and Bennermark (1967) due to driving of timber piles in the upper part of the slope. (13)

According to Torstensson (1973) shear strength was reduced by 10% within a zone of 1.5 pile diameter during driving in a soft sensitive clay. Any regain of strength was not observed. Holtz and Lowitz (1965) reported no significant loss of shear strength for driving 21 m long displacement piles in low sensitive clay. (13)

Roy et al. (1980) studied pile driving effect for 6 instrumented test piles in soft sensitive soil in Saint-Alban test site. In figure 2.15 normalized shear strength at different depth and location were plotted. It can be observed that, the value of undrained shear strength after pile driving is 60-75% of the initial shear strength close to the pile wall and the effect is not significant beyond 4 pile diameter.

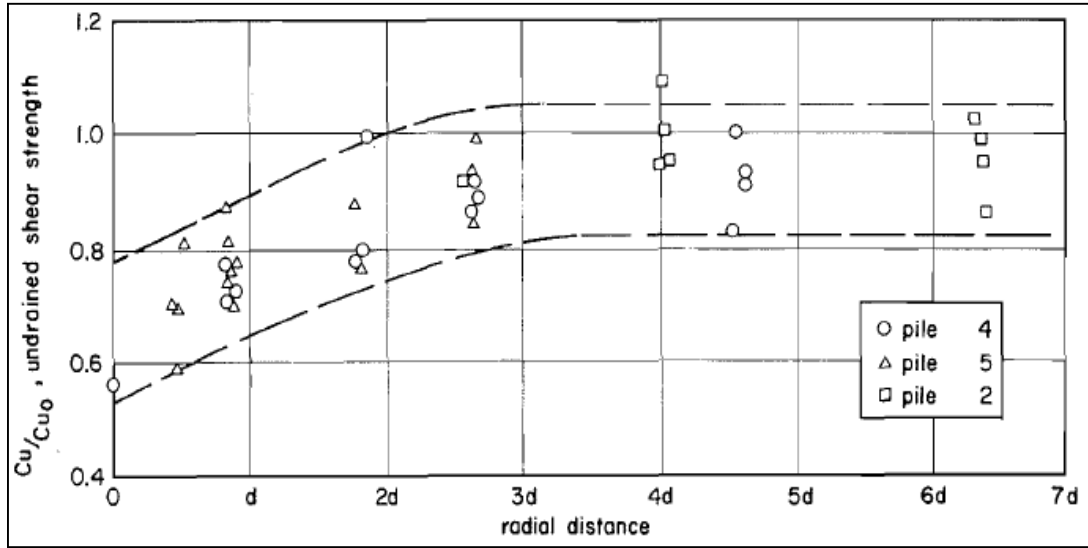


Figure 2.15 Variation of the normalized in-situ vane strength with the radial distance immediately after driving. (26)

2.3.3.2 The mechanism of shear strength reduction

Driving piles strongly squeezes adjacent soils, and causes buildup of excess pore water pressure, Δu . This provisional buildup of excess pore water pressure combined with the sensitivity of the clay leads the soil to lose a big part of its shear strength in the short term. The relation (2.4) expressing the shear strength after the increase of pore water pressure becomes:

$$\tau = c' + (\sigma_n - (u + \Delta u)) * \tan \varphi' \quad \dots \dots \dots (2.5)$$

After rearranging,

$$\tau = c' + (\sigma_n - u) - \Delta u * \tan \varphi'$$

And finally,

$$\tau = c' + (\sigma'_n - \Delta u) * \tan \varphi' \quad \dots \dots \dots (2.6)$$

Thus, the shear strength is reduced compared to the initial one. Mohr's circle will move on the left along the x axis.

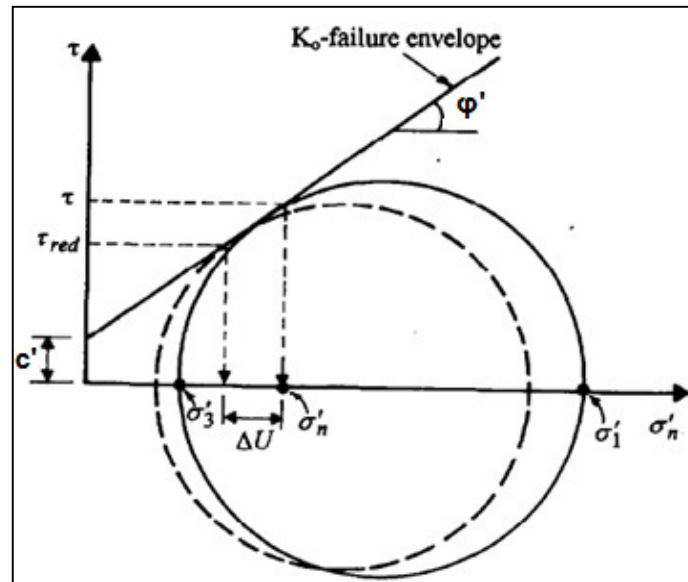


Figure 2.16 Mohr circle during pile driving (2)

If the variation of the pore water pressure is too high, the circle can reach the failure line. With regards to loose cohesionless soils, pile's adjoining soils are sheared and so tend to densify. As a result, it can be quite simple to drive pile in such soils. In this case, lateral effective stresses are smaller. In saturated cohesionless soils, the excess pore water pressure dissipates very quickly. Therefore, the soil recuperates its strength very rapidly. In a case of a dry cohesionless soil, there will be no pore pressure effects when the piles are driven. Thus, no temporary decrease of soil strength will occur.

Chapter III

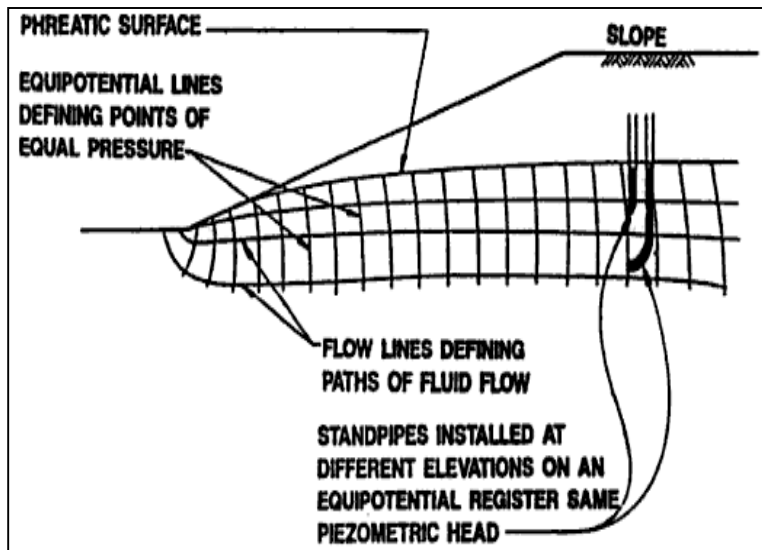
Excess pore pressure generation due to pile driving

Water has a significant role in slope stability analysis and design. Therefore, understanding of ground water condition is very important in Geotechnical Engineering. Water is filled in pores between the soil particles and the hydrostatic stress in the voids from the water is termed as pore water pressure, u_w . Total stress is the combination of effective stress and pore water pressure. The behavior of soil especially strength is controlled mostly by effective stress rather than total or pore pressure. The effective stress is then expressed as,

$$\sigma' = \sigma - u_w \quad \dots \dots \dots (3.1)$$

Where σ = Total stress acting on the plane.

Pore pressure may be divided into positive and negative pore pressures depending on the ground water table. At the phreatic level pore pressure is atmospheric, zero pressure datum. In the saturated zone pore pressure is above the atmospheric pressure and termed as positive. On the other hand in the unsaturated zone pore pressure is below the atmospheric pressure and hence negative. Figure 3.1 shows flow lines and equipotential lines which is known as flow nets. Equipotential lines are the points of



equal pressure where piezometer head is same at different level. Pore pressure is hydrostatic if there is no flow and piezometer head will coincide with water table. But the pore pressure is other than hydrostatic, if flow occurs.

Figure 3. 1 Pore pressures in an equipotential line (1)

3.1 Pile driving induced pore pressure

Excess pore pressure developed in a soil due to pile driving is a major concern in Geotechnical Engineering. This induced pore pressure at the pile face may become equal to or even greater than the effective overburden pressure (Lambe and Horn 1965, Orrje and Broms 1967, Poulos and Davis 1979, D'Appolonia and Lambe 1971). (24)

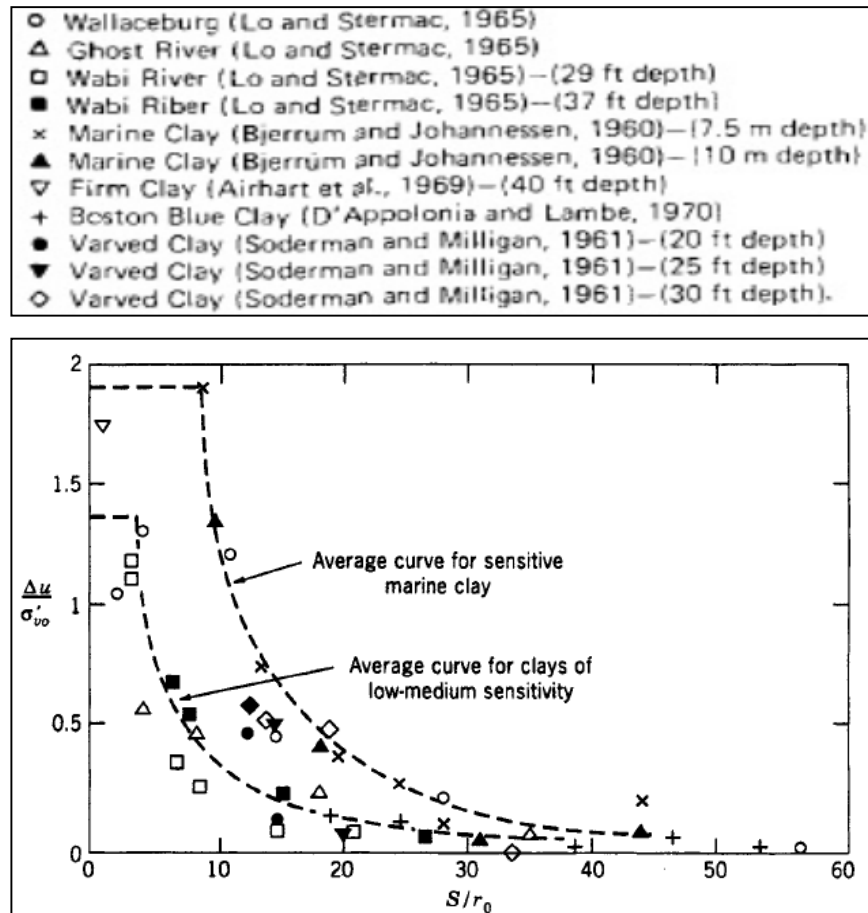


Figure 3.2 Summary of measured pore pressures (after Poulos and Davis 1979) (24)

Very high excess pore pressures are developed around the driven piles. In some cases, induced pore pressures exceed the in-situ vertical effective stress by 1.5 to 2.0 times and even amounting 3 to 4 times the in-situ vertical effective stress near the pile tip. However, the induced excess pore pressures decrease rapidly with distance from the pile. In Figure 3.2, the excess pore pressure Δu is expressed as $\Delta u/\sigma'_{vo}$, where σ'_{vo} is the vertical effective stress prior to driving a single pile and the radial distance s from the pile is expressed as s/r_0 , where r_0 is the pile radius. Due to soil type and sensitivity, the

resulting points are scattered. Figure 3.2 includes several tests with different soil type and depth. Beyond s/r_o distance of about 4 for normal clays and about 8 for sensitive clays, a rapid decrease in pore pressure occurs with distance and the excess pore pressures are virtually negligible beyond a distance of $s/r_o = 30$.

3.1.1 Lo and Stermac (1965) approach

Prediction of excess pore pressure generation due to pile driving in clay is very important for slope stability. Bjerrum et al. (1958) were the first to introduce driving pore pressures in clay around a group of precast pile. Bjerrum and johannessen (1960) and soderman and milligan (1961) reported similar observations around clay. (26)

Lo and Stermac (1965) were the first to introduce a method of prediction of this maximum driving pore pressure around the pile for normally consolidated clay. Pore pressure increase caused by either an increase of mean total stress or shearing of the soil to large strain around the pile. Based on this assumption, it is suggested that maximum excess pore pressure,

$$\Delta u_m = \Delta u_a + \Delta u_s \quad \dots \dots \dots (3.2)$$

Δu_a = From the change in total ambient pressure= $(1 - k_0)\sigma'_{vo}$

Δu_s =Caused by shearing = $(\frac{\Delta u}{p'})_m * \sigma'_{vo}$

Where, k_0 = Coefficient of earth pressure at rest= $1 - \sin\phi$

$(\frac{\Delta u}{p'})_m$ =Pore pressure ratio measured from consolidated undrained triaxial test.

p' =Initial consolidation stress.

σ'_{vo} = Effective overburden pressure.

Therefore, maximum pore pressure Δu_m for normally consolidated clays can be obtained from,

$$\Delta u_m = [(1 - k_0) + (\frac{\Delta u}{p'})_m * \sigma'_{vo} \quad \dots \dots \dots (3.3)$$

Analysis and Modelling of induced pore pressures due to pile driving.

With the common values of k_0 and $\left(\frac{\Delta u}{p'}\right)_m$ in equation (3.3), Δu_m becomes 1.0-1.3 times the effective overburden pressure. (26)

Orrje and Broms (1967), Koizumi and Ito (1967), Clark and Meyerhof (1972) reported, observed values equal to or more than the total overburden pressure for overconsolidated soil. This is one of the limitations of equation (3.3). Another drawback is that the equation is valid only for the immediate vicinity of the pile wall. The magnitude of the driving pore pressure reduces with the distance from pile wall. According to Bjerrum and Johannessen or Lo and Stermac (1965) reported, the driving pore pressures become negligible at a distance in the order of 10-20 pile diameter. (26)

3.1.1.1 Modification of the approach by Lo and Stermac Approach

Lo and Stermac proposed the equation for the pore pressure generated along the shaft close to a pile in normally consolidated soil. Roy et al. (1980) carried out investigation with six instrumented pile on saint-Alban test site, 80 km west of Quebec City. They carried out CIU test under various consolidation stresses, p' on samles from 6.5 to 7.5 m depth. The observed valued are plotted in figure 3.3.

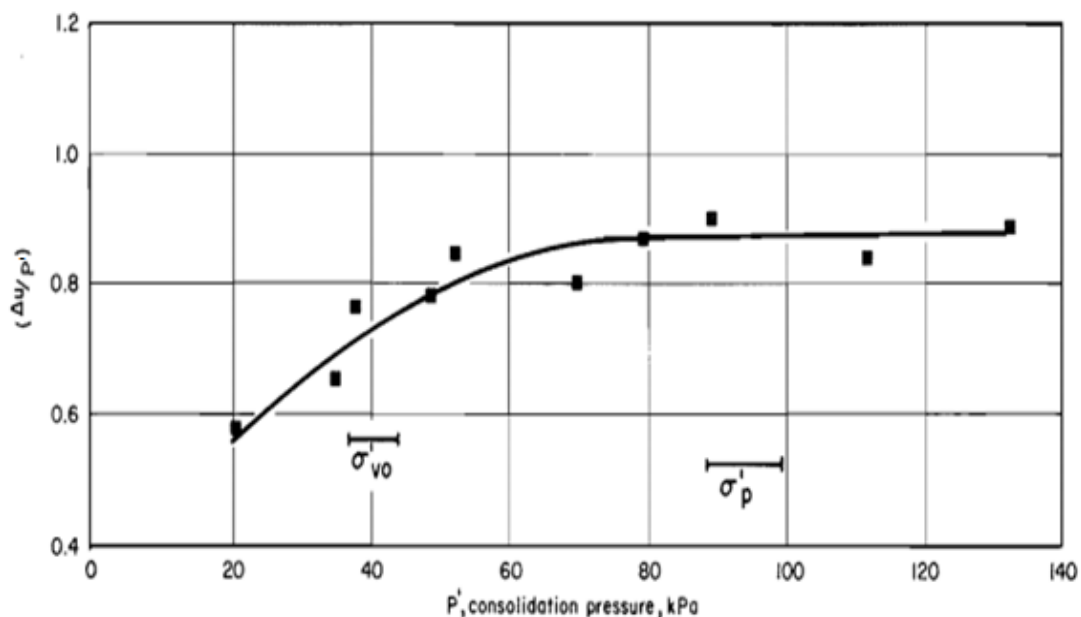


Figure 3.3 Variation of $\Delta u/p'$ in function of the consolidation pressure in CIU tests on Saint-Alban clay. (26)

Analysis and Modelling of induced pore pressures due to pile driving.

Maximum constant value of 0.87 was not achieved for p' equal to σ'_{vo} when the value reached maximum for larger consolidation stress but less than the preconsolidation pressure σ'_p . According to Tavenas et al. (1975), the coefficient of earth pressure at rest k_0 decreasing with depth from about 0.9 at 2m to 0.7 at 8m (26). With these values, Roy et al. (1980) measured the maximum driving pore pressure in saint-Alban site with equation (3.3) which is much lower than the observed value. This is because may be the saint-Alban clay is in the overconsolidated state. Applying the limit state concept by Tavenas and Lroueil (1977), the pore pressure induced by shear must be directly related to the preconsolidation pressure σ'_p of the clay. So, the equation (3.3) may be rewritten for overconsolidated clays as:

$$\Delta u_m = (1 - k_0)\sigma'_{vo} + \left(\frac{\Delta u}{p'}\right)_m \sigma'_p \quad \dots \dots \dots (3.4)$$

Where, σ'_p = Preconsolidated pressure.

The pore pressure computed from (3.4) agrees remarkably well with the observed values in the saint -Alban test site plotted in figure 3.4

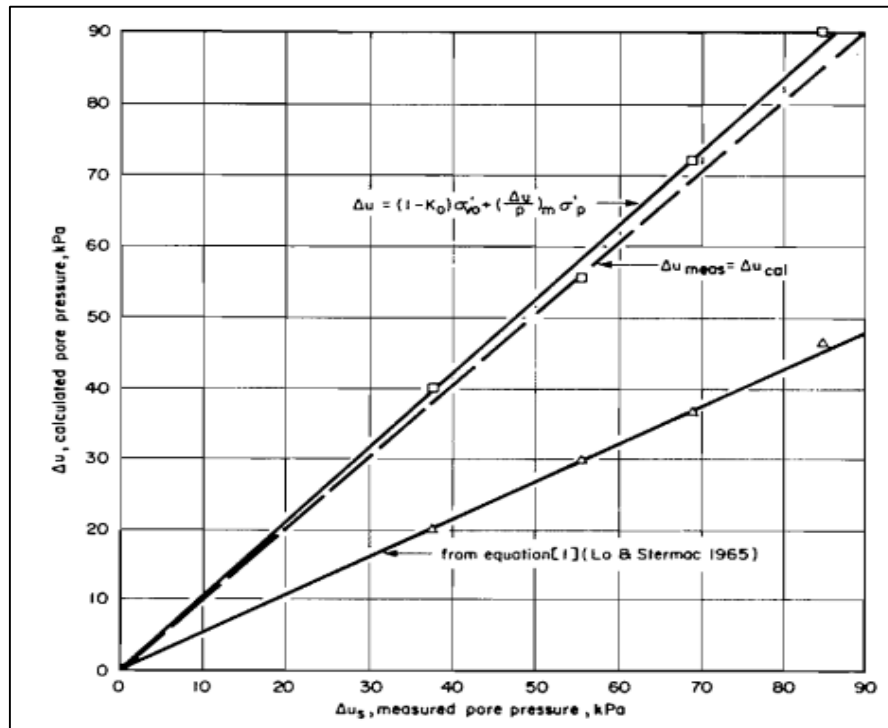
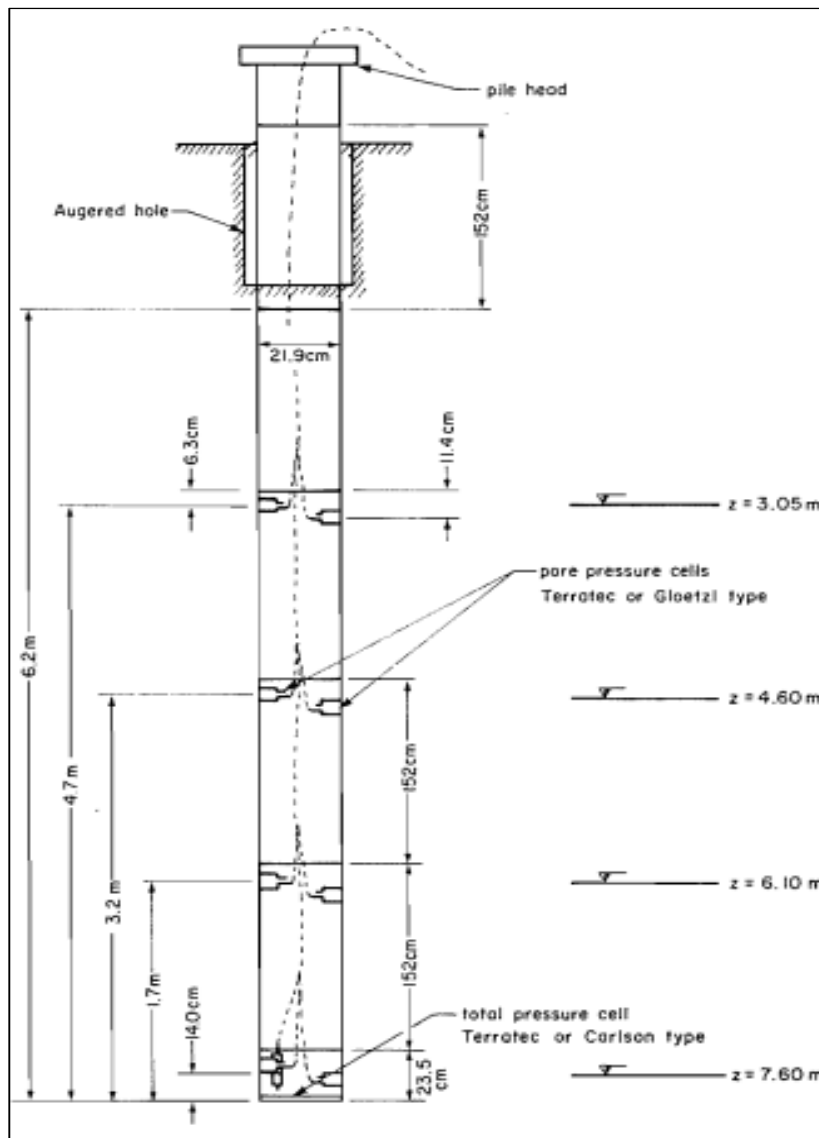


Figure 3. 4 Comparison of the pore pressure measured on the pile shaft and calculated from the original and modified Lo and Stermac (1965) solution. (26)

3.2 Variation of pore pressure generation at pile tip and pile shaft

The difference in pore pressure behavior near the pile tip and along the pile shaft was found by the Field observation Roy et al. (1980). Six instrumented test piles were driven into soft sensitive clay. To measure the pore pressure along the shaft, two types of pore pressure cells-Terratec cells and Gloetzel cells of pneumatic type were installed. Test



pile 1, 3 and 6 were instrumented at four different levels while for pile 2 and 5, only lower two levels were instrumented. In addition for pile 3 and 4, a Geonor electric piezometer type M.600 was attached on the outside of the pile wall at tip level to measure the pore pressure at pile tip. Figure 3.5 shows details of typical instrumented pile. Pore pressure cells were also installed in the soil near the pile.

Figure 3. 5 Details of typical instrumented pile in Saint-Alban test site. (26)

During driving of test pile 6, the generations of pore pressure at pile tip level and on the shaft were plotted in figure. 3.6. The pore pressure generated at the cells which are closed to pile tip is much higher than that of the pile shaft.

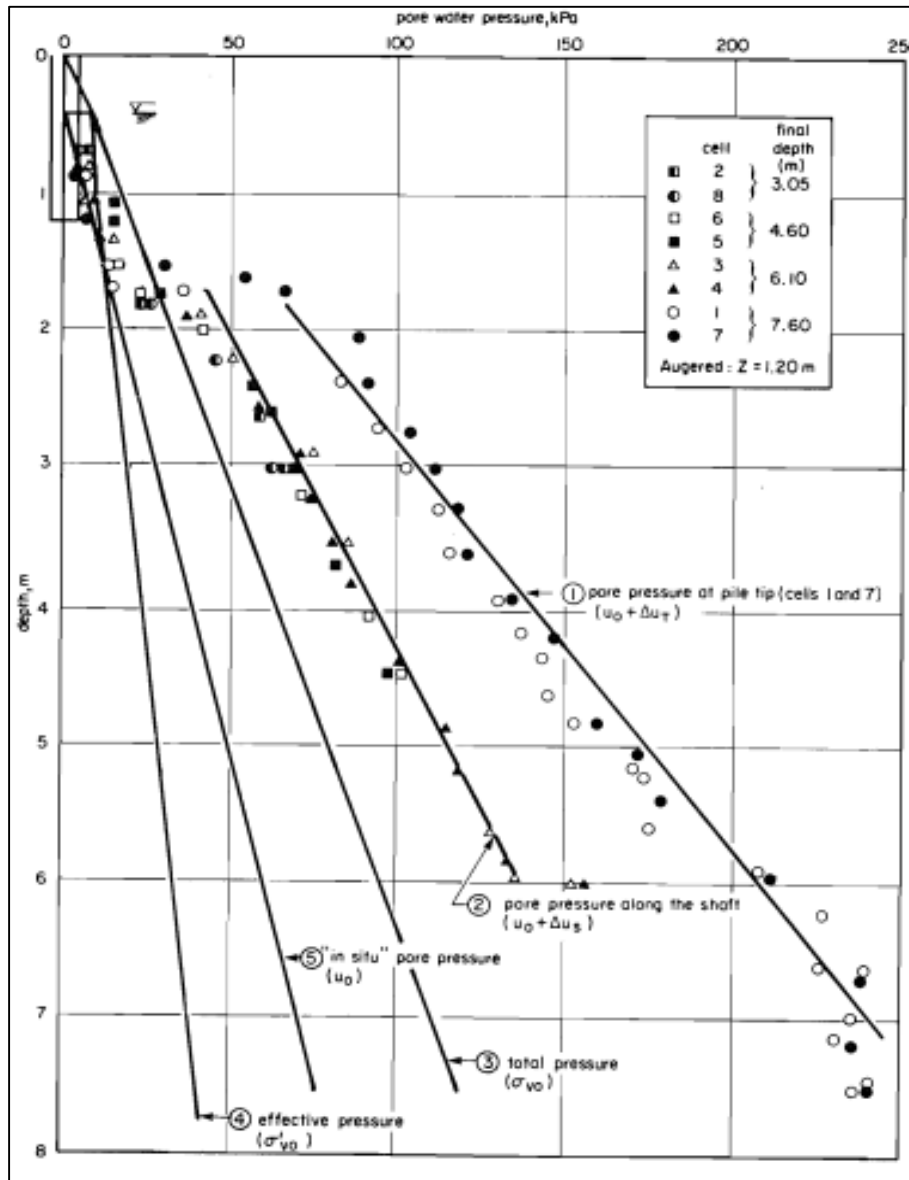


Figure 3. 6 Pore pressures measured on the pile shaft during the driving of test pile 6 in Saint-Alban test site. (26)

When the soil is displaced by pile, the changes in behavior of clay may result high pore pressure at tip level. It is hypothesized that high pore pressure at tip level is due to strong deformation in the cavity expansion required to let the pile penetrate the intact clay. Roy et al. (1980) compared the measured pore pressure at tip level and along shaft with σ'_{v0} , σ_{v0} and σ'_p which is plotted in table 3.1.

Analysis and Modelling of induced pore pressures due to pile driving.

Table 3.1 Induced pore pressure expressed in function of σ'_{vo} , σ_{vo} , σ'_p . (26)

| Depth (m) | σ'_{vo} | σ_{vo} | σ'_p | Tip pore pressure | | | Shaft pore pressure | | | | |
|-----------|----------------|---------------|-------------|-------------------|-----------------------------------|----------------------------------|--------------------------------|--------------|-----------------------------------|----------------------------------|--------------------------------|
| | | | | Δu_T | $\frac{\Delta u_T}{\sigma'_{vo}}$ | $\frac{\Delta u_T}{\sigma_{vo}}$ | $\frac{\Delta u_T}{\sigma'_p}$ | Δu_s | $\frac{\Delta u_s}{\sigma'_{vo}}$ | $\frac{\Delta u_s}{\sigma_{vo}}$ | $\frac{\Delta u_s}{\sigma'_p}$ |
| 2 | 15 | 32 | 34 | 56 | 3.73 | 1.75 | 1.65 | 31 | 2.07 | 0.97 | 0.91 |
| 3 | 20 | 47 | 47 | 79 | 3.95 | 1.68 | 1.68 | 43 | 2.15 | 0.91 | 0.91 |
| 4 | 27 | 59 | 102 | 102 | 3.78 | 1.57 | 1.73 | 56 | 2.07 | 0.68 | 0.95 |
| 5 | 32 | 70 | 125 | 125 | 3.91 | 1.54 | 1.79 | 67 | 2.09 | 0.83 | 0.96 |
| 6 | 36 | 84 | 147 | 147 | 4.08 | 1.53 | 1.75 | 77 | 2.14 | 0.80 | 0.92 |
| Average | | | | | 3.89 | 1.61 | 1.72 | | 2.10 | 0.87 | 0.93 |

It can be seen that the tip pore pressure is 190% of the pore pressure along the shaft. The average value of Δu_T can be expressed as,

$$\Delta u_T = 3.89 * \sigma'_{vo} = 1.61 * \sigma_{vo} = 1.72 * \sigma'_p$$

But the ratio $\frac{\Delta u_s}{\sigma'_{vo}}$ is about 2.1 which was much higher than the value calculated by Lo and Stermac (1965) equation 3.3 for the test site. The pore pressure development was obviously affected by the distance from the pile wall. For Saint-Alban site it is plotted in the figure 3.7, normalized by σ'_p against the radial distance.

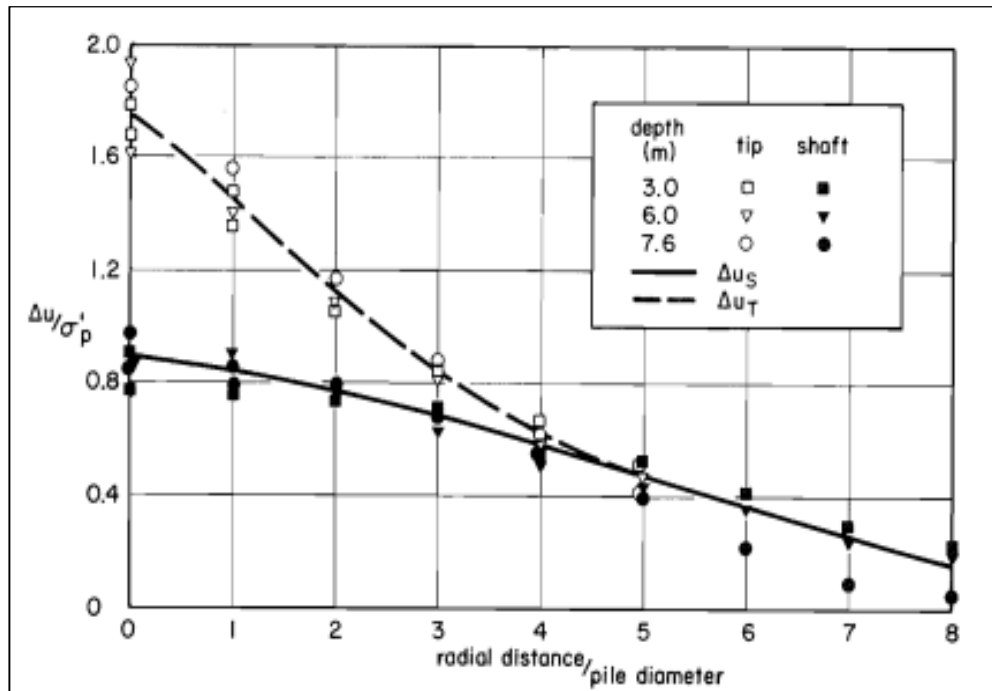


Figure 3.7 Variation of the normalized Pore pressures with the radial distance from the pile surface at Saint-Alban test site. (26)

3.3 Pore pressure variation during driving through different soil layers

During driving of piles in soft soils with low permeability, excess pore pressure generation may affect the stability of adjacent structure and slopes. The magnitude of the pore pressure prediction is difficult as they depend on a number of factors such as pile driving energy transferred into the soil, type of pile, local drainage conditions, soil density, stress history and soil type (11). Therefore, the follow up of excess pore pressure during driving is very important to maintain the safety margin especially for soft clays with high sensitivity.

K. D. Eigenbrod et al. (1996) observed high pore pressure increase in the clay when the piles were penetrated into the underlying very dense sand and gravel. The response while driving through the clay layer was very small. They reported that the clay was loaded from below, as the piles were driving into the very dense sand.

A series of steel pipe piles were driven through sensitive clay into the underlying dense sand and gravel for the construction of a school in the Fraser river lowlands in Canada. High plastic clay of 16-26 m thick, overlying very dense sand and gravel. The sensitivity of clay layer was found 3-5. The clay layer was slightly overconsolidated with $OCR=2$. The water content ranging from 40-50%. From the piezocone measurements it was reported that, the clay was highly contractive where as the sand layer reflects dilative behavior with low and negative pore pressure readings.

Two piezometer stations (Pneumatic type) P1 and P3 were installed at 9m and 18m each, for the pore pressure response due to driving. The piles were driven with two sections, first section was driven until 14m, after that the second section was welded onto the previous section and driven approximately at a depth of 22m. Figure 3.8 to 3.11 shows pore pressure response at P1 and P3 stations during piling of different section.

When the piles were penetrated into the dense layer, the clay layer was loaded from below due to heave caused by the displacement of soil. This was the possible reason for the high excess pore pressure during driving second stage. Another reason was considered as the dilation of the soil during shearing.

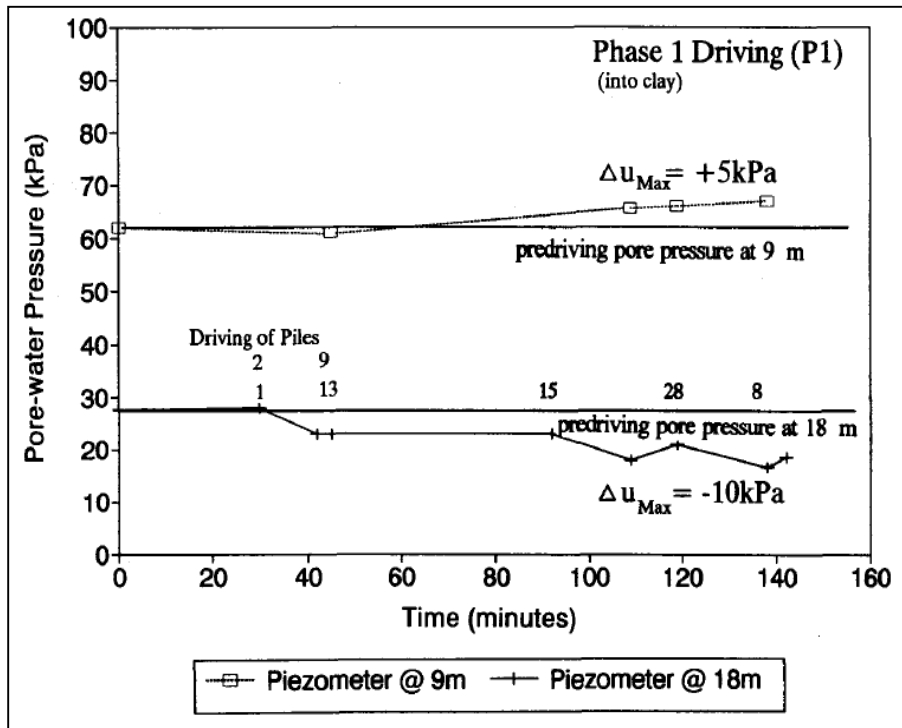


Figure 3. 8 Pore water pressures during driving in soft clay (first driving phase) near piezometer P1 (11).

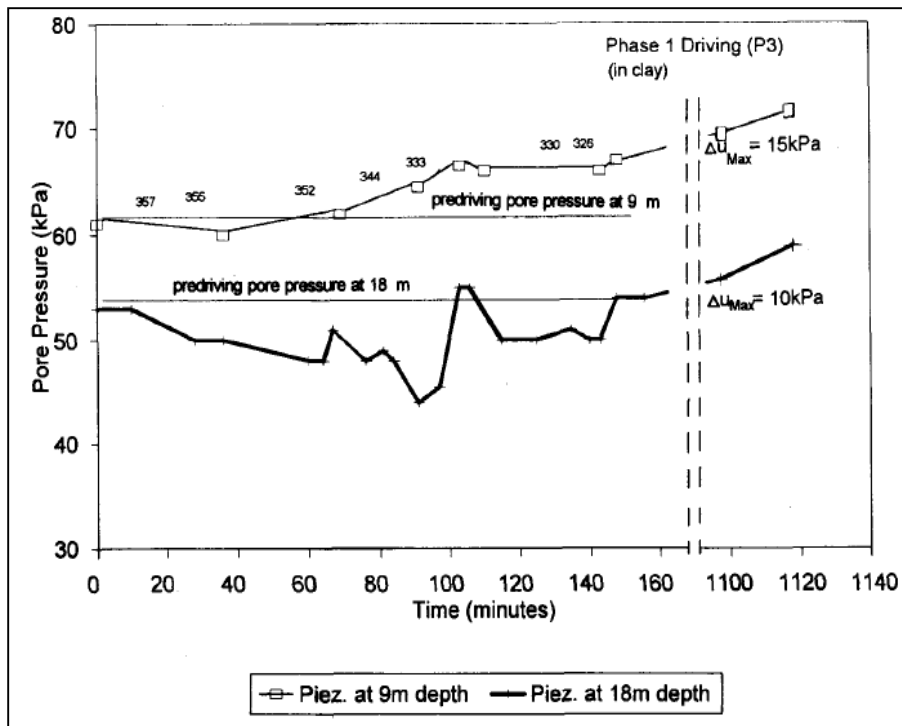


Figure 3. 9 Pore water pressures during driving in soft clay (first driving phase) near piezometer P3. (11)

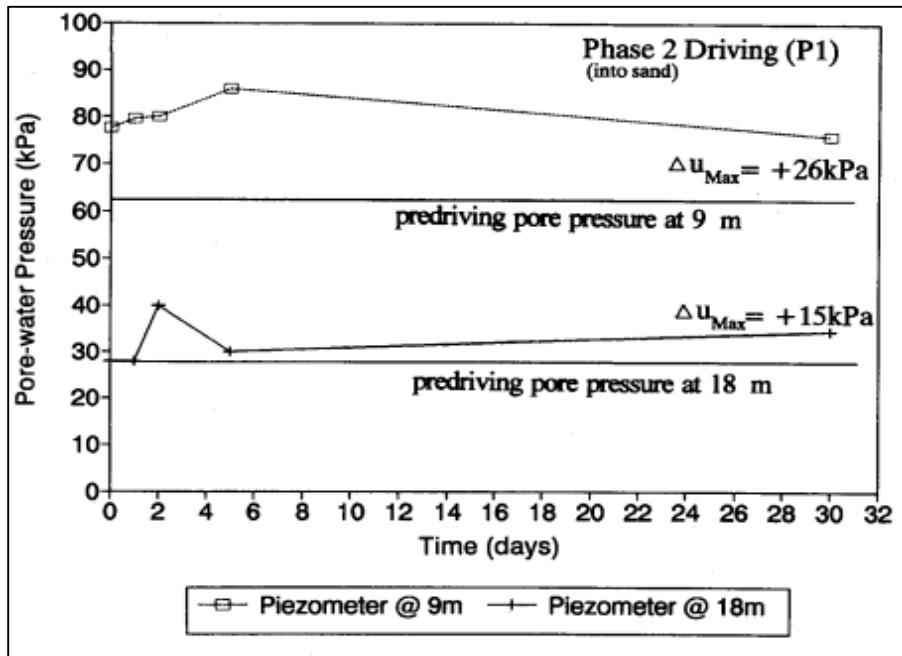


Figure 3. 10 Pore water pressures during driving in soft clay (second driving phase) near piezometer P1. (11)

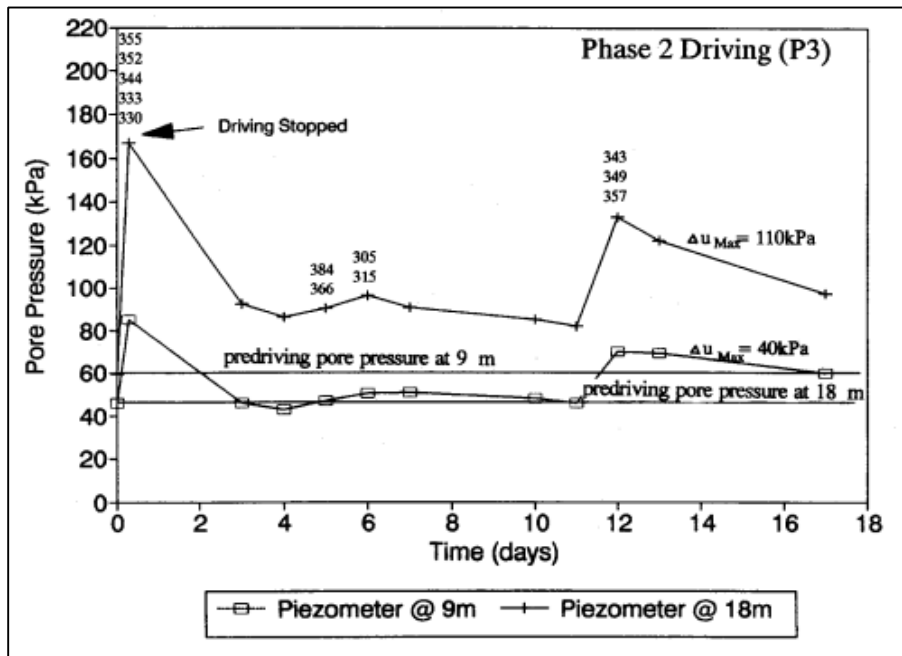


Figure 3. 11 Pore water pressures during driving in soft clay (second driving phase) near piezometer P3. (11)

During driving in clay layer for first driving phase (Fig. 3.8 & 3.9), the excess pore pressure was very little or even negative for both P1 and P3. While for driving second

phase, the response was as high as 110kPa at the station P3 (9m) and 40kPa at lower piezometer P3 (18m). Station P1 also showed higher response at second stage than driving during first stage.

3.4 Excess pore pressure dissipation

During pile installation excess pore pressure developed in clay. This may reduce shear strength of clay immediate after pile driving. After the pile driving process is stopped, the excess pore pressure will dissipate over time and equalize to the static condition which may increase effective strength and therefore shear strength. The dissipation of excess pore pressure is dependent on permeability of the soil. Clay has very low permeability, therefore it takes long time than sand to regain the strength by dissipation.

3.5 Techniques to reduce pore pressure during pile driving

A technique to decrease excess pore pressure during pile driving is described hereby used in a soil composed of soft varved silts and clay overlying fine sand with clay and silt for a bridge construction in the south of Stockholm where a small slide took place during pile driving (18). The team tried several solutions. First of all, removed clay before driving the piles but it was unsuccessful because the clay was too much soft and sensitive. Another solution was to wait for excess pore pressure to dissipate but it takes a lot of time and hence expensive. As these were not the best solution, Geotechnicians implemented the new “paper-plastic drain” to accelerate dissipation of excess pore water pressure. They used this method only on the east side. As the piles were driven into the ground, the drain was nailed down to the pile. The results showed that the maximum pore water pressure measured with a piezometer on the east side (even very close to driven pile) was half of the maximum given by a piezometer on the west side. So this technique allows excess pore pressure provoked by the piling to reduce to 50%. Moreover, this alternative is really less expensive than those proposed to the contractor at that time. Indeed, the extra cost was about 20% of the cost of the piles for the drain technique whereas removal of cores of clay might increase the piling costs about 50% excluding the cost of the delays. Another method which is cheaper and quicker is to install drains before beginning piling starts. It improves the dissipation of excess pore pressure.

Chapter IV

Theory of Cavity Expansion

Cavity expansion has a tremendous role in Geotechnical field because it provides useful and simple tool for modelling many complex Geotechnical problems. It deals with the theoretical study of changes in stresses, pore water pressure and displacements caused by the expansion and contraction of cylindrical or spherical cavities. In our present study, we will only focus on the expansion of cylindrical cavity.

Although steady progress has been made since the 1950's, the subject received significant amount of attention in the last 20 years. Various analytical solutions have been developed based on different constitutive models for cavity expansion at that certain period. Furthermore, these solutions have been used to solve different practical problems in Geotechnical Engineering such as the investigation of the capacity of pile foundations and earth anchors, the interpretation of in situ soil testing, analysis of the behavior of tunnels and underground excavations.

Pressuremeter and cone penetrometer are mostly used to measure in-situ soil properties. Menard (1957) and Gibson and Anderson (1961) had a great contribution to adopt the theory of cylindrical cavity expansion as the most important interpretation method for self-boring pressuremeter tests in soil and rock . Spherical cavity expansion is also widely used as a simple method for predicting the cone tip resistance in the cone penetration test (Yu and Mitchel, 1998). (35)

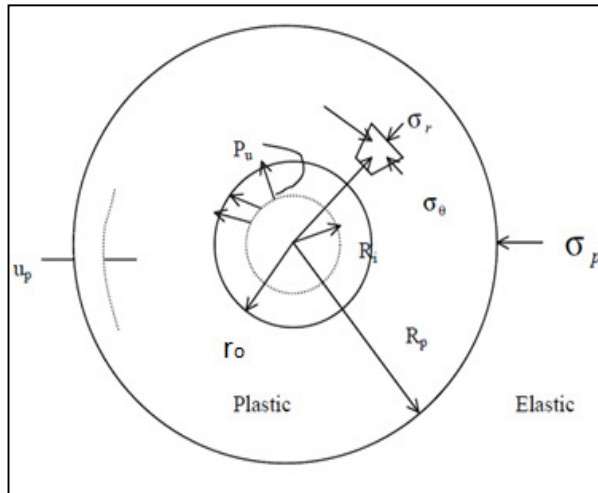
The prediction of end bearing and shaft capacities of a driven pile in soil remain a difficult problem in Geotechnical Engineering. In particular, following the early suggestion of Bishop et al. (1945), Hill (1950) and Gibson (1950), solutions of the limit pressures of cylindrical and spherical cavities are used to predict the end bearing and shaft capacities of piles in soil and rock.

Rowe (1986), Mair and Taylor (1993), Verruijt and Booker (1996), Sagaseta (1998), Logathan and Paulos (1998), Yu and Rowe (1999) used cavity expansion solutions to predict tunneling induced ground movement. Therefore, Cavity expansion has also been

applied to underground excavation and tunneling. To predict the borehole instability, cavity expansion has its applicability.

4.1 Expansion of cavity with perfectly plastic soil model

Cavity expansion theory was originally developed for application to the expansion of either cylindrical or spherical cavity indentation in metal. Vesic developed solutions to the expansion of cylindrical and spherical cavity in a soil with Mohr-Coulomb frictional parameters. To describe the solution of an expanding cavity, it is assumed that the cavity with an initial radius R_i expanded with the initial internal pressure p . As the cavity expands, the radial stresses acting along the walls will be increased and around the cavity a plastic zone will be introduced. This plastic zone will expand until the pressure reaches an ultimate value of p_u . At this moment, the cavity has a radius r_o . The radius of the plastic zone will be R_p . Beyond this radius, the rest of the soil mass remains in a state of elastic equilibrium.



Stress equilibrium,

$$\frac{\partial \sigma_r}{\partial r} + \frac{\sigma_r - \sigma_\theta}{r} = 0 \quad \dots \dots \dots (4.1)$$

σ_r = radial normal stress

σ_θ = circumferential normal stress.

r = distance to the center of cavity.

Figure 4. 1 Expansion of a cylindrical cavity. (38)

Mohr gives the failure conditions for soil in undrained shear, as induced during pile driving:

$$\sigma_r - \sigma_\theta = 2s_u \quad \dots \dots \dots (4.2)$$

Where, s_u is the undrained shear strength.

Analysis and Modelling of induced pore pressures due to pile driving.

Assuming soil as an ideal elastic-plastic material and that no volume changes occurred within the plastic zone, the width of the induced plastic zone can be determined:

$$\frac{R_p}{r_0} = \sqrt{I_r} \quad \dots \dots \dots (4.3)$$

R_p = Radius of plastic zone

r_0 = Radius of the cavity.

I_r = Rigidity index = $\frac{G}{s_u}$

G = Shear modulus = $\frac{E}{2(1+\nu)}$

E = Young's modulus.

ν = Poisson's ratio.

Therefore, the equation 4.3 becomes,

$$\frac{R_p}{r_0} = \sqrt{\frac{E}{2(1+\nu)s_u}} \quad \dots \dots \dots (4.4)$$

In order to determine total lateral stress due to expansion of cylindrical cavity (axially symmetrical), from the equations of equilibrium, condition of rupture (limiting equilibrium) and boundary conditions, the following equation is obtained for the plastic zone,

$$\sigma_r = p_u - 2s_u \ln \frac{r}{r_0} \quad \dots \dots \dots (4.5)$$

p_u = Ultimate pressure for the expansion of cylindrical cavity.

4.1.1 Ultimate pressure, p_u

$$p_u = s_u F_c + q F_q \quad \dots \dots \dots (4.6)$$

F_c and F_q are the dimensionless cylindrical cavity expansion factors are given for the cohesionless soil in undrained condition.

$$F_q = 1$$

$$F_c = \ln I_r + 1$$

q = Isotropic effective stress.

$$\sigma_r = p_u - 2s_u \ln \frac{R_p}{r_0} \text{ at } r = R_p \dots \dots \dots (4.7)$$

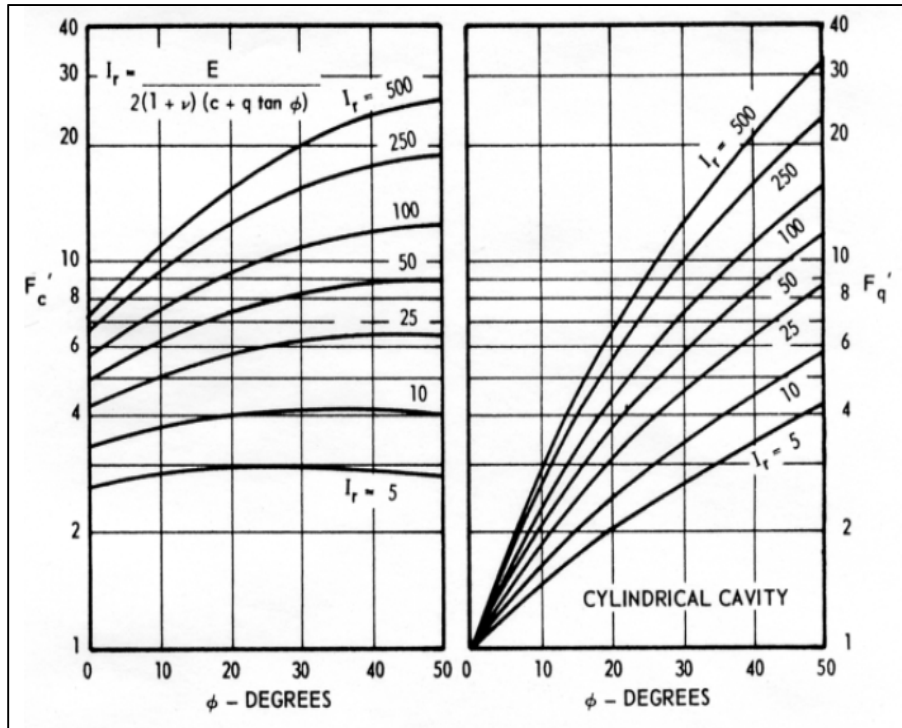


Figure 4.2 Cylindrical cavity expansion factor

4.1.2 Excess pore pressure

During penetration of a probe into a soil deposit, the excess pore pressure develops as a result of changes in the normal and shear stresses. The changes in normal stress results from displacement of soil grains and pore fluid caused by driving of the probe. However, changes in the shear stress at the interface between the pile surface and the soil deposit can be positive, exhibiting contracting behavior or negative, exhibiting dilating behavior. Therefore, the pore pressure measured at any given time is a combination of the normal and shear induced components, together with the hydrostatic pore pressure. (5)

Analysis and Modelling of induced pore pressures due to pile driving.

$$u_m = \Delta u_{oct} + \Delta u_{shear} + u_0 \quad \dots \dots \dots (4.8)$$

Where,

u_m = Measured pore pressure

Δu_{oct} = Excess pore pressure resulting from changes in octahedral normal stress.

Δu_{shear} = Excess pore pressure resulting from changes in octahedral shear stress.

u_0 = Hydrostatic pore pressure.

In order to determine the excess pore pressure during the expansion of cavity, Vesic proposed the following equation: (38)

$$\Delta u = \beta \Delta \sigma_0 + \alpha \Delta \tau_0 \quad \dots \dots \dots (4.9)$$

$\Delta \sigma_0$ = Mean normal stress change.

$\Delta \tau_0$ = Octahedral stress change.

α and β are henkel's pore pressure parameter.

$\beta = 1$ for saturated soil.

From the assumptions that the initial stress condition is an isotropic compressive stress, q and that the soil is saturated, the pore pressure for any point in the plastic zone of an expanded cylindrical cavity is equal to,

$$\Delta u = \Delta \sigma_0 + 0.817 \alpha_f s_u \quad \dots \dots \dots (4.10)$$

Where $\alpha_f = \alpha$ - parameter at failure.

For cylindrical expansion:

$$\Delta \sigma_0 = 2s_u \ln \left(\frac{R_p}{r} \right) \quad \dots \dots \dots (4.11)$$

From equations 4.10 and 4.11,

$$\Delta u = 0.817 \alpha_f s_u + 2s_u \ln \left(\frac{R_p}{r} \right) \quad \dots \dots \dots (4.12)$$

$$\alpha_f = \frac{1}{\sqrt{2}} [3A_f - 1] \quad \dots \dots \dots (4.13)$$

$A_f = 0.7$ For NC clay (Das, B.M. 1983) (38)

In the case of determining excess pore pressure in the elastic zone, the following equation is used,

$$\Delta u = 0.817\alpha_f s_u \left(\frac{R_p}{r}\right)^2 \quad \dots \dots \dots (4.14)$$

For spherical expansion:

$$\Delta u = \Delta\sigma_0 + 0.943\alpha_f s_u \quad \dots \dots \dots (4.15)$$

$$\Delta\sigma_0 = 4s_u \ln\left(\frac{R_p}{r}\right) \quad \dots \dots \dots (4.16)$$

Combining equations 4.15 and 4.16,

$$\Delta u = 0.943\alpha_f s_u + 4s_u \ln\left(\frac{R_p}{r}\right) \quad \dots \dots \dots (4.17)$$

Excess pore pressure on the surface of the pile:

$$\frac{\Delta u_{max}}{s_u} = \ln\left[\frac{E}{2(1+\nu)s_u}\right] + 1.73A_f - 0.58 \quad \dots \dots \dots (4.18)$$

4.2 Expansion of cavity by Modified cam clay model

Various constitutive models are used to describe the stress-strain behavior of an expanding body. Among them elastic perfectly plastic soil model (Hill, 1950; Chadwick, 1959; Gibson and Anderson, 1961; Vesic, 1972; Yu, 1990) are mostly used. Palmer (1972) presented an undrained solution without making any assumptions of the plain strain behavior for cylindrical cavity. A rigid/plastic idealization of the cam clay constitutive equation was applied by Palmer and Mitchel (1972) for normally consolidated clay. Collins and stimpson (1994) presented similarity solution for drained and undrained cavity expansions in strain hardening/softening soil. Large strain

undrained expansion in critical state soil model was presented by Collins and Yu (1996) for cylindrical and spherical cavities.

Some researchers (Battaglio et al., Mayne, 1991) combined the elastic perfectly plastic material with the modified cam clay. Cao et al. (1996), Chang et al. (2001) worked on undrained cavity expansion of modified cam clay. The modified cam clay is widely used to describe the elastic plastic behavior of soil incorporating the effect of stress histories (Chang et al., 1999). It is volumetric hardening elastoplastic material based on the critical state concept (Schofield and Wroth). It is also referred as the work hardening soil model. (8)

4.2.1 Modified cam clay parameter

The modified cam clay model which is often denoted as the cam clay model for short is based on the critical state soil mechanics. The preconsolidation pressure is used as a hardening parameter. In critical state soil mechanics, the state of a soil sample is characterized by three parameters:

- Effective mean stress, p'
- Deviatoric (shear stress), q
- Specific volume, v

Under general stress conditions, the mean stress p' and deviatoric stress, q can be calculated in terms of principal stresses σ_1, σ_2 and σ_3

$$p' = \frac{\sigma_1 + \sigma_2 + \sigma_3}{3} \quad \dots \dots \dots (4.19)$$

$$q = \frac{1}{\sqrt{2}} [(\sigma_1 - \sigma_2)^2 + (\sigma_2 - \sigma_3)^2 + (\sigma_3 - \sigma_1)^2]^{1/2} \quad \dots \dots (4.20)$$

Where, σ'_1, σ'_2 and σ'_3 are the major, intermediate and minor effective principal stresses respectively. When $\sigma'_2 = \sigma'_3$, the deviatoric stress in equation 4.20 becomes,

$$q = \sigma'_1 - \sigma'_3 \quad \dots \dots \dots (4.21)$$

Analysis and Modelling of induced pore pressures due to pile driving.

which is the definition of deviatoric stress in the MCC theory. The specific volume is defined as,

$$v = 1 + e \quad \dots \dots \dots (4.22)$$

Where, e is the void ratio.

The modified cam clay requires the specification of

five parameters as-

λ = the slope of the virgin consolidation line in $e - \ln p'$ space.

κ = the mean slope of the expansion and recompression line in $e - \ln p'$ space.

e_{cs} = the value of e at unit p' on the critical state line in $e - \ln p'$ space.

M = the value of the stress ratio q/p' at the critical state condition.

G = Elastic shear modulus.

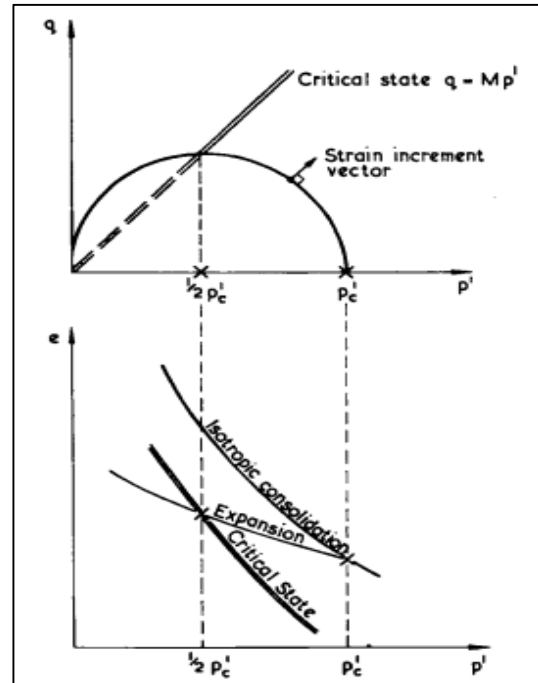


Figure 4.3 Modified Cam clay parameter. (7)

4.2.2 Cavity expansion solution

4.2.2.1 Basic assumption and definition

A cavity with a initial radius a_0 and an initial internal pressure p_0 in an unbounded three dimensional medium of modified cam clay is expanded by a uniformly distributed internal pressure, σ_a . A typical material point of the continuum now has a radial coordinate r , having moved from its original position r_0 resulting in a displacement $u_d = r - r_0$. The soil on the cavity wall will yield when the cavity pressure is sufficiently large. Further increase in cavity pressure will lead to the formation of a plastic zone around the cavity. The radial distance of the plastic zone around the cavity is r_p . The soil beyond the plastic zone would remain in a state of elastic equilibrium. (8)

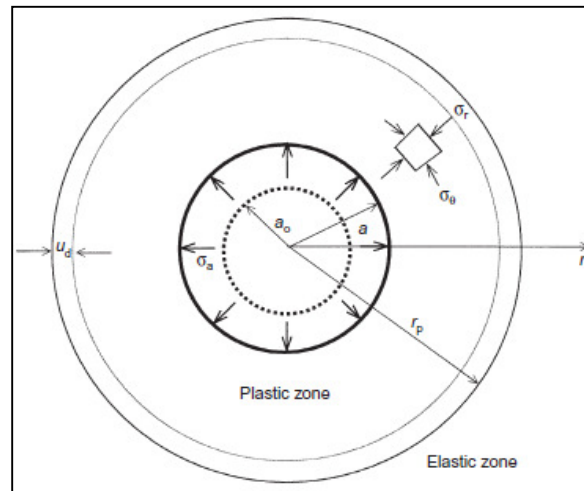


Figure 4. 4 Expansion of a cylindrical cavity. (8)

Condition of axial symmetry and plane strain prevails for cylindrical cavity and spherical symmetry for spherical cavity. Using a spherical polar coordinate system, the initial position of a soil element around a spherical cavity can be described as (r_0, θ, β) . The principal stresses σ_θ and σ_β are the same (Hill, 1950). Similarly, using cylindrical polar coordinate system, the initial position of a soil element around a cylindrical cavity can be described as (r_0, θ, z) . For a undrained condition the vertical stress σ_z is equal to the mean of radial stress σ_r and circumferential stress σ_θ . With this assumption the displacement in the medium are everywhere radial and the problem is one-dimensional.

The equation of equilibrium for both spherical and cylindrical cavity can be written as-

$$\frac{\partial \sigma_r}{\partial r} + m \frac{\sigma_r - \sigma_\theta}{r} = 0 \quad \dots \dots \dots (4.23)$$

Where, $m = 1$ for cylindrical cavity, and

$m = 2$ for spherical cavity.

4.2.2.2 Elastic analysis

With the assumption of small strain theory, the solution for stresses and displacement for the elastic zone during expansion of cavity can be easily determined. In the undrained condition, the volume change is zero and the mean effective stress is constant in the elastic zone. Consequently, no excess pore pressure is generated in the elastic zone. (10)

4.2.2.3 Plastic analysis

After the initial yielding at the cavity wall, a plastic zone, r_p will developed to a distance from the cavity wall as the cavity pressure continues to increase. For a soil obeying the MCC model, the deviator stress at the elastic-plastic boundary,

$$q_p = Mp_0\sqrt{R - 1} \quad \dots \dots \dots (4.24)$$

Here,

R is the isotropic overconsolidation ratio.

p_0 =initial mean effective stress.

M is the slope of the critical state line in the $p - q$ plane = $\frac{6 \sin \phi'}{3 - \sin \phi'}$

The total volumetric strain is the summation of the elastic and plastic volumetric strain after yielding. In an undrained condition, this total volumetric strain should be zero in the plastic zone. This condition leads to a relationship between the mean effective stress and the deviator stress:

$$q = Mp' \left[R \left(\frac{p}{p_0} \right)^{-\frac{1}{\Lambda}} - 1 \right]^{1/2} \quad \dots \dots \dots (4.25)$$

Λ is the plastic volumetric strain ratio defined as $(1 - \kappa/\lambda)$

When the cavity continues to expand indefinitely, position of the elastic-plastic boundary can be determined by, (8)

$$\left(\frac{r_p}{a_u} \right)^{m+1} = \frac{G\sqrt{m+2}}{q_p} \quad \dots \dots \dots (4.26)$$

a_u = Radius of cavity

4.2.2.4 An approximate closed form solution

The relation described above gives a simple numerical solution of the total stresses, whereas closed form solutions in terms of total stresses are more useful for the interpretation of in-situ tests. Such a solution can be obtained by simplifying the relationship between the deviator stress and the radial distance in the plastic zone. Assuming that q in the plastic zone is equal to q_u . The ultimate cavity pressure and the excess pore pressure at the cavity wall at the ultimate state can be approximately expressed as, (8)

$$\sigma_u = p_0 + \frac{m}{\sqrt{3^m}} Mp'_0 \left(\frac{R}{2}\right)^\Lambda \left[1 + \ln \left(\frac{G\sqrt{m+2}}{Mp'_0 \left(\frac{R}{2}\right)^\Lambda} \right) \right] \quad \dots \dots (4.27)$$

Here, p_0 = Initial total mean stress.

$$\Delta u_a = \frac{m}{\sqrt{3^m}} Mp'_0 \left(\frac{R}{2}\right)^\Lambda \ln \left[\frac{G\sqrt{m+2}}{Mp'_0 \left(\frac{R}{2}\right)^\Lambda} \right] + p'_0 \left[1 - \left(\frac{R}{2}\right)^\Lambda \right] \quad \dots \dots (4.28)$$

The excess pore pressure distribution in the plastic zone,

$$\Delta u = \frac{2m}{\sqrt{m+2}} q_u \ln \left(\frac{r_p}{r} \right) + p'_0 \left[1 - \left(\frac{R}{2}\right)^\Lambda \right] \quad \dots \dots \dots (4.29)$$

4.2.3 Factors affecting cavity pressure and excess pore pressure

Cao et al. (2001) illustrated the effects of different soil parameter on the soil stresses during the expansion of cavity. The relations have been determined based on Modified cam clay model. The normalized cavity pressure $(\sigma_a - p_0)/p_0$ is plotted against normalized cavity radius a/a_0 in figure.4.5 for a spherical cavity. The result shows the sensitivity of cavity expansion pressure with isotropic consolidation ratio, R . For a

Analysis and Modelling of induced pore pressures due to pile driving.

nearly normally consolidated soil, changing the other soil parameters while keeping R constant results small increase of the normalized cavity pressure $(\sigma_a - p_0)/p_0$. While keeping other parameters constant and changing R from 1 to 10, the normalized cavity pressure increased to 13.

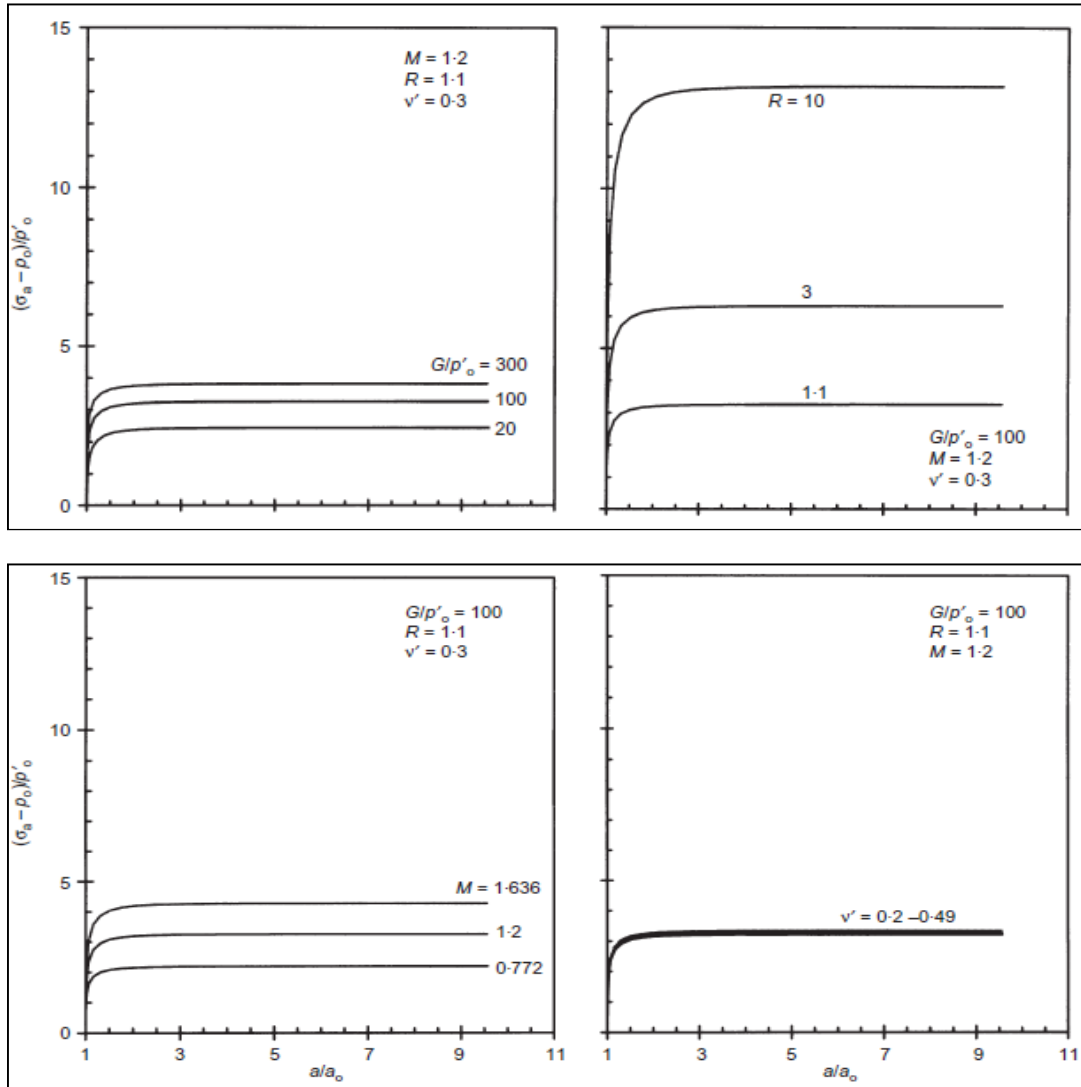


Figure 4.5 Variation of normalized cavity pressure with cavity radius during the expansion of a spherical cavity. (8)

They reported similar observation for cylindrical cavity expansion, which is described in figure.4.6

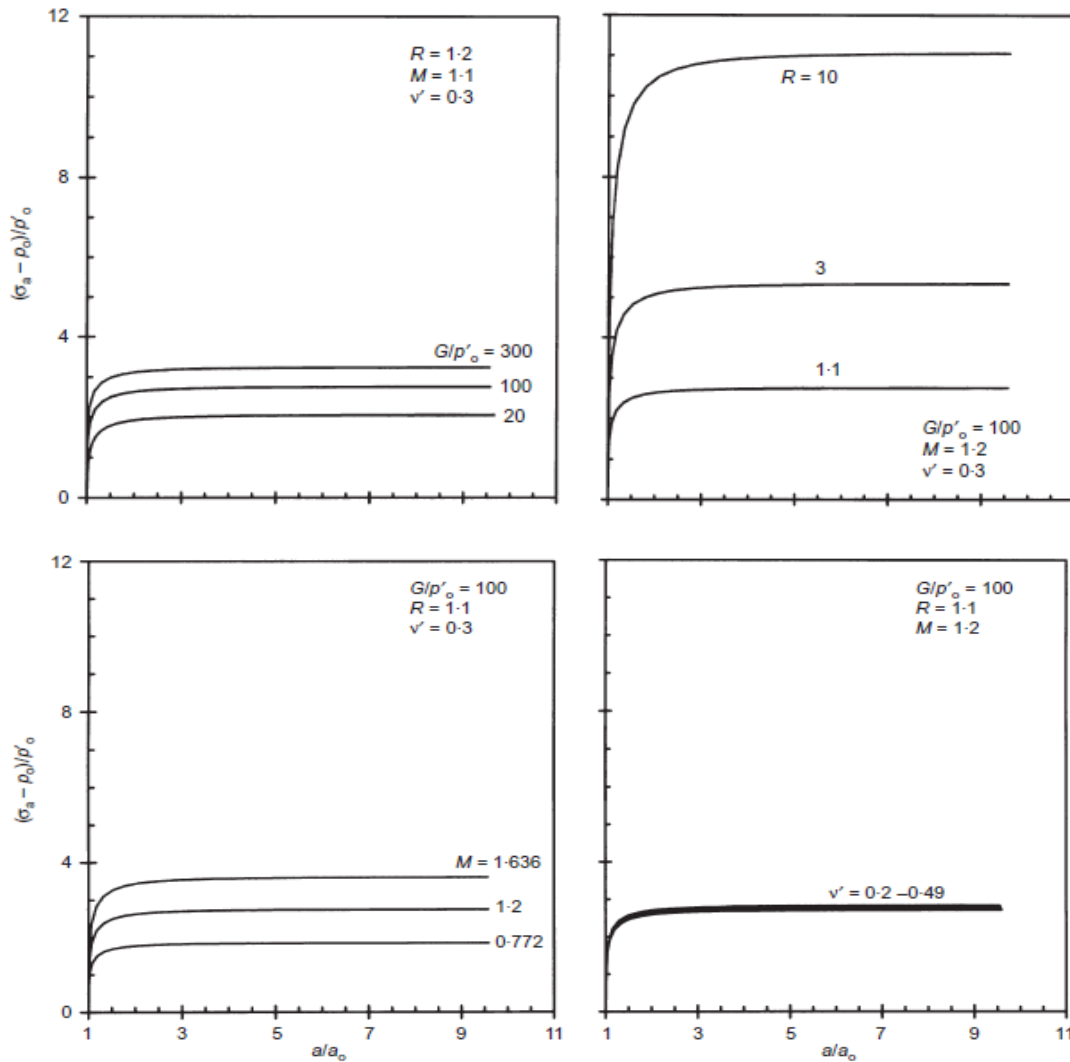


Figure 4. 6 Variation of normalized cavity pressure with cavity radius during the expansion of a cylindrical cavity. (8)

Figure 4.7 and 4.8 shows the dependency of the normalized excess pore pressure $\Delta U_a/p'_0$ with the isotropic consolidation ratio, R for spherical and cylindrical cavity respectively. To compare with the normalized cavity pressure $(\sigma_a - p_0)/p_0$, it is plotted in the same figure. For nearly normally consolidated soil with $R=1.1$, the value of $(\sigma_a - p_0)/p_0$ is close to $\Delta U_a/p'_0$.

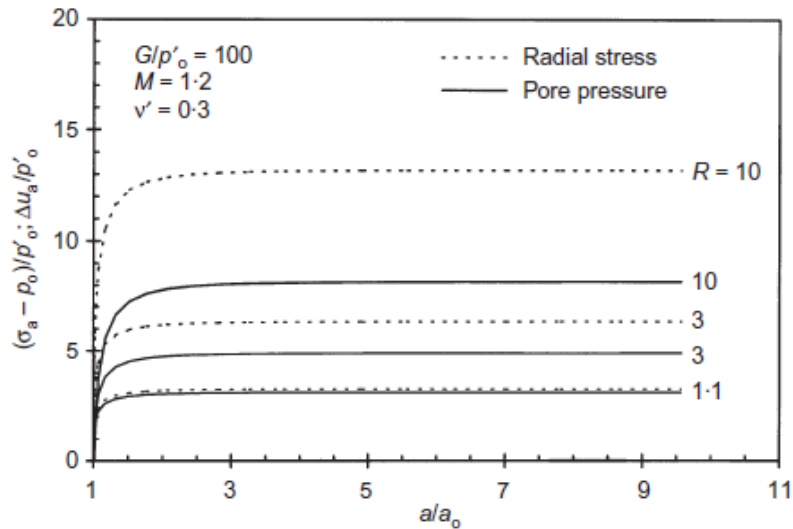


Figure 4.7 Variation of normalized excess pore pressure at the cavity wall and normalized cavity pressure with cavity radius during the expansion of a spherical cavity.(8)

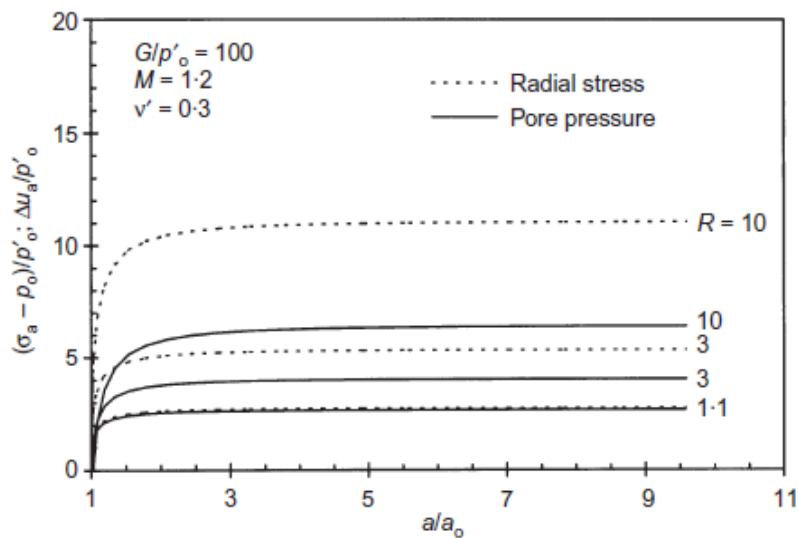


Figure 4.8 Variation of normalized excess pore pressure at the cavity wall and normalized cavity pressure with cavity radius during the expansion of a cylindrical cavity.(8)

The total radial and circumferential stress and the excess pore pressure around the expanded cavity when the cavity continues to expand indefinitely ($a/a_0 \rightarrow \infty$) are plotted as normalized quantities in figure 4.9 (a) for spherical and 4.9 (b) cylindrical cavity respectively. In both cases the normalized total stresses increase more rapidly with increase of R than the excess pore water pressure. When $R=1.1$ the excess pore

water distribution is slightly smaller than the normalized radial stress but larger than the circumferential stress. At $R=10$, both the radial and circumferential stresses are greater than the excess pore pressure.

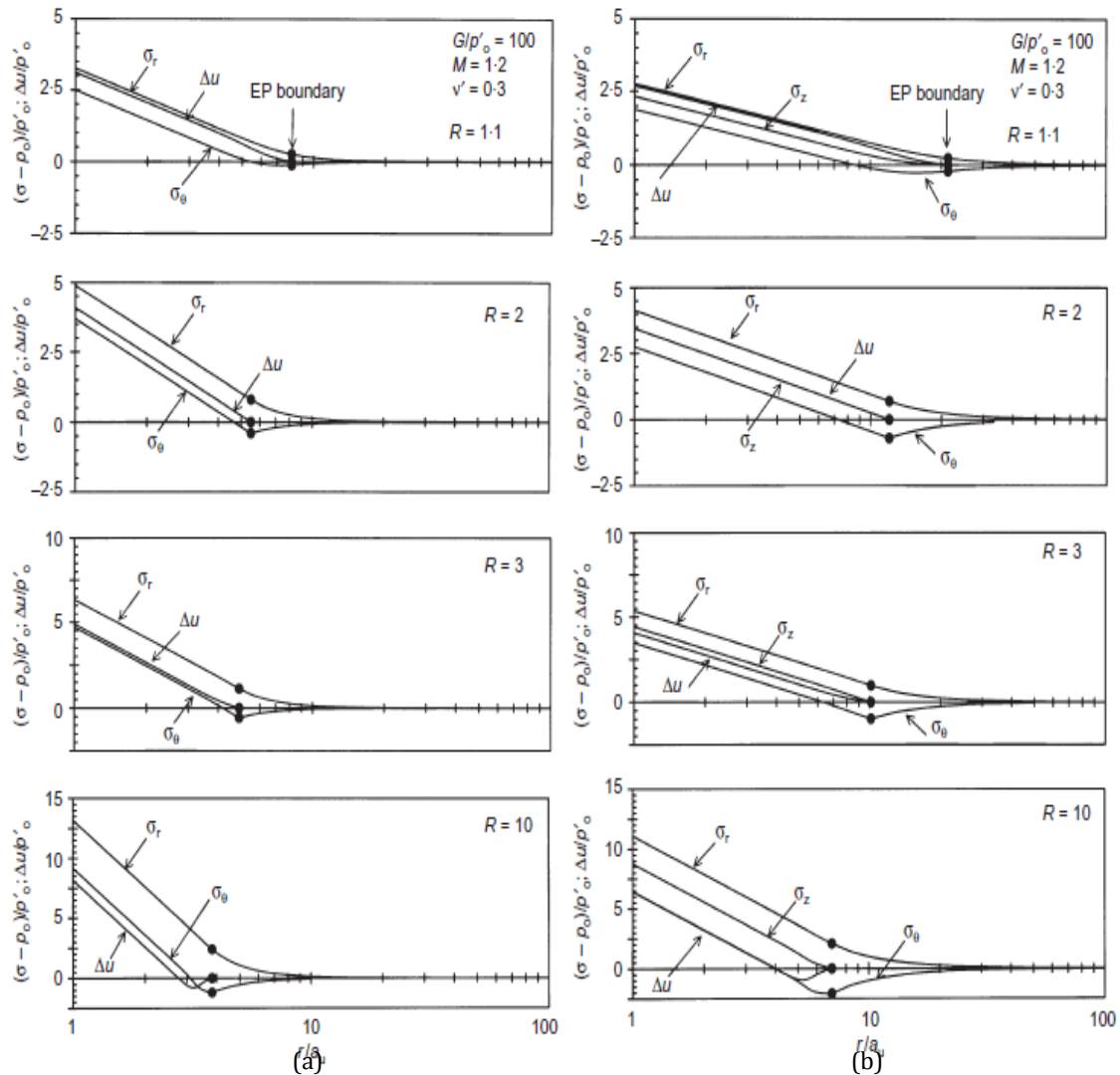


Figure 4. 9 Stress distribution around a (a) Spherical Cavity (b) cylindrical Cavity at the ultimate state. (8)

The variation of the radius of plastic zone at ultimate state with R is shown in figure 4.10. The size of the plastic zone is also sensitive to shear modulus, G . The size of the plastic zone in stiff soil ($G/p'_0 = 100$) is much larger than that in a soft soil ($G/p'_0 = 20$).

For $R < 5$, the size of the plastic zone decreases rapidly. Same trend has been observed for both spherical and cylindrical cavity.

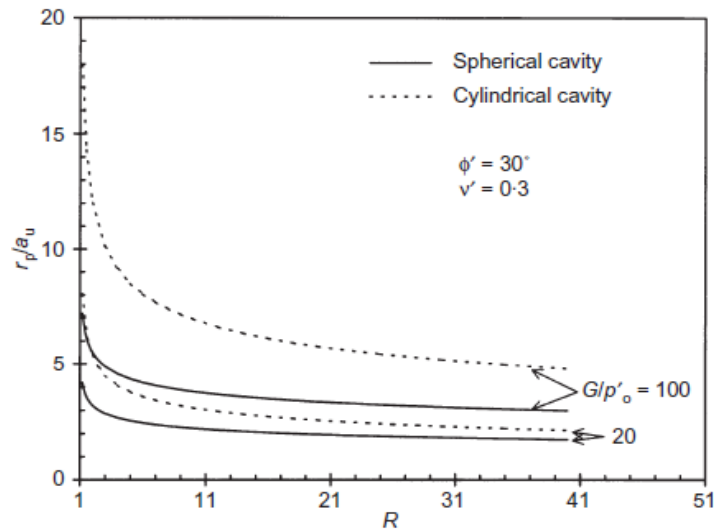


Figure 4.10 Variation of elastic-plastic boundary with isotropic overconsolidation ratio.(8)

4.3 Cavity expansion in pile driving

The analysis of the behavior of driven pile by cavity expansion solution is difficult because of its high material and geometric nonlinear nature. The capacity of pile, change of stress and pore water pressure can be analyzed by cavity expansion solutions and considerable progress has been made over last three decades. Randolph et al. (1979), Davis et al. (1984), Nystrom (1984), Collins and Yu (1996) reported the installation of piles into the clay as the expansion of cylindrical cavity.

4.3.1 Total stress analysis with perfectly plastic soil model

Perfectly plastic soil model is appropriate for modeling normally to lightly over consolidated soil. The advantage of total stress analysis by perfectly plastic soil model is that closed form solution is possible for cavity expansion problem.

The constant cavity pressure for expansion of a cylindrical cavity from zero radius-

For a cylindrical cavity
$$\sigma_{rr} = \sigma_{h0} + S_u \left[1 + \ln \frac{G}{S_u} \right] \dots \dots \dots (4.30)$$

Analysis and Modelling of induced pore pressures due to pile driving.

For a spherical cavity
$$\sigma_{rr} = \sigma_{h0} + \frac{4}{3}S_u \left[1 + \ln \frac{G}{S_u} \right] \dots \dots \dots (4.31)$$

σ_{h0} =In-situ total horizontal stress before pile driving.

G = Shear modulus.

S_u = Undrained shear strength.

The measured value of pile shaft normal stress by Coop and Wroth (1989) for model pile test in a normally consolidated clay is compared (35) with equation (4.30) in the figure 4.11.

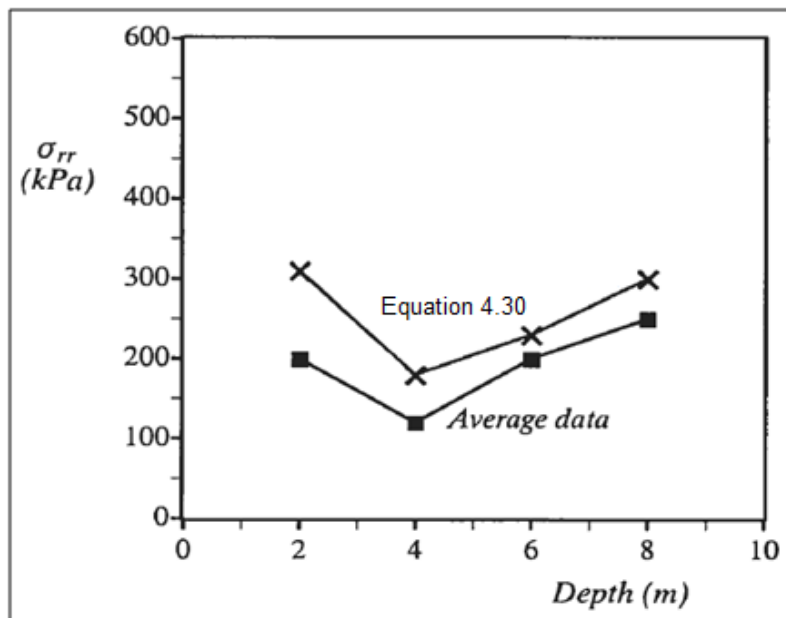


Figure 4. 11 Prediction of pile shaft normal stresses for normally consolidated Huntspill clays (Data from Coop and Wroth ,1989). (35)

The predicted value of total normal stress by cavity expansion is higher than that of measured value. The reduction of the measured value of shaft normal stress is due to some unloading along the pile shaft during pile installation. The total stress solution is not accurate for overconsolidated clays. This inaccuracy had been shown by Yu H.S. (2000) (35) by comparing the results from heavily overconsolidated Madingley clays by Coop and Wroth (1989) with the total stress cavity expansion solution. Figure 4.12 shows that equation 4.30 overestimates the measured normal stress by over 100% for heavily overconsolidated soil.

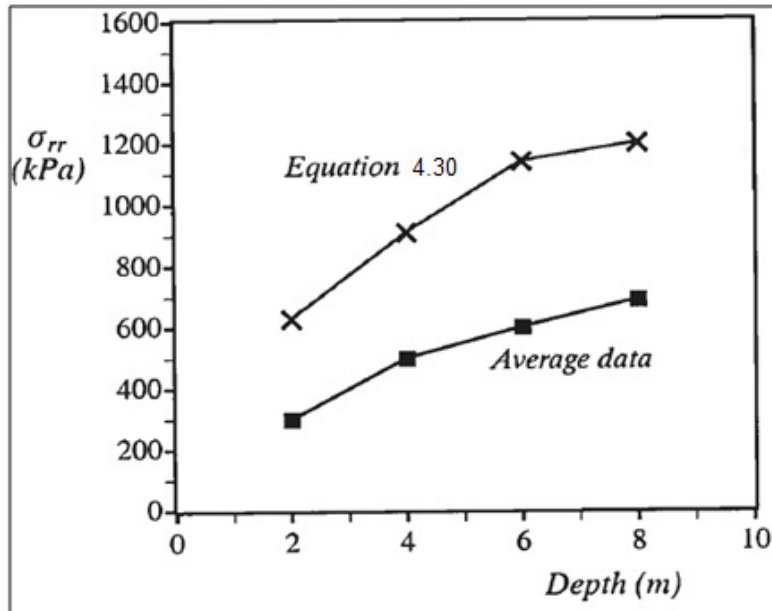


Figure 4. 12 Prediction of pile shaft normal stresses for heavily overconsolidated Madingley clays (Data from Coop and Wroth,1989). (35)

Randolph et al. (1979) and Collins and Yu (1996) reported two important shortcomings of the total stress analysis. First, pore pressure due to pure shear is not considered. The second limitation is that the perfectly plastic soil model is not able to link the strength of the soil and its change with the current effective stress state and stress history of soil.

4.3.2 Effective stress analysis with critical state soil model

Randolph et al. (1979) proposed the effective stress cavity expansion solution using a critical state soil model (Modified Cam Clay). Collins and Yu (1996) derived closed form solution for the same problem in soils. (35)

The cavity expansion prediction of radial effective stress is based on the assumption that the soil adjacent to the pile shaft is at a critical state under plane strain conditions with a major radial stress. The effective radial stress at the cavity wall may be expressed as follows:

$$\sigma'_{rr} = \left[1 + \frac{\sqrt{3}}{M} \right] S_u \quad \dots \dots \dots (4.32)$$

Where M is the slope of critical state line of $q - p'$ plot.

Analysis and Modelling of induced pore pressures due to pile driving.

The pore pressure results at the cavity wall proposed by Randolph et al. (1979) are represented by, (35)

$$\Delta U = U - U_0 = (P'_0 - P'_f) + S_u \ln \frac{G}{S_u} \quad \dots \dots \dots (4.33)$$

U_0 =In situ pore water pressure.

P'_0 and P'_f are the mean effective normal stress at the state of in-situ and failure respectively.

Many investigators as Kirbi and Esrig, 1979, Coop and wroth ((1989), Bond and Jardine (1991) have measured pore water pressure generated at the pile soil interface during pile installation in clay soils. Coop and Wroth (1989) noted that the excess pore pressure predicted by the cavity expansion theory of Randolph et al. (1979) for OCR clays are much higher than that of measured value. This was confirmed by Bond and Jardine (1991) in an independent research program. Coop and wroth (1989) applied the cavity expansion theory of Randolph et al. (1979) at the heavily overconsolidated London clay and showed that normalised excess pore pressure (the excess pore pressure devided by undrained shear strength) is in the range of 3.1 to 3.6. But the negative pore pressure

was recorded during piling.

Collins and Yu (1996) presented an analytical study of the undrained expansion of the cylindrical and spherical cavities in soil modelled by various critical state models. The cavity expansion results of London clay from three different critical state soil model

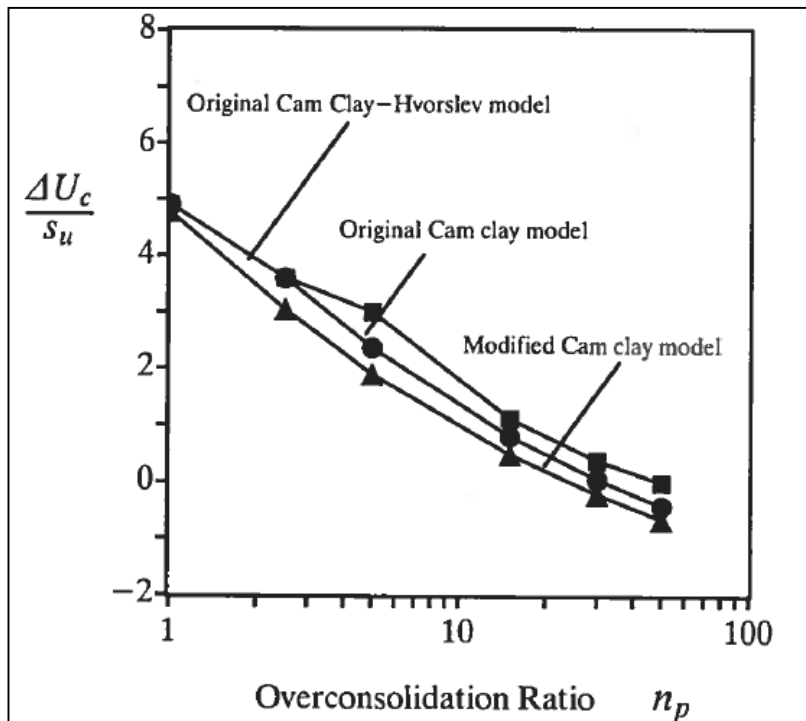


Figure 4.13 Variation of excess pore pressure at cavity wall with overconsolidation ratio. (35)

plotted in the figure 4.13 with the overconsolidation ratio.

The normalised excess pore pressure has a tendency to decrease with the increasing OCR. It shows that the excess pressure becomes negative when the OCR is more than 25. As the London clay is highly overconsolidated with 20-50, the negative excess pore pressure could be generated.

Chapter V

Soil condition and Geotechnical report

5.1 Project description

The Øvre sund Bridge project in Drammen, South-eastern Norway about 50km from Oslo, is the recently completed bridge construction across Drammen river which has officially open for public use on the 10th of September 2011. The bridge connects the Grønland part with the Hamborgstrøm part of the city (figure 5.1). The bridge is 148m long, 23.1 m wide and has spans of 25.8m and 32m long. The soil conditions on both sides of the river and in the river bed are relatively similar. A total of 191 concrete piles on the Grønland side, 32 steel pipe piles in the river and 100 concrete piles on the Hamborgstrøm side were installed. To follow up the development of excess pore pressure, a total of 8 piezometers in the Grønland side of the river, 6 piezometers in the river and 8 piezometers on the Hamborgstrøm side of the river were installed. (30)



Figure 5. 1 View of øvre sund bridge prject, Drammen.

Aas (1976) has described a slide that took place in the bank of Drammen River in 1971. The slide happened during the construction works for Union factories in Drammen. The slope failed due to the disturbances from the pile driving (32). Therefore, it was a great challenge to reduce and control the effects of driving for the øvre sund project.

5.2 Soil condition

The general soil conditions in both sides of the river and in the river bed are relatively similar. The ground is composed of mainly three different soil layers. There is a thin layer of silty sand soil overlying a thick layer of soft clay. This layer overlies a dense moraine. The clay layer is normally consolidated on both sides of the river and has undrained shear strength 10-15 kN/m² at the top of the layer and increases with depth to 20-30 kN/m² at the bottom of the layer. The unit weight is considered 19-20 kN/m² and the sensitivity 6-35. The depth of the bottom dense moraine layer is dipping in the direction of Hamborgstrøm side of the river. The depth of the bottom dense moraine layer varies from about 10m upstream side of Grønland to about 25m in the downstream of the Hamborgstrøm side of the river. (30)

5.3 Available test data

Geotechnical report was performed by "MULTICONCONSULT AS" one of the leading consulting company in Norway. The report compiles data from soil surveys conducted in 1997, 2002, 2003 and 2007. The concentration has been given on the data of Grønland part. There have been 7 total soundings along the riverbank in the Grønland. In addition, it was performed 4 total soundings far from river bank and studies had also included four sample series, 6 cone penetration test and 1 pore pressure measurement.

NPRA had installed 3 piezometers at different depth near the pile G182, referred as station P4, before 2 years of piling activities had started. It was observed that the pore pressure is approximately hydrostatic and varies with the water level in the river in terms of tides and flooding.

Figure 5.2 shows the boring plan in the Grønland side which were taken to evaluate the geotechnical condition of the grønland.

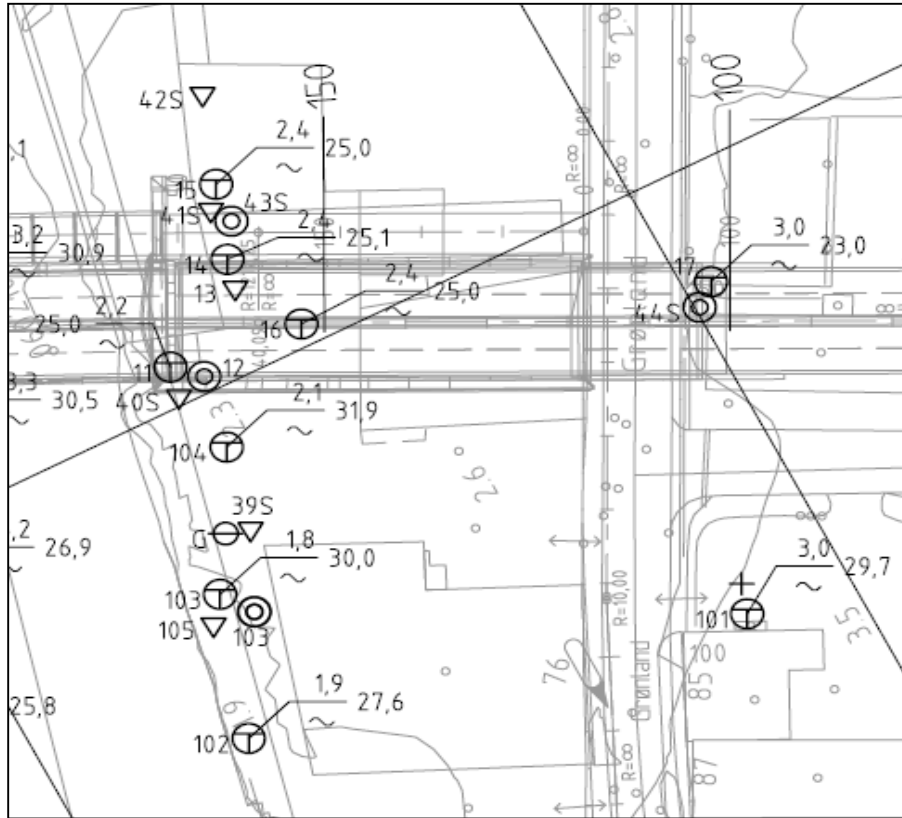



Figure 5.2 Boring Plan

5.3.1 Total sounding

Along Grønland side several total soundings have been performed. From figure 5.2 it is seen that total soundings have been performed at 7 locations namely 11, 14, 15, 16, 102, 103, 104 and indicated  in the figure as total sounding. From total sounding results it is observed that the thickness of the soft clay layer varies from 11-14m (Figure 5.3), whereas Hole 103 shows only 6m thickness of clay layer. The upper sand layer extends until 4-6m from the top of the ground surface.

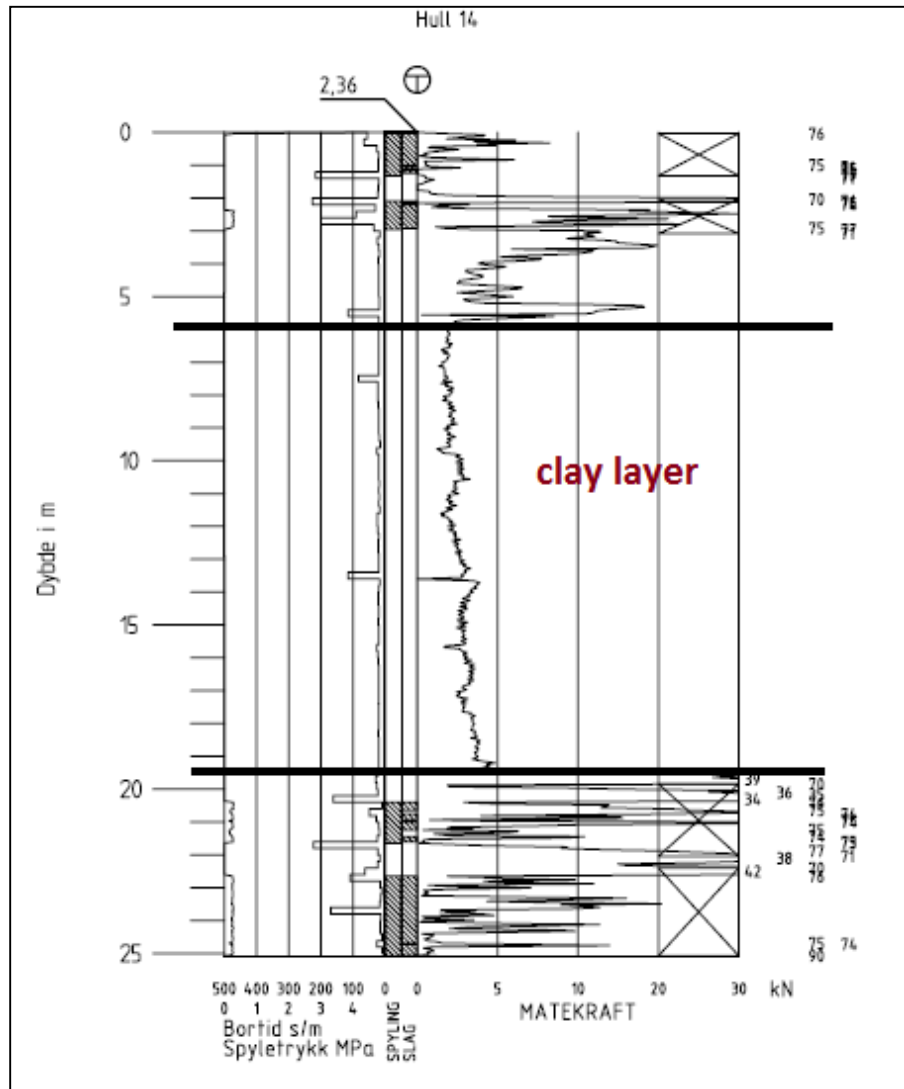


Figure 5.3 Total sounding result in Borehole 14.

5.3.2 Index test

Index test results provide soil identification and classification data. In our project, available data for index tests are at Hole 12, 43, 44, 103. Figure 5.4 shows the results of index test at bore hole 12. Summarized results of clay layer given later in the table 5.2.

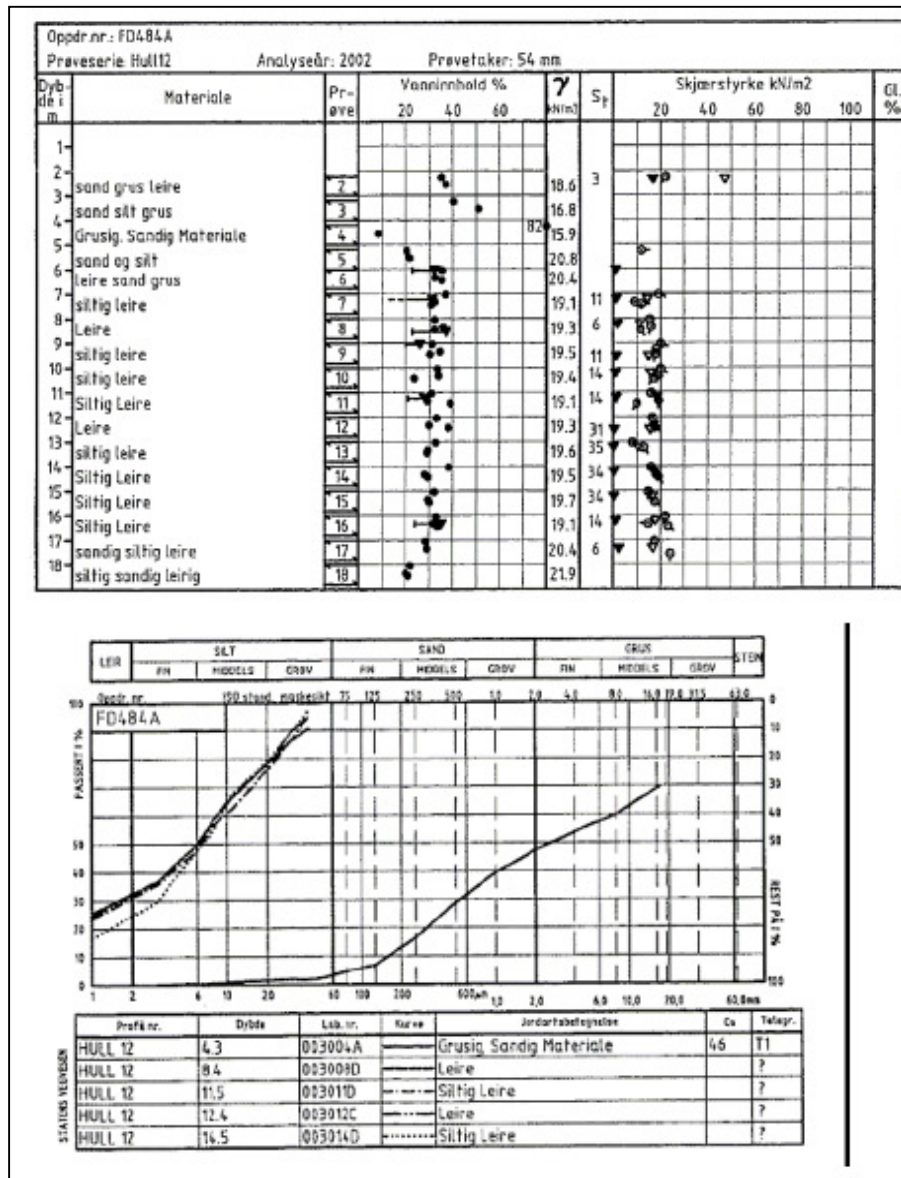


Figure 5. 4 Index test at borehole 12.

5.3.3 Cone penetration test

From Cone penetration test soil stratification is obtained by presenting the recorded cone resistance and pore pressure versus depth in parallel plots. Six CPT tests were carried out at hole 13, 39S, 40S, 41S, 42S, and 105. Results from hole 13 given below:

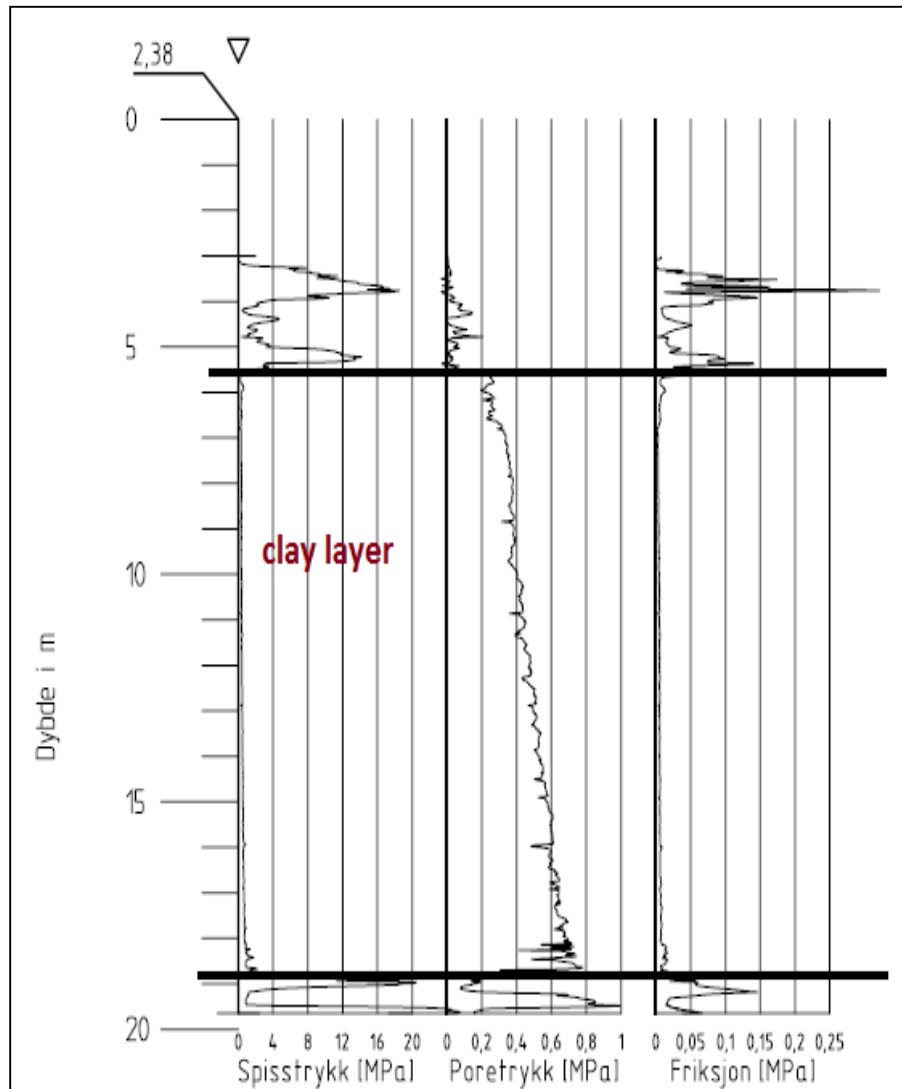


Figure 5. 5 CPTU result at borehole 13

5.3.4 Triaxial test

Fundamental material properties of the soil sample can be extracted from triaxial test data. Among them soil resistance to shear, apparent cohesion, dilatancy angle are important. These parameters are then used to predict soil behavior under different stress situation. Here triaxial tests are available in the Grønland part at hole 12, 43.

At point 12, active triaxial test, CAU tests at depth 8.4m, 11.4m and 15.3 m.

At point 43 passive triaxial test, CAU tests at depth 8.7m, 10.5m.

Analysis and Modelling of induced pore pressures due to pile driving.

At point 19 (in the river) Active, CIU tests at depth 3.2m, 3.3m, 3.5m.

At point 19 (in the river) Active, CIU tests at depth 5.3m, 5.4m, 5.5m.

At point 19(in the river) Active, CIU tests at depth 7.3m, 7.4m, 7.5m.

In Figure 5.6 it is plotted deviatoric stress against radial stress from the test data of borehole 12 has been plotted. From the slope of the curve, friction angle, φ has been calculated. Three graphs for three depths were plotted. The failure line intersects horizontal axis at 15 kPa which is the attraction value of soil sample.

$$\text{friction angle, } \varphi = \tan^{-1} \frac{S_f}{\sqrt{1 + 2S_f}}$$

$$\varphi = \tan^{-1} \frac{0.78}{\sqrt{1 + 2 * 0.78}} = 26^\circ$$

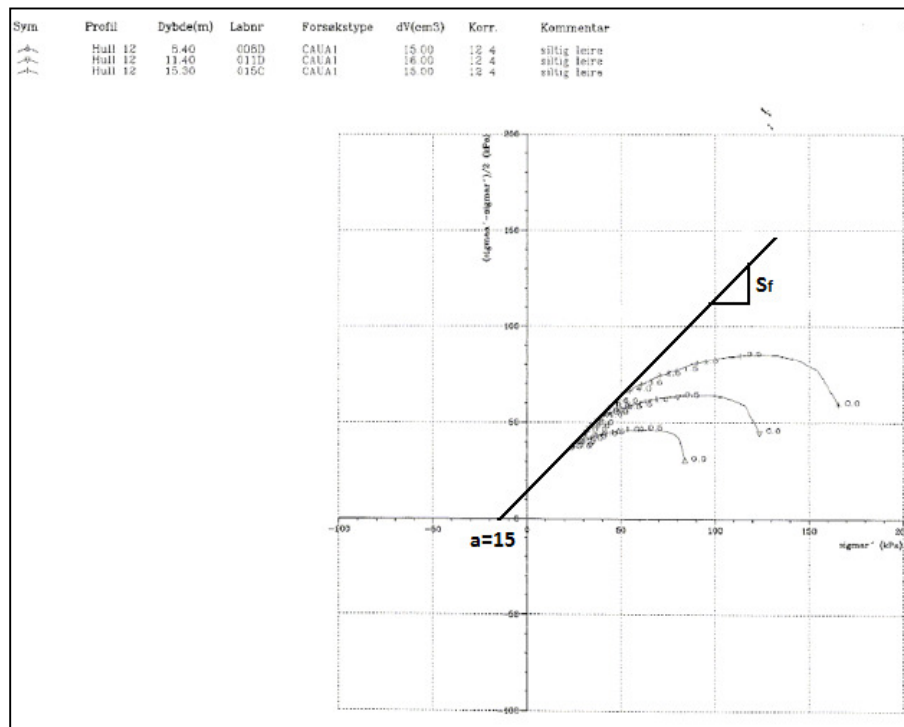


Figure 5. 6 Triaxial test result in a $\frac{1}{2} \sigma_d$ vs σ_3 diagram.

Analysis and Modelling of induced pore pressures due to pile driving.

In figure 5.7 Effective mean stress versus deviatoric stress graph has been plotted. It is clear from the plot that the three samples subjected to anisotropic stress condition during the consolidation. The $q - p'$ graph for isotropically consolidated sample from the river is plotted in figure 5.8.

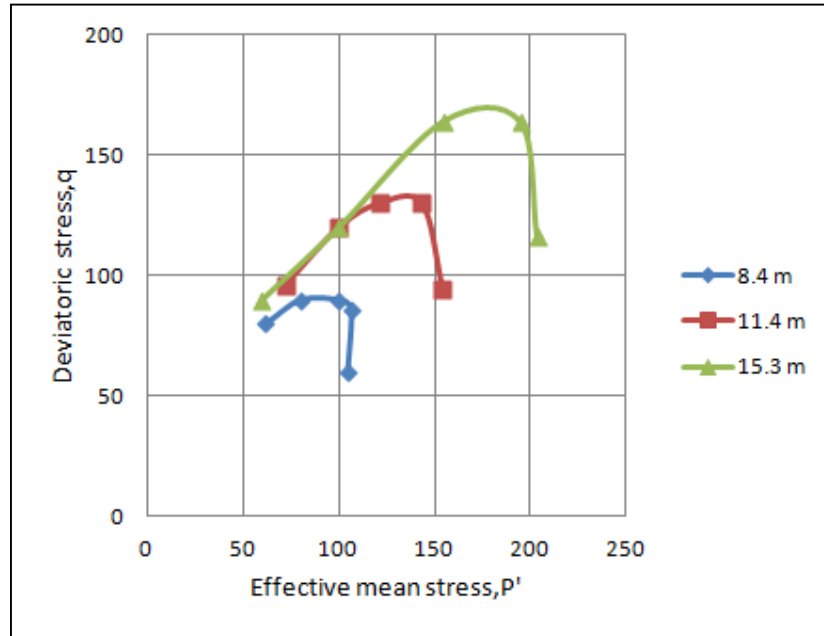


Figure 5. 7 q vs p' diagram for triaxial test at borehole 12

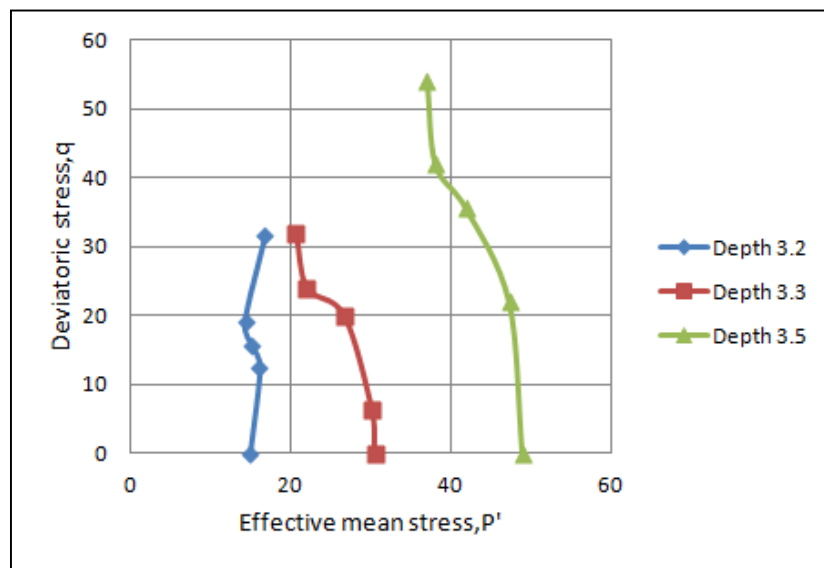


Figure 5. 8 q vs p' diagram for triaxial test borehole 19.

5.3.5 Oedometer test

Oedometer test is important to find the deformation properties of the soil. In this project Oedometer tests had carried out at borehole 12 and 44. Total Six oedometer tests were performed. Three samples from borehole 12 (9.5m, 12.1m, 16.5m) and three samples from bore hole 44 (4.5m, 8.5m, 11.5m). Calculation of finding stiffness parameters from the tests at hole 12 are given below.

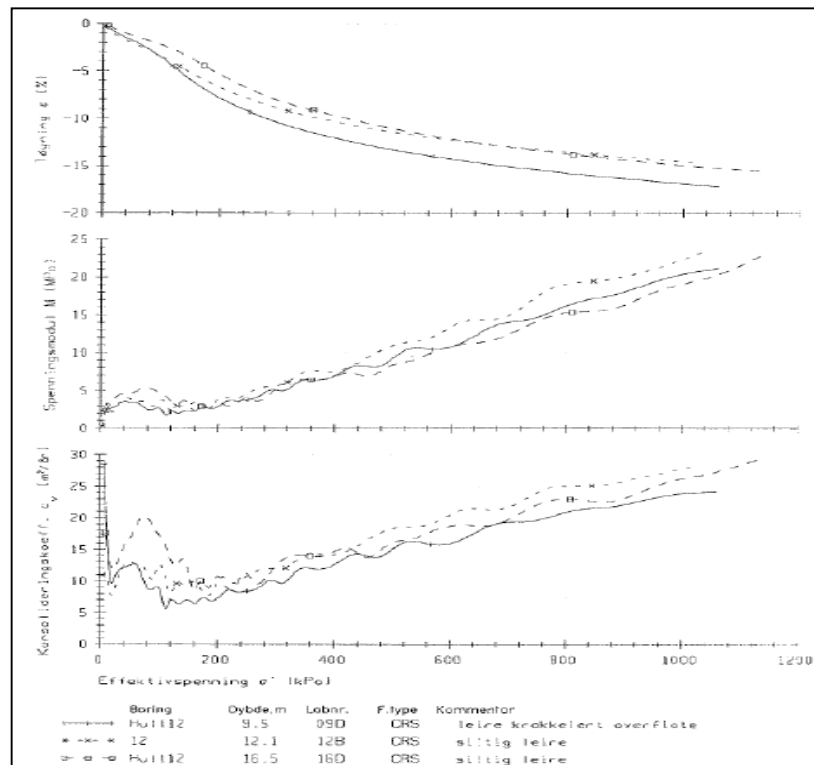


Figure 5.9 Oedometer test results at borehole 12

Preconsolidation stress

Depth 9.5m:

From fig 5.9 following values for the preconsolidation stresses can be read.

Stress-strain curve, $\sigma'_c = 110-130$ kPa

Analysis and Modelling of induced pore pressures due to pile driving.

Stress-modulus curve, $\sigma'_c = 90-130$ kPa

Stress- c_v curve, $\sigma'_c = 80-130$ kPa

Thus, the preconsolidation stress has a value around 120 kPa in average.

The effective overburden stress, $\sigma'_{vo} = 9.5 * 10 = 95$

Overconsolidation ratio, $OCR = \frac{\sigma'_c}{\sigma'_{vo}} = \frac{110}{95} = 1.15 > 1$, soil slightly overconsolidated.

Depth 12.1m:

Stress-strain curve, $\sigma'_c = 110-130$ kPa

Stress-modulus curve, $\sigma'_c = 110-130$ kPa

Stress- c_v curve, $\sigma'_c = 120-130$ kPa

Preconsolidation stress, $\sigma'_c = 120$ kPa

The effective overburden stress,
 $\sigma'_{vo} = 12.1 * 10 = 121$

Overconsolidation ratio,

$OCR = \frac{\sigma'_c}{\sigma'_{vo}} = \frac{120}{121} = 0.98 < 1$, normally

consolidated.

Depth 16.5m:

Stress-strain curve, $\sigma'_c = 140-160$ kPa

Stress-modulus curve, $\sigma'_c = 120-140$ kPa

Stress- c_v curve, $\sigma'_c = 120-140$ kPa

Preconsolidation stress, $\sigma'_c = 135$ kPa

The effective overburden stress,
 $\sigma'_{vo} = 16.5 * 10 = 165$

Overconsolidation ratio,

$OCR = \frac{\sigma'_c}{\sigma'_{vo}} = \frac{135}{165} = 0.811 < 1$, normally

consolidated.

Coefficient of consolidation, c_v

From the c_v vs stress curve, the c_v has been measured with the corresponding effective overburden stress which is equal to $8 \text{ m}^2/\text{yr}$.

Modulus, M

The constrained stiffness of the soil from the oedometer test is expressed by the oedometer modulus M .

Table 5. 1 The oedometer modulus M .

| Depth(m) | M_{nc} (kPa) | M_{oc} (kPa) |
|----------|----------------|----------------|
| 9.5 | 4000 | 8000 |
| 12.1 | 4000 | 8000 |
| 16.5 | 5000 | 8000 |

5.3.6 Undrained Shear Strength of clay layer

Depending on various it is suggested that the s_u can be evaluated from the relations below:

Active $s_{ua} = 6.4 + 2.7z$

Direct $s_{ud} = 0.64s_{ua}$

Passive $s_{up} = 0.32s_{ua}$

Z is the depth from ground in meter.

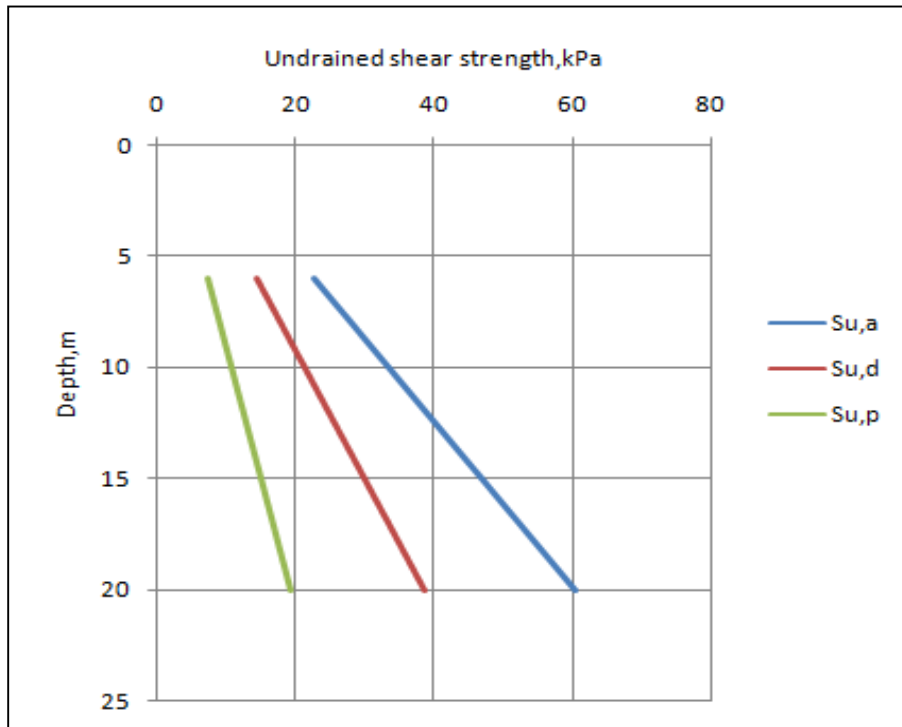


Figure 5. 10 Undrained shear strength for clay layers

Table 5. 2 Summerrized results of clay layer at øvre sund project,Drammen.

| Parameter | unit | value |
|---|-------------|----------------------------------|
| Water content (w) | % | 20-40 |
| Unit weight (γ) | kN/m^3 | 19-20 |
| Sensitivity (s_t) | - | 6-35 |
| Undrained shear strength, (s_u) | kN/m^2 | 10-15 (at top) 21.5 (average) |
| Friction angle (φ) | ° | 26 |
| Attraction (a) | kN/m^2 | 15 |
| Cohesion (c) | kN/m^2 | 7.3 |
| Preconsolidation stress (σ'_c) | kN/m^2 | 120 |
| Coefficient of consolidation | m^2/yr | 8 |
| Oedometer modulus, M_{nc} | kPa | 4000 |
| Oedometer modulus, M_{oc} | kPa | 8000 |

Chapter VI

Analysis of Pore pressure measurement of Øvre sund Project

6.1 Pore pressure measurements by Piezometers

An electric piezometer, introduced into a well, enables to have a proportional signal to the water level into it. This is possible with the sensor, a piezoelectric element, which converts the pressure to a directly proportional signal. This signal is then transferred by electric cables inside the inner rods and up to a data acquisition unit on the surface. What is required with piezometers is to have the lowest response time between the measured and the real pore pressure in the soil when there is a real variation of the water level. The response time depends on the shape, type, design of the sensor of the piezometer and on the permeability of the soil.

The development of pore water pressure during pile driving in the øvre sund bridge project had been monitored by piezometers at four locations in each side of the river banks and at three locations in the river bed. Because of the relative proximity to the river bank, pile driving activities in axes G4, G5, G6 and river front foundations were critical for the stability of the river bank slope. Fig. 6.1 shows the locations of piezometer stations in Grønland.

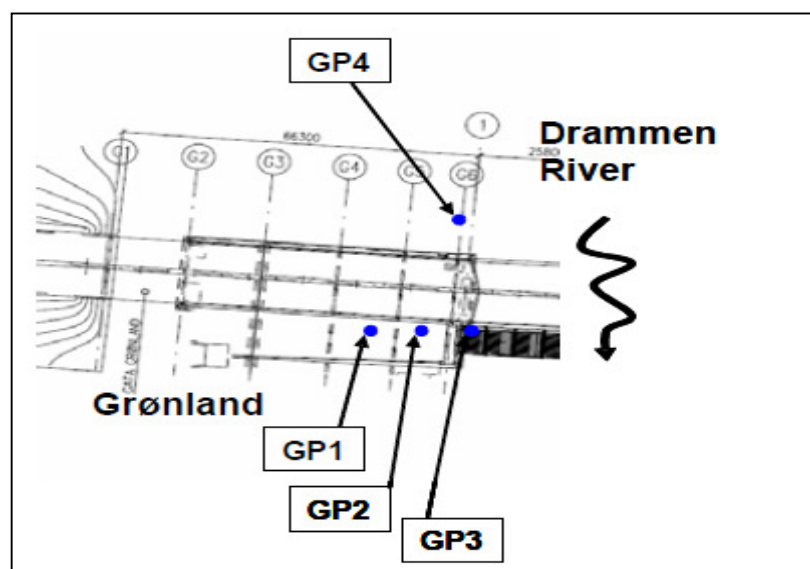


Figure 6. 1 Piezometer location at Grønland part. (30)

Analysis and Modelling of induced pore pressures due to pile driving.

In the contract it was the client's responsibility to cover the down-time (waiting time) cost due to excess pore-water pressure. On the Grønland side of the river, eight electric piezometers were installed in four different locations and depths (Table. 6.1):

Table 6. 1 Locations of piezometer (30)

| Station | Piezometer | Elevation, masl |
|---------|------------|-----------------|
| GP4 | G-71306 | -4.9 |
| | G-71606 | -9.9 |
| | G-71706 | -13.1 |
| GP3 | G-53108 | -10.0 |
| | G-52808 | -14.0 |
| GP2 | G-53008 | -9.0 |
| | G-52908 | -14.0 |
| GP1 | G-52508 | -7.0 |

From the figure 6.2 below, it is observed that the three piezometers at P4 station which were closely spaced. The piezometers at station GP4 were installed two years before the startup of the construction of the bridge. The piezometers at station GP1, GP2 and GP3 were installed two weeks before the piling activity had started.



Figure 6. 2 Pizometer location at station P4. (Photo : Tefera T.)

6.2 Piling activities in the project

For the construction of Øvre Sund bridge foundation, two different types of piles were used. The piles were designed to transfer the load through side friction and end bearing into the very dense moraine underlying the soft silty and sandy clay. Precast concrete piles with dimension 270 x 270mm for the construction of abutments and river fronts on both sides of the river and steel pipe piles with diameter 813mm for the construction of the main part of the bridge were used. In the Grønland side 191 prefabricated concrete piles, in the Hamborgstrøm side 104 prefabricated concrete piles including 4 piles used for the tower crane and in the river bed 32 steel pipe piles were installed.



Figure 6. 3 Piling in progress at Grønland side. (Photo : Tefera T.)

The piles were driven into the ground using hydraulic piling rig with drop hammer weight of 5 and 6 tons for concrete piles and 10 tons for steel pipe piles. The drop height of the hammer for concrete piles depended on hammer weight, length of the pile driven in the ground, the resistance of the soil and anticipated bearing capacity of the pile. The final pile depths were determined either by minimum penetration into the very dense moraine or by the specified drop height of the hammer and number of blows per specified penetration. For selected piles, bearing capacities were verified using PDA

Analysis and Modelling of induced pore pressures due to pile driving.

measurements. There was very little resistance met during pile driving in the soft sensitive clay layer. The piles were actually penetrating through this soft sensitive clay layer up to 6 m with zero drop height of the hammer. Penetration of the piles reduces dramatically with each drop of the hammer when the piles encounter the dense moraine deposit.

The test driving of 6 piles with PDA measurements were done 11 - 15 December, 2008. Piling started from 19th December, 2008 with Axis K7 and continue until 10th February, 2009, with Christmas break from 20 December to 4 January. During construction the contractor drove 121 piles of 17 to 31 m depth. They've finished 2980 m driving in 28 days, i.e. approximately 106 linear meters of pile per day. On the Grønland side, there were six axes G1, G2, G3, G4, G5, and G6. The piles were driven along these axes (Appendix A.2).

6.3 Measures taken to control pore pressure development

Different measures were taken to control the development of excess pore pressure. In addition to open ended steel pipe piles in axis 5 in the river, vertical drains (Mebradrain) were installed on the outside wall (Fig. 6.4)



Figure 6. 4 The four vertical drains installed on the outside wall of the open ended steel pipe piles in axis 5 in the river. (30)

Analysis and Modelling of induced pore pressures due to pile driving.

Based on the measured excess pore-water pressure, a technique commonly adopted in Scandinavia is preboring a slightly undersize hole (clay sausage) before driving. This method had been applied to the 6 concrete piles on the river bank. Fig. 6.5 shows the soft clay drilled out

of the hole before driving the concrete piles. To reduce the anticipated generation of high pore-water pressure during pile driving in axis 5 in the river, open ended steel pipe piles were used.



Figure 6. 5 The soft clay material (clay sausage) drilled/sucked out of the hole before driving the concrete pile. (30)

Based on the stability analyses, alarm limit for each piezometer station were developed. The alarming boundary zones of excess pore-water pressure at station GP1, GP2 and GP3 were 10, 50 and 60kPa respectively. Based on stability analysis, when the buildup of excess pore-water pressure along the critical failure plane at station GP3, GP2, and GP1 reaches a critical value of 60kPa, 50kPa and 10kPa respectively piling activity had stopped until it dissipated.(30)

To drive the piles, they adopted a particular procedure. Using an influence radius and knowing the location of the pile that they were driving, they were able to define an area where they were allowed to drive piles. It was planned to drive such a way that

Analysis and Modelling of induced pore pressures due to pile driving.

minimum distance of 8m between piles to be maintained in each day (Figure 6.6). Based on the measured excess pore water pressure the safety margin of the river bank slope was regularly checked.

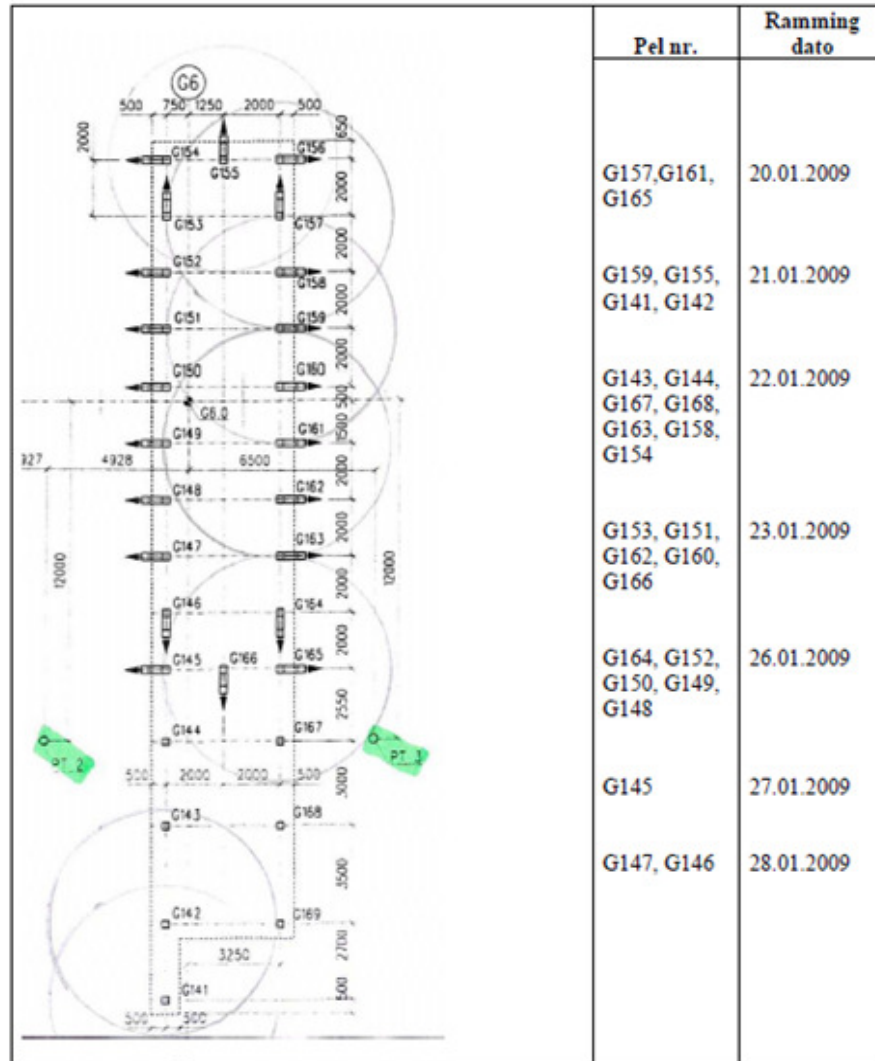


Figure 6. 6 Schedule of piling work at the axis of G6. (31)

6.4 Other factors that increase pore pressure

The pore pressure increase by the other activities had been measured also. Trucks led to an increase of 0.3 m on the piezometer P1 (G52508). A truck weights about 30 tons (10 tons axle load on three axes). Reinforcement of foundation G6 led to an increase of pore pressure at piezometer G53108 and G52808 at a distance of 0.5 m. It was noted that the

Analysis and Modelling of induced pore pressures due to pile driving.

pore pressure rose during the day and decreased during the nights. It is not clear whether the measurements are affected by the weight of the reinforcement or activities of the vehicles in the area. The casting was performed on Friday 6 February. Casting began 10:30 am and ended at 16:30. Pore pressure

increased at 13:30 and then stabilized at the last measurement at 15:30. It dropped down during the weekend.

6.5 Analysis of data

6.5.1 Pore pressure situation before driving

The intention was to analyze to what extent the measured pore pressure was due to pile driving. For this instance, it had measured the state of the soil was before piling. The average pore water pressure before piling for each piezometer had calculated and plotted with the calculated hydrostatic pore pressure versus depth. It was obtained for the 3 piezometers located in P4 (Figure 6.7).

As mentioned earlier, the piezometers at station GP4 were installed two years before the startup of the construction. The two years measurement shows that the pore-water pressure in the soil is close to hydrostatic and follows the seasonal as well as tidal variation of the river water level.

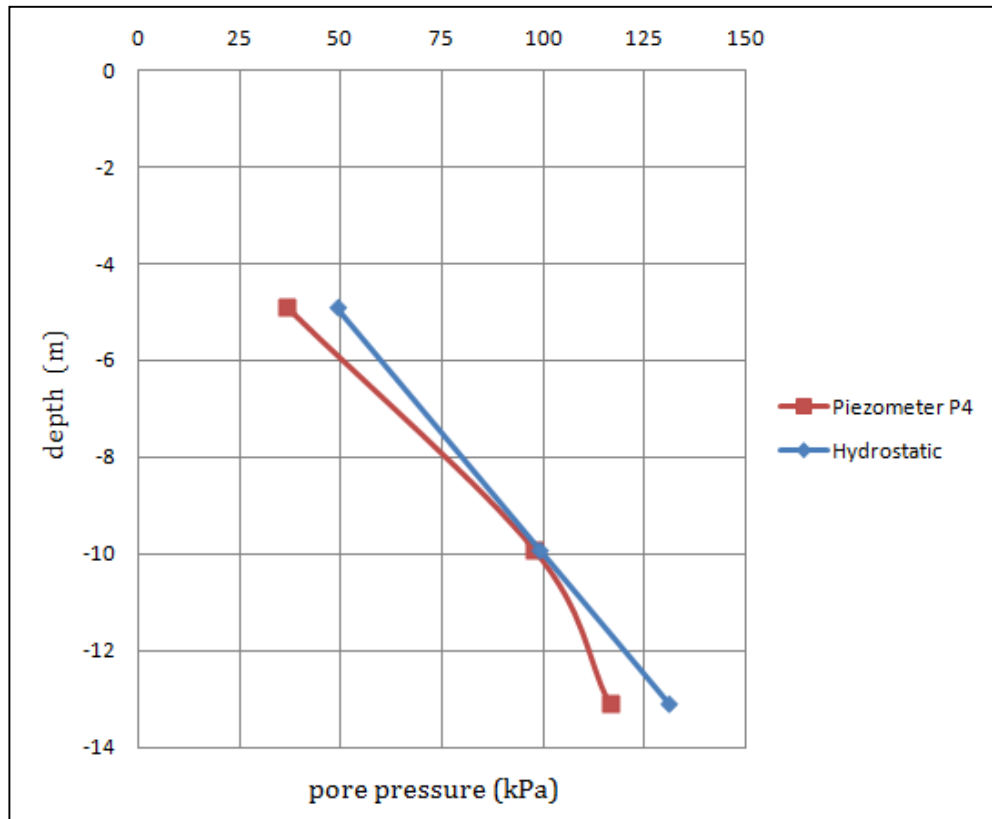


Figure 6. 7 Comparisons of hydrostatic pore pressure and piezometric pore pressure before pile driving at P4 station.

Therefore, pore pressure before piling was close to hydrostatic pore pressure, especially at 9,9m depth. We observe the same tendency at the other locations P1, P2 and P3 which were installed two weeks before driving starts (See appendices). As the pore pressure is hydrostatic before piling, the effect of the rain, snow or the river water fluctuation can be neglected.

6.5.2 Overview of Pore pressure increase

To have a general overview of the evaluation of pore water pressure in each piezometer, driving pore pressure u and the average, maximum and minimum pore water pressure before piling has been plotted.. For each piezometer, an increase of pore water pressure is observed when they start piling. It is obtained for P3 at 10m depth (Figure 6.8).

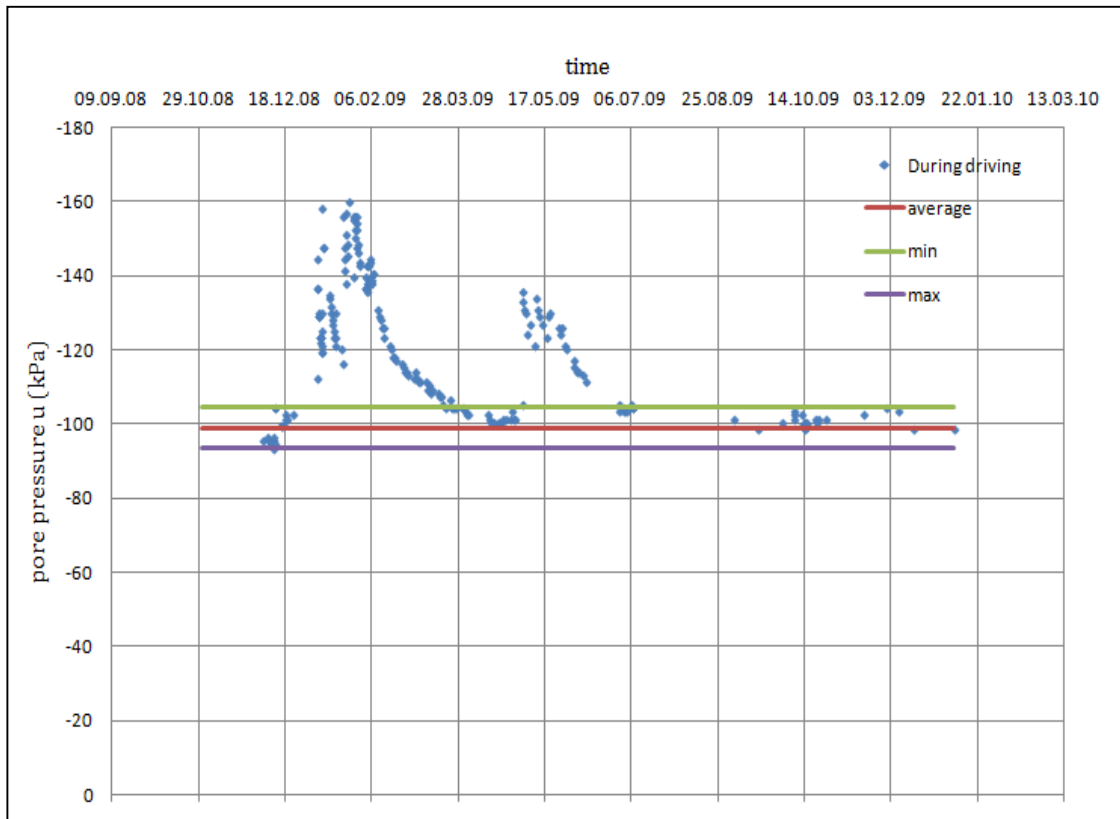


Figure 6. 8 Comparison of hydrostatic pore pressure and piezometric pore pressure before pile driving

Pore water pressure start increasing when piling start. During piling period, several increases and decreases in pore pressure depending on the distance between pile and piezometer occurred. During this period, pore water pressure goes down the maximum pore water pressure before piling but never reaches the average.

Finally, when piling is finished, pore water pressure decreased slowly and reached for the value of average pore pressure before piling on around the 20th of September, so approximately 3 months after the end of piling activities. After that, pore water pressure varies a bit between average and maximum pore pressure before piling. When water level measurement stopped, pore pressure is totally stabilized.

We can describe general pore pressure situation at different dates by the Figure 6.9 and 6.10 below. Two major increases in piezometer level are around 8m on 5th of January and around 4m on 7th of May which were extremely high for stability.

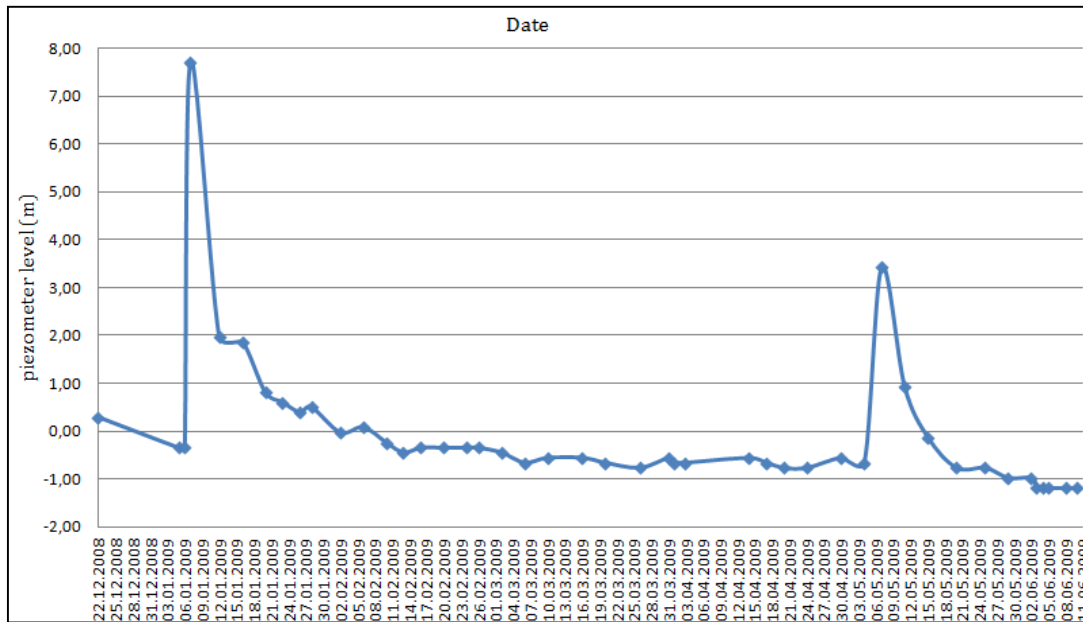


Figure 6. 9 Excess pore pressure at P4 (-9.9m) with time

Figure 6.11 will simplify the situation of pore water response at different piezometer for any individual pile. The excess pore pressure developed for driving half of G194 was highest at P3 station.

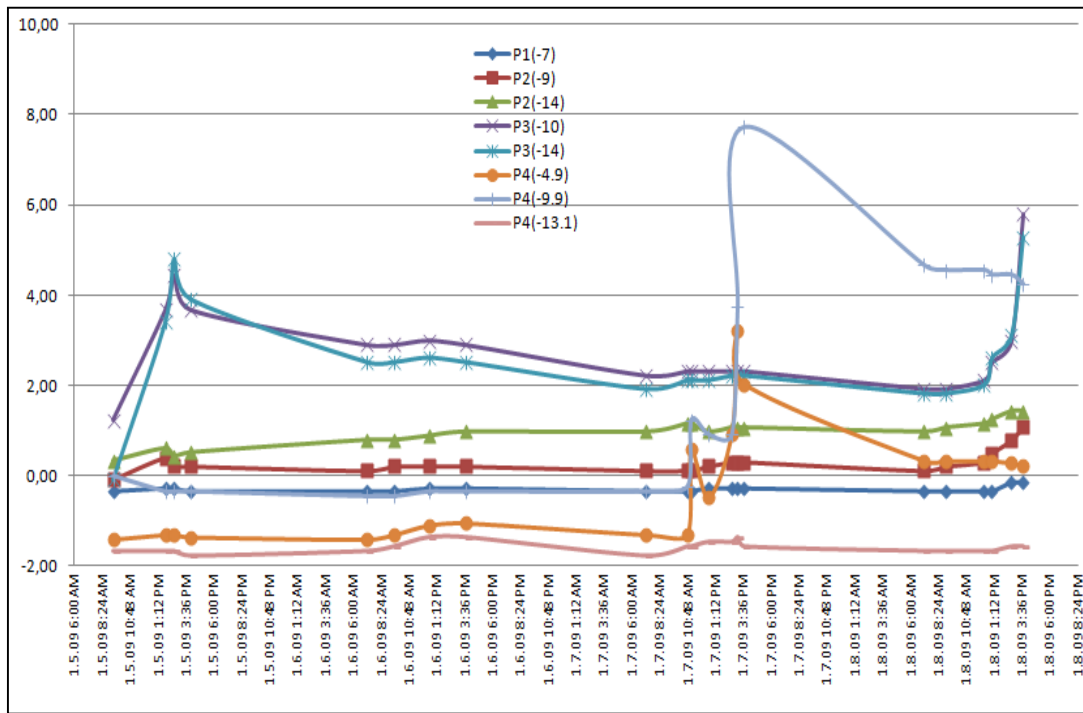


Figure 6. 10 Piezometer level in meter during piling.

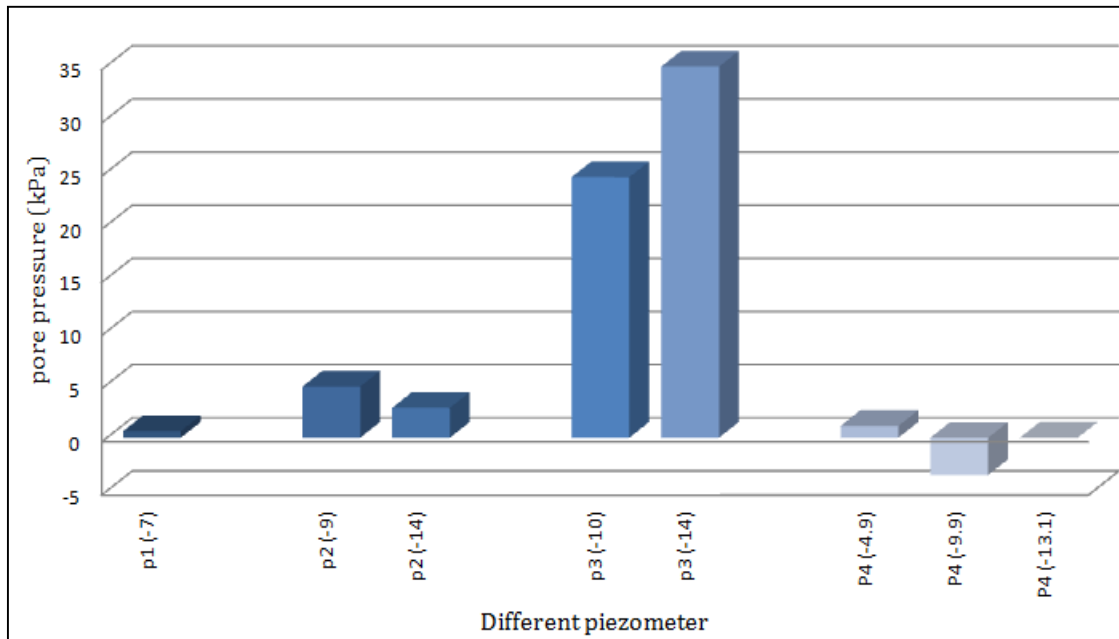


Figure 6. 11 Pore pressure response at different piezometer after driving half of G194.

We can conclude that pore water pressure increases and decreases with time. This can depend on the distance between pile and piezometer, the soil and the time of response of the

piezometer. Pile driving may be the major cause of this situation though we have other factors to consider such as movement of the pile driving equipment, transportation vehicles etc.

6.5.3 River water fluctuation

River water level of øvre sund remains almost constant throughout the year. Seasonal and tidal response in the river is not so pronounced. This situation is described in figure 6.12 where river water level variation with time has been showed. The highest river water level is +0.6m and the lowest is -0.5m from the zero reference point.

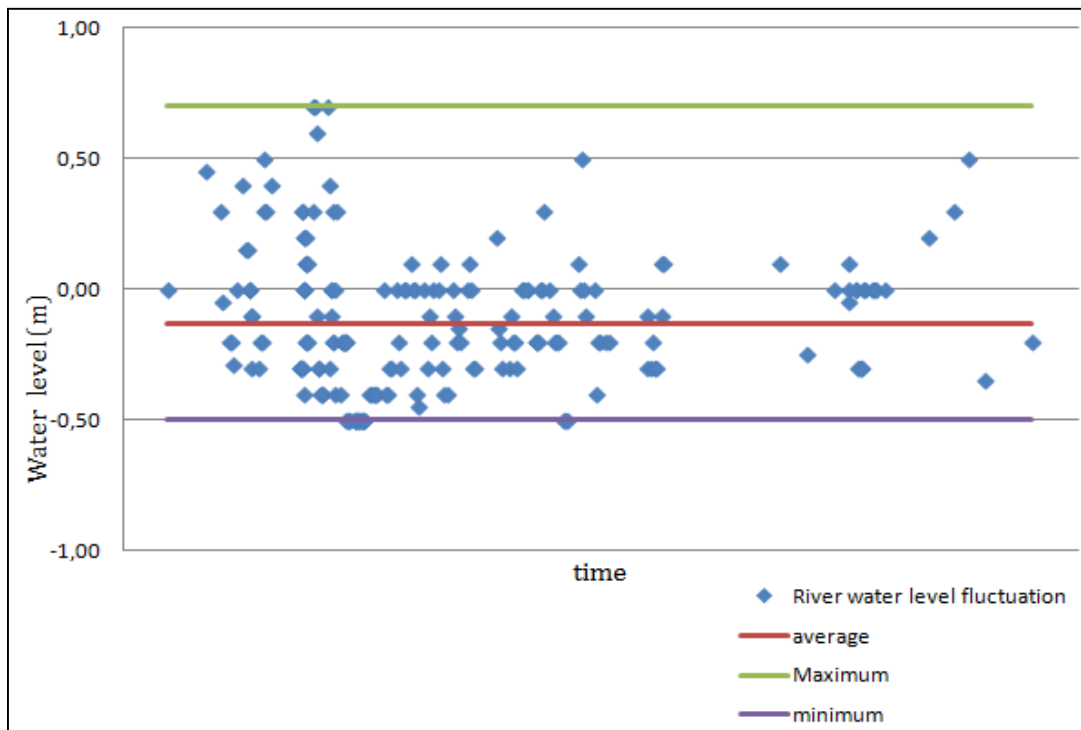


Figure 6. 12 River water fluctuation during driving.

6.5.4 Excess pore pressure with distance from driven pile

The most pronounced factor that affects the pore pressure generation during pile driving is the distance from the driven pile. Pore pressure generation close to the pile wall is extremely high. The magnitude of the driving pore pressure decreases rapidly with increasing distance. Several studies have been performed to describe this factor. Lo and Stermac (1965) reported maximum pore pressure in a limited volume of soil around the pile wall.

To see the effect of distance between pile and piezometer on the increase of pore water pressure, Figure 6.13 has been plotted. During driving of pile G201 in the axis K7, the responses of pore pressure at 8 different piezometers were plotted against the distance. The development of pore pressure was maximum at piezometer station P3. The value was recorded 50 kPa and 30 kPa for the two piezometers at P3 located at depth 14m and 10m respectively. This induced pore pressure decreases gradually with distance. Station P1 and P4 give no response due to driving as they are located far from the pile G201.

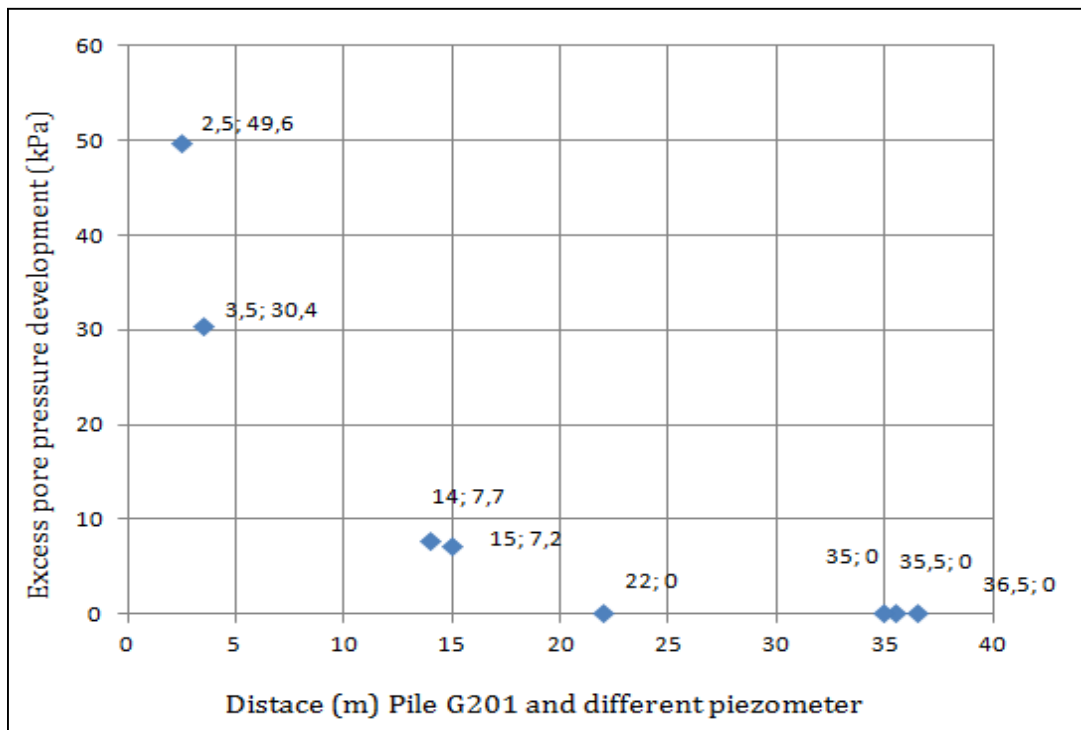


Figure 6. 13 Pore pressure response with distance

From the investigation of Lambe and Horn 1965, Orrje and Broms 1967, Poulos and Davis 1979, D'Appolonia and Lambe 1971, it can conclude that the excess pore pressures at the pile face may become equal to or even greater than the effective overburden pressure. Poulos and Davis (1979) summarized the excess pore pressure generation in terms of effective overburden with the increasing depth. The distance between pile and piezometer was normalized by the pile diameter. (Section 3.1 in chapter 3).

This dependency for øvre sund bridge project analyzed in the figure 6.14 below. During driving of different piles, the response in P3 (-10) has taken into account. The excess pore pressure is 30% of the effective overburden at the $\frac{\text{distance}}{\text{diameter}}$ ratio of 6, which is lower compared to the findings of Poulos and Davis (1979). This is may be because of the fact that the clay layer was thicker compared to the øvre sund. The pore pressure measurement along the pile wall and at the pile tip was not available for this study as the pile were not instrumented with the pore pressure cells. Poulos and Davis

Analysis and Modelling of induced pore pressures due to pile driving.

(1979) reported the excess pore pressures are virtually negligible beyond a distance of $s/r_o = 30$ which is also true for the øvre sund measurement.

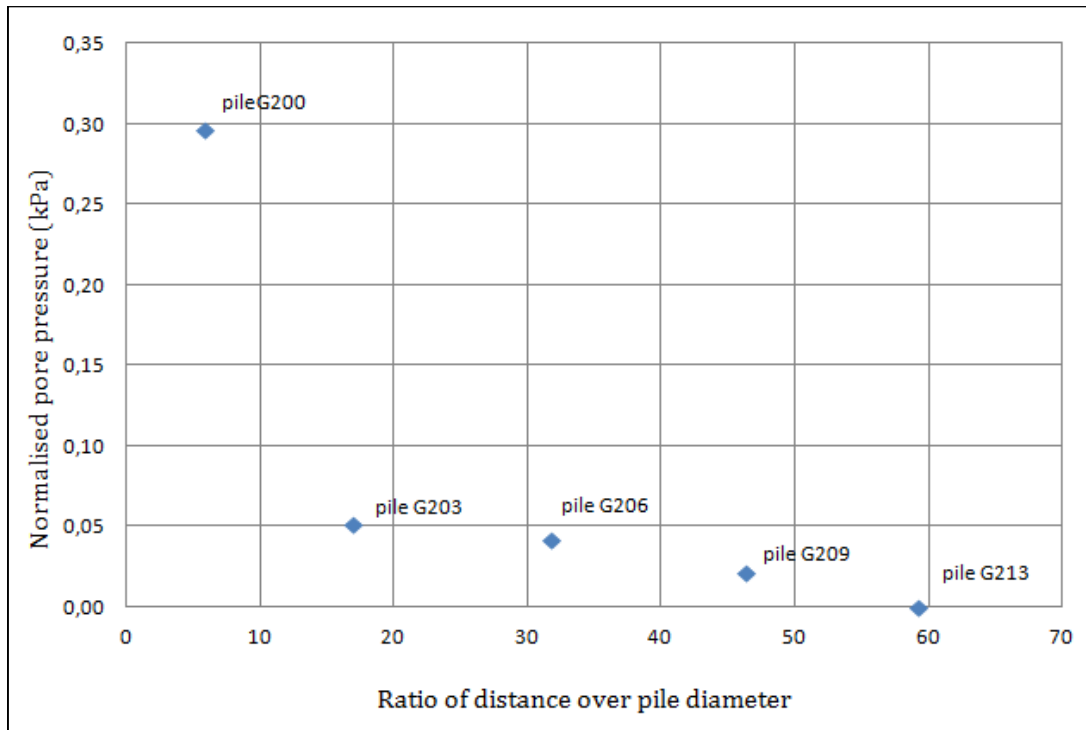


Figure 6. 14 Normalized pore pressure with distance-pile diameter ratio at P3. (-10)

The pore pressure dependency with the distance can be explained in another way. Different investigation have been taken to measure the distance beyond which the pore pressure response is negligible. According to Lo and Stermac (1965) or Bjerrum and Johannessen (1960), the driving pore pressure becomes negligible in the order of 10-20 pile diameter. (26) Same tendency has been observed in the case of øvre sund measurement. It can be shown for different piles. In figure 6.15 the response is plotted against the distance during driving Pile 184, 182, 213, 209, 206, 203 and 200. For every case induced pore pressure response is measurable within the distance 13 m from the pile wall. Therefore, the excess pore pressure becomes negligible beyond 13m from the pile center.

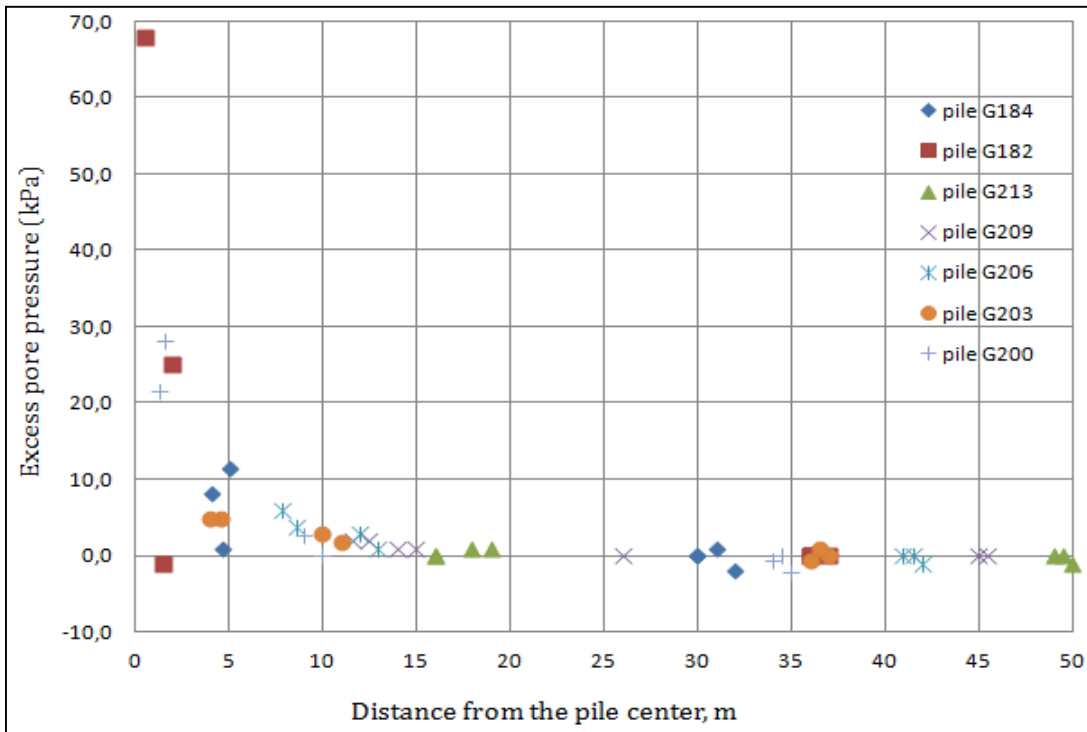


Figure 6. 15 Excess pore pressure response at all piezometers for driving of different pile.

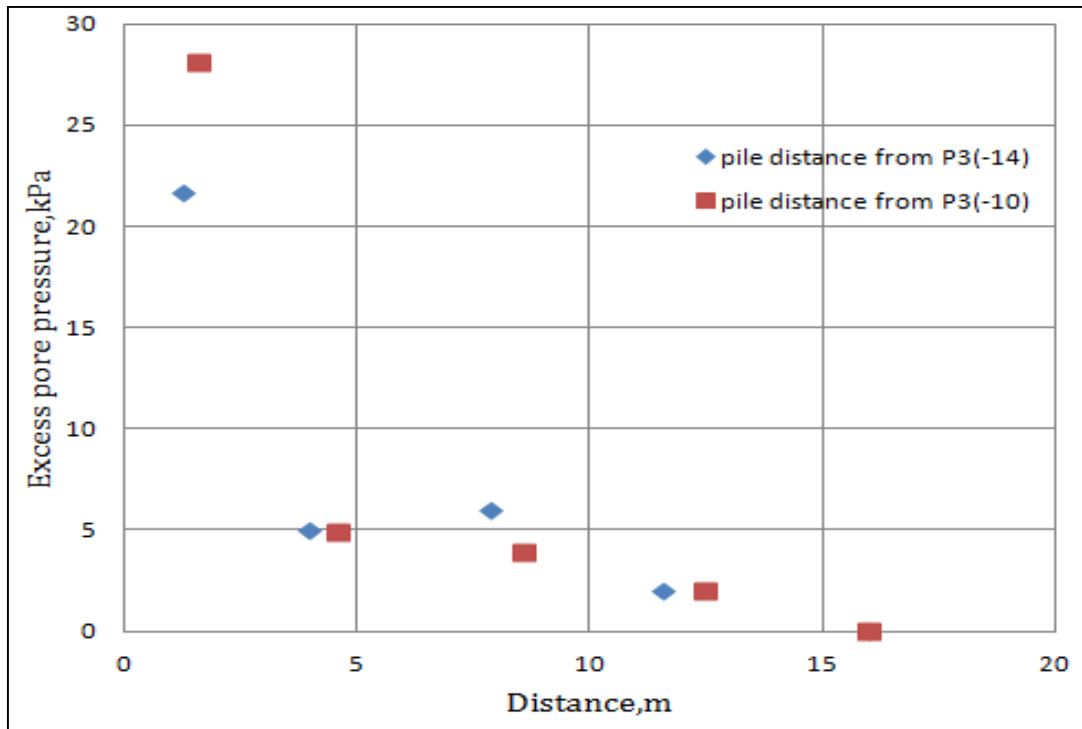


Figure 6. 16 Induced pore pressure variation with distance

Analysis and Modelling of induced pore pressures due to pile driving.

Figure 6.16 shows, even for the same station P3, pore pressure response differs significantly with the distance. During driving pile G200, P3(10) and P3(14) has variation in the pore pressure development. For both piezometer depth of 10m and 14m at station P3, pile no. G200 is the closest one, higher response can be found compared to other piles. The pore pressure development is small when a single pile is installed compared to several piles in a pile group. To keep the pore pressure increase in a certain limit closely spaced piles were not driven together.

When the increased pore pressure is very high for stability then the next pile had installed far from that specific pile.

6.5.5 Excess pore pressure with soil type

We will now look at similar diagrams as the above one, located at different depths. The first one (Figure 6.17) represent results from a piezometer located in clay and the second one results from a piezometer located in sand. (Figure 6.18)

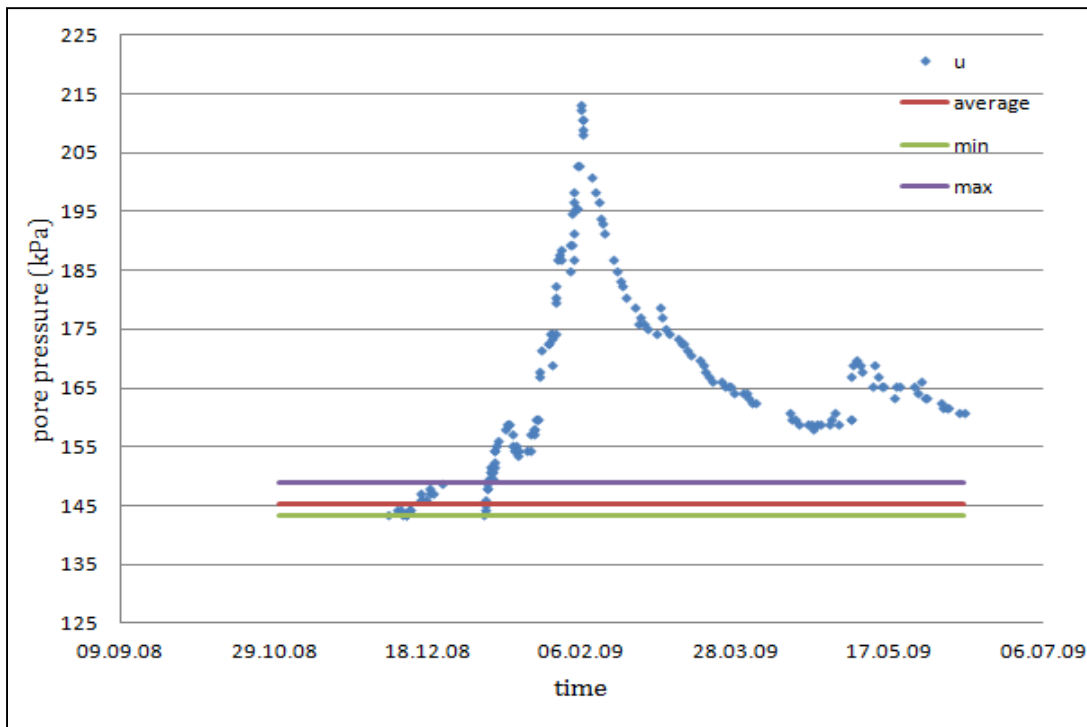


Figure 6. 17 Pore pressure responses from the clay layer

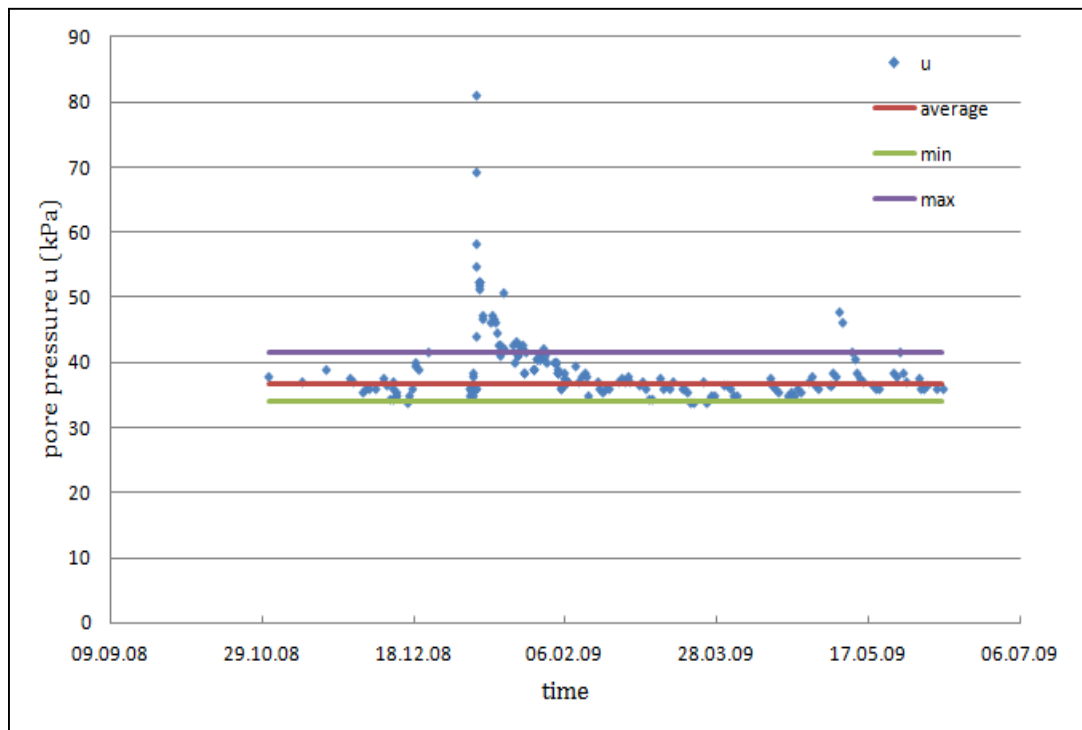


Figure 6.18 Pore pressure response from the sand layer

We observe that pore pressure increase for both at the beginning of piling activities but for the second one (Figure 6.18), pore pressure dissipates very quickly and reaches rapidly the average pore pressure before piling. During all period of piling, this piezometer only shows small variation between minimum and maximum pore pressure before piling. This is the typical behavior of a cohesionless soil.

On the other hand, the diagram (6.17) describes the response in a cohesive soil as pore pressure decreases more slowly.

6.5.6 Induced pore pressure variation with the depth of clay layer

Pore pressure development during pile driving also varies with the depth of clay layer. Higher response of pore pressure observed when the clay layer is thick. From the geotechnical report the clay layer is thin (5-6m) where pile G183 and G185 are located compared to the location of pile G202 and G205. The response of the pore pressure with distance is less pronounced for pile G183 and G185 with the only exception at P4 (9.9m) which is very close to the pile. The other piezometers give no response even

Analysis and Modelling of induced pore pressures due to pile driving.

which is only 4m away from the pile in figure 6.19. Therefore, it can conclude that the excess pore pressure development depends not only with the distance but also with the thickness of clay layer.

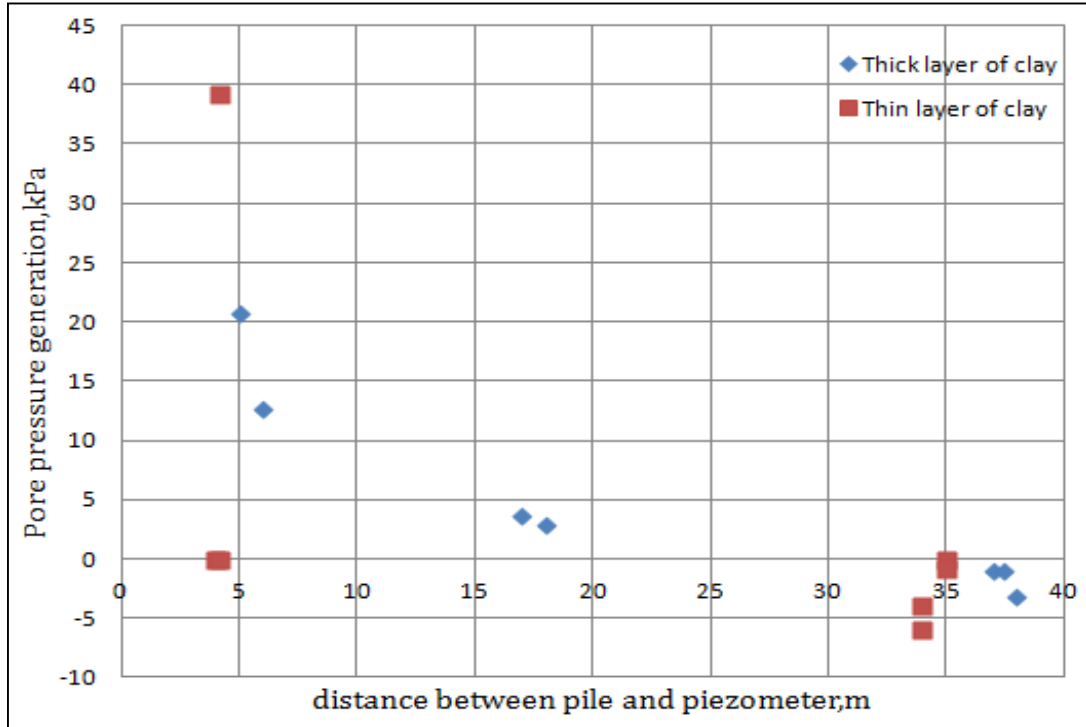


Figure 6. 19 Induced pore pressure variation with clay layer depth.

6.5.7 Pore pressure variation during driving through different soil layer

K. D. Eigenbrod et al. (1996) reported higher pore pressure development in the clay layer while driving through the underlying dense sand than driving through the clay layer. This mechanism has been described in section 3.3 in chapter 3. They reported that the clay was loaded from below as the piles were driving into the very dense sand.

This tendency has been observed in the case of Øvre sund project. To analyze this fact, three piles namely G184, G182, G201 has been considered. The piles are 25 m long. The pore pressure measurement after driving 12m and full driving has been plotted in the figure 6.20 to compare the contribution. During driving in the first phase i.e. until 12m, the pile went through clay layer, while in the second phase, piles met the underlying

dense moraine. The response of pile G182 and G201 were as high as 70 and 50 kPa respectively during second phase.

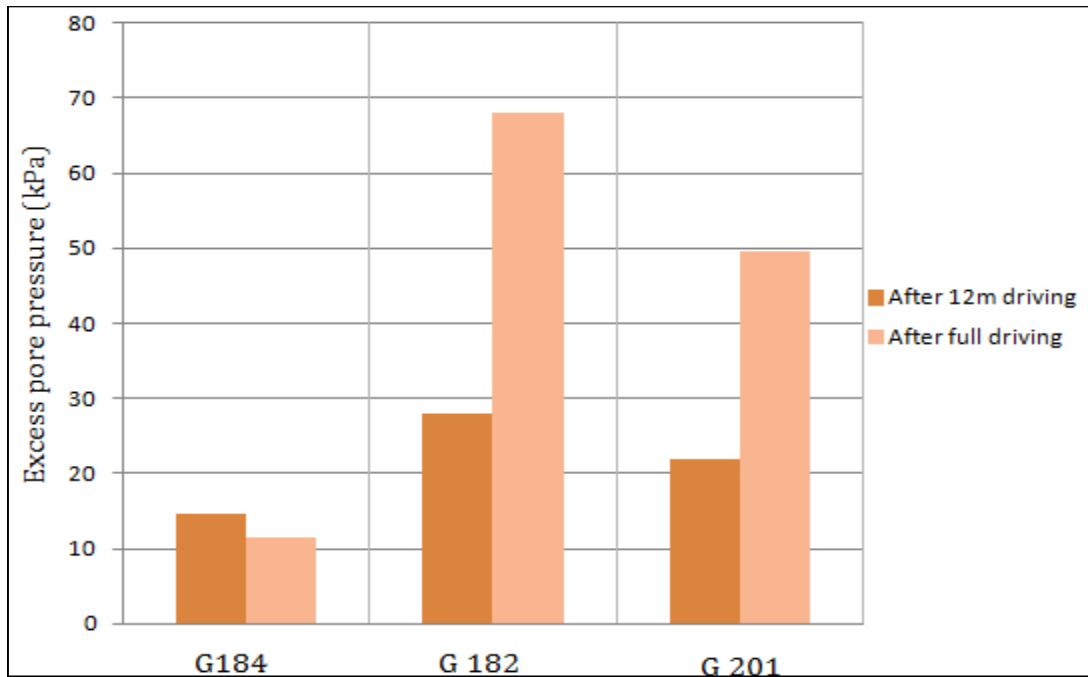


Figure 6.20 Induced pore pressure variation with clay layer depth.

6.5.8 Driving pore pressure at øvre sund by Lo and Stermac approach

Lo and Stermac (1965) proposed the solution to predict the driving pore pressure around the pile wall. The equation described in the section 3.1.1 in chapter 3, which is valid for normally consolidated soil.

$$\Delta u_m = [(1 - k_0) + \left(\frac{\Delta u}{p'}\right)_m * \sigma'_{v0}] \dots \dots \dots (6.1)$$

Where,

k_0 = Coefficient of earth pressure at rest = $1 - \sin\phi$

p' = initial consolidation pressure

σ'_{v0} = effective overburden pressure.

$\left(\frac{\Delta u}{p'}\right)_m$ = Pore pressure ratio measured at CIU triaxial test

Analysis and Modelling of induced pore pressures due to pile driving.

The pore pressure ratio measure in the conventional consolidated-undrained triaxial test with pore pressure measurements generally assumes in the order 0.6-0.8 (26). Blanchet (1976) found that the pore pressure ratio becomes constant when the consolidation pressure used in the test is preconsolidation pressure, σ'_p . He proposed maximum pore pressure ratio of 0.70 for marine clay (4). From friction angle φ we calculated the coefficient of earth pressure at rest. Putting the values into equation (6.1), we got the maximum calculated driving pore pressure which was compared with measured value from the field. The predicted pore water pressure was considerably higher than the measured one. This is may be due to the fact that pore pressure measurements were made far from the pile whereas the Lo and stermac equation is applicable at the pile surface.

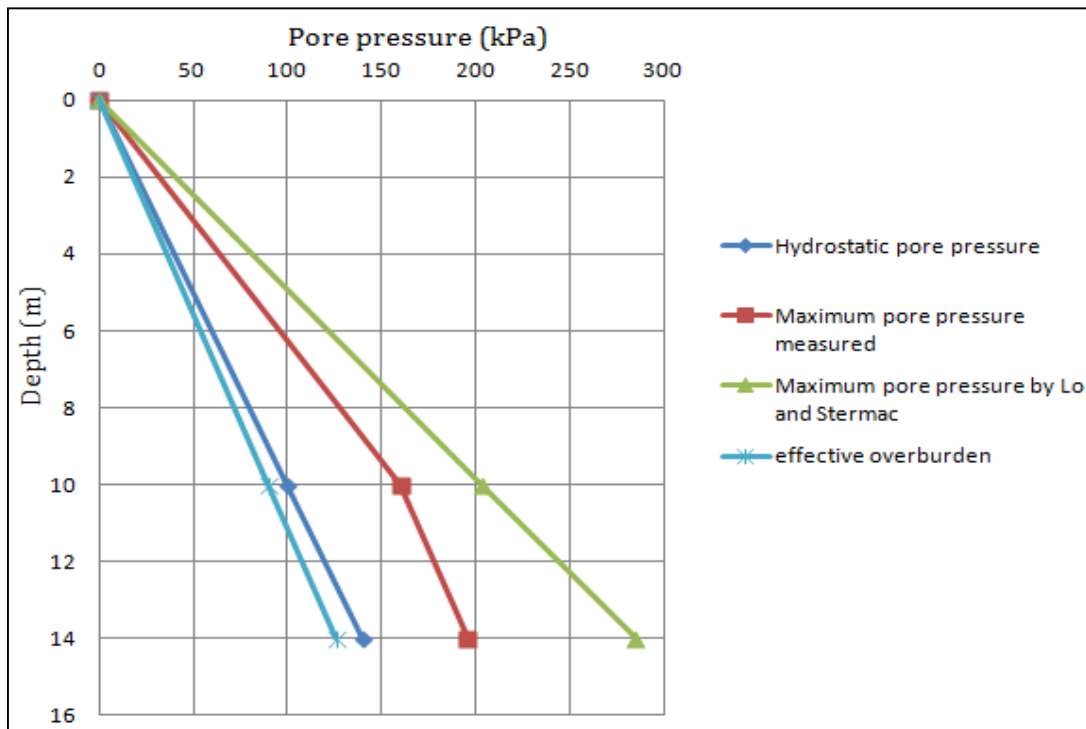


Figure 6. 21 Comparison of measured and calculated pore pressure at piezometer location P2 in Øvre sund project, Drammen.

6.5.9 Pore pressure as a function of overburden pressure

The maximum pore pressure developed in the different piezometer stations are compared to the effective and total overburden pressure of the øvre sund project. In

Analysis and Modelling of induced pore pressures due to pile driving.

figure 6.22, the pore pressure is plotted against the depth. As the ground water level is at surface, the hydrostatic pore pressure has plotted in the graph for P3 at the level 10m and 14m from the ground level. The figure 6.22 shows that the excess pore pressure is 70-80% the effective overburden pressure which is much lower than the value observed by Roy et al. (1981) (Table 3.1 for pore pressure along the shaft) at Saint-Alban test site, whereas the ratio $\frac{\Delta u_m}{\sigma_{vo}}$ is about 0.2 which also lower than Roy et al. (1981). This lower value results from the fact that the pore pressure was not measured along the shaft as the piezometers were placed far from the piles at Øvre sund.

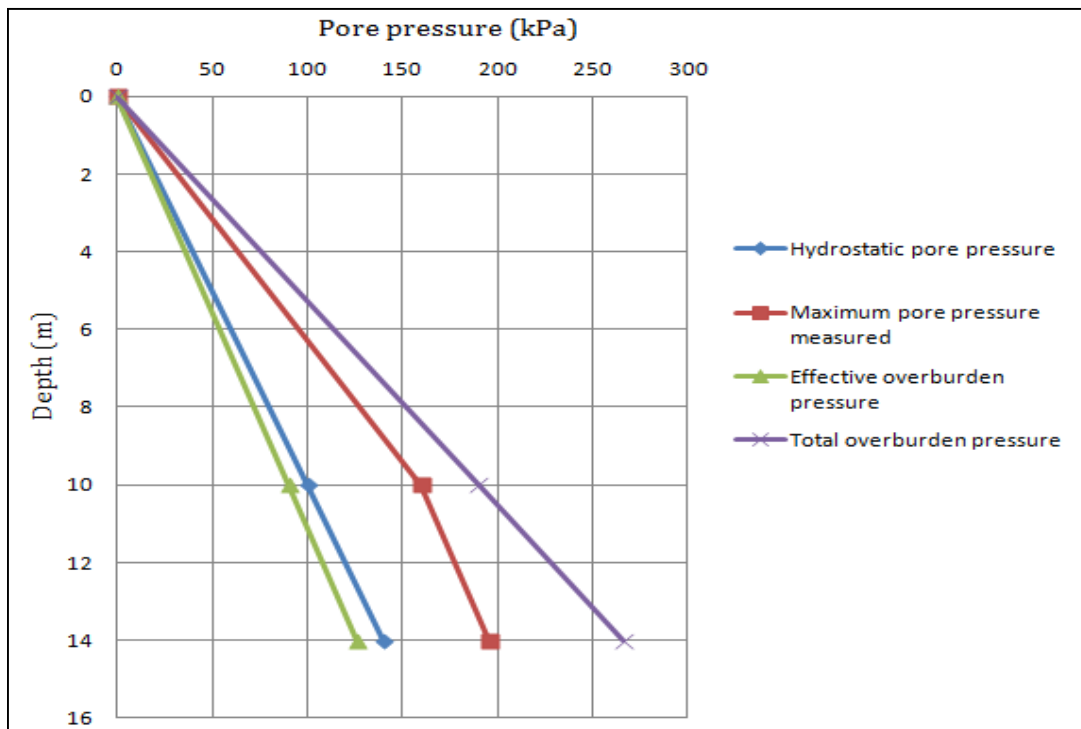


Figure 6. 22 Comparison of measured pore pressure at piezometer location P3 with the effective and total overburden pressure in Øvre sund project, Drammen.

6.6 Analysis of øvre sund data with cavity expansion theory

6.6.1 Perfectly plastic soil model

If the soil is modeled as an ideal linear-elastic, perfectly plastic material, the stresses and pore pressures induced within the soil surrounding an expanding cavity can be calculated using closed-form solutions. (Gibson and Anderson, 1961 and Vesic, 1972).

Analysis and Modelling of induced pore pressures due to pile driving.

The solutions have been described in section 4.1 in chapter 4. In the analysis only the clay layer has been considered. Therefore, the clay parameters was used for the calculations.

6.6.1.1 Radial cavity pressure

Cavity expansion from zero radiuses is expected to take place at a constant cavity pressure. This constant radial cavity pressure from equation 4.30,

$$\sigma_{rr} = \sigma_{h0} + s_u \left[1 + \ln \frac{G}{s_u} \right]$$

σ_{h0} = Total horizontal stress.

s_u = Undrained shear strength.

G = Shear modulus = $\frac{E}{2(1+\nu)}$

E = Elastic modulus = $\frac{3}{2}$ Oedometer modulus = $\frac{3}{2} * 4000 = 6000 \text{ kPa}$

ν = undrained poison's ratio = 0.5 (38)

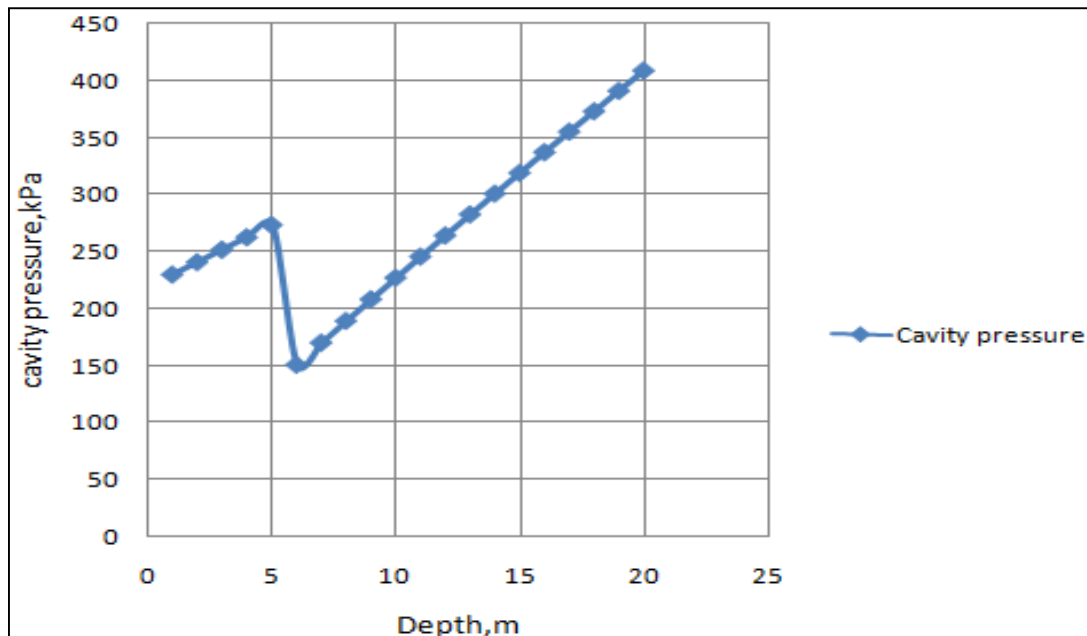


Figure 6. 23 Radial pressure to expand the cavity with depth.

Analysis and Modelling of induced pore pressures due to pile driving.

The pressure which extends the cavity from zero radiuses varies with the depth. This pressure is a function of total horizontal stress and undrained shear strength those increase with depth. Other parameters in the equation considered constant. Elastic modulus is taken to $3/2$ times of oedometer modulus in the normally consolidated range (Section 5.25 in chapter 5). Taking undrained Poisson's ratio is equal to 0.5, the shear modulus can be calculated as 2000 kPa. The variation of cavity pressure with depth is plotted in figure 6.23. It has been observed that the cavity pressure increases until 5m, after sudden reduction it increases again with the depth. In øvre sund project, the top sand layer is located within 5m in average, below this layer clay is located. When the layer changes from sand to clay, the cavity pressure drop down as it is the function of undrained shear strength. To show this affect, average undrained shear strength value was not used. This phenomenon has been described in chapter 4 (Figure 4.11) which matches with this finding.

6.6.1.2 Radius of the plastic zone

Due to the increase in cavity pressure, the expansion of a cavity occurs. Further increase in cavity pressure will lead to the formation of a plastic zone around the cavity. This zone is considered as the most disturbed zone of soil during expansion of cavity. Beyond this radius, the rest of the soil mass remains in a state of elastic equilibrium. As the soil mass is disturbed high excess pore pressure generated in this zone. The radius of this plastic zone can be determined by the relation described in equation 4.4 in chapter 4.

$$\frac{R_p}{r_0} = \sqrt{\frac{E}{2(1 + \nu)s_u}}$$

Here,

R_p =radius of the plastic zone.

$$\frac{R_p}{r_0} = \sqrt{\frac{6000}{2(1 + 0.5) * 21.5}}$$

r_0 =Radius of the pile=0.135m

$$R_p = 1.3 \text{ m}$$

Considering the average s_u value, the radius of plastic zone using Elastic-plastic soil model becomes 1.3m.

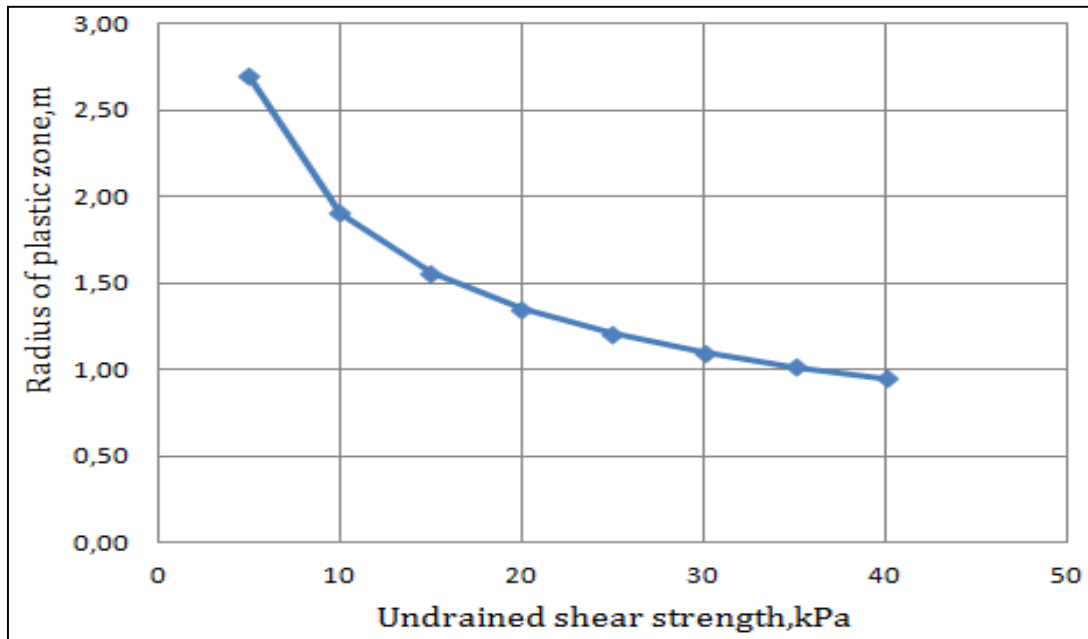


Figure 6.24 Radius of plastic zone with undrained shear strength.

Although it was assumed constant average s_u in the calculation, the Radius varies with the different s_u value. It has been described in figure 6.24. The radius of the plastic zone has an inverse relation with s_u . For undrained shear strength value less than 10, the radius becomes more than 2.0m, which is high. The clay layer of øvre sund has s_u value in the range of 10-30 kPa varying with depth.

6.6.1.3 Excess pore pressure within the plastic zone

As it is mentioned earlier, the response of pore pressure in the plastic zone is high because of the disturbance of soil around the cavity. This high excess pore pressure development is calculated by the relation described in equation 4.12 and 4.13 in chapter 4.

$$\Delta u = 0.817\alpha_f s_u + 2s_u \ln\left(\frac{R_p}{r}\right)$$

Here,

$$\alpha_f = \frac{1}{\sqrt{2}}[3A_f - 1]$$

$$\Delta u = 0.817 * 0.778 * 21.5 + 2 * 21.5 \ln\left(\frac{R_p}{r}\right)$$

$$\alpha_f = \frac{1}{\sqrt{2}}[3 * 0.7 - 1] = 0.778$$

$$\Delta u = 13.7 + 43 \ln\left(\frac{R_p}{r}\right)$$

Analysis and Modelling of induced pore pressures due to pile driving.

Taking the radius of plastic zone $R_p = 1.3$, for different distance from the pile center, the excess

pore pressure calculated has given in table 6.2 below-

Table 6. 2 Pore pressure generation in plastic zone by cavity expansion theory.

| Distance from pile center, r in meter. | Excess pore pressure, Δu in kPa |
|--|---|
| 0.25 | 85 |
| 0.50 | 55 |
| 0.75 | 37 |
| 1.00 | 25 |
| 1.25 | 15 |

6.6.1.4 Excess pore pressure within the elastic zone

Beyond the plastic zone, the soil is considered to be in a state of elastic equilibrium. Therefore the equation to determine the pore pressure in the elastic zone is different from that of plastic zone. From equation 4.14,

$$\Delta u = 0.817 \alpha_f s_u \left(\frac{R_p}{r}\right)^2$$
$$\Delta u = 0.817 * 0.778 * 21.5 * \left(\frac{R_p}{r}\right)^2$$
$$\Delta u = 13.7 * \left(\frac{R_p}{r}\right)^2$$

For different distance from pile center, the response of pore pressure in the elastic zone is given in table 6.3.

Table 6.3 Pore pressure generation in the elastic zone by cavity expansion theory.

| Distance from pile center, r in meter. | Excess pore pressure, Δu in kPa |
|--|---|
| 2.0 | 5.80 |
| 2.5 | 3.70 |
| 3.5 | 1.90 |
| 14.0 | 0,20 |
| 15.0 | 0,10 |
| 25.0 | 0,04 |
| 35.0 | 0,02 |
| 36.0 | 0,02 |
| 40 | 0.01 |

Beyond the distance 15m from pile center the response become constant and negligible.

6.6.1.5 Excess pore pressure at cavity wall

For a saturated elastic completely plastic material abiding by Mohr-Coulomb yield criterion, the pore pressure development on the surface of the pile from equation 4.18 in chapter 4:

$$\frac{\Delta u_{max}}{s_u} = \ln \left[\frac{E}{2(1 + \nu)s_u} \right] + 1.73A_f - 0.58$$

Where $A_f=0.7$ for NC clay (Das, B.M 1983)

To simplify the analysis it is assumed average undrained shear strength of clay, $s_u=21.5$ kPa.

$$\frac{\Delta u_{max}}{s_u} = \ln \left[\frac{6000}{2(1 + 0.5) * 21.5} \right] + 1.73 * 0.7 - 0.58$$

$$\Delta u_{max} = 111 \text{ kPa}$$

According to cavity expansion theory, the excess pore pressure development at cavity wall is as high as 111 kPa.

6.6.1.6 Comparison of measured and calculated value by cavity expansion

The excess pore pressure measured in the øvre sund fits very well with the calculated value by cavity expansion. In figure 6.25, the comparison is plotted against the distance. During driving of pile G201, the excess pore pressure response is considered in this case. However, the measured value is bit high, both results shows the same dependency with the distance. The excess pore pressures becomes negligible beyond the distance 13-15m from the pile center by cavity expansion solution.

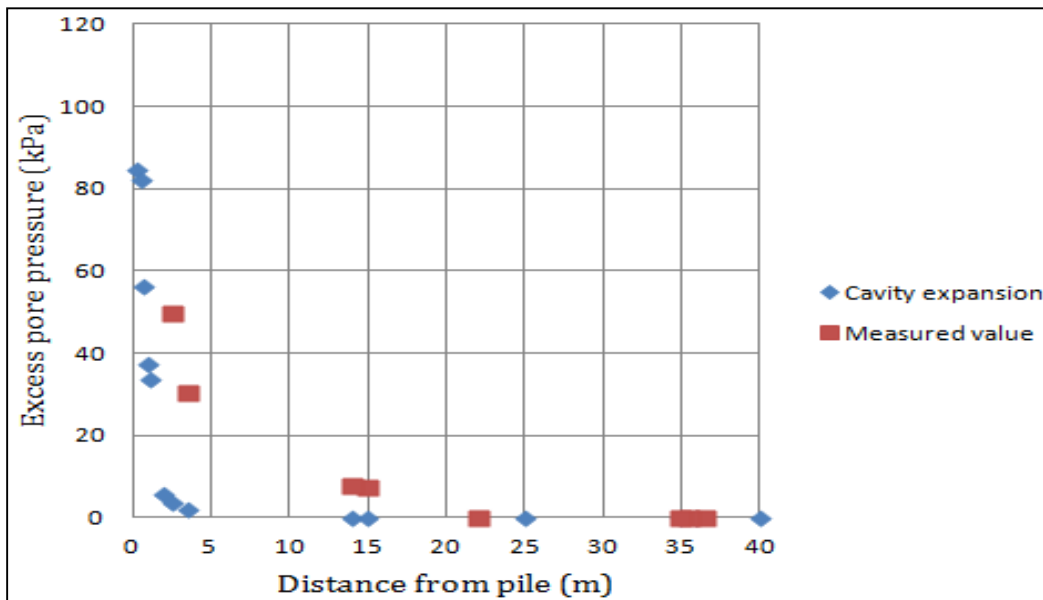


Figure 6. 25 Comparison of the development of pore pressure in the plastic and elastic zone by cavity expansion and øvre sund.

6.6.2 Modified Cam clay model

6.6.2.1 Radial cavity pressure

Immediately after driving, the soil adjacent to the pile is at failure, with the effective stresses given by the conditions at the critical state in the Cam-clay model in Equation 4.32:

$$\sigma'_{rr} = [1 + (\sqrt{3}/M)]s_u$$

$M = \text{slope of the } p' - q \text{ graph}$

Analysis and Modelling of induced pore pressures due to pile driving.

M can be determined from the friction angle, φ' in the way,

$$M = \frac{6 \sin \varphi'}{3 - \sin \varphi'} = \frac{6 \sin 26^\circ}{3 - \sin 26^\circ} = 1.03$$

Considering three depths in bore hole 12 Grønland part (8.4m, 11.4m and 15.3 m) from which the samples were taken for CAU triaxial tests. Considering corresponding S_u value at these depths, the radial pressure required to expand the cavity is given in the table below:

$$\sigma'_r = [(\sqrt{3}/M) + 1]s_u = [(\sqrt{3}/1.03) + 1] * 31 = 83 \text{ kPa}$$

Table 6. 4 Radial cavity pressure with MCC model for different depth.

| Depth, m | S_u , kPa | σ'_r , kPa |
|----------|-------------|-------------------|
| 8.4 | 20 | 53.6 |
| 11.4 | 24 | 64.3 |
| 15.3 | 31 | 83 |

6.6.2.2 Radius of the plastic zone

After the initial yielding at the cavity wall, a zone of soil extending from the cavity wall to a radial distance r_p will become plastic as the cavity pressure continues to increase. The radius of plastic zone using Cam clay model depends on various factors, such as deviatoric stress at the elastic-plastic boundary. This deviatoric stress is sensitive to the isotropic overconsolidation ratio, R .

Determination of isotropic overconsolidation ratio, R :

Isotropic overconsolidation ratio R is different from the conventional overconsolidation ratio (OCR). The later is defined in terms of effective vertical stress.

Isotropic overconsolidation ratio, $R = \frac{p'_c}{p'_0}$ (6.2)

Where,

p'_c is the maximum isotropic mean preconsolidation stress. p'_0 =initial mean effective stress.

Analysis and Modelling of induced pore pressures due to pile driving.

Modified cam clay model was developed based on triaxial compression test on isotropically consolidated samples (9). The samples from the grønlund side of Øvre sund for triaxial test was anisotropically consolidated. Therefore, samples from the river at borehole 19 has been considered (Figure 5.8 in chapter 5). The clay layer in the river is slightly overconsolidated. The initial mean effective stress $p'_0 = 49$ kPa for samples at 3.5m depth. To calculate the maximum isotropic mean preconsolidation stress p'_c , the following procedure has been followed (39):

The initial confining pressure is 49 kPa.

The past vertical effective stress σ'_y ,

$$\sigma'_y = \text{OCR} * 49 = 1.25 * 49 = 61.25 \text{ kPa (assuming OCR} = 1.25)$$

$$K_0 = 1 - \sin \varphi = 1 - \sin 26^\circ = 0.56$$

$$\sigma'_z = \sigma'_x = 0.56 * 61.25 = 34.3 \text{ kPa}$$

$$\sigma'_{mean} = (61.25 + 34.3 + 34.3) / 3 = 43.3 \text{ kPa}$$

The shear stress q at the past mean stress,

$$q = \frac{1}{\sqrt{2}} \sqrt{(\sigma'_y - \sigma'_x)^2 + (\sigma'_z - \sigma'_y)^2 + (\sigma'_x - \sigma'_z)^2}$$

$$q = 26.95 \text{ kPa}$$

Currently the sample is isotropically consolidated to 49 kPa.

Now, the maximum isotropic mean preconsolidation stress, $p'_c = \frac{1}{M^2 p} q^2 + M^2 p = 61.75$

kPa

Using equation 6.2, the calculated $R = \frac{61.75}{49} = 1.26$

Therefore, the size of plastic zone has been determined using this average $R=1.26$

The deviatoric stress at the elastic-plastic boundary,

$$q_p = M p'_0 \sqrt{R - 1}$$

$$q_p = 1.03 * 49 \sqrt{1.26 - 1} = 25.7 \text{ kPa}$$

Table 6. 5 Different parameters to calculate size of the plastic zone.

| Depth | p'_0 | R | q_p |
|-------|--------|------|-------|
| 3.2 | 15 | 1.26 | 7.8 |
| 3.3 | 31 | 1.26 | 16.3 |
| 3.5 | 49 | 1.26 | 25.7 |

Considering various deviatoric stress, the radius of plastic zone can be determined by,

$$\left(\frac{r_p}{a_u}\right)^{m+1} = \frac{G\sqrt{m+2}}{q_p}$$

Here,

a_u =cavity radius.

$m=1$ for cylindrical cavity.

r_p = radius of the plastic zone.

Table 6. 6 Size of the plastic zone with depth.

| Depth | r_p |
|---------|-------|
| 3.2 | 2.8 |
| 3.3 | 1.96 |
| 3.5 | 1.5 |
| average | 2.08 |

The width of the plastic zone decrease with the depth as the deviatoric stress increases. The plastic radius calculated by Elastic-plastic model was 1.3 which is much lower than the value calculated by MCC. The plastic radius for Elastic-plastic model has been calculated for average depth. In the upper layer where s_u is lower, the radius is higher which is shown in Fig. (6.24). For MCC model, the radius is also decreasing with increasing depth. Therefore, the plastic radius calculated by two methods fits very well.

6.6.2.3 Excess pore pressure distribution in the plastic zone

Excess pore pressure development by MCC model in the plastic zone from equation 4.29:

$$\Delta u = \frac{2m}{\sqrt{m+2}} q_u \ln\left(\frac{r_p}{r}\right) + p'_0 \left[1 - \left(\frac{R}{2}\right)^\Lambda\right]$$

Where,

$m = 1$ for cylindrical expansion.

$R =$ Isotropic overconsolidation ratio $= \frac{p'_c}{p'_0}$

$M = 1.03$

$\Lambda =$ Plastic volumetric strain ratio,
Typical value = 0.75

$q_u =$ ultimate deviatoric stress $= p'_0 \left(\frac{R}{2}\right)^\Lambda$

$r =$ distance from the center of the cavity, m.

$p'_0 = 49 =$ initial mean effective stress.

$p'_c = 61.75 =$ Maximum isotropic mean
preconsolidation stress.

Table 6. 7 Ultimate deviatoric stress with depth.

| Depth | q_u |
|-------|-------|
| 3.2 | 10.7 |
| 3.3 | 22 |
| 3.5 | 34.8 |

Putting different value of q_u , p'_0 and R , the excess pore distribution with different depth is plotted in the figure. 6.26. Very high pore pressure development has been observed at depth 3.5m compared to depth 3.2m.

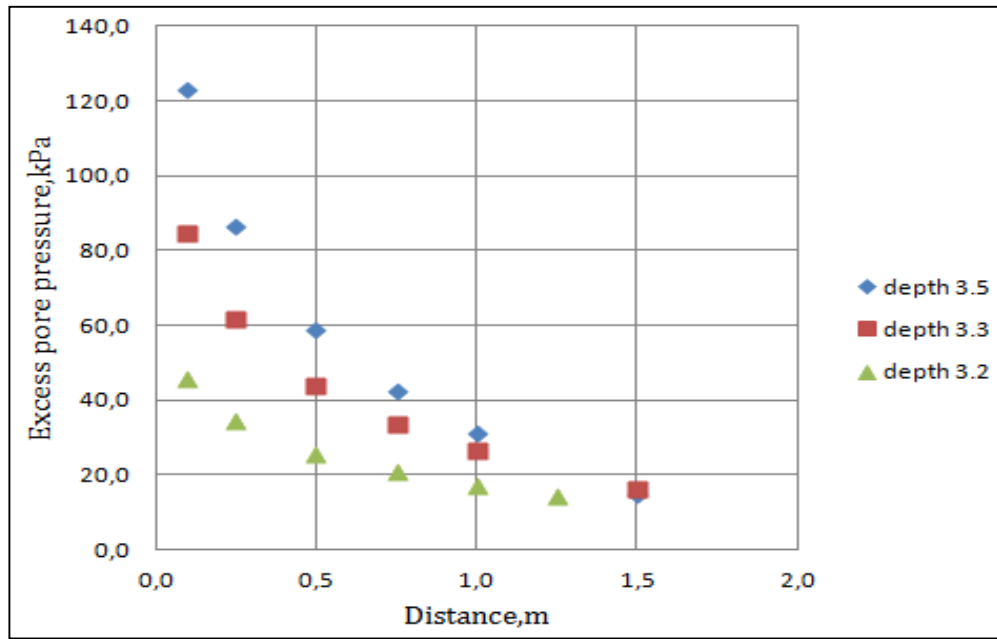


Figure 6. 26 Excess pore pressure at plastic zone by MCC at different depth.

The excess pore water distribution with the perfectly plastic model is compared with the MCC model. Taking the average value of excess pore pressure by MCC, it has been plotted in the figure 6.27 against the distance limited in the plastic zone.

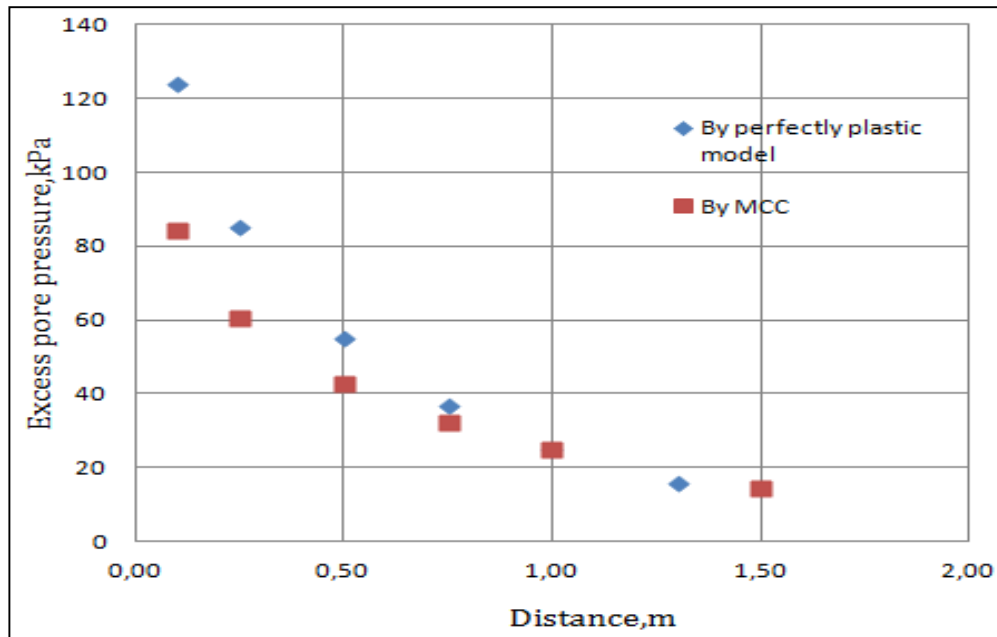


Figure 6. 27 comparison of excess pore pressure at plastic zone by MCC and perfectly plastic model.

6.6.2.4 Excess pore pressure at cavity wall

The pore pressure results at the cavity wall proposed by Randolph et al. (1979) are represented in equation 4.33:

$$\Delta U = U - U_0 = (P'_0 - P'_f) + S_u \ln \frac{G}{S_u}$$

P'_0 =in-situ mean effective normal stress.

P'_f = mean effective normal stress at failure.

From the triaxial test results in the form of $p' - q$ graph (Figure 5.7), P'_0 and P'_f can be found at different depth. Taking the corresponding value of S_u for depth 8.4m, 11.4m and 15.3m, the excess pore pressure at cavity wall is given in table 6.8:

Table 6. 8 Excess pore pressure at cavity wall at different depth wih MCC model.

| Depth , m | P_0 (Kpa) | P_f (kpa) | $P_0 - P_f$ (Kpa) | S_u (Kpa) | Δu (Kpa) |
|-----------|-------------|-------------|-------------------|-------------|------------------|
| 8.4 | 105 | 85 | 20 | 20 | 112 |
| 11.4 | 154 | 136 | 18 | 24 | 124 |
| 15.3 | 203 | 180 | 23 | 31 | 153 |

6.7 Pore pressure dissipation

At the Drammen site pile driving was completed at mid of May, 2009. After driving had finished excess pore pressures start to dissipate with time. The dissipation at piezometer P3 (-14) is plotted in the Figure 6.28

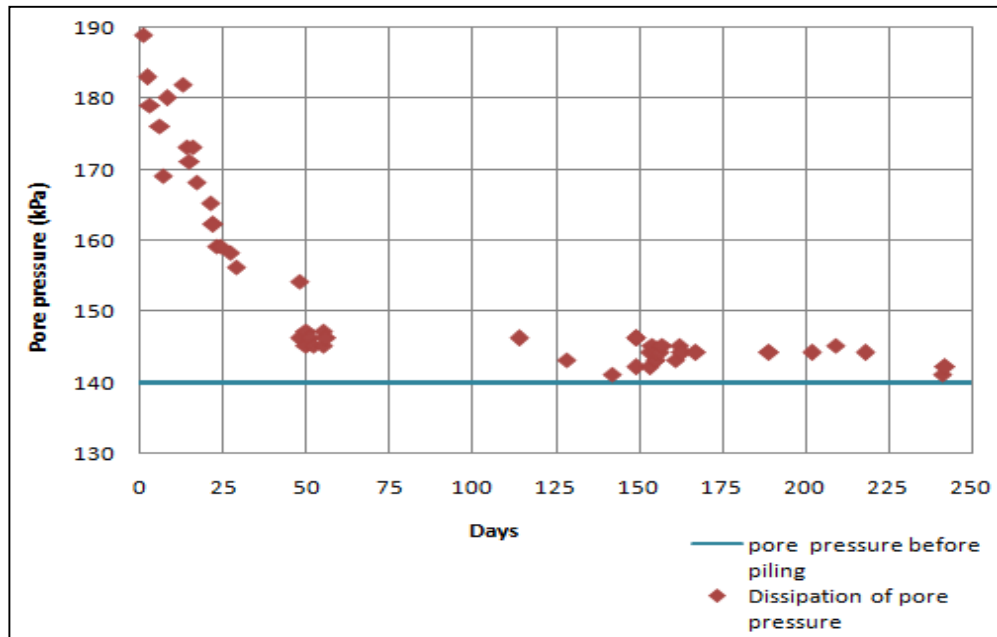


Figure 6. 28 Excess pore pressure dissipation with time after driving at P3 (-14).

The excess pore pressure after driving has been reduced gradually with time. The rate of dissipation is very rapid within first 30 days. After that pore pressure dissipates very slowly with time. On 19.05.2009 (After 7 days), the pore pressure was increased little though there was no driving at that time, may be this is because of construction of pile cap or moving of pile driving machines. Within the first one month, 70% of the excess pore pressure was dissipated whereas only 10% of excess pore pressure had remained after 3 months. The same situation was observed at piezometer P3 (-10) which was very close to P3 (-14) as because the permeability and the coefficient of consolidation were same. For other piezometer stations, the measurement after driving were available for one month only. The latest driving piles were G202 and G205 which were close to station P3. Therefore, the response were rapid at these stations.

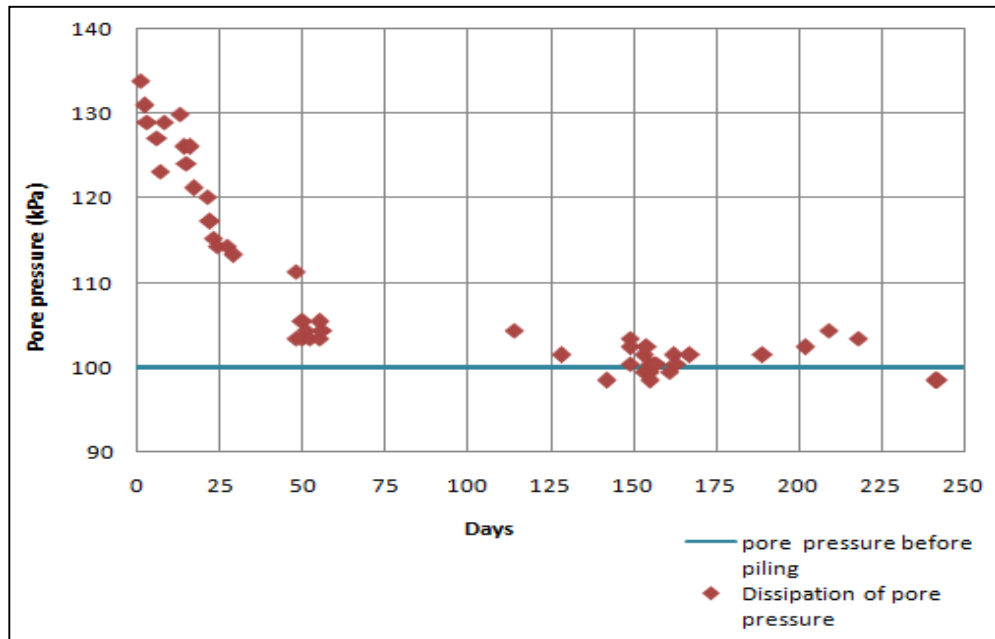


Figure 6.29 Excess pore pressure dissipation with time after driving at P3 (-10).

At the other stations P1, P2 and P4 at different depth the pore pressure dissipates 20-50% within first one month depending on the distance from the pile G201 and G205. Though P4 (-4.9) is far from the piles, the excess pore pressure dissipation was rapid as the location of the piezometer was at the upper sand layer.

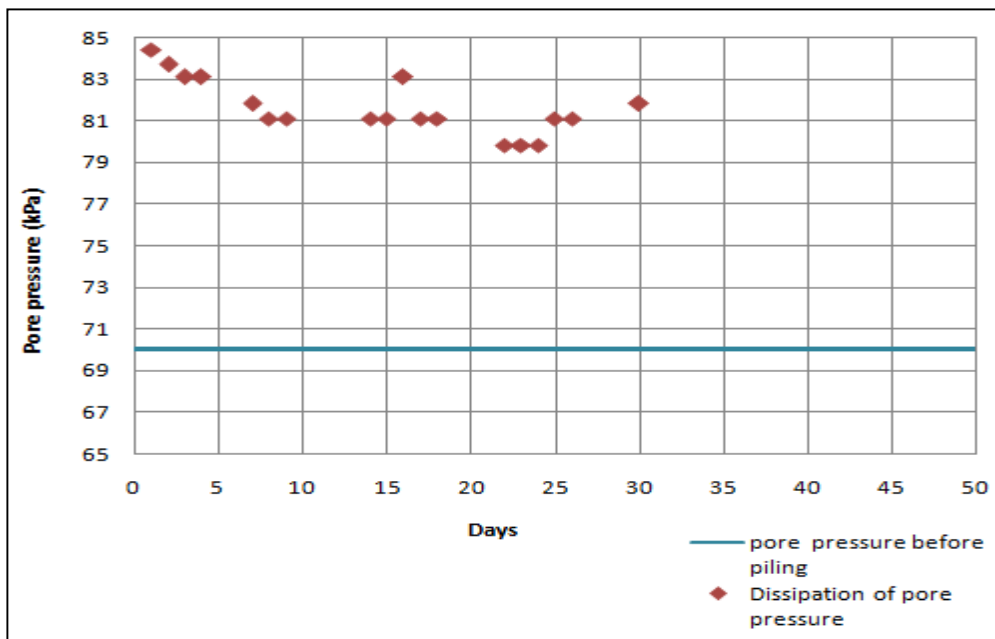


Figure 6.30 Excess pore pressure dissipation with time after driving at P1 (-7).

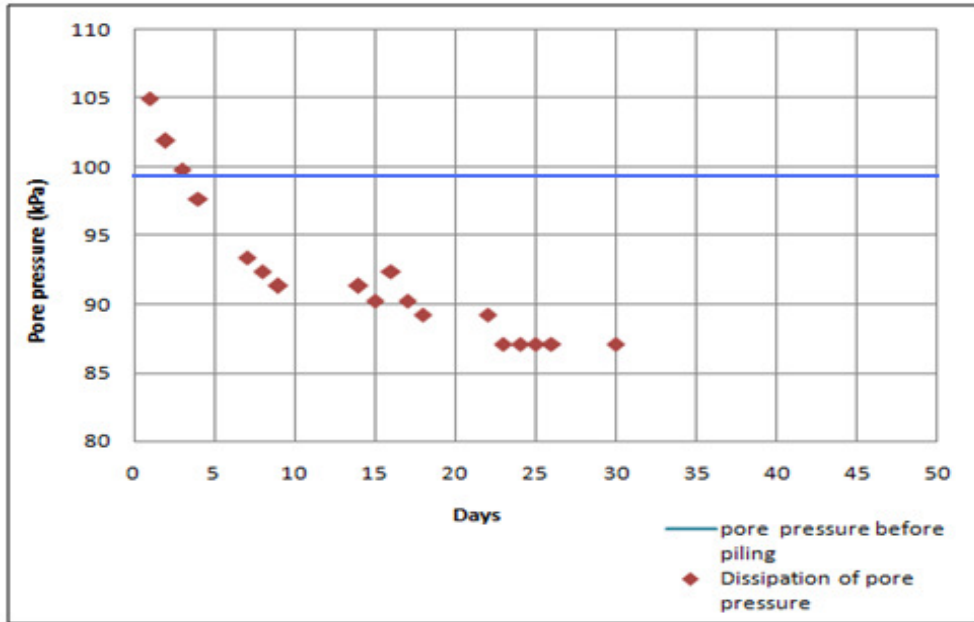


Figure 6.31 Excess pore pressure dissipation with time after driving at P4 (-9.9).

6.7.1 Calculation of primary consolidation time

During consolidation phase the pore water is expelled from soil layer. For this consequence the excess pore pressure dissipates. The time to back the pore pressure to initial value termed as primary consolidation time, t_p . The permeability of the soil measures the consolidation time.

The formula for primary consolidation time, $t_p = T \frac{H^2}{c_v}$ (6.3)

H= drainage distance, m

c_v = coefficient of consolidation, $\frac{m^2}{yr}$

T= dimensionless time factor.

In the piezometer P3 location 10 m clay layer is located in between sand layers. So, assuming two way of drainage.

$c_v = 9 \frac{m^2}{yr}$ from oedometer test. (Borehole 12)

T=1 for 100% dissipation.

$$t_p = T \frac{H^2}{c_v} = 1.00 \frac{7^2}{9} = 5.4 \text{ year.}$$

It is observed from the figure 6.28 and 6.29 that soil took approximately 150 days or 5 months to back to its original pore pressure. As clay has less permeability the excess pore pressure took more time to decapitate.

The formula (6.3) relates only the vertical permeability but the major pore pressure gradients are radial over most of the length of the pile. For this instance the primary consolidation time = 5 months from øvre sund project is valid.

Chapter VII

Numerical analysis

The intension of software analysis is to model the piling activities by finite element software PLAXIS and describe the pore pressure generation and the effect on stability. How the piling activity reduced the short-term stability was also analyzed by Limit equilibrium software SLIDE and GeoSuite-Stability.

Due to pile driving in the øvre sund project, excess pore pressure was developed in the clay layer which reduces the stability of the slope in the short term. Therefore, these pore pressure generations were monitored frequently.

The profile for numerical analysis was selected in the grønland side of the river and along the axis of piling. Figure 7.1 shows the profile section used in the analysis. The soil layering and other geotechnical properties are taken from the geotechnical report of the øvre sund project.

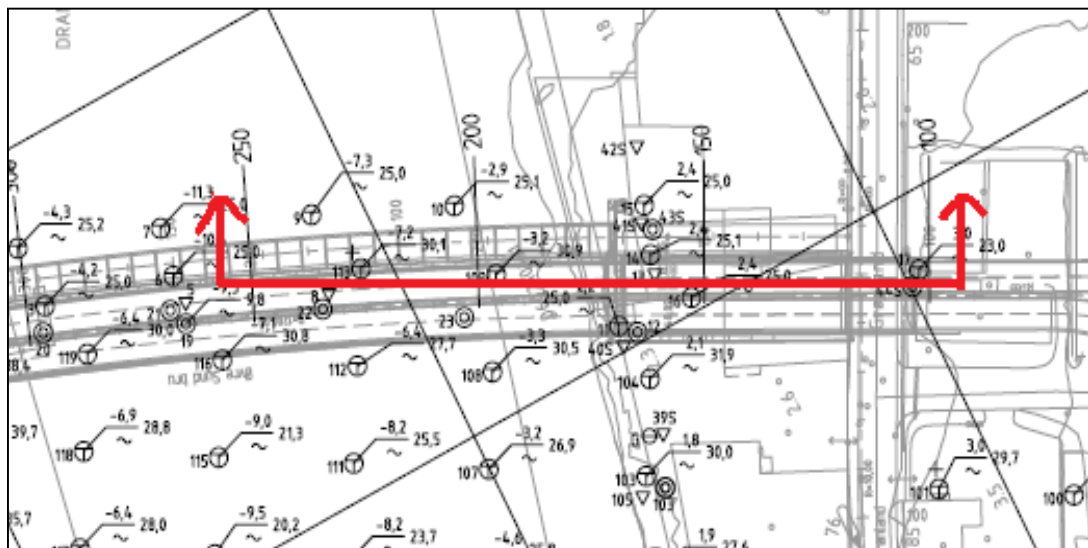


Figure 7.1 Profile section for numerical analysis

7.1 Stability analysis by SLIDE

Slide is a program for two-dimensional slope stability analysis developed by Rocscience. Slide can be used to design and/or analyze natural slopes or manmade (engineered)

slopes such as cuts, embankments and fills (including earth dams and retaining structures such as tie-back walls, and soil nail structures), and waste dumps formed from mining or industrial by-products. Slide has the ability to analyze both a single user-defined non-circular failure surface and to search for the minimum non-circular failure surface. Composite surfaces containing both a circular and non-circular component can also be analyzed. Slide has an appealing and easy-to use graphical interface and provides a wide range of modeling and data interpretation functionalities. It calculates safety factors for circular and noncircular slope failure surfaces using a number of widely used limit equilibrium analysis approaches such as the Bishop, Janbu, Spencer, Corp Engineers 1&2, Lowe-Karafiath, and GLE methods. SLIDE version 6 was used in the analysis (28).

7.1.1 Geometry and input parameter

Figure 7.2 shows the soil layering and water table with their coordinates. The top sand is overlying the clay layer. The depth of the underlying dense moraine layer varies from 10m to 25m from Grønland side to the Hamborgstrøm side. The thickness of the clay layer varies 11-17m from left to right in Figure 7.2. The water table follows the ground surface. The river water which is at the zero reference level also shown in the figure.

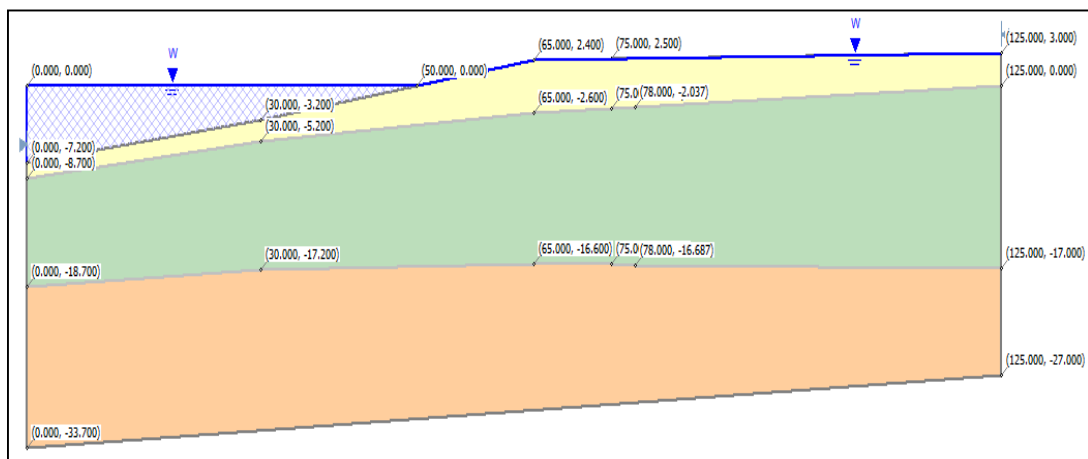


Figure 7. 2 Section of Soil profile used in Slide.

The soil tests were performed mainly in the clay layer. The input parameter for the upper sand and dense moraine were assumed to typical values. These two layers were modeled by Mohr-coulomb strength type and effective stress parameters were chosen.

For the clay layer Both the Mohr-coulomb effective stress and undrained total stress analysis were performed to compare the stability.

Table 7.1 Input parameters of soil

| Soil layer | Unit weight, (kN/m^3) | Cohesion (kPa) | Friction angle ($^{\circ}$) | Undrained shear strength, kPa |
|---------------|---------------------------|----------------|-------------------------------|-------------------------------|
| Upper sand | 18.5 | 1 | 30 | - |
| Clay | 19.5 | 7.3 | 26 | 21.5(avg) |
| Dense moraine | 21 | 10 | 25 | - |

7.1.2 The stability of the slope before pile driving

From the stability analysis of the slope with effective stress parameter (Figure 7.3), the slope has a factor of safety of 2.14 by Janbu simplified method which is higher in Bishop simplified with FOS=2.19. With undrained total stress parameter the slope has Factor of safety of 1.48 (Figure 7.4).

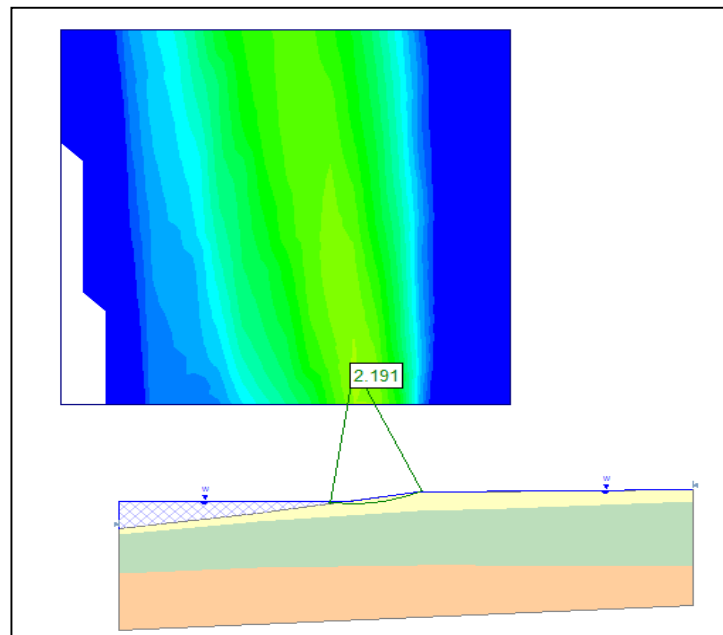


Figure 7.3 Effective stress analysis considering river water.

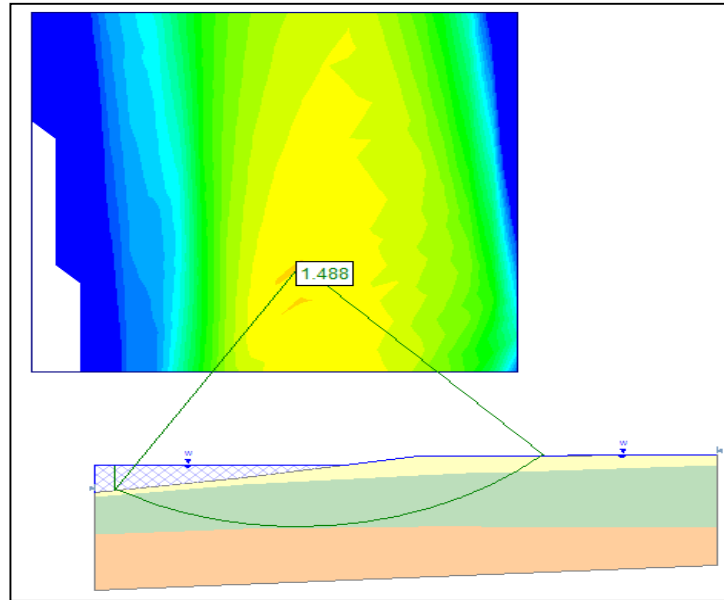


Figure 7.4 Undrained total stress analysis considering river water.

Without considering the river water level, SLIDE gives lower FOS both in effective (Figure7.5) and total undrained analysis (Figure7.6) of 1.94 and 0.95 respectively. It has been observed that, the slope fails without considering river water with total stress parameter. Therefore the river water has remarkable effect to stabilize the slope.

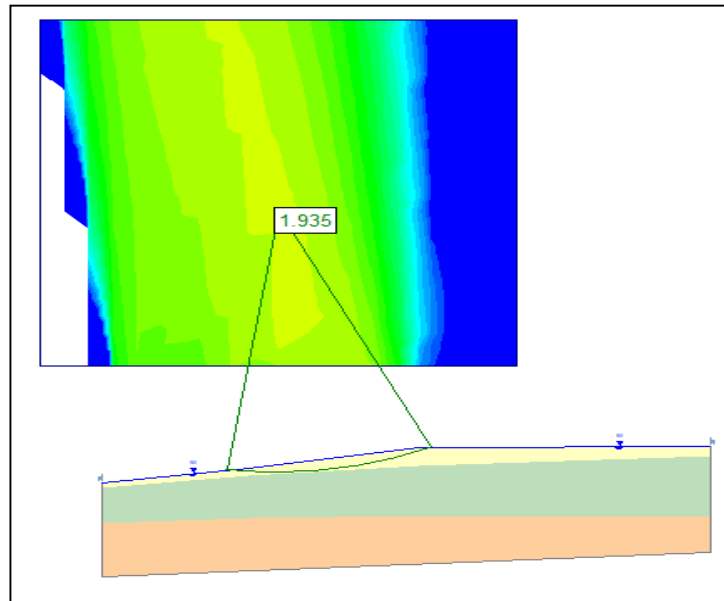


Figure 7.5 Effective stress analysis without considering river water.

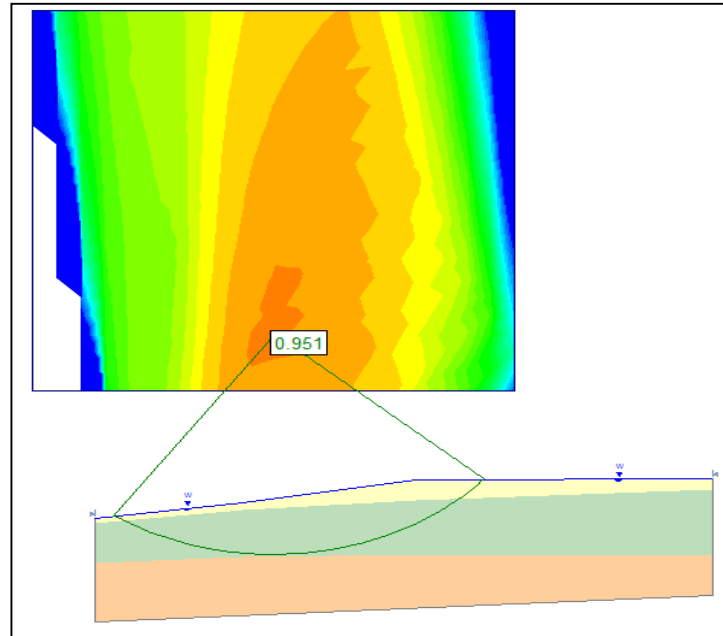


Figure 7. 6 Undrained total stress analysis without considering river water.

Using the effective parameter of the clay layer gives shallow failure surface which is limited in the upper sand layer, where undrained analysis of clay gives comparatively deeper failure surface which is extended in the clay layer.

7.1.3 The stability considering the piling activity

SLIDE has limitations to describe the piling activity by means of volume expansion or mass displacement. Therefore, reduced undrained stability can be evaluated by increasing the pore pressure in the calculation. This is possible either by increasing the water table or increases the unit weight of water to provide excess pore pressure which is the effect of pile driving. In this analysis the unit weight of water has increased from 9.8 kPa until the slope fails. From analysis, it is found that the slope is close to failure with an increase of 40% of pore pressure (Figure 7.7). From the measured value in the øvre sund the extreme pore pressure increment was 80 kPa at P4 (-9.9) on 7th january, 2009. As the hydrostatic pore pressure at the depth 9.9m from the ground is 99 kPa, the excess pore pressure development was almost 80%. Therefore, this excess pore pressure development of 80kPa was indeed very high for the stability. Any piling activity without dissipating this pore pressure might be crucial. In the slope analysis, the river water level was adjusted as the unit weight of water was increased. The river water level

was lowered 2m, so that the water gives same overburden on the soil. The effective stress analysis was used.

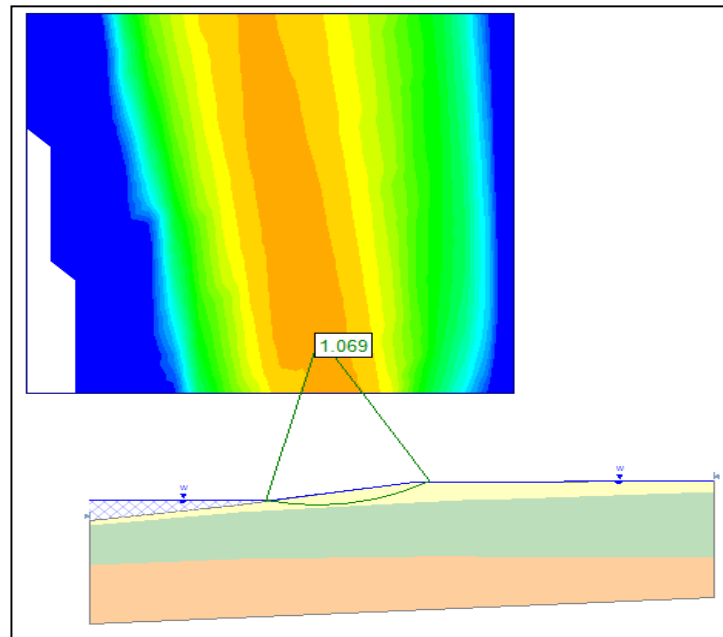


Figure 7.7 Effective stress analysis considering the pile effect.

7.2 PLAXIS

Plaxis is a finite element program for Geotechnical applications in which soil models are used to simulate the soil behavior. Plaxis 2D is intended for the two dimensional analysis of deformation and stability in geotechnical engineering. Geotechnical applications requires advanced constitutive model for the simulation of the non linear, time dependent and anisotropic behavior of soils and rock. Development of Plaxis began in 1987 at the Technical University of Delft as an initiative of the Dutch Department of Public Works and Water Management (22).

7.2.1 Geometry and material properties

In the Plaxis analysis same profile has used as in the slide with only difference the river water level was added in the initial condition stage. Mohr coulomb material model and undrained behavior had selected for soil layers. For pile material elastic non-porous behavior was used. Interface for pile-soil interaction was used with roughness value 0.8.

Table 7.2 Input parameters of soil in Plaxis

| Parameter | Upper sand | Clay | Dense moraine | Pile | Unit |
|-------------------------|------------|-----------|---------------|-----------|------------|
| Material model | MC | MC | MC | Elastic | - |
| Type of behavior | undrained | undrained | undrained | Non-porus | - |
| Unit weight | 18.5 | 19.5 | 21 | 24 | kN/m^3 |
| Horizontal permeability | 1.0 | 0.0002 | 0.5 | - | m/day |
| Vertical permeability | 1.0 | 0.0002 | 0.5 | - | m/day |
| Young's modulus | 30 | 6 | 20 | 30000 | Mpa |
| Cohesion | 1 | 7.3 | 10 | - | kPa |
| Poisson's ratio | 0.3 | 0.3 | 0.3 | 0.1 | - |
| Friction angle | 30 | 26 | 25 | - | $^{\circ}$ |
| Dilatancy angle | 0 | 0 | 0 | - | $^{\circ}$ |

The total stress parameter is also compared with the effective stress parameter. For total stress parameter, friction angle $\phi = 0$ and average undrained shear stress, $s_u=21.5$ kPa has been used as cohesion value for clay layer.

7.2.2 Mesh generation

A two dimension plane strain finite element Model is created using 15-noded, triangular elements. The fine Mesh used for the following FEM analyses is shown in the figure 7.8 below. The characteristic mesh data is given in the table 7.3 below.

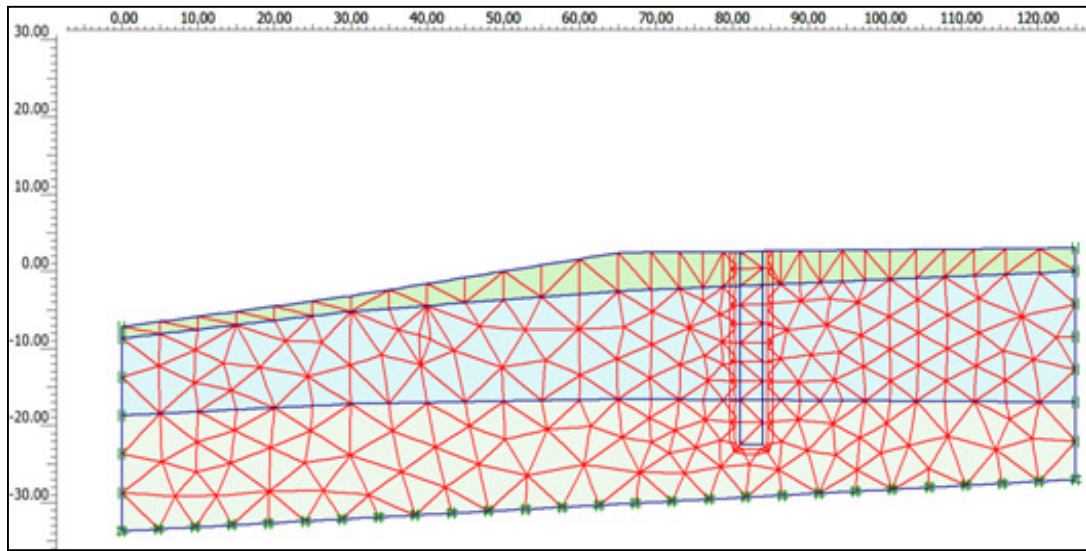


Figure 7.8 Working mesh with 454 elements

Table 7.3 General informations of mesh generation

| | |
|---------------------|------|
| No. of elements | 454 |
| No. of nodes | 3858 |
| No. of stress point | 5448 |

7.2.3 Stability of the slope without pile

The stability of the slope before piling activity started had been checked in plaxis. It is possible by ϕ/c -reduction in the calculation phase. After mesh generation the initial condition was generated considering the river water level. The ground water table was at surface. After generating the initial pore pressure, k_0 procedure had skipped as it is not suitable for slopes. In the calculation stage, first phase was the gravity loading. In this phase the undrained behavior was ignored. In the second calculation phase ϕ/c -reduction was defined with $Msf = 0.1$ and the additional steps with 100. Any displacements from previous step were reset. The undrained analysis with drained parameter was compared with the undrained parameter, taking friction angle $\phi = 0$ and putting the cohesion value equal to undrained shear strength, s_u .

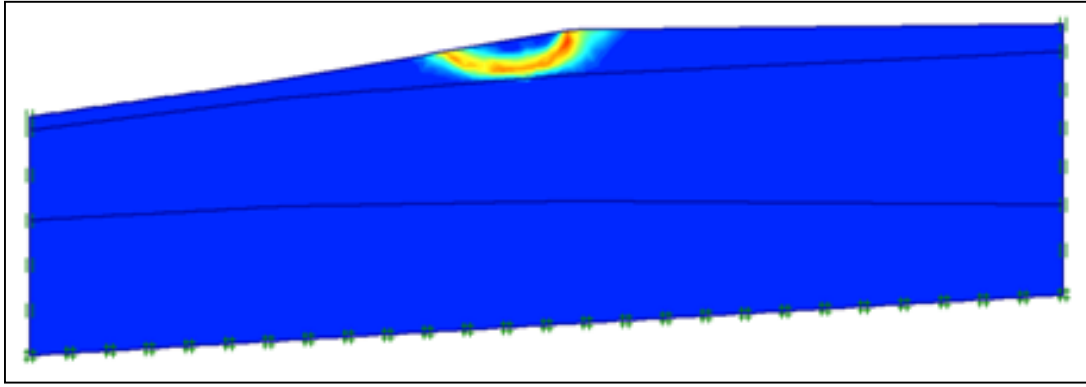


Figure 7.9 Failure surface for effective stress parameter.

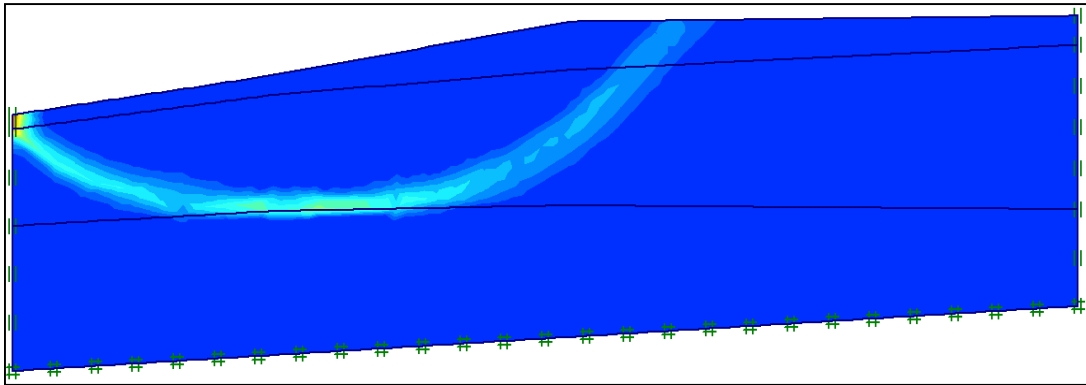


Figure 7.10 Failure surface for total stress parameter.

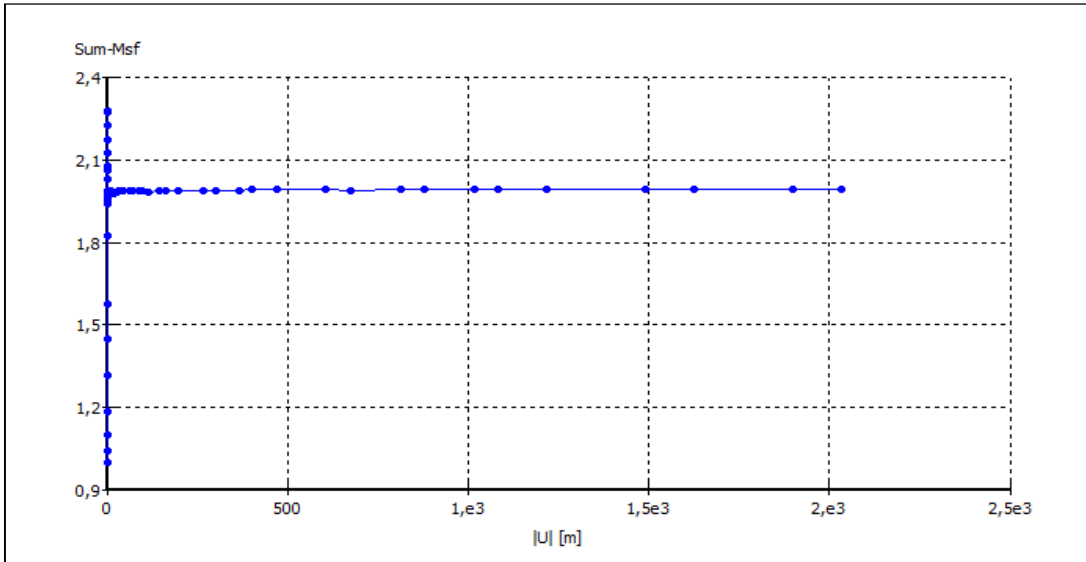


Figure 7.11 FOS for effective stress parameter.

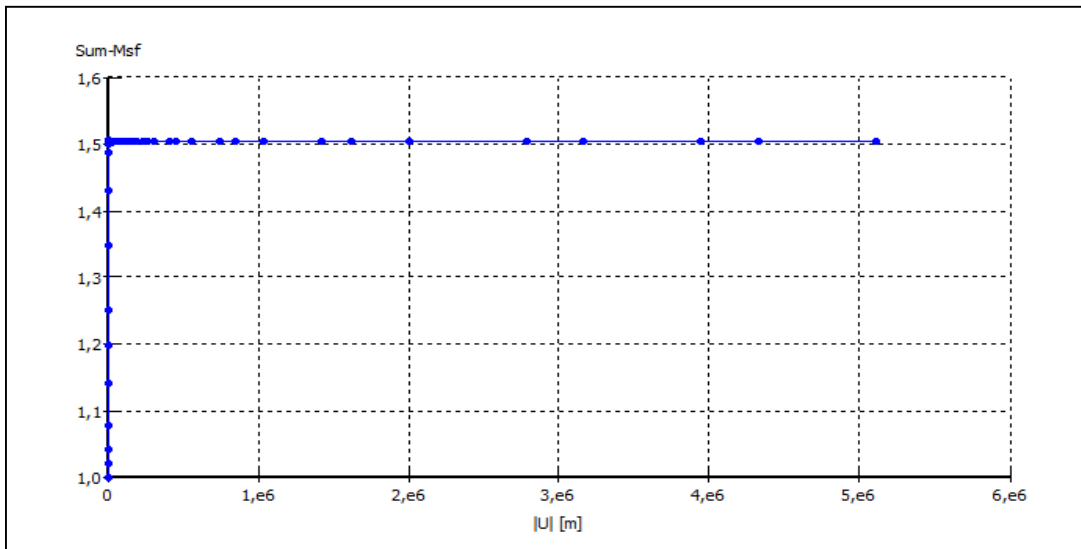


Figure 7.12 FOS for total stress parameter.

7.2.3.1 Effects of river water

Water level in the Drammen River is almost constant. It is at the zero reference level. It increases the stability of the slope. In the Plaxis analysis it is shown that, with keeping the other parameters constant, without considering the river water the Factor of safety reduced to 1.4 from 1.5 for total stress parameter, (Figure 7.13). This is because of the fact that river water acts to stabilize the slope.

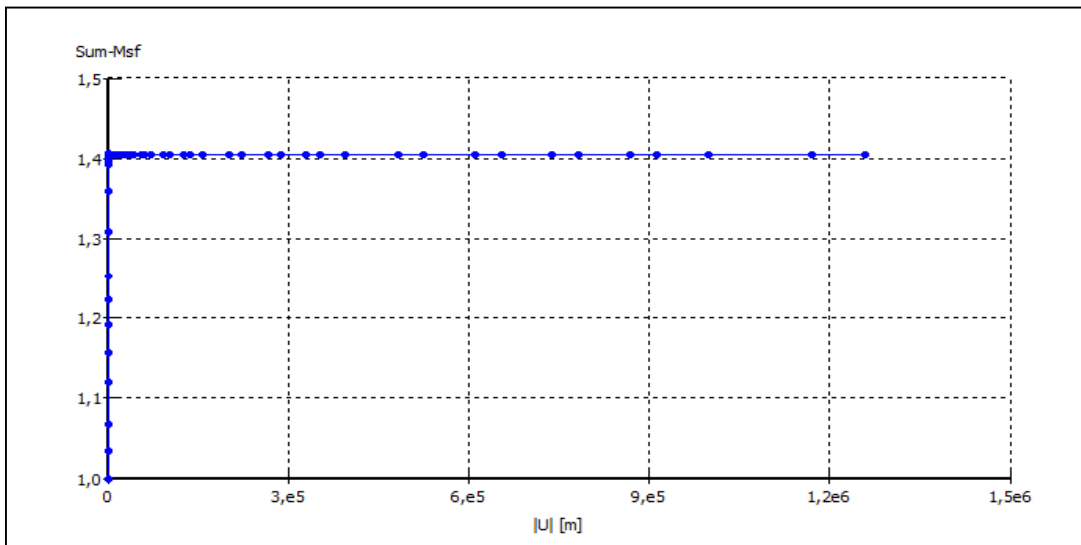


Figure 7.13 Reduced stability of slope without river water.

Another important effect of river water in Plaxis calculation is that it gives deeper failure surface (Figure 7.14) which is extended to the clay layer, though it is realistic to consider the river water level.

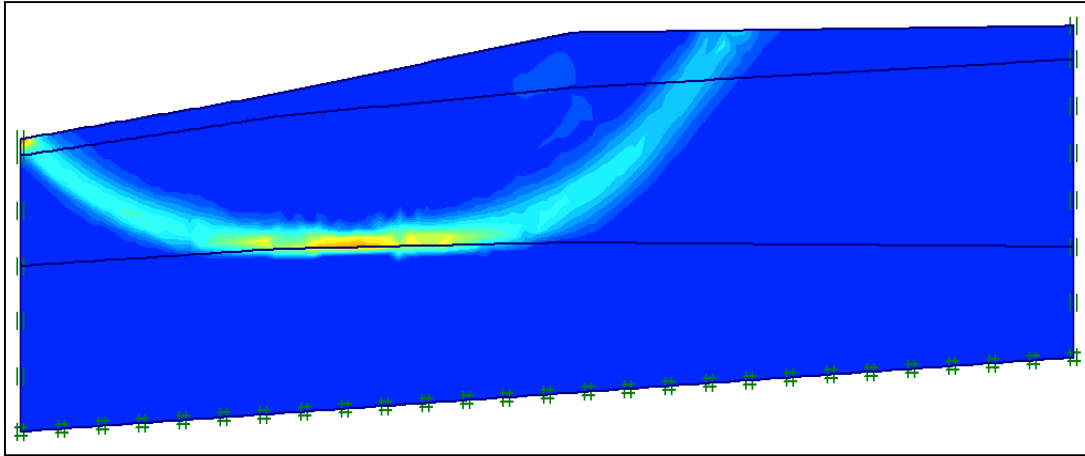


Figure 7. 14 Effects of river water on failure surface.

7.2.4 Effects of piling

Driving of displacement pile produces large excess pore pressure and reduces the stability of the slope in the short term. In the Plaxis analysis it has considered volumetric expansion and prescribed displacement to show the effects of piling.

7.2.4.1 Volumetric expansion

Pile driving induced ground movements was taken into account in this method. When a pile is driven into the ground, some amount of soil is replaced. The soil pile volume replacement must be equal to the soil volume moved to the neighboring region and the volume of soil consumed in the densification process. (32)

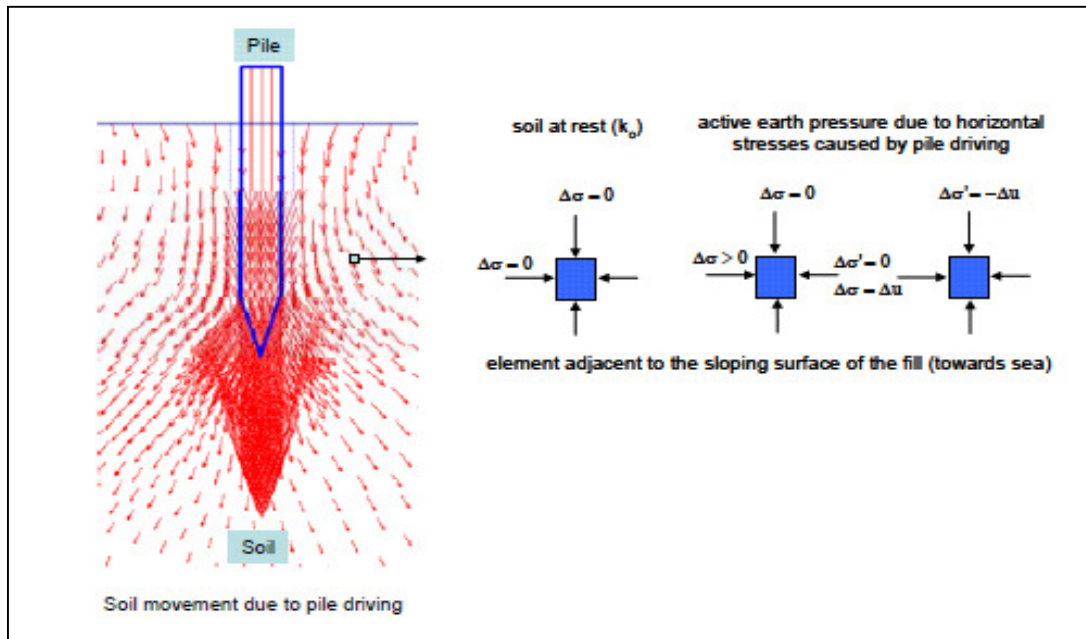


Figure 7.15 Soil movement due to pile driving. (32)

In figure 7.15 a soil element adjacent to the pile, and towards the sloping surface of the fill has been considered. Before piling has been started, this soil element is subjected to the overburden pressure ($\sigma'_y = \gamma' * \text{height of overburden}$) and the lateral pressure ($\sigma'_x = k'_0 * \sigma'_y$). At this stage there is no stress change ($\Delta\sigma = \Delta\sigma' + \Delta u = 0$). However, during pile driving this soil is subjected to additional pressure due to soil displacement. The horizontal stress in the soil will increase and the vertical stress will remain unchanged; $\Delta\sigma_x > 0$ and $\Delta\sigma_y = 0$. This scenario is little different for undrained and effective stress point of view. For undrained case, change in the horizontal stress must be equal to change in the pore water pressure. Therefore, $\Delta\sigma_x = \Delta u$, and so $\Delta\sigma'_x = 0$, whereas $\Delta\sigma_x = 0$ and $\Delta\sigma'_y = -\Delta u$. Therefore the vertical effective stresses will reduce and so the undrained capacity of the soil will also decrease. Pile driving can be so crucial while calculating the structural stability. (32)

From the stability analysis, some alarm-limit for excess pore pressure generation were developed and maintained in the øvre sund project. The driving was scheduled in such a way that the pore pressure generation never exceeds the limit. In this analysis it is considered only the piles in axis G5. Before piling started in G5, the driving in the axis K7

and G6 had completed. Therefore these piles may have positive effects on the stability of the slope when driving in the axis G5. However, it is assumed only the individual effects from G5.

There are 28 Piles in the axis G5. Pile cluster have been made in the geometry to simulate the effect of soil movement. The total pile area per meter depth must be equal to $28 \times 0.27 \text{m} \times 1.0 \text{m} = 7.56 \text{m}^2$. In calculation, a single pile cluster is assumed instead of 28 different pile clusters. Also, only around half of the total pile area (3.0m^2) per meter depth is assumed. The pile cluster is then subjected to volumetric expansion to 100%. From the plaxis analysis volume expansion causes outward movements in the soil adjacent to the pile. Soil in active regions (towards river side) moves more than the soil in passive zone (grønland side). Soil movement causes excess pore pressure build-up in different layers. Higher excess pore pressure observed close to the pile and then decreases with the distance from the pile face.

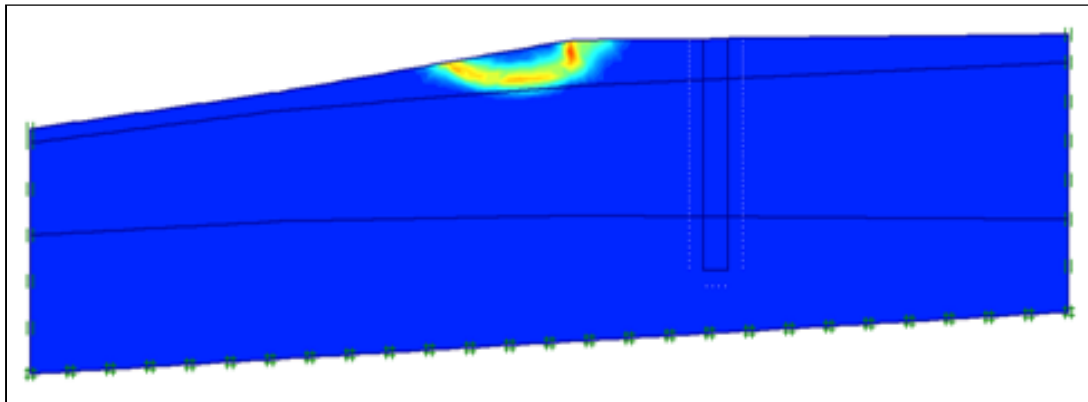


Figure 7.16 short time stability of the slope including pile effect.

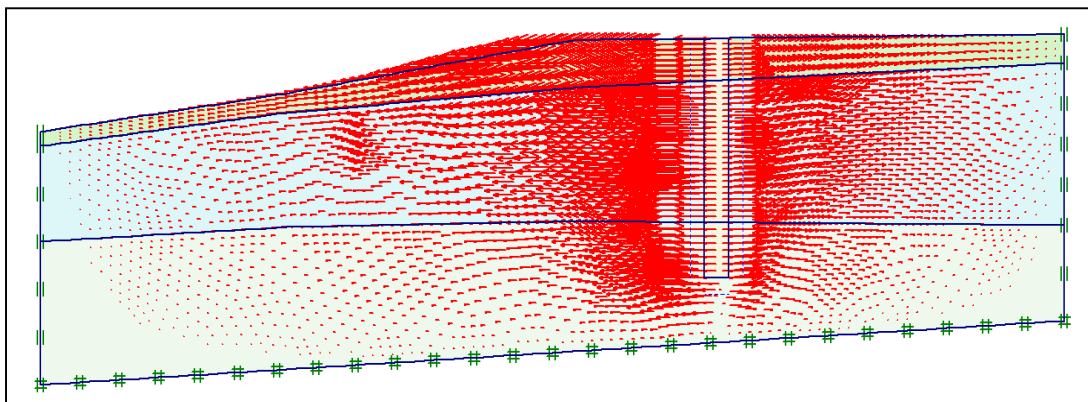


Figure 7. 17 Horizontal displacement by volume expansion.

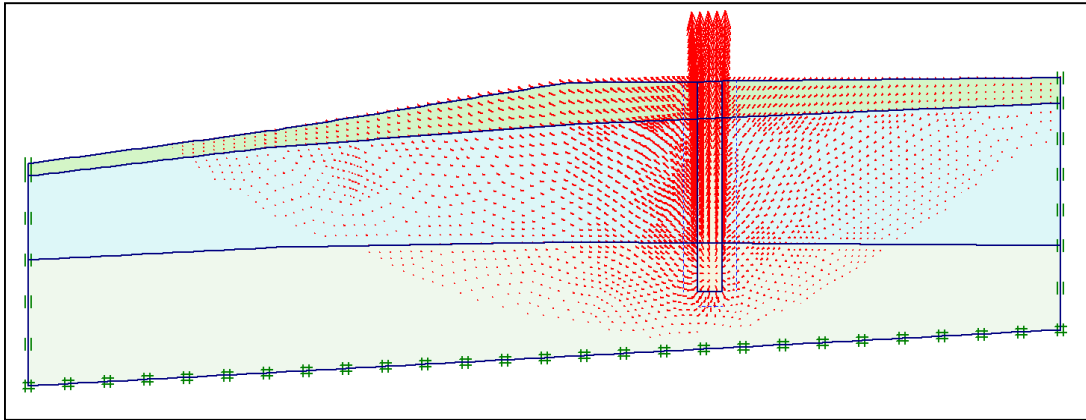


Figure 7. 18 Total displacement by volume expansion.

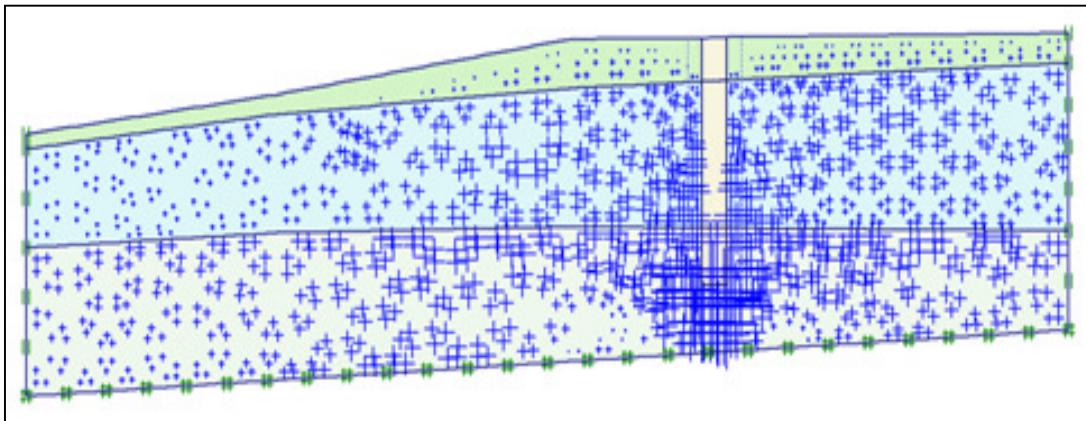


Figure 7. 19 Excess pore pressure developed due to pile effect

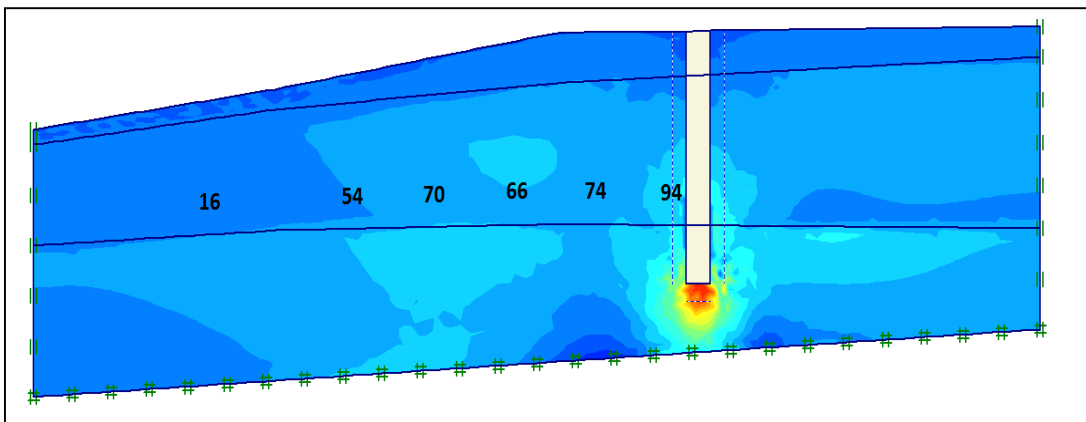


Figure 7. 20 Excess pore pressure generation in clay layer.

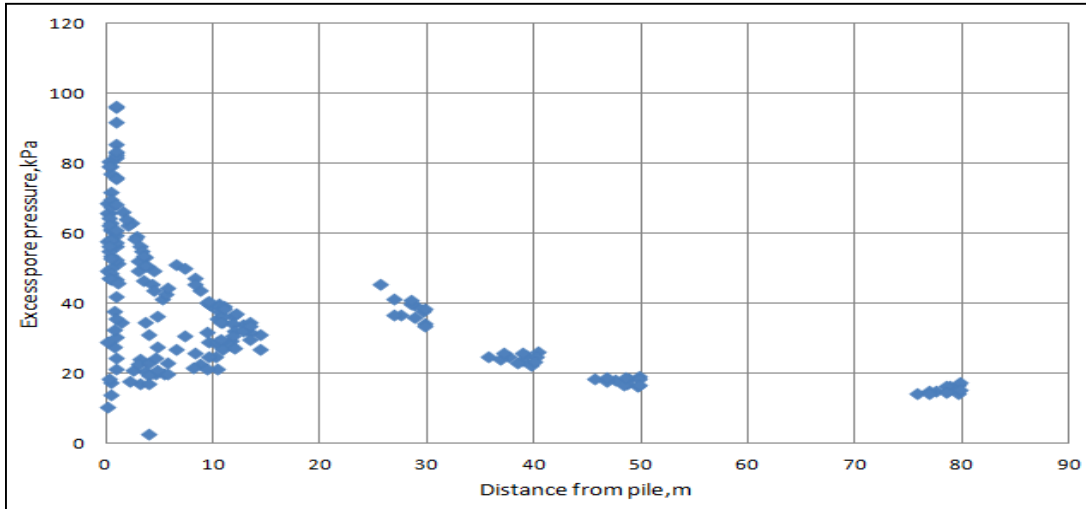


Figure 7. 21 excess pore pressure with distance from plaxis analysis

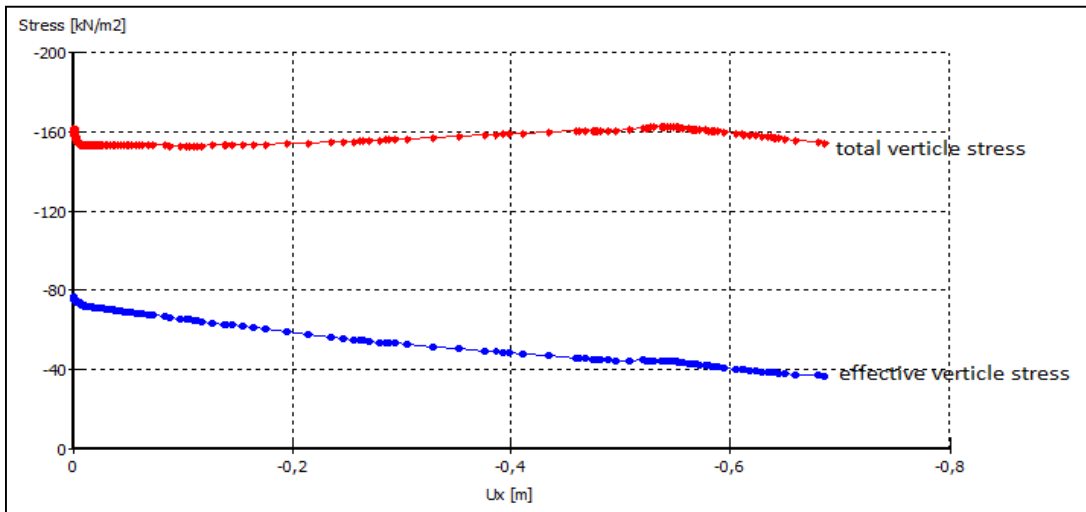


Figure 7. 22 Total and effective verticle stress with horizontal displacement.

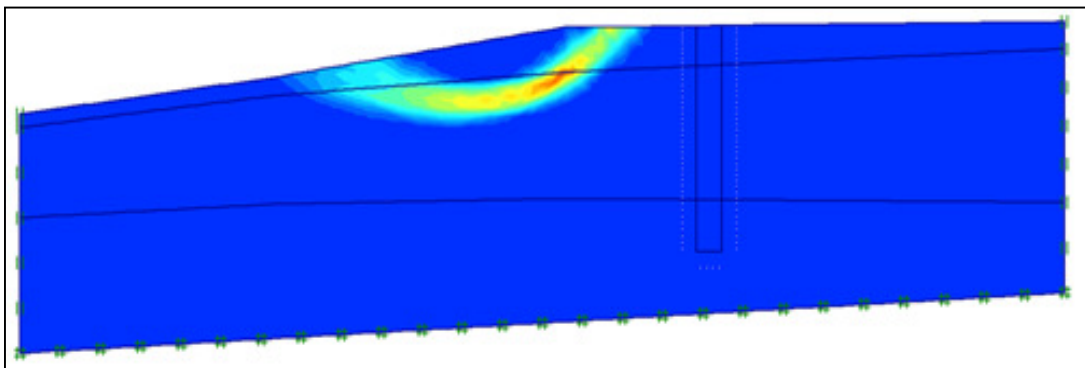


Figure 7. 23 failure surface with sand layer cohesion=5.

7.2.4.2 Prescribed displacement

To simulate pile installation process, a prescribed displacement, equivalent to pile diameter 27cm was applied to the soil along the perimeter in the direction of the slope as shown in figure 7.24. 8cm diameter pile was first created as the initial size of the cavity to facilitate the computational process. Plain strain condition and 15 nodes triangle elements were used. Linear elastic constitutive model was utilized to describe the behavior of concrete pile. It was considered single pile driving process into the soil and to simulate the failure mechanism and excess pore pressure development in the clay. In the first calculation phase gravity loading was done. In the second phase an initial opening of 8cm was created in the soil layer and described as pile element, interface was used at the pile soil interface Finally a prescribed displacement equal to pile diameter was introduced to represent the pile installation process (27).

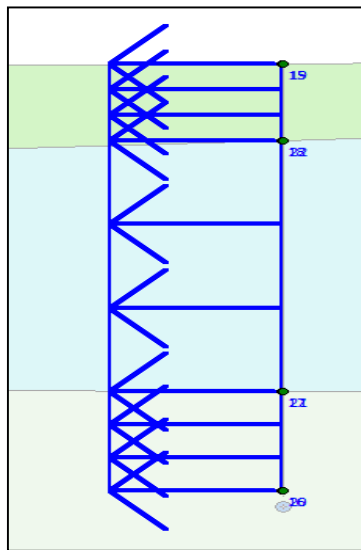


Figure 7. 24 Prescribed displacement

From different measures taken to predict the failure mechanism it is observed that due to pile driving front tip of the slope always subject to failure (Figure 7.25). Excess pore pressure developed around the pile in different soil layers are shown in figure 7.26. From figure it is observed extreme pore pressure development is at the pile tip and in dense moraine layer is 225kPa which is extremely high compared to field value. Figure 7.27 shows maximum excess pore pressure in the clay layer with distance which is also

very high. Suction developed at the other side of the slope may be this is because the prescribed displacement was introduced in the slope side only.

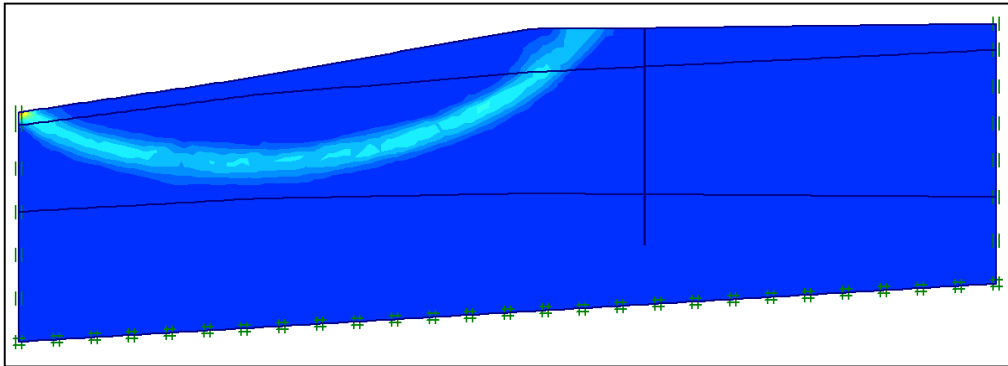


Figure 7.25 Failure surface with prescribed displacement

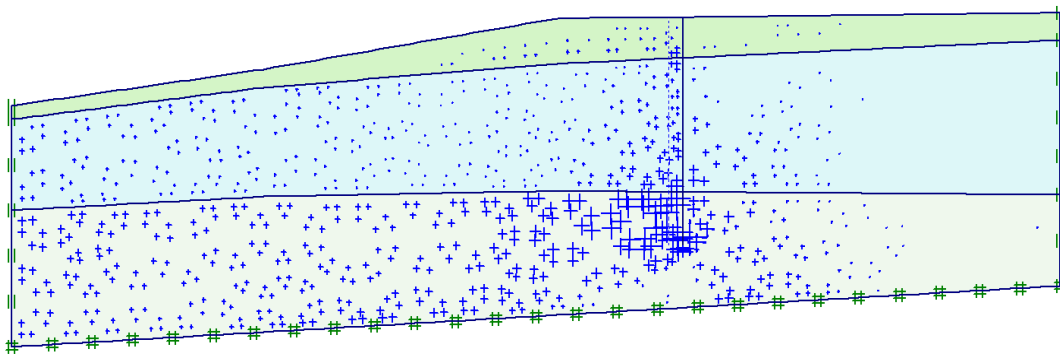


Figure 7.26 Excess pore pressure with prescribed displacement

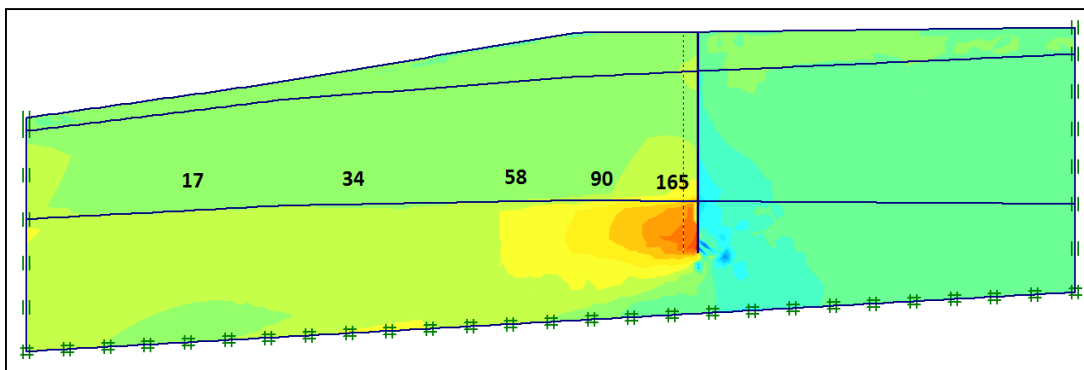


Figure 7.27 Excess pore pressure generation in clay layer with prescribed displacement.

7.2.5 Limitations

The study has been performed assuming static load condition only. However pile driving may cause dynamic loading. Very simple Elasto-plastic soil model has been used for the analysis. However, pile driving can cause liquefaction in the materials. Therefore, advance material model has been suggested.

PLAXIS 2D analysis has been used for the analysis. To describe the piling effect properly, it is strongly suggested 3D analysis. The analysis has been made simple considering 2D analysis due lack of time.

To describe the effect of piling, volumetric expansion and prescribed displacement has been used. Total pile area in the axis has been used rather than single pile. Therefore it would be more realistic to follow the schedule of driving as in the site. When considering the piles in axis G5, few piles have been driven in axis G6, which may have effect on the stability. This effect has not considered.

7.3 GeoSuite-stability

GS Stability is a 2D slope stability program for evaluating stability of circular or non-circular failure surfaces in slopes. It is a part of the Novapoint GeoSuite Toolbox, which is a tool for making presentations and calculations in geotechnical design. Profiles for modelling of undrained shear strength and pore water pressure, gives powerful abilities to simulate any state in the soil. GS Stability is based on AutoCAD. It is possible to specify terrain geometry, soil layering, groundwater level, load conditions and other factors as needed. The search area is to be specified for a critical shear surface. There are four different methods of calculation:

- Force equilibrium
- Bishop simplified
- Bishop modified
- BEAST 2003

7.3.1 Analysis without pile effect

The stability of the Øvre sund project has analyzed by GeoSuite Stability. The reduced stability due to piling effect also considered and compared with the previous one. Stability before pile driving has been calculated using total and effective stress parameters. C-profile has been used to describe the variable undrained shear strength with depth. Stability without pile considering various factors has been given in figures below:

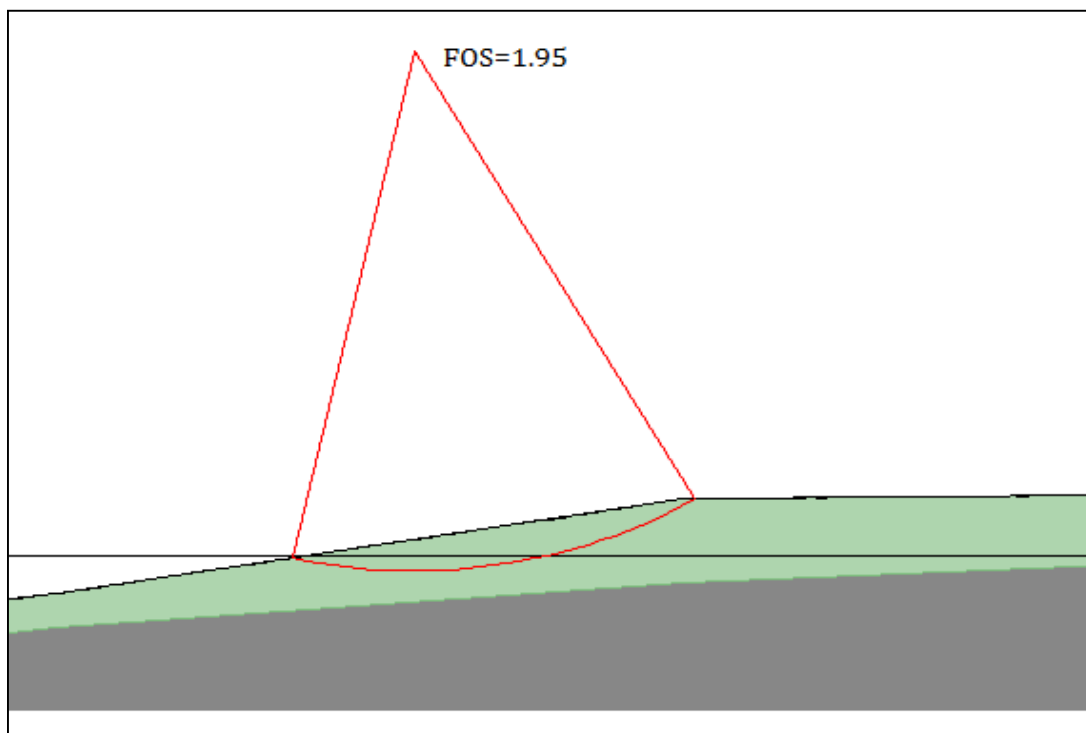


Figure 7. 28 Stability of slope using effective stress parameter before piling starts without considering river water.

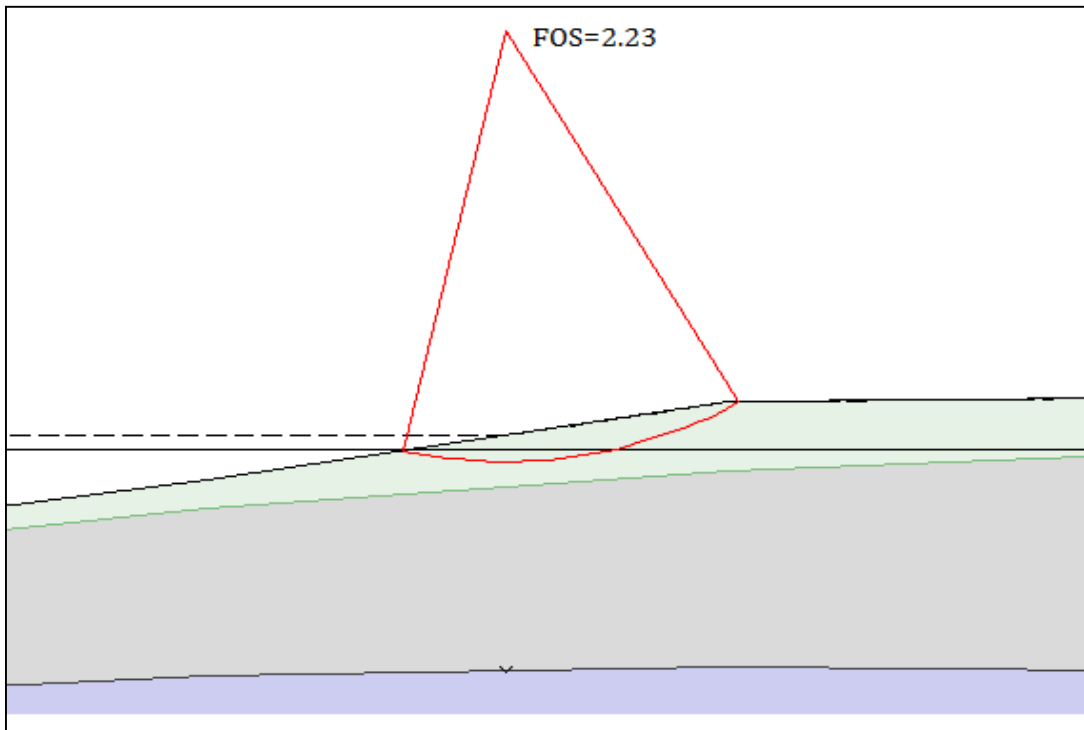


Figure 7. 29 Stability of slope using effective stress parameter before piling starts considering river water.

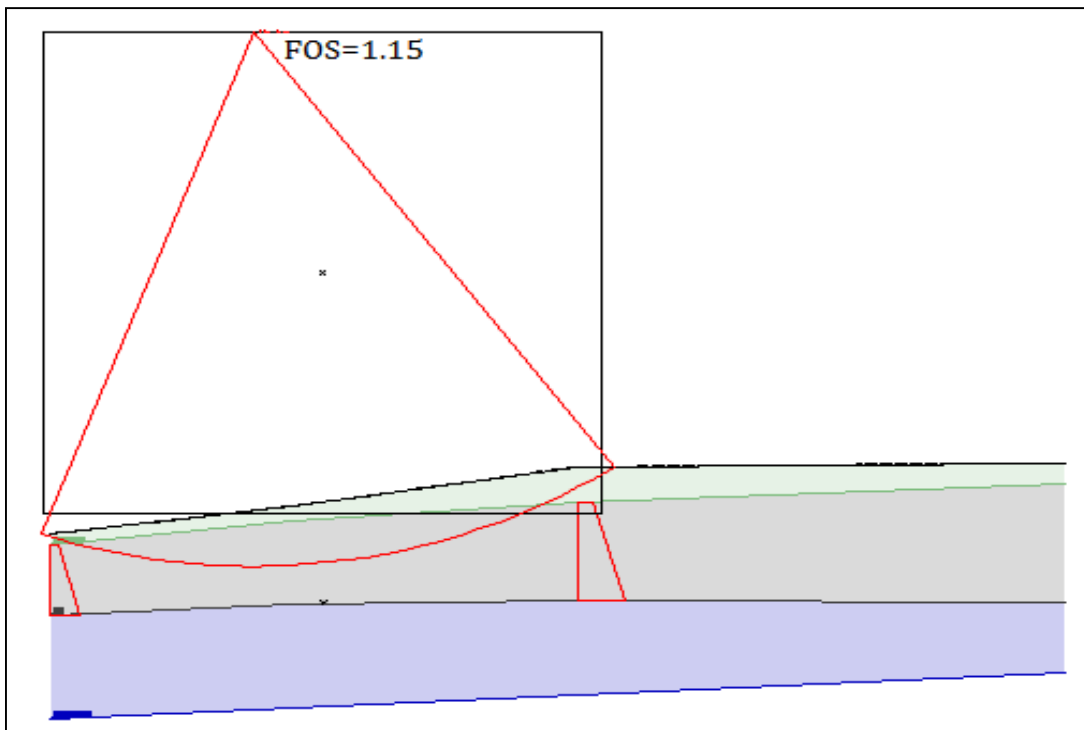


Figure 7. 30 Stability of slope using total stress parameter before piling starts without considering river water

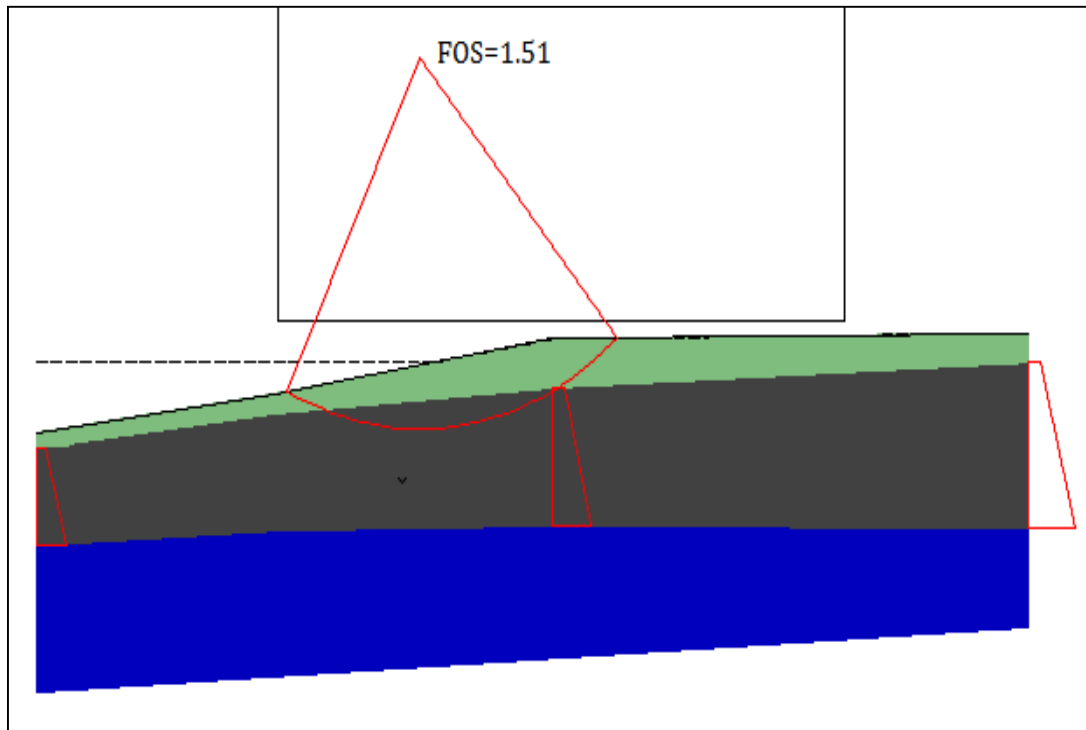


Figure 7. 31 Stability of slope using total stress parameter before piling starts considering river water.

7.3.2 Considering pile effect

Pile driving activities increases the pore pressure in the clay. It has been considered in the GS-stability and increased the hydrostatic pore pressure by 40% using the option “pore profile”. The GeoSuite has been considered this excess pore pressure and calculate the combined vaule pore pressure. The FOS is less than unity due to 40% increase of pore pressure in the clay layer which is relevant with the slide analysis. The effective stress parameter has been used.

Table 7. 4 Effective stress parameter.

| Calculation Data | | | | | | | | | | | |
|--------------------|------------|--------------|-----------------------------|-------------------------------------|------------|------------------|-----------|--|------|---|------|
| Soil | | | | | | | | | | | |
| C Profile | | | | | | | | | | | |
| GW & Pore Pressure | | | | | | | | | | | |
| Loads | | | | | | | | | | | |
| Model Data | | | | | | | | | | | |
| Materials | | | | | | | | | | | |
| New Layer | | Delete Layer | | Edit Soil Surface | | New Rock Surface | | <input type="checkbox"/> Combined analysis | | <input checked="" type="checkbox"/> Advanced grid | |
| Name | CAD | Color | ρ [kN/m ³] | Drained | ϕ [°] | C' [kPa] | C [kPa] | Add | Aa | Ad | Ap |
| upper sand | Geometry < | | 18,50 | <input checked="" type="checkbox"/> | 30,0 | 1,0 | | | 1,00 | 1,00 | 1,00 |
| clay | Geometry < | | 19,50 | <input checked="" type="checkbox"/> | 26,0 | 7,3 | | | 1,00 | 1,00 | 1,00 |
| dense moraine | Geometry < | | 21,00 | <input checked="" type="checkbox"/> | 25,0 | 10,0 | | | 1,00 | 1,00 | 1,00 |

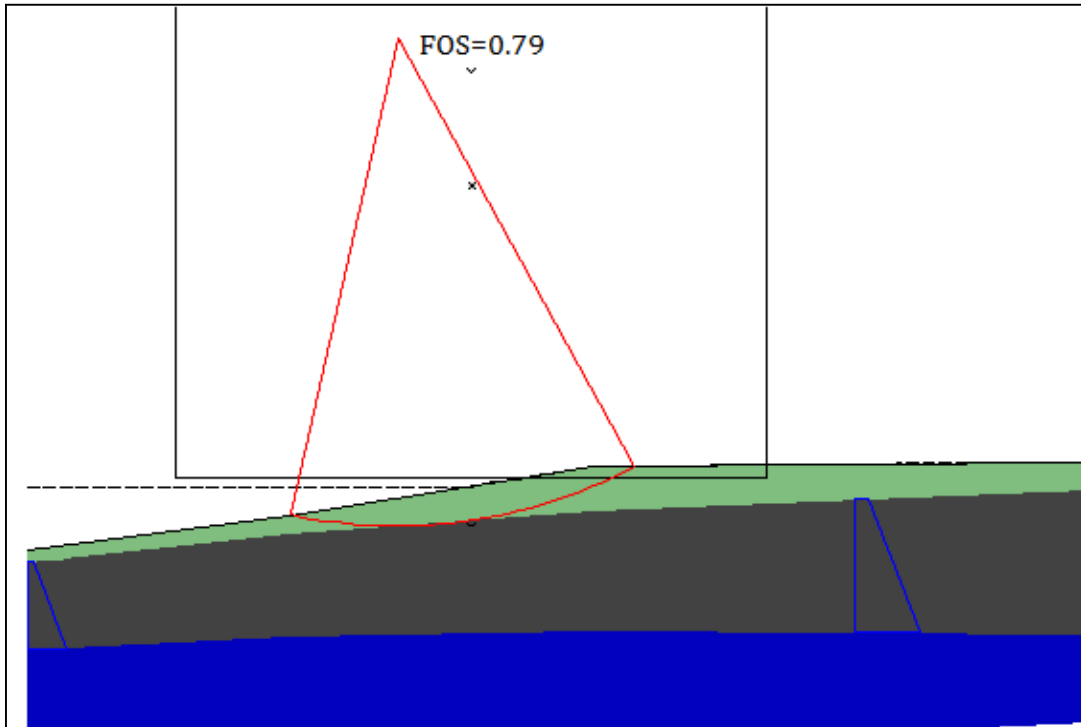


Figure 7. 32 Stability of slope considering pile effect.

Conclusion and Recommendations

Pile driving affects significantly the surrounding soil and modifies its properties. One of the consequences is that pore pressure develops and provokes a reduction of the undrained shear strength. Lateral displacement and soil heave also occur and need to be taken into consideration. Several studies have included in the literature survey part. The excess pore pressure generation factors have been discussed briefly. It has been found that the theory of cavity expansion describes the stress and pore pressure change in soil around the driven pile. Finally, pore water pressure dissipates. This phenomenon lasts longer or shorter and depends on type of soil. Cohesive soil will take more time to reach pore pressure that had before piling.

In the second part, water level measurements enabled to highlight some important points:

- It has been showed that the closer the driven pile is, the higher the piezometer response is. In the Øvre sund project, it was measured 68 kPa of extra pore pressure at 0.5m away from the driven pile. This excess pore measure became negligible 12-15 m from the pile center. Due to lack of pore pressure measurement along the pile shaft, it was not possible to compare the data with theory very well.
- The excess pore pressure development had also influenced by other factor such as thickness of the clay layer, soil type where piezometer is located or the layer through which piles were driven. Driving pore pressure dissipated very rapidly for sand layer whereas it took 4-5 months in case of clay layer.
- For the clay layer with thickness of 14m gave a higher response compared to the layer which is 6m thick.
- High pore pressure increase in the clay has been observed when the piles were penetrated into the underlying dense moraine than into the clay layer.
- It was not possible to measure shear strength reduction due to pile driving because of the unavailability of data.
- Pile driving procedure has described by the expansion of cylindrical cavity. The disturbance due to pile driving and excess pore pressure predicted through cavity expansion and compared with the measured value. Perfectly plastic and

modified cam clay model had used for the cavity expansion solution. The measured and predicted value of excess pore pressure was quite close.

Furthermore, pore pressure dissipate some time after the pile is driven until progressively attain equilibrium value. Numerical analysis has also been performed to show the effects of driving on clay and stability of slope. LE method using GeoSuite – Stability, SLIDE and FEM method Plaxis have been used. River water showed positive affect for slope stability in every case. Total stress and effective stress parameter gives different factor of safety for the slope. According to SLIDE and Geo-Suite, 40% excess pore pressure in the clay layer became crucial. From PLAXIS analysis, the development of excess pore pressure with distance gave reasonable results.

Several recommendations can be suggested for the future study:

- Same analysis is recommended for the Hamborgstørm side and in the river.
- It is recommended to analysis the soil movements as well as movement of previously driven piles due to driving of later piles. To what extent soil is heaved and the disturbance to the nearby structures may be analyzed. As there was no available data from Øvre sund, it is suggested to study this affect for any new project.
- Reduced shear strength due to driving is suggested to be analyzed.
- The piles were not instrumented to measure the pore pressure at the tip and shaft of the pile. Therefore, the analysis was limited to the measurement far from the piles. Therefore, instrumented test piles with pore pressure measurement at tip and shaft is suggested.
- FEM method Plaxis 2D version has been used for modeling. However, 3D analysis is strongly suggested to model the excess pore pressure development and soil disturbance during piling activities to get more realistic scenario.
- Another renowned LEM software “SLOPE/W” is recommended to compare with “SLIDE” and “GeoSuite-stabilty”.

References

1. Abramson L. W. et al. (2002). ***"Slope stability and stabilization method"***, Second Edition, pp. 102-130.
2. Al-Karni A. A. (2001). ***"Shear strength reduction due to excess pore water pressure"***. 4th international conference on recent advances in geotechnical earthquake engineering and soil dynamics and symposium in honor of professor W.D. Liam Finn, San Diego, California.
3. Arora K.R. (2000), ***"Soil Mechanics and Foundation Engineering"***, Fifth edition, pp.671-675.
4. Bozozuk M., Felleneius B. H. and Samson L. (1978). ***"Soil disturbance from pile driving in sensitive clay"***. Canadian geotechnical journal, vol. 15, pp. 346-361.
5. Burns S.E., Mayne P.W. (1999). ***"Pore pressure dissipation behavior surrounding driven piles and cone penetrometers"***. Journal of the Transportation Research Board, Vol. 1675, pp 17-23.
6. Carter J.P., Booker J.R., Yeung S.K. (1986): ***"Cavity expansion in cohesive frictional soils"***. Geotechnique 36,No.3,349-358.
7. Carter J. P., Randolph M. F. and Wroth C. P. (1979), ***"Stress and pore pressure changes in clay during and after the expansion of a cylindrical cavity"***. International Journal for Numerical and Analytical Methods in Geomechanics Vol. 3, pp. 305-322.
8. Cao, L.F., Teh, C.I. and Chang M.F., (2001). ***"Undrained Cavity Expansion in Modified Cam Clay I: Theoretical Analysis"***, Geotechnique, Vol. 51, No. 4, pp. 323-334.
9. Chang M.F., Teh, C.I. and Cao, L.F., (1999). ***"Critical state strength parameters of saturated clays from the modified Cam clay model"***. Canadian geotechnical journal, vol. 36, pp. 876-890.
10. Cao, L.F., Teh, C.I. and Chang, M.F. (2001). ***"Undrained Cavity Expansion in Modified Cam Clay"***, CSE Research bulletin No. 14.
11. Eigenbrod K. D., Issigonis T. (1996). ***"Pore-water pressures in soft to firm clay during driving of piles into underlying dense clay"***. Canadian geotechnical journal, vol. 33, pp. 209-218.

12. Emdal A., Grande L. (2006). ***“Geotechnics and Geohazards”***. Lecture Notes-TBA 5100 - Theoretical Soil Mechanics, Norwegian University of Science and Technology.
13. Fellenius B.H. and Samson L. (1975). ***“Testing of drivability of concrete piles and disturbance to sensitive clay”***. Canadian geotechnical journal, vol. 13, pp 139-160.
14. Flaate K. (1972). ***“Effects of Pile Driving in Clays”***. Canadian Geotechnical Journal, Vol. 9, No. 1, pp. 81-88
15. Fleming K., Weltman A., Randolph M. and Elson K. (2008) ***“Piling Engineering”***, Third Edition, pp. 253-262.
16. Gue, S.S. (1984), ***“Ground heave around driven piles in clay”***, PhD Thesis, University of Oxford.
17. Guihai F., Limin W. and Hui Z. (2011), ***“Analysis on Excess Pore Water Pressure caused by Prestressed Concrete pipes Construction in Saturated Clay Ground”***. Advanced Materials Research Vols. 168-170, pp 1238-1244.
18. Holtz R. D. and Boman P. (1974). ***“A new technique for reduction of excess pore pressures during pile driving”***. Canadian geotechnical journal, 1974, vol.2, no.3, pp. 423-429.
19. Ismael, N.F. and Klym J.W. (1979). ***“Pore-Water Pressure Induced by Pile Driving”***. Journal of the Geotechnical Division, ASCE, Vol. 105, November, pp. 1349-1354.
20. Lo K.Y. and Stermac A.G. (1965). ***“Induced Pore Pressures During Pile Driving Operations”***. Proceedings of the 6th International Conference on Soil Mechanics and Foundation Engineering, Montreal, Vol. 2, pp. 285-289.
21. Nordal S. (2008). ***“Finite element in Geotechnical Engineering”***. Lecture Notes-TBA 4115, Norwegian University of Science and Technology.
22. ***PLAXIS 2D*** Reference Manual, Version 9.
23. Poulos H. G. (1994). ***“Effect of pile driving on adjacent piles in clay”***. Canadian Geotechnical journal, 31, pp 856-867.
24. Poulos H. G and Davis E. H (1980). ***“Pile-Foundation- Analysis and Design”***, Geotechnical Engineering Series, Wiley Medical Publication, pp. 6-12.
25. Prakash S. and Sharma H. D. (1990), ***“Pile foundations in Engineering practice”***, pp. 1-10.

26. Roy M., Blanchet R., Tavenas F. and Rochelle P.L.(1981), "***Behavior of a sensitive clay during pile driving***". Canadian Geotechnical Journal, 18, pp. 67-85.
27. Sabry M. (2005), "***In situ stresses and capacity of driven piles in sands***". PhD thesis, Concordia University, Montreal, Quebec, Canada.
28. **SLIDE** Tutorial Version 6.
29. Swan C.C, "**Changes in soil during pile driving**". 53-139 Foundation Engineering, the University of Iowa, pp 1-3.
30. Tefera T. , Tvedt G. and Oset F. (2009). "***Excess pore pressure during pile driving in soft sensitive clay***". Norwegian public road administration, Norway.
31. Tvedt. G & Tefera T. (2009), "***Øvre Sund bru erfaringer med poretrykk og bæreevne under peleramming på Grønland***".Notat (In Norwegian).
32. Thakur V., Bæverfjord M.G., and Grande L.O. (2008). "***Pile Movements induced Instability of Engineered Slopes***". The 12th International Conference of International Association for Computer Methods and Advances in Geomechanics (IACMAG), pp. 4105-4112.
33. Vesic, A.S. (1972). "***Expansion of Cavities in Infinite Soil Mass***". Journal of the Soil Mechanics and Foundations Division, ASCE Proceedings, Vol. 98, No. SM3, pp. 265-290.
34. Weech C.N. (1996), "***Installation and load testing of helical piles in a sensitive fine-grained soil***". Master's thesis, The University of Waterloo, Canada.
35. Yu H.S. (2000). "***Cavity Expansion Methods in Geomechanics***". Kluwer Academic Publishers, pp. 275-289.

Internet sources:

36. Pile Foundation Design: A Student Guide:
<http://www.ctu.edu.vn/colleges/tech/bomon/ktxd/baigiang/pile%20foundation/Pile%20Foundation%20Design-Chapter%201.htm>
[viewed on 11/05/2012].
37. Soil Mechanics & Foundations, Lecture 11.1, Shear Strength of Soil I
<http://www.engr.uconn.edu/~lanbo/CE240LectW111shearstrength1.pdf>
[viewed on 05/04/2012].

38. National University of Singapore:

http://scholarbank.nus.edu/bitstream/handle/10635/13882/Appendix_A.pdf?sequence=10 [viewed on 25/05/2012].

39. GEO-SLOPE International Ltd, Calgary, Alberta, Canada: Modified Cam-clay triaxial test simulations:

<http://downloads.geo-slope.com/geostudioresources/7/examples/MCC%20-%20triaxial%20tests.pdf>

[viewed on 06/06/2012].

40. Bridge-info.org:

<http://www.bridge-info.org/bridge/index.php?ID=67>

[viewed on 15/06/2012].

Appendix

Appendix-A: Data from Øvre sund Project

Table A. 1 : Piezometer readings at different dates

| Date | time | G-71306 P4(K-4,9) | G-71606 P4(K-9,9) | G-71706 P4(K-13,1) | G-52508- P1 (K-7,0) | G-52908- P2 (K-14,0) | G-53008- P2 (K-9,0) | G-53108- P3 (K-10,0) | G-52808- P3 (K-14,0) | comments |
|------------|-------|----------------------|----------------------|-----------------------|------------------------|-------------------------|------------------------|-------------------------|-------------------------|----------|
| 10/31/2008 | 9:15 | -1.10 | -0.03 | -1.47 | 0.00 | 0.00 | 0.00 | 0.00 | 0.00 | |
| 11/5/2008 | 0:00 | | | | | | | | | |
| 11/11/2008 | 9:45 | -1.20 | -0.03 | -1.37 | 0.00 | 0.00 | 0.00 | 0.00 | 0.00 | |
| 11/19/2008 | 13:40 | -0.99 | 0.08 | -1.17 | 0.00 | 0.00 | 0.00 | 0.00 | 0.00 | |
| 11/27/2008 | 9:45 | -1.15 | -0.13 | -1.27 | 0.00 | 0.00 | 0.00 | 0.00 | 0.00 | |
| 11/28/2008 | 11:50 | -1.20 | -0.13 | -1.47 | 0.00 | 0.00 | 0.00 | 0.00 | 0.00 | |
| 12/1/2008 | 13:00 | -1.35 | -0.24 | -1.66 | 0.00 | 0.00 | 0.00 | 0.00 | 0.00 | |
| 12/2/2008 | 12:15 | -1.30 | -0.24 | -1.47 | 0.00 | 0.00 | 0.00 | 0.00 | 0.00 | |
| 12/3/2008 | 13:35 | -1.30 | -0.24 | -1.57 | 0.00 | 0.00 | 0.00 | 0.00 | 0.00 | |
| 12/5/2008 | 13:25 | -1.30 | -0.13 | -1.47 | -1.02 | 0.33 | -0.47 | -0.45 | -0.49 | |
| 12/8/2008 | 12:15 | -1.15 | -0.03 | -1.27 | -0.82 | 0.42 | -0.37 | -0.35 | -0.39 | |
| 12/9/2008 | 13:20 | -1.25 | -0.13 | -1.47 | -0.82 | 0.42 | -0.37 | -0.45 | -0.49 | |
| 12/10/2008 | 11:45 | -1.46 | -0.24 | -1.57 | -0.82 | 0.33 | -0.47 | -0.55 | -0.69 | |
| 12/11/2008 | 8:30 | -1.46 | -0.35 | -1.66 | -0.69 | 0.33 | -0.47 | -0.65 | -0.69 | |
| 12/11/2008 | 13:55 | -1.30 | -0.13 | -1.57 | -0.55 | 0.33 | -0.37 | -0.45 | -0.49 | |
| 12/11/2008 | 15:30 | -1.20 | -0.03 | -1.47 | -0.42 | 0.33 | -0.37 | -0.35 | -0.49 | |
| 12/12/2008 | 9:15 | -1.41 | -0.24 | -1.66 | -0.62 | 0.42 | -0.47 | -0.55 | -0.69 | |
| 12/12/2008 | 12:45 | -1.41 | -0.13 | -1.66 | -0.55 | 0.42 | -0.18 | 0.44 | 0.32 | |
| 12/12/2008 | 15:00 | -1.35 | -0.13 | -1.57 | -0.49 | 0.42 | -0.08 | 0.44 | 0.42 | |
| 12/15/2008 | 12:05 | -1.51 | -0.35 | -1.66 | -0.55 | 0.70 | 0.02 | -0.06 | 0.02 | |
| 12/15/2008 | 13:50 | | | | | 0.61 | -0.08 | -0.06 | -0.08 | |
| 12/16/2008 | 12:30 | -1.41 | -0.35 | -1.66 | -0.49 | 0.61 | 0.02 | -0.06 | -0.08 | |
| 12/17/2008 | 13:30 | -1.30 | -0.24 | -1.57 | -0.49 | 0.61 | -0.08 | -0.06 | -0.08 | |
| 12/18/2008 | 9:05 | -0.89 | 0.08 | -1.17 | -0.35 | 0.79 | 0.21 | 0.24 | 0.32 | |
| 12/18/2008 | 13:40 | -0.94 | -0.03 | -1.27 | -0.42 | 0.70 | 0.11 | 0.14 | 0.12 | |
| 12/19/2008 | 12:35 | -0.99 | -0.03 | -1.17 | -0.42 | 0.70 | 0.11 | 0.14 | 0.12 | |

Analysis and Modelling of induced pore pressures due to pile driving.

| | | | | | | | | | | |
|------------|-------|-------|-------|-------|-------|------|-------|------|-------|--|
| 12/22/2008 | 11:55 | -0.74 | 0.29 | -1.17 | -0.35 | 0.88 | 0.11 | 0.24 | 0.22 | |
| 1/5/2009 | 9:20 | -1.41 | 0.00 | -1.66 | -0.35 | 0.33 | -0.08 | 1.23 | -0.08 | after G192 |
| 1/5/2009 | 13:50 | -1.30 | -0.35 | -1.66 | -0.29 | 0.61 | 0.40 | 3.68 | 3.41 | after G192 and half of G194 |
| 1/5/2009 | 14:35 | -1.30 | -0.35 | -1.66 | -0.29 | 0.42 | 0.21 | 4.46 | 4.79 | after G192 G194 G197 |
| 1/5/2009 | 16:00 | -1.35 | -0.35 | -1.76 | -0.35 | 0.52 | 0.21 | 3.68 | 3.91 | |
| 1/6/2009 | 7:10 | -1.41 | -0.45 | -1.66 | -0.35 | 0.79 | 0.11 | 2.90 | 2.52 | |
| 1/6/2009 | 9:30 | -1.30 | -0.45 | -1.57 | -0.35 | 0.79 | 0.21 | 2.90 | 2.52 | |
| 1/6/2009 | 12:30 | -1.10 | -0.35 | -1.37 | -0.29 | 0.88 | 0.21 | 3.00 | 2.62 | after G53, G54 |
| 1/6/2009 | 15:40 | -1.04 | -0.35 | -1.37 | -0.29 | 0.97 | 0.21 | 2.90 | 2.52 | etter peln. G53, G54, G55, G56 rammet. |
| 1/7/2009 | 7:15 | -1.30 | -0.35 | -1.76 | -0.35 | 0.97 | 0.11 | 2.22 | 1.92 | |
| 1/7/2009 | 10:45 | -1.30 | -0.24 | -1.57 | -0.35 | 1.16 | 0.11 | 2.31 | 2.12 | før pelnr. G184 rammet |
| 1/7/2009 | 11:05 | 0.58 | 1.23 | -1.57 | -0.35 | 1.16 | 0.11 | 2.31 | 2.12 | halv pelnr. G184 rammet (12m) |
| 1/7/2009 | 12:35 | -0.48 | 0.92 | -1.47 | -0.29 | 0.97 | 0.21 | 2.31 | 2.12 | etter pelnr. G184 rammet |
| 1/7/2009 | 14:35 | 0.94 | 0.92 | -1.47 | -0.29 | 1.07 | 0.31 | 2.31 | 2.22 | før pelnr. G182 rammet og etter pelnr. G217 rammet. |
| 1/7/2009 | 15:05 | 3.21 | 3.73 | -1.37 | -0.29 | 1.07 | 0.31 | 2.31 | 2.22 | halv pelnr. G182 rammet (12m) |
| 1/7/2009 | 15:40 | 2.03 | 7.72 | -1.57 | -0.29 | 1.07 | 0.31 | 2.31 | 2.22 | etter pelnr. G182 rammet |
| 1/8/2009 | 7:10 | 0.33 | 4.66 | -1.66 | -0.35 | 0.97 | 0.11 | 1.92 | 1.82 | før pelnr. G213 rammet. |
| 1/8/2009 | 9:00 | 0.33 | 4.56 | -1.66 | -0.35 | 1.07 | 0.21 | 1.92 | 1.82 | etter pelnr. G213 rammet. |

Analysis and Modelling of induced pore pressures due to pile driving.

| | | | | | | | | | | |
|-----------|-------|-------|------|-------|-------|------|------|------|------|--|
| 1/8/2009 | 12:20 | 0.33 | 4.56 | -1.66 | -0.35 | 1.16 | 0.31 | 2.12 | 2.02 | etter pelnr. G209 rammet. |
| 1/8/2009 | 13:00 | 0.33 | 4.46 | -1.66 | -0.35 | 1.25 | 0.50 | 2.51 | 2.62 | etter pelnr. G206 rammet. |
| 1/8/2009 | 14:40 | 0.28 | 4.46 | -1.57 | -0.15 | 1.43 | 0.79 | 3.00 | 3.12 | etter pelnr. G203 rammet. |
| 1/8/2009 | 15:40 | 0.23 | 4.25 | -1.57 | -0.15 | 1.43 | 1.07 | 5.81 | 5.28 | etter pelnr. G200 rammet. |
| 1/9/2009 | 10:35 | -0.23 | 3.32 | -1.76 | -0.29 | 1.52 | 1.07 | 4.75 | 4.30 | |
| 1/9/2009 | 13:30 | -0.18 | 3.22 | -1.57 | -0.29 | 1.61 | 1.07 | 4.75 | 4.11 | |
| 1/12/2009 | 7:35 | -0.28 | 1.86 | -1.27 | -0.22 | 1.80 | 1.07 | 3.39 | 3.02 | |
| 1/12/2009 | 15:40 | -0.18 | 1.97 | -1.17 | -0.02 | 1.89 | 1.27 | 3.49 | 3.12 | |
| 1/13/2009 | 7:40 | -0.23 | 1.76 | -1.17 | -0.09 | 1.89 | 1.17 | 3.19 | 2.82 | |
| 1/13/2009 | 15:40 | -0.28 | 1.65 | -1.27 | 0.05 | 1.89 | 1.17 | 3.00 | 2.72 | |
| 1/14/2009 | 7:20 | -0.43 | 1.44 | -1.37 | -0.02 | 1.70 | 1.07 | 2.71 | 2.32 | |
| 1/14/2009 | 15:30 | -0.63 | 1.13 | -1.66 | -0.22 | 1.52 | 0.98 | 2.80 | 2.42 | |
| 1/15/2009 | 7:50 | -0.63 | 1.23 | -1.57 | -0.22 | 1.43 | 0.88 | 2.51 | 2.22 | |
| 1/15/2009 | 14:40 | -0.79 | 1.02 | -1.86 | -0.22 | 1.52 | 0.88 | 2.31 | 1.92 | |
| 1/16/2009 | 8:00 | -0.69 | 1.02 | -1.66 | -0.15 | 1.43 | 0.79 | 2.12 | 1.82 | |
| 1/16/2009 | 10:30 | -0.69 | 1.02 | -1.66 | -0.15 | 1.43 | 0.88 | 3.00 | 1.92 | etter st lror rammet p  pel Nr G200 |
| 1/16/2009 | 13:00 | 0.18 | 1.86 | -1.86 | -0.15 | 1.34 | 0.79 | 2.31 | 1.72 | etter st lror rammet p  all peler. |
| 1/19/2009 | 9:00 | -0.63 | 0.71 | -1.27 | -0.09 | 1.43 | 0.88 | 2.02 | 1.82 | |
| 1/20/2009 | 7:10 | -0.89 | 0.50 | -1.57 | -0.22 | 1.43 | 0.79 | 1.63 | 1.42 | |
| 1/20/2009 | 15:30 | -0.58 | 0.81 | -1.27 | -0.09 | 1.70 | 1.46 | 5.61 | 4.20 | etter pelnr. G157, G161og G165 rammet. |

Analysis and Modelling of induced pore pressures due to pile driving.

| | | | | | | | | | | |
|-----------|-------|-------|------|-------|-------|------|------|------|------|-------------------------------|
| 1/21/2009 | 7:10 | -0.79 | 0.50 | -1.47 | -0.15 | 1.70 | 1.17 | 4.17 | 3.32 | |
| 1/21/2009 | 10:30 | -0.79 | 0.50 | -1.47 | -0.09 | 1.80 | 1.46 | 4.75 | 4.01 | etter pel G141 og G142 rammet |
| 1/21/2009 | 15:30 | -0.63 | 0.71 | -1.37 | -0.02 | 1.80 | 1.55 | 4.46 | 3.81 | etter pel G155 og G159 rammet |
| 1/22/2009 | 7:10 | -0.69 | 0.50 | -1.57 | -0.09 | 1.98 | 1.55 | 3.78 | 3.32 | før pelnr. G168 |
| 1/22/2009 | 10:45 | -0.69 | 0.50 | -1.57 | -0.09 | 1.98 | 1.94 | 5.71 | 4.40 | etter pel nr. G168 og G167 |
| 1/22/2009 | 15:00 | -0.63 | 0.81 | -1.27 | 0.05 | 1.98 | 2.03 | 5.13 | 4.30 | |
| 1/23/2009 | 7:10 | -1.04 | 0.39 | -1.76 | -0.02 | 2.79 | 2.51 | 4.55 | 4.11 | |
| 1/23/2009 | 10:30 | -1.04 | 0.39 | -1.76 | -0.02 | 2.70 | 2.70 | 4.84 | 4.40 | før pel nr. G166 |
| 1/23/2009 | 15:20 | -0.74 | 0.60 | -1.37 | 0.25 | 3.15 | 2.51 | 6.00 | 5.58 | etter pel nr. G166 |
| 1/26/2009 | 7:10 | -0.99 | 0.29 | -1.66 | 0.18 | 3.24 | 2.51 | 3.97 | 4.01 | |
| 1/26/2009 | 10:20 | -0.99 | 0.29 | -1.66 | 0.05 | 3.24 | 2.70 | 5.61 | 4.99 | etter pel nr. G164 |
| 1/26/2009 | 14:00 | -0.99 | 0.39 | -1.66 | 0.25 | 3.42 | 2.89 | 5.52 | 5.19 | |
| 1/27/2009 | 7:10 | -0.84 | 0.50 | -1.57 | 0.18 | 3.42 | 2.79 | 5.04 | 4.89 | før pel nr. G145 |
| 1/27/2009 | 9:15 | -0.84 | 0.50 | -1.57 | 0.25 | 2.88 | 3.27 | 5.61 | 5.38 | etter pel nr. G145 |
| 1/27/2009 | 14:50 | -0.84 | 0.50 | -1.76 | 0.38 | 3.33 | 3.36 | 5.23 | 5.09 | |
| 1/28/2009 | 7:00 | -0.84 | 0.50 | -1.76 | 0.45 | 3.96 | 3.17 | 4.75 | 4.70 | før pel nr. G147 |
| 1/28/2009 | 9:10 | -0.84 | 0.50 | -1.76 | 0.31 | 4.05 | 3.27 | 5.23 | 4.99 | etter pel nr. G147 |
| 1/28/2009 | 10:15 | -0.84 | 0.50 | -1.76 | 0.38 | 3.42 | 3.17 | 5.61 | 5.28 | etter pel nr. G146 |
| 1/28/2009 | 15:15 | -0.84 | 0.50 | -1.76 | 0.51 | 4.23 | 2.98 | 5.42 | 5.19 | |
| 1/29/2009 | 9:10 | -0.69 | 0.50 | -1.66 | 0.38 | 4.68 | 3.27 | 4.84 | 4.89 | |
| 1/29/2009 | 15:10 | -0.84 | 0.39 | -1.76 | 0.71 | 4.77 | 3.27 | 4.65 | 4.70 | |
| 1/30/2009 | 8:00 | -0.79 | 0.29 | -1.76 | 0.45 | 4.68 | 3.17 | 4.36 | 4.40 | |

Analysis and Modelling of induced pore pressures due to pile driving.

| | | | | | | | | | | |
|-----------|-------|-------|-------|-------|------|------|------|------|------|---|
| 1/30/2009 | 12:30 | -0.89 | 0.18 | -1.86 | 0.71 | 4.86 | 3.27 | 4.26 | 4.30 | etter pel nr. G85, G86, G87, G101 og G102 |
| 2/2/2009 | 8:15 | -0.89 | -0.03 | -1.86 | 0.71 | 4.50 | 3.17 | 3.68 | 3.71 | |
| 2/2/2009 | 12:20 | -0.89 | -0.03 | -1.86 | 1.11 | 4.95 | 3.27 | 3.68 | 3.71 | etter pel nr. G117, G132 |
| 2/2/2009 | 15:00 | -0.89 | -0.03 | -1.86 | 1.24 | 5.48 | 3.36 | 3.68 | 3.81 | etter pel nr. 133 |
| 2/2/2009 | 15:30 | -0.89 | -0.03 | -1.96 | 0.65 | 4.95 | 3.17 | 3.97 | 3.91 | |
| 2/3/2009 | 7:00 | -1.04 | -0.13 | -1.96 | 0.85 | 4.68 | 3.17 | 3.58 | 3.51 | |
| 2/3/2009 | 9:10 | -1.04 | -0.03 | -1.96 | 1.11 | 5.12 | 3.36 | 3.78 | 3.61 | etter pel G116 rammet |
| 2/3/2009 | 12:20 | -0.99 | -0.03 | -1.76 | 0.71 | 5.66 | 3.45 | 4.26 | 4.11 | etter pel G111 og G138 rammet |
| 2/3/2009 | 14:30 | -1.04 | -0.13 | -1.86 | 0.71 | 5.83 | 3.55 | 4.26 | 4.11 | etter pel G137 og G112 rammet |
| 2/4/2009 | 7:00 | -1.30 | -0.13 | -1.96 | 0.85 | 5.57 | 3.55 | 3.78 | 3.41 | 0 |
| 2/4/2009 | 11:00 | -1.30 | -0.03 | -1.76 | 0.91 | 5.57 | 3.64 | 3.88 | 3.51 | 0 |
| 2/4/2009 | 14:00 | -1.25 | -0.13 | -1.86 | 0.85 | 6.27 | 4.58 | 4.26 | 3.81 | etter pel G113 og G136 rammet |
| 2/5/2009 | 7:00 | -1.25 | -0.13 | -1.86 | 1.44 | 6.27 | 3.83 | 3.88 | 3.41 | 0 |
| 2/5/2009 | 12:20 | -1.15 | 0.08 | -1.66 | 1.97 | 7.24 | 4.58 | 4.46 | 3.91 | etter pel nr. G115, G134 rammet |
| 2/5/2009 | 15:00 | -1.04 | 0.18 | -1.66 | 2.36 | 7.33 | 5.43 | 4.36 | 3.81 | etter pel nr. G105, G106, G83, G84 rammet |
| 2/6/2009 | 7:00 | -1.20 | -0.03 | -1.86 | 1.97 | 6.80 | 5.33 | 3.78 | 3.32 | 0 |
| 2/6/2009 | 10:30 | -1.20 | -0.03 | -1.86 | 2.23 | 6.89 | 5.52 | 3.88 | 3.41 | 0 |
| 2/6/2009 | 13:25 | -1.20 | -0.03 | -1.86 | 2.23 | 7.07 | 5.61 | 4.07 | 3.51 | 0 |
| 2/6/2009 | 15:30 | -1.20 | 0.08 | -1.76 | 2.23 | 7.07 | 5.61 | 4.07 | 3.51 | 0 |
| 2/9/2009 | 7:35 | -0.94 | 0.08 | -1.76 | 2.75 | 6.10 | 5.05 | 3.10 | 3.22 | 0 |

Analysis and Modelling of induced pore pressures due to pile driving.

| | | | | | | | | | | |
|-----------|-------|-------|-------|-------|------|------|------|------|------|------------------------------|
| 2/10/2009 | 7:55 | -1.20 | -0.24 | -1.76 | 2.88 | 5.83 | 4.96 | 2.90 | 2.92 | 0 |
| 2/11/2009 | 8:15 | -1.10 | -0.13 | -1.66 | 3.01 | 5.66 | 4.87 | 2.80 | 2.92 | 0 |
| 2/12/2009 | 7:20 | -1.04 | -0.03 | -1.66 | 3.01 | 5.39 | 4.68 | 2.61 | 2.72 | 0 |
| 2/12/2009 | 15:58 | -1.10 | -0.03 | -1.66 | 3.08 | 5.30 | 4.68 | 2.61 | 2.52 | 0 |
| 2/13/2009 | 11:45 | -1.41 | -0.45 | -1.96 | 3.08 | 5.12 | 4.58 | 2.31 | 2.32 | is på elven |
| 2/16/2009 | 12:00 | -1.20 | -0.35 | -1.76 | 3.21 | 4.68 | 4.30 | 2.12 | 2.12 | is på elven |
| 2/17/2009 | 8:20 | -1.30 | -0.35 | -1.96 | 3.21 | 4.50 | 4.21 | 2.02 | 2.02 | is på elven |
| 2/18/2009 | 9:45 | -1.35 | -0.35 | -1.96 | 3.14 | 4.32 | 4.02 | 1.82 | 1.82 | Målt o.k. is på elva |
| 2/19/2009 | 9:20 | -1.30 | -0.35 | -1.86 | 3.21 | 4.23 | 4.02 | 1.82 | 1.82 | Målt o.k. is på elva |
| 2/20/2009 | 9:00 | -1.30 | -0.35 | -1.96 | 3.21 | 4.05 | 3.83 | 1.72 | 1.62 | Målt o.k. is på elva |
| 2/23/2009 | 8:45 | -1.20 | -0.35 | -1.76 | 3.27 | 3.87 | 3.74 | 1.63 | 1.52 | 0:00 |
| 2/24/2009 | 8:30 | -1.15 | -0.35 | -1.76 | 3.14 | 3.60 | 3.64 | 1.53 | 1.52 | Målt o.k. is på elva |
| 2/25/2009 | 8:40 | -1.20 | -0.35 | -1.86 | 3.14 | 3.69 | 3.55 | 1.43 | 1.42 | Målt o.k. is på elva |
| 2/26/2009 | 10:00 | -1.10 | -0.35 | -1.76 | 3.21 | 3.60 | 3.55 | 1.43 | 1.42 | Målt o.k. is på elva |
| 2/27/2009 | 9:00 | -1.20 | -0.45 | -1.76 | 3.08 | 3.51 | 3.36 | 1.33 | 1.42 | Målt o.k. is på elva |
| 3/2/2009 | 9:40 | -1.25 | -0.45 | -1.76 | 3.34 | 3.42 | 3.36 | 1.23 | 1.22 | Nå er isen borte |
| 3/3/2009 | 10:15 | -1.20 | -0.35 | -1.66 | 3.60 | 3.87 | 3.83 | 1.43 | 1.42 | Oppfylling med ca 1,0 masser |
| 3/4/2009 | 8:10 | -1.30 | -0.45 | -1.86 | 3.53 | 3.69 | 3.64 | 1.23 | 1.22 | |
| 3/5/2009 | 8:10 | -1.46 | -0.56 | -2.06 | 3.53 | 3.51 | 3.45 | 1.13 | 1.12 | |
| 3/6/2009 | 8:10 | -1.46 | -0.66 | -2.06 | 3.40 | 3.42 | 3.36 | 1.13 | 1.02 | |
| 3/9/2009 | 8:30 | -1.15 | -0.45 | -1.76 | 3.34 | 3.33 | 3.27 | 1.13 | 1.12 | |
| 3/10/2009 | 9:40 | -1.30 | -0.56 | -1.96 | 3.27 | 3.24 | 3.08 | 0.94 | 0.92 | |
| 3/11/2009 | 8:45 | -1.25 | -0.45 | -1.76 | 3.27 | 3.24 | 3.08 | 1.03 | 1.02 | |
| 3/12/2009 | 9:20 | -1.30 | -0.56 | -1.86 | 3.21 | 3.15 | 2.98 | 0.84 | 0.82 | |
| 3/13/2009 | 9:40 | -1.20 | -0.45 | -1.76 | 3.14 | 3.06 | 2.98 | 0.94 | 0.92 | |
| 3/16/2009 | 9:30 | -1.30 | -0.56 | -1.76 | 3.01 | 2.97 | 2.79 | 0.84 | 0.82 | |
| 3/17/2009 | 8:15 | -1.30 | -0.56 | -1.86 | 2.95 | 2.88 | 2.70 | 0.74 | 0.72 | |
| 3/18/2009 | 8:00 | -1.35 | -0.56 | -1.96 | 2.95 | 2.79 | 2.60 | 0.74 | 0.62 | |

Analysis and Modelling of induced pore pressures due to pile driving.

| | | | | | | | | | | |
|-----------|-------|-------|-------|-------|------|------|------|------|------|----------------------------------|
| 3/19/2009 | 8:10 | -1.51 | -0.66 | -2.06 | 2.88 | 2.70 | 2.51 | 0.54 | 0.52 | |
| 3/20/2009 | 10:00 | -1.51 | -0.66 | -2.06 | 2.82 | 2.61 | 2.41 | 0.44 | 0.52 | |
| 3/23/2009 | 13:45 | -1.20 | -0.45 | -1.76 | 2.69 | 2.61 | 2.41 | 0.64 | 0.62 | |
| 3/24/2009 | 10:55 | -1.51 | -0.66 | -1.96 | 2.69 | 2.52 | 2.32 | 0.44 | 0.52 | |
| 3/25/2009 | 13:00 | -1.46 | -0.77 | -1.96 | 2.62 | 2.52 | 2.22 | 0.44 | 0.42 | |
| 3/26/2009 | 8:00 | -1.41 | -0.77 | -1.76 | 2.56 | 2.52 | 2.22 | 0.44 | 0.52 | |
| 3/27/2009 | 8:30 | -1.41 | -0.77 | -1.96 | 2.56 | 2.43 | 2.13 | 0.44 | 0.42 | |
| 3/30/2009 | 12:20 | -1.25 | -0.66 | -1.76 | 2.43 | 2.43 | 2.13 | 0.44 | 0.52 | |
| 3/31/2009 | 8:15 | -1.25 | -0.56 | -1.76 | 2.43 | 2.43 | 2.13 | 0.44 | 0.52 | |
| 4/1/2009 | 9:00 | -1.30 | -0.66 | -1.86 | 2.36 | 2.34 | 2.03 | 0.34 | 0.42 | |
| 4/2/2009 | 8:10 | -1.41 | -0.77 | -1.96 | 2.29 | 2.25 | 1.94 | 0.24 | 0.32 | |
| 4/3/2009 | 8:45 | -1.41 | -0.66 | -1.96 | 2.29 | 2.25 | 1.94 | 0.24 | 0.22 | |
| 4/14/2009 | 10:40 | -1.15 | -0.56 | -1.76 | 1.97 | 2.07 | 1.65 | 0.24 | 0.32 | |
| 4/15/2009 | 8:30 | -1.25 | -0.56 | -1.86 | 2.03 | 1.98 | 1.65 | 0.14 | 0.32 | |
| 4/16/2009 | 8:20 | -1.30 | -0.56 | -1.96 | 1.90 | 1.98 | 1.65 | 0.04 | 0.12 | |
| 4/17/2009 | 8:05 | -1.35 | -0.66 | -2.06 | 1.84 | 1.89 | 1.46 | 0.04 | 0.12 | |
| 4/20/2009 | 9:35 | -1.41 | -0.77 | -2.06 | 1.77 | 1.89 | 1.55 | 0.04 | 0.02 | |
| 4/21/2009 | 12:40 | -1.35 | -0.77 | -1.96 | 1.84 | 1.89 | 1.55 | 0.04 | 0.12 | |
| 4/22/2009 | 12:45 | -1.41 | -0.77 | -1.96 | 1.77 | 1.80 | 1.36 | 0.04 | 0.02 | |
| 4/23/2009 | 8:25 | -1.30 | -0.77 | -1.86 | 1.84 | 1.89 | 1.46 | 0.14 | 0.12 | |
| 4/24/2009 | 9:30 | -1.35 | -0.77 | -1.86 | 1.84 | 1.89 | 1.46 | 0.14 | 0.12 | |
| 4/27/2009 | 9:10 | -1.20 | -0.66 | -1.76 | 1.64 | 1.89 | 1.36 | 0.14 | 0.22 | |
| 4/28/2009 | 8:30 | -1.10 | -0.66 | -1.66 | 1.70 | 1.98 | 1.36 | 0.34 | 0.32 | |
| 4/29/2009 | 12:00 | -1.25 | -0.77 | -1.86 | 1.64 | 2.07 | 1.36 | 0.14 | 0.22 | |
| 4/30/2009 | 7:10 | -1.30 | -0.56 | -1.96 | 1.64 | 1.89 | 1.36 | 0.14 | 0.22 | |
| 5/4/2009 | 7:10 | -1.25 | -0.66 | -1.96 | 1.51 | 1.98 | 1.36 | 0.54 | 0.62 | før pel G201 rammet |
| 5/4/2009 | 11:31 | -1.25 | -0.66 | -1.96 | 1.51 | 1.98 | 1.36 | 3.29 | 2.82 | etter halv pel G201 rammet |
| 5/4/2009 | 14:57 | -1.25 | -0.66 | -1.96 | 1.51 | 2.70 | 2.13 | 3.58 | 5.58 | etter pel G201 rammet |
| 5/5/2009 | 7:05 | -1.04 | -0.56 | -1.66 | 1.57 | 2.88 | 2.03 | 3.10 | 4.50 | |

Analysis and Modelling of induced pore pressures due to pile driving.

| | | | | | | | | | | |
|-----------|-------|-------|-------|-------|------|------|------|------|------|---|
| 5/6/2009 | 7:50 | -1.10 | -0.56 | -1.76 | 1.51 | 2.97 | 2.13 | 3.00 | 4.11 | |
| 5/7/2009 | 7:58 | -0.12 | 3.42 | -1.76 | 1.51 | 2.88 | 2.13 | 2.41 | 3.71 | etter pel. G183 og 185 rammet |
| 5/8/2009 | 8:23 | -0.28 | 2.38 | -1.57 | 1.51 | 2.79 | 2.13 | 2.71 | 3.61 | |
| 5/11/2009 | 7:51 | -0.74 | 0.92 | -1.76 | 1.37 | 2.52 | 1.84 | 2.12 | 2.82 | |
| 5/12/2009 | 10:45 | -0.84 | 0.60 | -1.86 | 1.44 | 2.88 | 2.13 | 3.39 | 4.89 | etter pel. nr. G202, G205 rammet |
| 5/13/2009 | 7:51 | -1.04 | 0.29 | -2.06 | 1.37 | 2.70 | 1.94 | 3.10 | 4.30 | |
| 5/14/2009 | 7:53 | -1.15 | 0.08 | -2.06 | 1.31 | 2.52 | 1.84 | 2.90 | 3.91 | |
| 5/15/2009 | 8:20 | -1.20 | -0.13 | -2.16 | 1.31 | 2.52 | 1.84 | 2.71 | 3.61 | |
| 5/18/2009 | 7:30 | -1.25 | -0.56 | -2.06 | 1.18 | 2.34 | 1.74 | 2.31 | 2.92 | |
| 5/19/2009 | 7:30 | -1.30 | -0.66 | -2.16 | 1.11 | 2.52 | 1.84 | 2.90 | 4.01 | |
| 5/20/2009 | 8:59 | -1.30 | -0.77 | -2.16 | 1.11 | 2.52 | 1.94 | 3.00 | 4.20 | |
| 5/25/2009 | 7:46 | -1.04 | -0.77 | -1.86 | 1.11 | 2.52 | 1.74 | 2.61 | 3.32 | |
| 5/26/2009 | 8:35 | -1.10 | -0.88 | -1.86 | 1.11 | 2.43 | 1.74 | 2.41 | 3.12 | |
| 5/27/2009 | 9:20 | -0.74 | -0.66 | -1.57 | 1.31 | 2.61 | 1.94 | 2.61 | 3.32 | |
| 5/28/2009 | 12:30 | -1.04 | -0.88 | -1.86 | 1.11 | 2.34 | 1.65 | 2.12 | 2.82 | |
| 5/29/2009 | 8:05 | -1.20 | -0.98 | -1.96 | 1.11 | 2.34 | 1.65 | 2.02 | 2.52 | |
| 6/2/2009 | 15:40 | -1.15 | -0.98 | -1.96 | 0.98 | 2.25 | 1.55 | 1.72 | 2.22 | |
| 6/3/2009 | 8:50 | -1.30 | -1.19 | -2.16 | 0.98 | 2.16 | 1.46 | 1.53 | 1.92 | |
| 6/4/2009 | 7:51 | -1.30 | -1.19 | -2.06 | 0.98 | 2.16 | 1.46 | 1.43 | 1.92 | |
| 6/5/2009 | 8:23 | -1.25 | -1.19 | -2.06 | 1.11 | 2.16 | 1.46 | 1.43 | 1.82 | |
| 6/8/2009 | 9:55 | -1.30 | -1.19 | -2.06 | 1.11 | 2.07 | 1.36 | 1.33 | 1.62 | |
| 6/10/2009 | 9:30 | -1.30 | -1.19 | -2.16 | 1.18 | 2.07 | 1.36 | 1.13 | 1.42 | |
| 6/29/2009 | 8:28 | | | | | | | 0.34 | 0.62 | |
| 6/29/2009 | 13:50 | | | | | | | 0.54 | 0.72 | |
| 7/1/2009 | 8:45 | | | | | | | 0.34 | 0.52 | |
| 7/1/2009 | 12:15 | | | | | | | 0.44 | 0.62 | |
| 7/2/2009 | 9:30 | | | | | | | 0.34 | 0.52 | |
| 7/3/2009 | 8:56 | | | | | | | 0.34 | 0.52 | |
| 7/6/2009 | 9:40 | | | | | | | 0.54 | 0.72 | |
| 7/6/2009 | 14:12 | | | | | | | 0.44 | 0.62 | |

Analysis and Modelling of induced pore pressures due to pile driving.

| | | | | | | | | | | |
|------------|-------|--|--|--|--|--|--|-------|------|--|
| 7/7/2009 | 9:41 | | | | | | | 0.44 | 0.62 | |
| 9/3/2009 | 15:07 | | | | | | | 0.14 | 0.32 | |
| 9/17/2009 | 9:41 | | | | | | | -0.15 | 0.12 | |
| 10/1/2009 | 13:33 | | | | | | | 0.04 | 0.22 | |
| 10/8/2009 | 7:46 | | | | | | | 0.34 | 0.62 | |
| 10/8/2009 | 8:37 | | | | | | | 0.24 | 0.62 | |
| 10/8/2009 | 12:33 | | | | | | | 0.14 | 0.42 | |
| 10/12/2009 | 8:10 | | | | | | | -0.06 | 0.22 | |
| 10/12/2009 | 13:41 | | | | | | | 0.24 | 0.52 | |
| 10/13/2009 | 9:54 | | | | | | | -0.06 | 0.32 | |
| 10/14/2009 | 8:30 | | | | | | | -0.15 | 0.32 | |
| 10/14/2009 | 12:20 | | | | | | | 0.04 | 0.42 | |
| 10/14/2009 | 12:36 | | | | | | | 0.04 | 0.42 | |
| 10/15/2009 | 8:41 | | | | | | | 0.04 | 0.52 | |
| 10/16/2009 | 10:00 | | | | | | | -0.06 | 0.32 | |
| 10/20/2009 | 9:00 | | | | | | | 0.14 | 0.52 | |
| 10/21/2009 | 12:57 | | | | | | | 0.04 | 0.42 | |
| 10/22/2009 | 10:08 | | | | | | | 0.14 | 0.42 | |
| 10/26/2009 | 13:30 | | | | | | | 0.14 | 0.42 | |
| 11/17/2009 | 9:06 | | | | | | | 0.24 | 0.42 | |
| 11/30/2009 | 9:15 | | | | | | | 0.44 | 0.52 | |
| 12/7/2009 | 13:44 | | | | | | | 0.34 | 0.42 | |
| 12/16/2009 | 10:15 | | | | | | | -0.15 | 0.12 | |
| 1/8/2010 | 11:56 | | | | | | | -0.15 | 0.22 | |

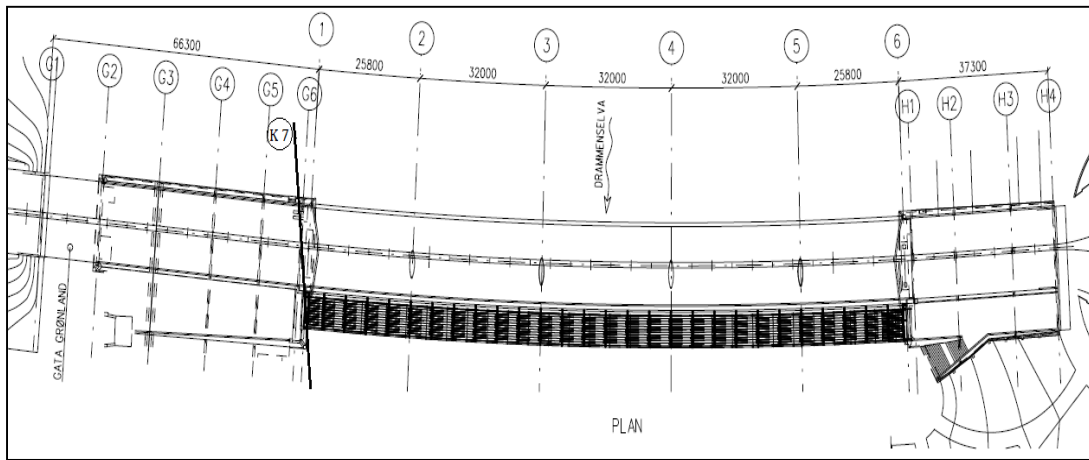


Figure A. 1 : Plan view of Bridge showing pile axis

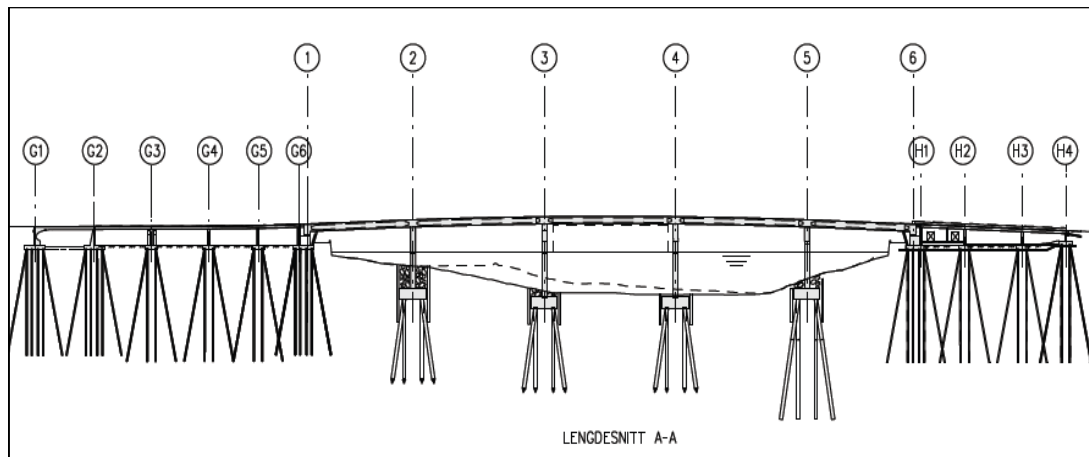


Figure A. 2 : Cross sectional view of Bridge showing pile axis

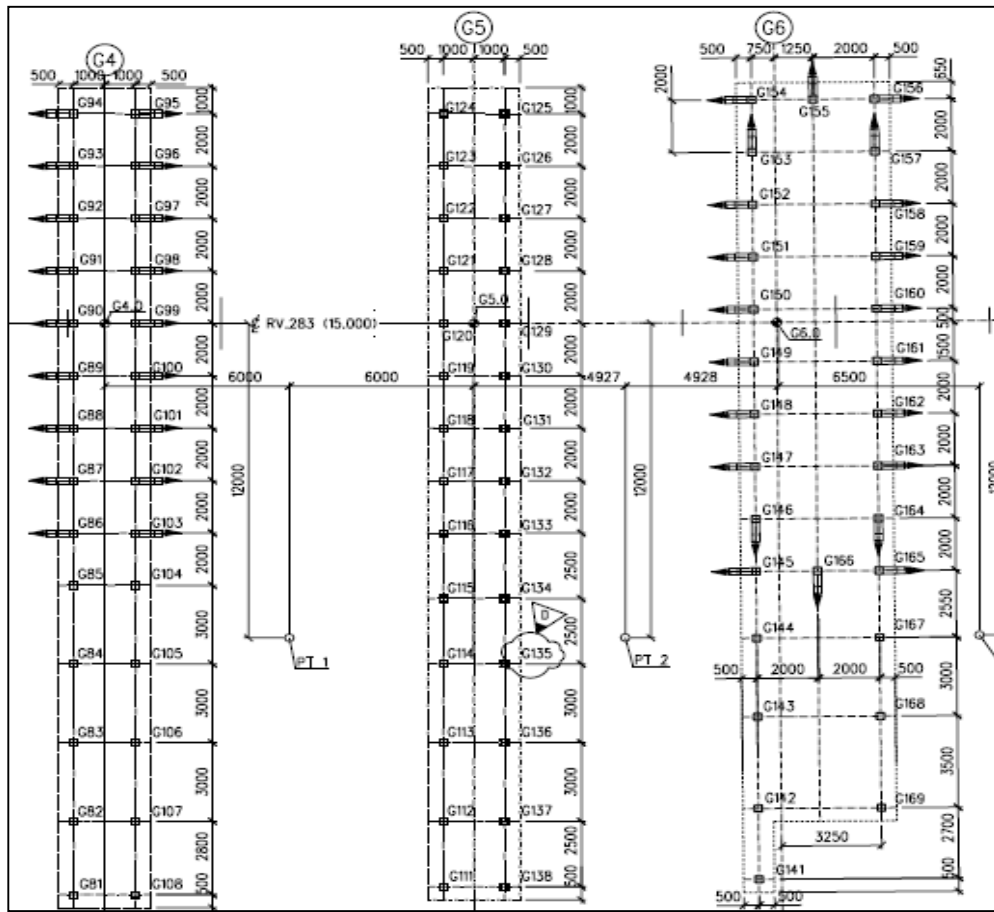


Figure A. 3 : Pile plan at different axis.

Table A. 2 : Lengths of piles below the cutting elevation. The ground level is at 0,5m and the cutting elevation is at 0,7m

| Lengths of piles below the cutting elevation. The ground level is at 0,5m and the cutting elevation is at 0,7m. | | | | | | | | | |
|---|------------|----------|------------|----------|------------|----------|------------|----------|------------|
| Axis 7 | | Axis G6 | | Axis G5 | | Axis G4 | | Axis G3 | |
| Pile nr. | Length (m) | Pile nr. | Length (m) | Pile nr. | Length (m) | Pile nr. | Length (m) | Pile nr. | Length (m) |
| G182 | 22,10 | G141 | 29,90 | G111 | 25,70 | G81 | 23,95 | G51 | 21,70 |
| G184 | 26,30 | G142 | 29,70 | G112 | 23,10 | G82 | 23,70 | G52 | 25,30 |
| G186 | 25,30 | G143 | 28,00 | G113 | 23,30 | G83 | 23,05 | G53 | 21,80 |
| G188 | 25,30 | G144 | 28,10 | G114 | 25,60 | G84 | 23,95 | G54 | 22,30 |
| G190 | 31,30 | G145 | 27,30 | G115 | 25,65 | G85 | 23,15 | G55 | 22,10 |
| G192 | 28,40 | G146 | 27,40 | G116 | 25,75 | G86 | 22,80 | G56 | 21,10 |
| G194 | 28,30 | G147 | 26,30 | G117 | 26,30 | G87 | 23,00 | G57 | 22,00 |
| G197 | 30,30 | G148 | 23,85 | G118 | 27,30 | G88 | 23,00 | G58 | 22,20 |
| G200 | 23,40 | G149 | 24,70 | G119 | 24,10 | G89 | 24,00 | G59 | 22,00 |
| G203 | 29,80 | G150 | 24,70 | G120 | 22,10 | G90 | 24,70 | G60 | 22,40 |
| G206 | 30,90 | G151 | 24,20 | G121 | 22,80 | G91 | 25,00 | G61 | 21,50 |
| G209 | 31,30 | G152 | 25,30 | G122 | 22,30 | G92 | 25,90 | G62 | 24,60 |
| G213 | 30,80 | G153 | 23,70 | G123 | 24,70 | G93 | 25,60 | G63 | 23,20 |
| G217 | 32,30 | G154 | 25,50 | G124 | 23,70 | G94 | 25,30 | G64 | 23,15 |
| | | G155 | 24,80 | G125 | 23,80 | G95 | 20,31 | G65 | 25,30 |
| | | G156 | 24,10 | G126 | 24,30 | G96 | 22,70 | G66 | 25,60 |
| | | G157 | 23,35 | G127 | 27,70 | G97 | 22,30 | G67 | 24,50 |
| | | G158 | 25,55 | G128 | 23,10 | G98 | 22,60 | G68 | 24,80 |
| | | G159 | 25,55 | G129 | 23,90 | G99 | 22,30 | G69 | 24,10 |
| | | G160 | 25,60 | G130 | 24,50 | G100 | 22,30 | G70 | 23,50 |
| | | G161 | 24,20 | G131 | 25,70 | G101 | 22,20 | G71 | 22,00 |
| | | G162 | 23,30 | G132 | 25,60 | G102 | 22,00 | G72 | 24,10 |
| | | G163 | 29,40 | G133 | 24,75 | G103 | 22,20 | G73 | 22,30 |
| | | G164 | 28,40 | G134 | 25,65 | G104 | 22,20 | G74 | 22,00 |
| | | G165 | 31,80 | G135 | 25,90 | G105 | 23,70 | G75 | 21,50 |
| | | G166 | 30,00 | G136 | 24,90 | G106 | 24,00 | G76 | 21,40 |
| | | G167 | 28,80 | G137 | 25,05 | G107 | 23,95 | G77 | 22,10 |
| | | G168 | 29,00 | G138 | 25,50 | G108 | 24,00 | G78 | 21,60 |
| | | G169 | 29,80 | | | | | | |

Table A. 3 : Pile distances from piezometers

| Piezometers | | Elvation (m) | Pile nr. | Distance (m) |
|-------------|---------|--------------|----------|--------------|
| P4 | G-71306 | -4,9 | G184 | 4,1 |
| | | | G182 | 2,0 |
| | G-71606 | -9,9 | G184 | 5,1 |
| | | | G182 | 0,5 |
| | G-71706 | -13,1 | G184 | 4,7 |
| | | | G182 | 1,5 |
| P3 | G-53108 | -10 | G213 | 16,0 |
| | | | G209 | 12,5 |
| | | | G206 | 8,6 |
| | | | G203 | 4,6 |
| | | | G200 | 1,6 |
| | G-52808 | -14 | G213 | 16,0 |
| | | | G209 | 11,6 |
| | | | G206 | 7,9 |
| | | | G203 | 4,0 |
| | | | G200 | 1,3 |

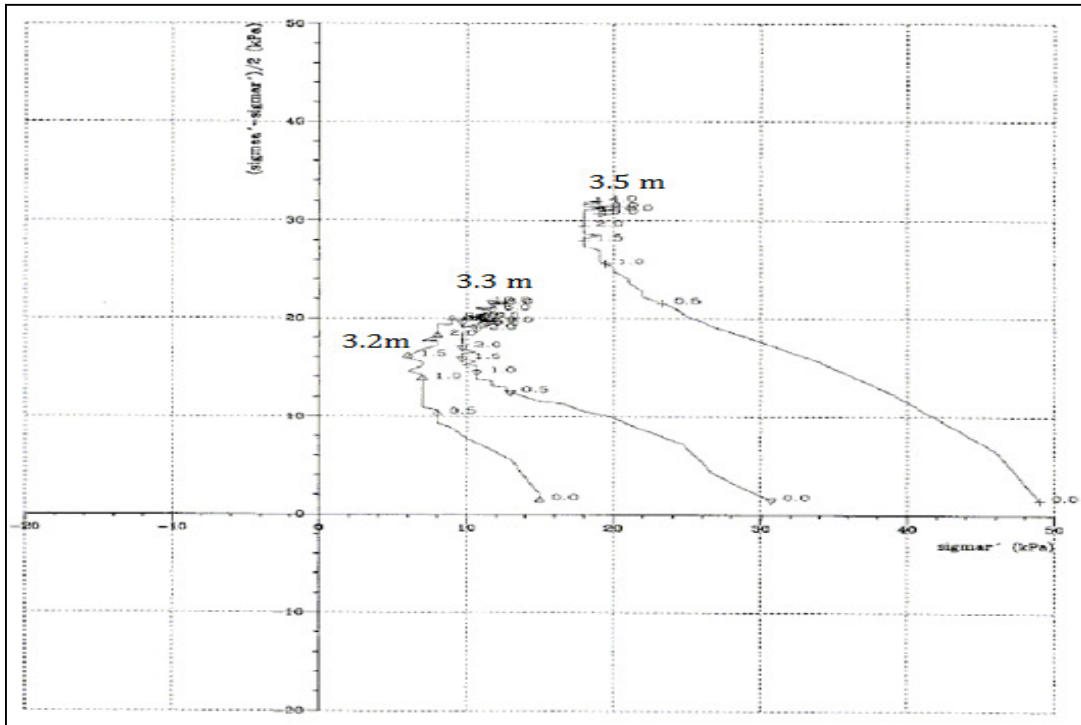


Figure A. 4 : CIU triaxial test at borehole 19

Appendix-B: Analysis of piezometric data from Øvre sund Project

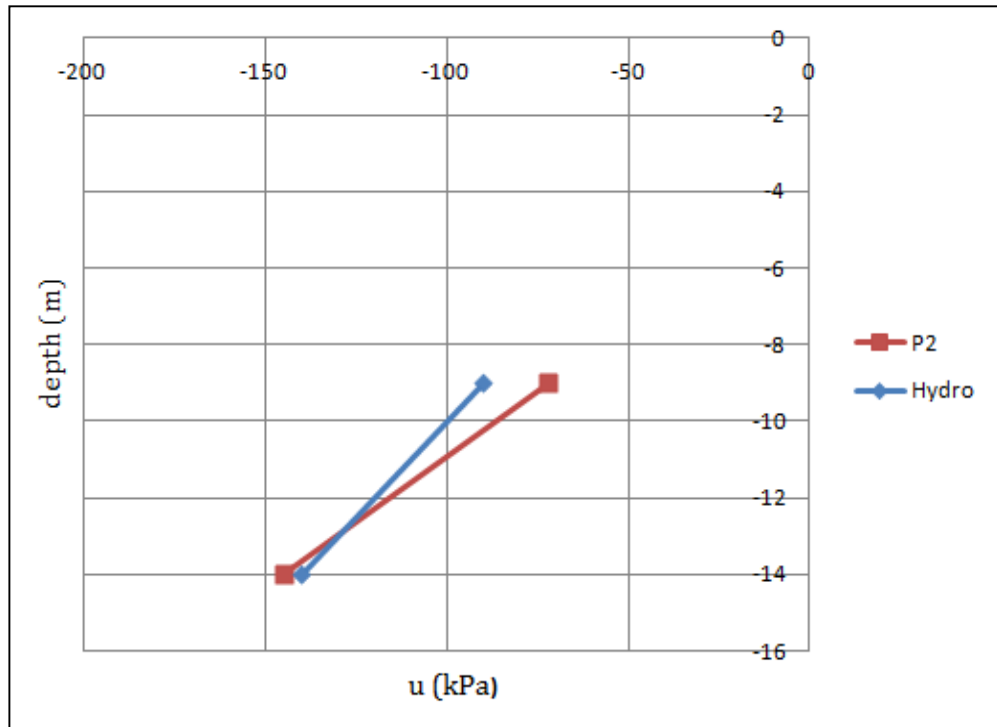


Figure B. 1 : Comparison of Hydrostatic and piezometric pore pressure before piling at station P2

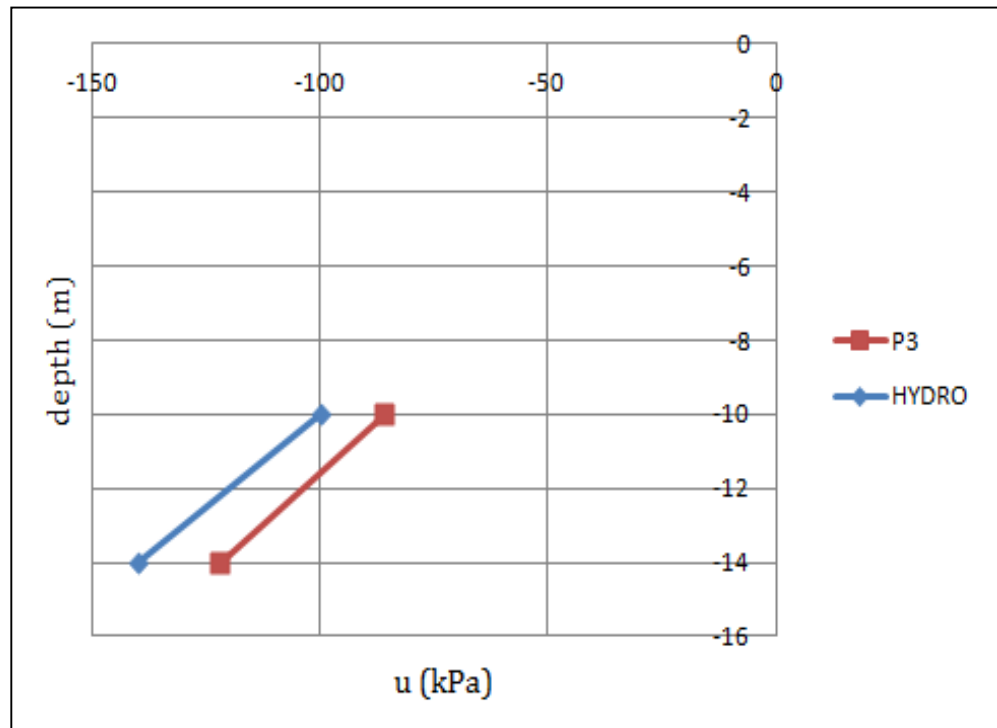


Figure B. 2 : Comparison of Hydrostatic and piezometric pore pressure before piling at station P3

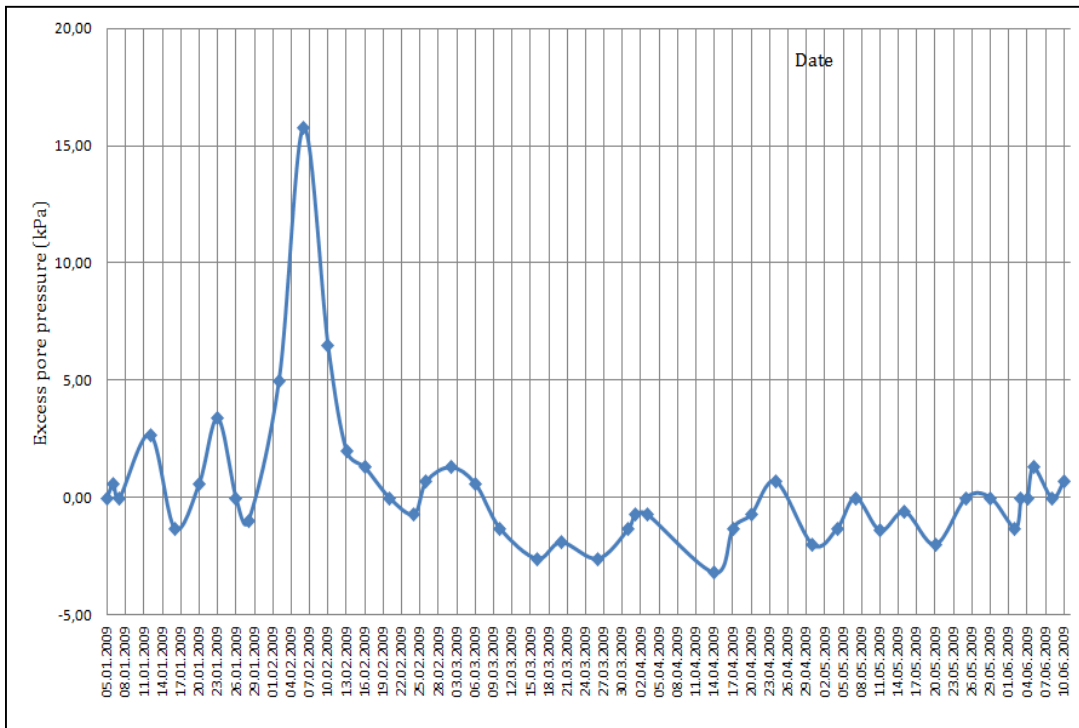


Figure B. 3 : Excess pore pressure developed at P1(-7m)

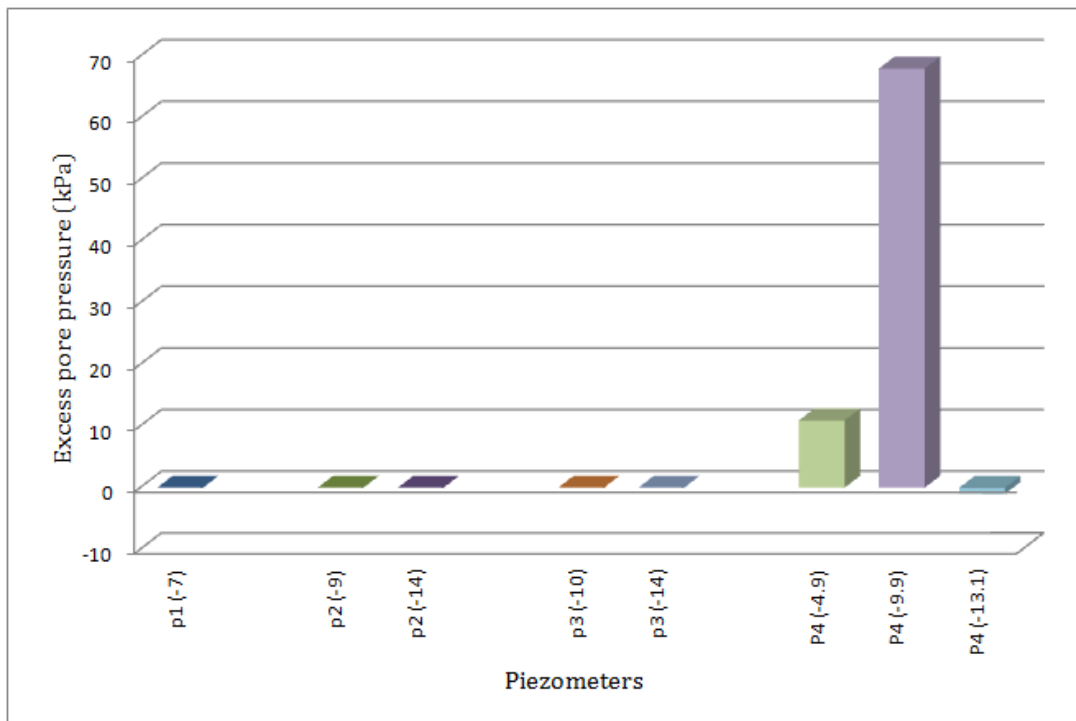


Figure B. 4: Excess pore pressure after driving G 182

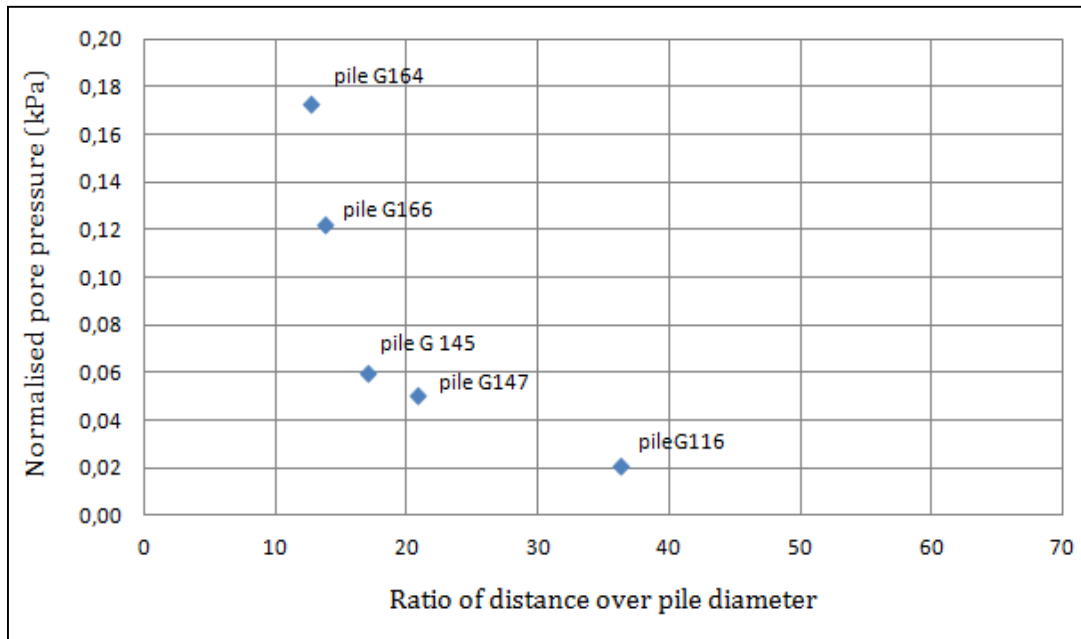


Figure B. 5 Normalized pore pressure with distance-pile diameter ratio at P3 (-10).

Table B. 1 : Radial cavity pressure with depth.

| Depth ,m | $s_{u,a}$ | $s_{u,d}$ | $s_{u,p}$ | σ_{vo} | k_o | σ_{ho} | $s_u [1 + \ln G/s_u]$ | σ_{rr} |
|----------|-----------|-----------|-----------|---------------|-------|---------------|-----------------------|---------------|
| 1,0 | 46,0 | 46,0 | 46,0 | 19,5 | 0,6 | 10,9 | 219,5 | 230,4 |
| 2,0 | 46,0 | 46,0 | 46,0 | 39,0 | 0,6 | 21,8 | 219,5 | 241,4 |
| 3,0 | 46,0 | 46,0 | 46,0 | 58,5 | 0,6 | 32,8 | 219,5 | 252,3 |
| 4,0 | 46,0 | 46,0 | 46,0 | 78,0 | 0,6 | 43,7 | 219,5 | 263,2 |
| 5,0 | 46,0 | 46,0 | 46,0 | 97,5 | 0,6 | 54,6 | 219,5 | 274,1 |
| 6,0 | 22,6 | 14,5 | 7,2 | 117,0 | 0,6 | 65,5 | 85,8 | 151,3 |
| 7,0 | 25,3 | 16,2 | 8,1 | 136,5 | 0,6 | 76,4 | 94,2 | 170,6 |
| 8,0 | 28,0 | 17,9 | 9,0 | 156,0 | 0,6 | 87,4 | 102,4 | 189,8 |
| 9,0 | 30,7 | 19,6 | 9,8 | 175,5 | 0,6 | 98,3 | 110,5 | 208,8 |
| 10,0 | 33,4 | 21,4 | 10,7 | 195,0 | 0,6 | 109,2 | 118,4 | 227,6 |
| 11,0 | 36,1 | 23,1 | 11,6 | 214,5 | 0,6 | 120,1 | 126,2 | 246,3 |
| 12,0 | 38,8 | 24,8 | 12,4 | 234,0 | 0,6 | 131,0 | 133,8 | 264,9 |
| 13,0 | 41,5 | 26,6 | 13,3 | 253,5 | 0,6 | 142,0 | 141,3 | 283,3 |
| 14,0 | 44,2 | 28,3 | 14,1 | 273,0 | 0,6 | 152,9 | 148,8 | 301,6 |
| 15,0 | 46,9 | 30,0 | 15,0 | 292,5 | 0,6 | 163,8 | 156,1 | 319,9 |
| 16,0 | 49,6 | 31,7 | 15,9 | 312,0 | 0,6 | 174,7 | 163,3 | 338,0 |
| 17,0 | 52,3 | 33,5 | 16,7 | 331,5 | 0,6 | 185,6 | 170,4 | 356,0 |
| 18,0 | 55,0 | 35,2 | 17,6 | 351,0 | 0,6 | 196,6 | 177,4 | 374,0 |
| 19,0 | 57,7 | 36,9 | 18,5 | 370,5 | 0,6 | 207,5 | 184,3 | 391,8 |
| 20,0 | 60,4 | 38,7 | 19,3 | 390,0 | 0,6 | 218,4 | 191,2 | 409,6 |

Table B. 2 : Excess pore pressure due to cavity expansion by plastic soil model

| Distance from pile, r (m) | Excess pore pressure, kPa |
|---------------------------|---------------------------|
| 0,25 | 84,59 |
| 0,50 | 54,79 |
| 0,75 | 37,35 |
| 1,00 | 24,98 |
| 1,25 | 15,39 |
| 2,00 | 5,79 |
| 2,50 | 3,70 |
| 3,50 | 1,89 |
| 14,00 | 0,12 |
| 15,00 | 0,10 |
| 25,00 | 0,04 |
| 35,00 | 0,02 |
| 36,00 | 0,02 |
| 40,00 | 0,01 |

Table B. 3 : Excess pore pressure due to cavity expansion by MCC model

| Distance from pile, r (m) | Excess pore pressure, kPa | | | Average |
|---------------------------|---------------------------|-------------|-------------|---------|
| | depth 3.2 m | depth 3.3 m | depth 3.5 m | |
| 0,10 | 45,50 | 84,60 | 123,00 | 84,37 |
| 0,25 | 34,20 | 61,40 | 86,40 | 60,67 |
| 0,50 | 25,70 | 43,90 | 58,60 | 42,73 |
| 0,75 | 20,70 | 33,60 | 42,40 | 32,23 |
| 1,00 | 17,20 | 26,30 | 30,90 | 24,80 |
| 1,50 | 12,20 | 16,10 | 14,70 | 14,33 |